

IMPLEMENTATION AND ASSESSMENT OF DEMAND RESPONSE AND VOLTAGE/VAR CONTROL WITH DISTRIBUTED GENERATORS

A Dissertation
Presented to
The Academic Faculty

by

Zhaoyu Wang

In Partial Fulfillment
Of the Requirements for the Degree
Doctor of Philosophy in the
School of Electrical and Computer Engineering

Georgia Institute of Technology
August 2015

Copyright © 2015 by Zhaoyu Wang

IMPLEMENTATION AND ASSESSMENT OF DEMAND RESPONSE AND VOLTAGE/VAR CONTROL WITH DISTRIBUTED GENERATORS

Approved by:

Dr. Ronald G. Harley, Advisor
School of Electrical and Computer
Engineering
Georgia Institute of Technology

Dr. Thomas Habetler
School of Electrical and Computer
Engineering
Georgia Institute of Technology

Dr. Nigel Hampton
School of Electrical and Computer
Engineering
Georgia Institute of Technology

Dr. Maryam Saeedifard
School of Electrical and Computer
Engineering
Georgia Institute of Technology

Dr. Santiago Grijalva
School of Electrical and Computer
Engineering
Georgia Institute of Technology

Dr. Andy Sun
School of Industrial and Systems
Engineering
Georgia Institute of Technology

Date Approved: June 12, 2015

ACKNOWLEDGEMENTS

The doctoral study at Georgia Tech is a challenging but enjoyable experience. This long-distance journey would not have been accomplished without the inspiration, encouragement, support and help from many people. I would like to express my heartfelt gratitude to all of them at this time.

First of all, I would like to extend my deepest gratitude to my advisor, Dr. Ronald G. Harley. I could not have imagined having a better advisor and mentor during my Ph.D. study. It is due to his patience, motivation, inspiration, support and immense knowledge that I have gained a deeper understanding of power engineering. His careful guidance on solving problems, writing papers and oral communicating with profession rewards my entire research life. Without his illuminating instruction, consistent encouragement, and confidence in my capability, this dissertation work could not be completed in the present form. Besides research, my advisor also shares his valuable experience in being professionals in power industry, which is highly beneficial to my future development. I am deeply grateful for my advisor's guidance and support during my Ph.D. life. Dr. Ronald G. Harley shares his valuable experience in being an effective instructor and researcher. During the preparation of this dissertation and my job hunting, I received continuous support and help from Dr. Harley. His professional expertise is always excellent and admirable.

I am extremely grateful for the support from NEETRAC (National Electric Energy Testing Research and Applications Center). My Ph.D. study is sponsored by NEETRAC.

I appreciate the supervision from Mr. Frank Lambert, Dr. Yamille Valle, Dr. Nigel Hampton and all other personnel in NEETRAC.

I would also like to extend my sincere gratitude to Dr. Santiago Grijalva, Dr. Thomas Habetler, Dr. Maryam Saeedifard, and Dr. Andy Sun for serving as my dissertation committee members and for their valuable time contribution in reviewing the drafts. Their insightful comments and suggestions have also made considerable contribution to the completion of this work.

I am thankful to all my friends at Georgia Tech. They supported me academically, personally, and especially during difficulties.

I am especially thankful to Dr. G. Tong Zhou, who established the dual master degree program between Georgia Tech and Shanghai Jiaotong University.

Most of all, I owe my loving thanks to my family. My parents' encouragement and support kept me focused and motivated. Thanks to their love, encouragement, support and understanding, I eventually reached the final stage of this doctoral degree.

TABLE OF CONTENTS

ACKNOWLEDGEMENTS	iii
LIST OF TABLES	viii
LIST OF FIGURES	x
SUMMARY	xviii
CHAPTER 1 INTRODUCTION.....	1
1.1 Research Motivations and Problem Statement	1
1.2 Research Objectives.....	6
1.3 Dissertation Outline	11
CHAPTER 2 LITERATURE REVIEW	14
2.1 Overview	14
2.2 Review of Demand Response Programs.....	14
2.3 Review of Implementation and Assessment of Voltage/VAR Control	23
2.3.1 Implementation of Voltage/VAR Control	23
2.3.2 Concept of conservation voltage reduction	26
2.3.3 Performance Assessment of Conservation Voltage Reduction	29
2.3.4 Implementation of Conservation Voltage Reduction	34
2.4 Planning of DG Penetration in Distribution Grids.....	37
2.5 Load Forecasting Techniques	38
2.6 Load Modeling and Identification	40
2.7 Summary	42
CHAPTER 3 INTRODUCTION TO STOCHASTIC OPTIMIZATION OF POWER SYSTEMS	44
3.1 Overview	44
3.2 Stochastic Optimization	44
3.3 Scenario Generation and Reduction.....	46
3.4 Multiple Replication Procedure	49
3.5 Summary	51

CHAPTER 4 IMPLEMENTATION OF VOLTAGE/VAR CONTROL IN DISTRIBUTION GRIDS.....	53
4.1 Overview	53
4.2 Models for Distribution Grids and Loads	54
4.3 Stochastic Rolling Horizon Optimization-Based Voltage/VAR Control	57
4.3.1 Rolling Horizon Optimization	57
4.3.2 Mathematical Formulation for Stochastic Voltage/VAR Control	57
4.3.3 Simulation Results	64
4.4 Stochastic DG Placement for Voltage/VAR Control.....	74
4.4.1 Mathematical Formulation for Stochastic DG Placement	76
4.4.2 Proposed Solution Algorithm	82
4.4.3 Case Study	89
4.5 Summary	95
CHAPTER 5 ASSESSMENT OF VOLTAGE/VAR CONTROL/CONSERVATION VOLTAGE REDUCTION EFFECTS.....	98
5.1 Overview	98
5.2 Data-driven Assessment by Multistage Support Vector Regression	100
5.2.1 Support Vector Machine and Support Vector Regression.....	100
5.2.2 Data-driven Assessment by Multistage Support Vector Regression.....	106
5.2.3 Impacts of Load Estimation Error on Conservation Voltage Reduction Assessment	115
5.2.4 Numerical Studies for Data-driven Assessment	119
5.2.5 Statistical Analysis.....	121
5.3 Model-driven Assessment.....	125
5.3.1 Load Model Identification	126
5.3.2 Model-Driven Assessment of Conservation Voltage Reduction Effects	127
5.3.3 Simulation Verification	136
5.3.4 Numerical Studies for Model-driven Assessment	145
5.3.5 Statistical Analysis of Assessment Results by Unscented Kalman Filter	182
5.4 Summary	184
CHAPTER 6 IMPLEMENTATION OF DEMAND RESPONSE WITH DGs AND ENERGY STORAGE SYSTEMS.....	187
6.1 Overview	187

6.2 Mathematical Formulation.....	188
6.3 Numerical Results.....	193
6.3.1 Parameter Settings of Case Studies	193
6.3.2 Simulation Results for Small Commercial/Industrial Buildings	196
6.3.3 Simulation Results for Large Commercial/Industrial Campuses	201
6.4 Summary	208
CHAPTER 7 CONCLUSIONS AND FUTURE WORK DIRECTION.....	209
7.1 Conclusions and Contributions.....	209
7.2 Future Work Directions	213
7.2.1 Future Work for Voltage/VAR Control and DG Placement	213
7.2.2 Future Work for Assessment of Conservation Voltage Reduction	215
7.2.3 Future Work for Demand Response	216
CHAPTER 8 OUTCOMES.....	218
CHAPTER 9 APPENDICES.....	220
Appendix A: IEEE 33-Node Distribution Test System	220
Appendix B: 37-Bus Distribution Test System	223
REFERENCES	229

LIST OF TABLES

Table 1.1 Comparison of existing papers and the proposed method on demand response.	7
Table 1.2. Comparison of existing papers and proposed method on voltage/VAR control.	9
Table 2.1. Demonstration of conservation voltage reduction.	34
Table 2.2. Voltage reduction techniques.	36
Table 4.1. Load types and exponent values.	56
Table 4.2. Nomenclature for stochastic voltage/VAR control formulation.	57
Table 4.3. The relationship among s, a and c.	62
Table 4.4. Node types for stochastic voltage/VAR control simulations.	66
Table 4.5. Nomenclature for stochastic DG placement formulation.	76
Table 4.6. The relationship among a, b and c.	81
Table 4.7. Base case of the test system.	90
Table 4.8. DG placement results.	90
Table 4.9. Values of optimality gaps in multiple replication procedure.	93
Table 5.1. Estimation errors of support vector regression and multi-linear regression	113
Table 5.2. Results of conservation voltage reduction factor calculations of feeders	123
Table 5.3. Summary of conservation voltage reduction factors of all test feeders	125
Table 5.4. Comparison of existing approaches and proposed method for assessment of conservation voltage reduction effects	136
Table 5.5. Calculation results of Euclidian distance-based indices in example 1	160
Table 5.6. Calculation results of Euclidian distance-based indices in example 2	169

Table 5.7. Calculation results of Euclidian distance-based indices in example 3	179
Table 6.1 Nomenclature for demand response formulation.	189

LIST OF FIGURES

Figure 1.1. Illustration of voltage/VAR control with DGs.	3
Figure 2.1. Reported potential peak reduction from 2004 to 2012.	15
Figure 2.2. Summary of cost-effectiveness results [4].	16
Figure 2.3. Categories of demand response programs.	17
Figure 2.4. Demonstration of conservation voltage reduction.	28
Figure 2.5. Simulation based methods.	32
Figure 4.1. Schematic diagram of a radial distribution grid.	54
Figure 4.2. Demonstration of rolling-horizon optimization.	56
Figure 4.3. Test distribution system [82].	65
Figure 4.4. Profiles of active and reactive load multipliers.	66
Figure 4.5. Profiles of solar power and wind power.	67
Figure 4.6. Tap positions with exponential model (Tap EXL) and constant power model (Tap CP).	69
Figure 4.7. Switch status of capacitors at nodes 2 and 3 with exponential model (Cap EXL) and constant power model (CAP CP).	70
Figure 4.8. Switch status of capacitors at nodes 6 and 11 with exponential model (Cap EXL) and constant power model (CAP CP).	70
Figure 4.9. Switch status of capacitors at nodes 20 and 23 with exponential model (CAP EXL) and constant power model (CAP CP).	71
Figure 4.10. Voltage profiles.	71
Figure 4.11. Peak-time voltage profiles.	72

Figure 4.12. Active power losses and max voltage deviations (EEV refers to the expected results of using the expected value solution).	73
Figure 4.13. Demonstration of voltage drop along a feeder.	75
Figure 4.14. Flowchart of combined multiple replication procedure and sample average approximation.	86
Figure 4.15. The 37-bus distribution system.	89
Figure 4.16. Voltage profile of the 37-buse distribution system.	91
Figure 4.17. Active load consumption of the 37-buse distribution system.	92
Figure 4.18. Optimality gap in multiple replication procedure (the optimality gap is defined in equation 4.74).	93
Figure 4.19. Comparison of the expected results of using the expected value solution (EEV) and Monte Carlo simulation.	94
Figure 5.1. Load profiles with and without voltage reduction.....	99
Figure 5.2. A non-separable example with support vectors shown in ringed points.	103
Figure 5.3. Demonstration of conservation voltage reduction test.	107
Figure 5.4. Multistage support vector regression framework for conservation voltage reduction analysis (MAPE represents mean average percentage error).	109
Figure 5.5. Load profiles with and without voltage reduction.....	110
Figure 5.6. Comparison of support vector regression and multi-linear regression.....	112
Figure 5.9. Comparison of support vector regression with and without pre-selection in forming the training dataset for a single normal-voltage day.....	115
Figure 5.7. Relationship of estimation errors of load, actual conservation voltage reduction factors and estimation errors of conservation voltage reduction factors.	117

Figure 5.8. Contour of estimation errors of load, actual conservation voltage reduction factors and estimation errors of conservation voltage reduction factors.	118
Figure 5.10. Voltage profile, actual load profile (with conservation voltage reduction) and estimated load profile by multistage support vector regression (MSVR based on 63 training days).	120
Figure 5.11. Conservation voltage reduction factors calculated by multistage support vector regression.	120
Figure 5.12. Band for actual conservation voltage reduction factors in data-driven assessment.	121
Figure 5.13. Cumulative probability of conservation voltage reduction factors of Feeder 1	122
Figure 5.14. Histogram of CVR factors of Feeder 1	123
Figure 5.15. Cumulative normal distribution functions of conservation voltage reduction factors of all test feeders.	124
Figure 5.16. Time-varying load modeling framework for assessing conservation voltage reduction effects.	134
Figure 5.17. Values of c	138
Figure 5.18. Mean average percentage estimation errors with different values of q and r in simulation example 1.	139
Figure 5.19. Actual and estimated values of b	139
Figure 5.20. Actual and estimated values of A	140
Figure 5.21. IEEE 123-bus distribution system.	141

Figure 5.22. Voltage profiles with and without conservation voltage reduction in simulation example 2.....	141
Figure 5.23. Load profiles with and without voltage reduction in simulation example 2.....	142
Figure 5.24. Mean average percentage estimation errors with different values of $P(0)$, $k_p(0)$, q and r in simulation example 2.....	143
Figure 5.25. Simulated and estimated load profiles with different combinations of $P(0)$, $k_p(0)$, q and r in simulation example 2.....	144
Figure 5.26. Comparison of actual and estimated conservation voltage reduction factors in simulation example 2.....	144
Figure 5.27. Voltage profile with conservation voltage reduction in example 1.....	148
Figure 5.28. Measured load profiles in example 1.....	149
Figure 5.29. Mean average percentage estimation errors with different values of q and r in example 1.....	150
Figure 5.30. Measured and estimated load profiles with different combinations of q and r in example 1.....	151
Figure 5.31. Estimated load-to-voltage sensitivities with different combinations of q and r in example 1.....	151
Figure 5.32. Conservation voltage reduction factors calculated by estimated load-to-voltage sensitivities in example 1 (only the period of 140-422 minutes is CVR period).....	152
Figure 5.33. Mean average percentage estimation errors with different values of $P_0(0)$, $k_p(0)$, q and r in example 1.....	153

Figure 5.34. Measured and estimated load profiles with different combinations $P_0(0)$, $k_p(0)$, q and r in simulation example 1.....	154
Figure 5.35. Estimated load-to-voltage sensitivities with different combinations of $P_0(0)$, $k_p(0)$, q and r in example 1.....	155
Figure 5.36. Conservation voltage reduction factors calculated by estimated load-to-voltage sensitivities in example 1 (only the period of 140-422 minutes is CVR period).	155
Figure 5.37. Conservation voltage reduction factors during voltage reduction period in example 1.....	156
Figure 5.38. Contour of relationship of estimation errors of k_p , estimated values of k_p , and estimation errors of conservation voltage reduction factors.....	158
Figure 5.39. Band of conservation voltage reduction factors in example 1.....	159
Figure 5.40. Load profiles with and without voltage reduction in example 1.....	161
Figure 5.41. Voltage profiles with voltage reduction and without voltage reduction in example 1.....	162
Figure 5.42. Conservation voltage reduction factors calculated by model-driven method and comparison method in example 1.....	162
Figure 5.43. Voltage profile with conservation voltage reduction in example 2.....	163
Figure 5.44. Measured load profiles in example 2.....	164
Figure 5.45. Mean average percentage estimation errors with different values of $P_0(0)$, $k_p(0)$, q and r in simulation example 2.....	165
Figure 5.46. Measured and estimated load profiles with different combinations $P_0(0)$, $k_p(0)$, q and r in simulation example 2.....	166

Figure 5.47. Estimated load-to-voltage sensitivities in example 2.....	166
Figure 5.48. Conservation voltage reduction factors calculated by estimated load-to-voltage sensitivities in example 2 (only the period of 123-181 minutes is CVR period).	167
Figure 5.49. Conservation voltage reduction factors during voltage reduction period in example 2.....	167
Figure 5.50. Band of conservation voltage reduction factors in example 2.	168
Figure 5.51. Load profiles with and without voltage reduction in example 2.....	171
Figure 5.52. Voltage profiles with voltage reduction and without voltage reduction in example 2.....	172
Figure 5.53. Conservation voltage reduction factors calculated by model-driven method and comparison method in example 2.	172
Figure 5.54. Voltage profile with conservation voltage reduction in example 3.....	173
Figure 5.55. Measured load profiles in example 3.....	174
Figure 5.56. Mean average percentage estimation errors with different values of $P_o(0)$, $k_p(0)$, q and r in simulation example 3.....	175
Figure 5.57. Measured and estimated load profiles with different combinations $P_o(0)$, $k_p(0)$, q and r in simulation example 3.....	176
Figure 5.58. Estimated load-to-voltage sensitivities in example 2.....	176
Figure 5.59. Conservation voltage reduction factors calculated by estimated load-to-voltage sensitivities in example 3 (only the period of 184-363 minutes is CVR period).	177

Figure 5.60. Conservation voltage reduction factors during voltage reduction period in example 3.....	177
Figure 5.61. Band of conservation voltage reduction factors in example 3.	178
Figure 5.62. Load profiles with and without voltage reduction in example 3.....	180
Figure 5.63. Voltage profiles with voltage reduction and without voltage reduction in example 3.....	181
Figure 5.64. Conservation voltage reduction factors calculated by model-driven method and comparison method in example 3.	181
Figure 5.65. Histogram of conservation voltage reduction factors calculated by unscented Kalman filter.....	182
Figure 5.66. Cumulative distribution curves of conservation voltage reduction factors calculated by unscented Kalman filter.....	183
Figure 6.1. Two-stage demand response selection and energy management.	188
Figure 6.2. Five load scenarios for small commercial/industrial buildings.....	194
Figure 6.3. Five load scenarios for large commercial/industrial campuses.....	194
Figure 6.4. Price deviations of demand response programs.	195
Figure 6.5. Flowchart of simulation.....	196
Figure 6.6. Load shifting results of a small commercial/industrial building in the first year.	198
Figure 6.7. Aggregated charging/discharging of battery units of a small commercial/industrial building in the first year.....	199
Figure 6.8. Power imported from the grid of a small commercial/industrial building in the first year.	200

Figure 6.9. Power imported from the grid of a small commercial/industrial building without batteries in the first year.	201
Figure 6.10. Load shifting results of a large commercial/industrial building in the first year.....	202
Figure 6.11. Load shifting of a large commercial/industrial campus without batteries in the first year.	203
Figure 6.12. Aggregated charging/discharging of battery units of a large commercial/industrial campus in the first year.....	204
Figure 6.13. Power imported from the grid of a large commercial/industrial campus in the first year.	205
Figure 6.14. Power imported from the grid of a large commercial/industrial campus in the fifth year.....	206
Figure 6.15. Power imported from the grid of a large commercial/industrial campus in the fifth year (with peak-time rebate and time-of-use).	207
Figure 6.16. Power imported from the grid of a large commercial/industrial campus without batteries in the first year.	207

SUMMARY

The main topic of this research is the efficient operation of a modernized distribution grid from both the customer side and utility side. For the customer side, this dissertation discusses the planning and operation of a customer with multiple demand response programs, energy storage systems and distributed generators; for the utility side, this dissertation addresses the implementation and assessment of voltage/VAR control and conservation voltage reduction in a distribution grid with distributed generators.

The objectives of this research are as follows: (1) to develop methods to assist customers to select appropriate demand response programs considering the integration of energy storage systems and DGs, and perform corresponding energy management including dispatches of loads, energy storage systems, and DGs; (2) to develop stochastic voltage/VAR control techniques for distribution grids with renewable DGs; (3) to develop optimization and validation methods for the planning of integration of renewable DGs to assist the implementation of voltage/VAR control; and (4) to develop techniques to assess load-reduction effects of voltage/VAR control and conservation voltage reduction.

In this dissertation, a two-stage co-optimization method for the planning and energy management of a customer with demand response programs is proposed. The first level is to optimally select suitable demand response programs to join and integrate batteries, and the second level is to schedule the dispatches of loads, batteries and fossil-fired backup generators. The proposed method considers various demand response programs, demand

scenarios and customer types. It can provide guidance to a customer to make the most beneficial decisions in an electricity market with multiple demand response programs.

For the implementation of voltage/VAR control, this dissertation proposes a stochastic rolling horizon optimization-based method to conduct optimal dispatches of voltage/VAR control devices such as on-load tap changers and capacitor banks. The uncertainties of renewable DG output are taken into account by the stochastic formulation and the generated scenarios. The exponential load models are applied to capture the load behaviors of various types of customers.

A new method to simultaneously consider the integration of DGs and the implementation of voltage/VAR control is also developed. The proposed method includes both solution and validation stages. The planning problem is formulated as a bi-level stochastic program. The solution stage is based on sample average approximation (SAA), and the validation stage is based on multiple replication procedure (MRP) to test the robustness of the sample average approximation solutions of the stochastic program.

This research applies big data-driven analytics and load modeling techniques to propose two novel methodologies to assess the load-reduction effects of conservation voltage reduction. The proposed methods can be used to assist utilities to select preferable feeders to implement conservation voltage reduction.

CHAPTER 1 INTRODUCTION

1.1 Research Motivations and Problem Statement

The U.S. Energy Policy Act of 2005 (EPACT) states that it is the policy of the United States to encourage time-based pricing and other forms of demand response and encourage States to coordinate, on a regional basis, State energy policies to provide reliable and affordable demand response services to the public. Demand response is defined as the changes in electric use by demand-side resources from their normal consumption patterns in response to changes in the price of electricity, or to incentive payments designed to induce lower electricity use at times of high wholesale market prices or when system reliability is jeopardized [1].

Demand response offers a variety of financial and operational benefits for electricity customers, load-serving entities and grid operators. Demand response benefits include avoided capacity costs, avoided transmission and distribution costs, avoided ancillary service costs, revenues from wholesale Demand response programs, market price suppression effects, avoided environmental costs, participant bill savings, financial incentives, improved reliability, etc. There are various demand response programs which can be classified into two main categories according to how load changes are brought about: price-based programs and incentive-based programs. Price-based demand response programs refer to changes in usage by customers in response to changes in the prices they pay. Incentive-based demand response programs are established by utilities, load-serving entities, or a regional grid operator to provide rebates to customers to reduce the load consumption in certain periods.

Utilities usually provide multiple options of demand response programs to customers, so as to reduce or shift the peak-time demand, and improve the system operation and reliability. For example, Pacific Gas and Electric Company (PG&E) offers time-of-use (TOU) program, peak-time rebate program, and critical peak pricing program. A customer can select multiple programs to participate in. To facilitate the implementation of demand response, energy storage systems can be installed at the customer level. Energy storage can store energy when there is less demand and release the stored energy back to the system during peak periods, which make it an ideal candidate to improve the demand response performance. A customer may also have DGs such as fossil-fired backup generators. The operation of these DGs can be optimized to coordinate with the demand response schedules and energy storage systems.

The challenge is that a customer can opt-in/out from multiple demand response programs. The variety of customer demand scenarios and the integration of customer-owned DGs and energy storage bring further challenges. The problem is to design a method to assist various types of customers to make the most beneficial plan to participate in demand response programs, and to integrate customer-owned energy storage and DGs. Meanwhile, the developed method should help the customers to schedule DG generation, charging/discharging of batteries, and perform load management accordingly. Multiple objectives should be considered in the decision-making process, which include costs, reliability, and discomfort. The costs include electricity purchases as well as investments and operation of energy storage and DGs. The reliability is defined as the curtailment index of loads. The discomfort is defined as the index of load shifts. The methods developed in this dissertation require computational

abilities which may not be available to the average customer. A possible solution is to integrate the proposed method with an online computation platform so that a customer can upload the data to a server and take advantage of the computational ability of the server to receive an optimal result.

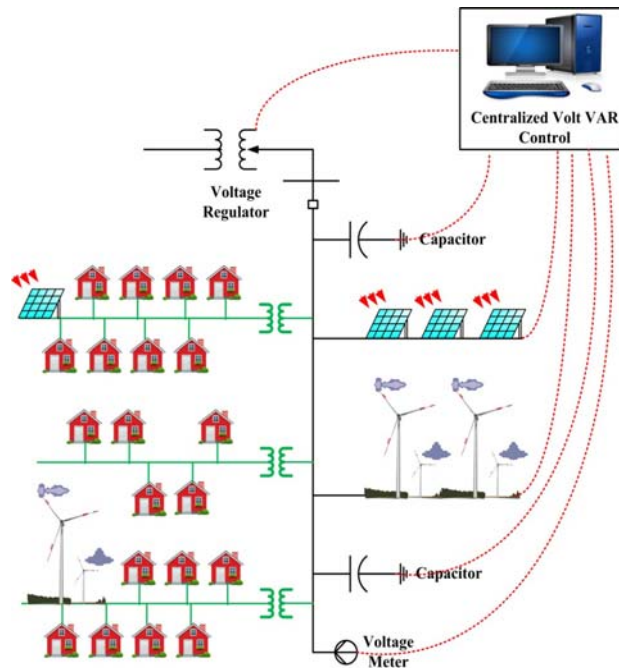


Figure 1.1. Illustration of voltage/VAR control with DGs.

Demand response can be implemented on the customer side to increase the efficiency and reliability of a power system. On the utility side, voltage/VAR control (VVC) can be used to improve the system operation. Voltage/VAR control refers to the process of managing voltage levels and reactive power throughout the distribution systems. voltage/VAR control is achieved by controlling the tap positions of on-load tap changers and VAR compensation devices such as capacitor banks. Fig. 1.1 shows an example of a centralized voltage/VAR control for a distribution grid with renewable DGs. The increasing penetration of DGs has great impacts on conventional voltage/VAR

control because of the uncertain outputs of renewable energy sources-based DGs. The stochasticity of renewable DG outputs should be taken into account when making the voltage/VAR control dispatches.

On the other hand, the load behaviors also impact the voltage/VAR control. However, most existing literature ignores the load-to-voltage relationship and uses constant-power models to represent load behaviors, which may not be accurate in practice. Load models have significant impacts on power system operation and analysis. The studies of power system stability, operation and planning strongly depend on the accuracy of load models and their parameters. The conventional constant-power load models which are normally used in previous studies assume that the load is insensitive to voltage, which may not be realistic and lead to inaccurate voltage/VAR control dispatches. A variety of load-to-voltage behaviors exist for different types of customers. This is especially true in distribution systems since the load-to-voltage sensitivities may vary from one node to another due to the complicated load compositions. The load-to-voltage sensitivities greatly impact the effectiveness of voltage/VAR control. The voltage control of power systems is a multi-objective optimization problem that requires more effective and robust control strategies. A novel voltage/VAR control technique is needed to take into account both the uncertain DG outputs and load behaviors. In this dissertation, the exponential load model is selected to represent the load-to-voltage relationship; this load model is selected because it is a frequently used voltage dependent model in existing papers [2, 3]. However, a rigorous way to validate the exponential load model is still outstanding. A possible way to validate the load model is to run a few trials to change the tap positions

of tap changers to check if the exponential load model can track the load-to-voltage behaviors.

One important function of voltage/VAR control is conservation voltage reduction. The main purpose of conservation voltage reduction is to reduce the voltage level of distribution grids so as to reduce peak demand and energy consumption. Thus, conservation voltage reduction has a similar objective as demand response programs. But unlike demand response programs, conservation voltage reduction is imposed by utilities. conservation voltage reduction works on the principle that many loads are voltage dependent and consume less power when the supplied voltage is reduced. As a popular and economical energy-saving measure, conservation voltage reduction has attracted many utilities for implementation in their distribution systems. One of the critical problems about conservation voltage reduction is how to assess its energy-saving effect, which is useful for utilities in selecting candidate feeders to implement voltage reduction and conduct cost/benefit analysis. conservation voltage reduction effects are evaluated by a conservation voltage reduction factor (CVRf), which is defined as the percentage of load consumption reduction resulting from one percent reduction in voltage. Calculating CVR factors is challenging for many reasons: there is no benchmark for comparison, i.e., the load consumption without voltage reduction during the conservation voltage reduction period cannot be measured; conservation voltage reduction factors are small, which can be biased by the measurement noises and estimation errors; and conservation voltage reduction effects are stochastic since the load behaviors are uncertain. Methodologies are needed to assess conservation voltage reduction effects.

Besides the implementation of demand response and stochastic voltage/VAR control, another important feature of a modernized distribution grid is the integration of distributed generators (DGs), which is driven by the energy deficit, load growth, environmental consciousness and constraints on building new transmission and distribution lines. DG has impacts on voltage profile, power quality, energy efficiency, and reliability of distribution systems. The location and size of DG units should be carefully selected in order to take advantage of DGs and limit their negative impacts on system operations. Because of the uncertain outputs of renewable DGs, the placement of such DGs is typically a stochastic mixed-integer multi-objective optimization problem. In this dissertation, a solution and validation method is designed for the planning of DG integration with the objective to assist the implementation of voltage/VAR control.

1.2 Research Objectives

The dissertation objectives are listed as follows:

(1) Develop a two-stage framework for the implementation of demand response. The designed framework is a co-optimization method of planning and operation of a customer with demand response programs. The main objective is to maximize the benefits to the customer. The first stage is to assist customers in optimally selecting demand response programs and integrating energy storage systems. The second stage is to perform energy management including load dispatch, generation scheduling of controllable DGs, and charging/discharging of energy storage systems. A variety of demand response programs and customer demand scenarios are considered in the proposed method. The impacts of energy storage systems on the planning and operation of demand response programs are analyzed. Table 1.1 summarizes some representative papers on demand response in

recent years. This table evaluates whether a paper has considered the energy management with demand response, the planning problem (i.e., to select most beneficial programs to participate), the existence of DGs and batteries, and multiple demand response programs. No paper listed in the table has studied the co-optimization of energy management and planning with demand response. The proposed method in this dissertation can assist customers to make the most beneficial decision to participate in demand response programs, install batteries, and perform the corresponding energy management. Thus, the co-optimization of planning and energy management used in the proposed method and is a novel contribution of this work.

Table 1.1 Comparison of existing papers and the proposed method on demand response.

Papers	Energy management	Planning	DG/Battery	Multiple DR programs
Aalami (2010) [4]		X		X
Pourmousavi (2012) [5]	X		X	
Dietrich (2012) [6]	X		X	
Peng (2012) [7]	X		X	
Nunna (2013) [8]	X		X	
Vlot (2013) [9]	X		X	
Parvania (2013) [10]	X		X	
Chen (2014) [11]	X		X	
Meng (2014) [12]	X		X	
Chapter 6 in dissertation	X	X	X	X

(2) Develop a stochastic rolling horizon optimization-based method for the optimal dispatch of on-load tap changer and capacitor banks considering the load behaviors and the uncertainty of DG outputs. A practical distribution system may consist of various

types of customers such as residential, commercial and industrial loads. The constant-power load model which is frequently used in existing voltage/VAR control techniques should be replaced by models that can represent load-to-voltage relationships. Specifically, an exponential load model is introduced in this dissertation. Each type of customer is assigned with assumed exponents in the exponential load models. The uncertainties of prediction errors of DG outputs and load consumption are taken into account using a scenario-based approach. The probabilistic prediction errors result from the integration of renewable DGs, i.e., wind turbines and photovoltaic systems in this dissertation. Monte-Carlo simulations are used to generate scenarios. The simultaneous backward scenario reduction method is applied to increase the calculation speed while maintaining the accuracy of the solution. The stochastic rolling horizon optimization-based voltage/VAR control problem is formulated as a mixed integer nonlinear program with reduced scenarios and then solved by the general algebraic modeling system. Table 1.2 summarizes some representative journal papers on voltage/VAR control in recent years. Most papers have considered the control of on-load tap changers and capacitors. There are a few papers have taken into account the stochasticity of load consumption and renewable generation. All of the listed papers use constant-power models instead of voltage-dependent models to represent load behaviors. However, the aggregated load behavior of a feeder is not pure constant-power. At the end of this table is the voltage/VAR control method proposed in this dissertation. The novel contribution of the proposed method is that it simultaneously considers the load-to-voltage relationship and the stochasticity of load consumption and renewable generation.

Table 1.2. Comparison of existing papers and proposed method on voltage/VAR control.

Papers	OLTC*	Capacitors	Stochastic DG output	Stochastic load	Voltage-dependent load model
Viawan (2007) [13]	X	X			
Hong (2009) [14]	X	X	X		
Souza (2010) [15]	X	X			
Niknam (2012) [16]	X	X	X	X	
Farag (2012) [17]	X	X	X		
Borghetti (2013) [18]	X	X			
Medina (2013) [19]		X	X		
Agalgaonkar (2014) [20]	X	X			
Capitanesccu (2014) [21]	X	X			
Chapter 4 in dissertation	X	X	X	X	X

*OLTC=on-load tap changer

(3) Develop novel methods to assess the load-reduction effect of conservation voltage reduction. Two methods are proposed in this dissertation.

The *first* one is based on a big data-driven technique. A multistage support vector regression-based method is designed and used to estimate the load consumption at normal voltage levels during the conservation voltage reduction period. As a powerful machine learning method, support vector regression (SVR) is considered as one of the best non-parametric regression techniques, since it can approximate any nonlinear function. In order to increase the accuracy of the support vector regression model, only the set of profiles that are close to the load

profile under prediction is used to train the support vector regression model. The selection process is performed by calculating a Euclidian distance-based index in the first stage. Support vector regression is used for load estimation in the second stage. The model accuracy can be improved by performing the pre-selection of the training data. To further lower down estimation errors, the estimated profiles are re-selected in the third stage.

The *second* method is to model loads as functions of voltage and calculate conservation voltage reduction factors estimating the load-to-voltage sensitivities. A conservation voltage reduction factor is subject to different types of uncertainties, depending on load mix, feeder configurations, weather conditions, human behaviors, etc. Therefore, this dissertation proposes a probabilistic analysis framework based on the Kolmogorov-Smirnov (K-S) goodness-of-fit test to identify the most suitable probability distribution representing conservation voltage reduction factors of different feeders.

(4) Develop a solution and validation method to simultaneously consider stochastic placement of renewable DGs and voltage/VAR control for energy saving and peak demand reduction. This dissertation proposes a novel stochastic DG placement model to minimize load consumptions of a distribution grid and maintain the voltage deviations along the feeder within a predefined range. The proposed method assumes a centralized decision maker such as the distribution system operator who can make the DG placement plan for the voltage/VAR control implementation since voltage/VAR control is a measure initiated by the utilities. In order to effectively deal with the probabilistic nature of DG outputs and load consumption, the DG placement is formulated as a two-stage stochastic

programming problem. The first stage includes deterministic variables. The second stage includes variables adjusted according to the uncertainties. Sample Average Approximation is used to solve the two-stage stochastic formulation. Sample average approximation can converge to an optimal solution if the number of samples is large enough. Since the sample size cannot be infinite in practice, a new method is proposed by combining multiple replications procedure with sample average approximation to measure the quality of the solution and find the confidence interval of the gap between the sample average approximation solution and the optimal solution.

1.3 Dissertation Outline

The outline of the remaining parts of this dissertation is as follows.

In Chapter 2, background information is provided on the origin of the topic along with presently available technologies that are being used. In addition, a thorough literature survey is presented that summarizes related research work efforts. In particular, this chapter starts with an introduction to existing demand response programs and corresponding energy management techniques. The presently utilized technologies for voltage/VAR control along with its biases and limitations are presented. The chapter also gives a summary of the current technologies and limitations of the implementation and assessment of conservation voltage reduction. A literature review on the state-of-the-art algorithms utilized for DG placement problem follows. Finally, the load forecasting and load model identification technologies are summarized.

Chapter 3 presents the preliminary research on stochastic optimization in power systems. Specifically, it discusses the sample average approximation, scenario generation

and reduction for renewable DG outputs and load consumptions, and multiple replication procedure for solution validation.

Chapter 4 presents the detailed mathematical formulations for the rolling horizon optimization-based voltage/VAR control and DG placement to assist voltage/VAR control. The uncertainties of DG outputs and load consumptions are taken into account by modeling the problems as bi-level stochastic programs. The load-to-voltage sensitivities and various customer types are considered. This chapter also presents the combined sample average approximation-multiple replication procedure solution and validation method. Simulation results on an IEEE distribution test system are given at the end.

Chapter 5 presents in detail the big data-driven and load modeling-driven techniques to assess conservation voltage reduction effects. More specifically, a multistage support vector regression-based method and a load modeling and identification method are presented in details. To deal with the stochasticity of conservation voltage reduction effects, a Kolmogorov-Smirnov test-based probabilistic analysis framework is also given. Finally, demonstration results with practical utility test data are presented.

Chapter 6 describes a two-stage co-optimization framework for the planning and energy management of a customer with demand response programs. The first stage is to assist a customer to select multiple demand response programs to join and make plans to integrate energy storage systems to coordinate with demand response programs. The second stage is to conduct energy management which includes dispatches of loads, DGs and energy storage systems according to the decisions in the first stage. Case studies with various practical demand response programs, customer types, and demand scenarios are presented in this chapter.

Finally, Chapter 7 summarizes the research work and outlines the results and contributions of this dissertation.

CHAPTER 2 LITERATURE REVIEW

2.1 Overview

This chapter provides the background information of existing technologies related to the proposed research along with a literature review of the research efforts on these topics. For the implementation of demand response, section 2.2 presents a review on various demand response programs and the existing techniques on optimal operation of power systems with demand response programs. For the research on voltage/VAR control, section 2.3 summarizes the currently utilized methods in conducting voltage/VAR control and assessing the corresponding effects. Section 2.4 introduces the optimal planning of distributed generation in distribution grids to assist the implementation of voltage/VAR control. In this dissertation, load forecasting and modeling techniques are used to assess the performance of voltage/VAR control. Section 2.5 provides a literature review on the state-of-the-art algorithms utilized for load forecasting. Section 2.6 summarizes the load modeling and identification techniques.

2.2 Review of Demand Response Programs

Demand response is a tariff or program established to motivate changes in electricity consumption by end-use customers in response to changes in the electricity price over time. Further, it can be defined as programs to give incentive payments designed to induce lower electricity use at times of high market prices or when grid reliability is jeopardized [1]. In the past several years, significant progress has been achieved for both wholesale and retail demand response thanks to the support by the U.S. Energy Policy Act and the American Recovery and Reinvestment Act. Fig. 2.1 shows the reported

potential peak demand reduction from 2004 to 2012 [1-2]. demand response programs were estimated to be about 72,000 MW or nearly 9.2 percent of U.S. peak demand in 2012 [22]. This shows the tremendous increase of demand response programs since the demand response capability was estimated to be about 20,500MW, or 3 percent of U.S. peak demand by the Department of Energy (DOE) in 2004 [1].

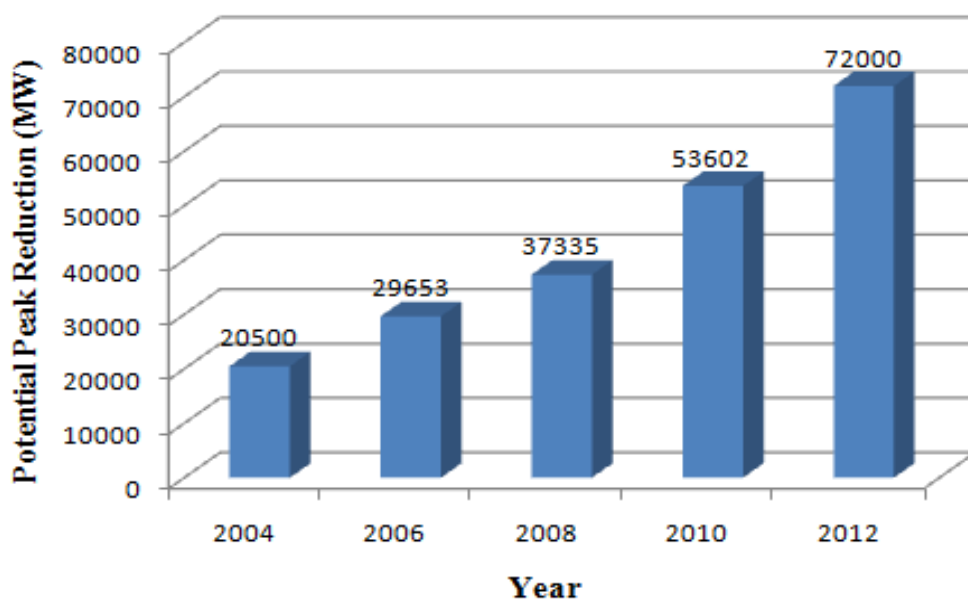


Figure 2.1. Reported potential peak reduction from 2004 to 2012.

Demand response offers a variety of financial and operational benefits which can be categorized into four parts: participant, system, reliability, and market performance [23]. Customers participating in demand response programs can expect savings in electricity bills. Demand response programs also have system-wide benefits such as an overall electricity price reduction, a more efficient utilization of existing infrastructures, and an avoided or deferred generation/transmission expansion costs. From the perspective of reliability, the operator will have more options and resources to maintain system

reliability, thus reducing forced outages and interruptions. The electricity market performance has been improved by demand response programs since the participants have more choices in the market and can affect the market. The price volatility in the spot market has also been reduced. Fig. 2.2 shows a cost/benefit analysis for the demand response programs in Consolidated Edison Company [24]. The company offers its customers direct load control programs, commercial system relief programs (CSR) and distribution load relief programs (DLRP). It can be seen in Fig. 2 that all the demand response programs implemented in ConEdison are beneficial.

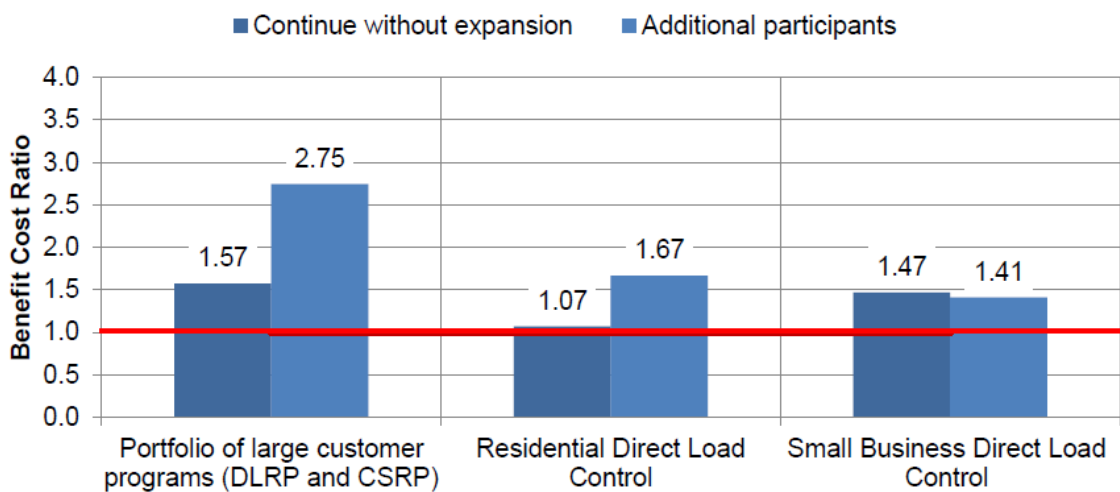


Figure 2.2. Summary of cost-effectiveness results [4].

There are many types of demand response programs. As shown in Fig. 2.3, demand response programs can be classified into two categories: incentive-based programs and price-based programs [1]. The incentive-based programs offer participating customers rebates when load reduction is requested by the programs sponsor, which can be triggered by a grid reliability problem or high electricity prices. Typical incentive-based programs

include: direct load control, interruptible/curtailable programs, demand bidding, emergency demand response, capacity market, ancillary service market and peak time rebate. The price-based programs give customers time-varying rates which reflect the value and cost of electricity in different time periods so that customers tend to consume less electricity during peak-price periods. Typical price-based programs include real-time pricing, critical-peak pricing and time of use tariffs.

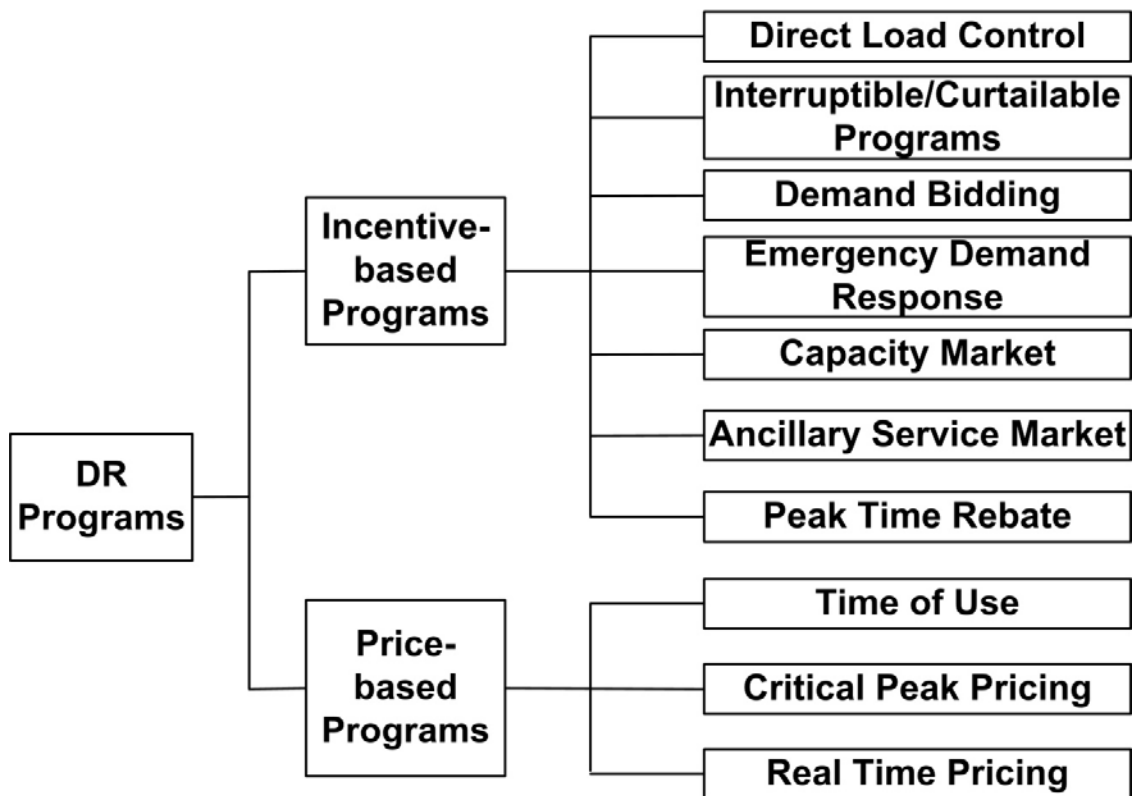


Figure 2.3. Categories of demand response programs.

Direct load control refers to the load management scheme that allows utilities to shed the end-use customer loads unilaterally in order to curtail the system peak load [25]. Loads such as air-conditioners and water heaters are good candidates for direct load

control. The customers sign contracts with utilities to specify the maximum number of events per year and the maximum duration of the given event (usually 4 hours). The utilities usually issue little advance notification prior to initiating an event. If the customer overrides an event, there could be penalties. Direct load control is one of the most economical and straightforward ways to conduct demand response. However, there are some drawbacks with the direct load control: the consumers suffer from the discomfort and inconvenience due to the load shedding; the reconnection of disconnected load may cause another load peak; the effects of pre-scheduling direct load control are affected by load uncertainties. Reference [26] proposed a profit-based load direct load control technique with the objective to maximize the profit of utilities. The formulation was solved by a linear programming algorithm. Reference [25] presented an adaptive control strategy for integrating direct load control with interruptible load management to provide instantaneous reserves for ancillary services in deregulated power systems.

In interruptible/curtailable programs, customers receive a discount or incentive in exchange for agreeing to reduce load during system contingencies. Interruptible/curtailable programs are typically offered by utilities. Customers on interruptible/curtailable programs agree to either curtail a specific block of electric load or curtail their consumption to a pre-specified level. The participating customers must curtail within 30 to 60 minutes when being notified by the utility. The number of hours that a utility can request an interruption is usually no more than 200 hours per year. It is clear that customers with continuous processes are not suitable for interruptible/curtailable programs. Reference [27] introduced the concepts of price

elasticity of demand and customer benefit function and presented the economic model of interruptible/curtailable programs to maximize the benefits of customers.

Capacity market programs are another traditional and common type of demand response programs which are driven by both reliability and economic needs. Customers who join this program are responsible to provide pre-specified load reductions when system contingencies arise, and are subject to penalties if they do not curtail when directed [27]. Capacity market programs are different from interruptible/curtailable programs since capacity market programs are usually offered by wholesale market providers such as independent system operators (ISOs) and program providers need to call the participated customers when needed. There are some requirements for customers to qualify for capacity market programs. The requirements of New York ISO are: minimum load reductions of 100 kW, minimum four hour reduction, two hour notification, and to be subject to one test or audit per capability period. If no events are called, the participants will still receive payments. Reference [27] proposed an economic model based on demand-price elasticity and incentives/penalties to maximize the benefits of participants.

In demand bidding programs, consumers bid on specific load reduction in the electricity wholesale market. A bid is accepted if it is less than the market price. The customer must curtail corresponding to the load specified in the bid once the bid is accepted. Otherwise, there will be penalties [23].

Emergency demand response programs provide incentive payments to customers for load reduction achieved during an emergency event. In certain cases, customers can receive up to \$65,000 per MW per year to be on standby to reduce a portion of their

energy consumption when the supply of the electricity on the grid is threatened. The participants are paid even if no event has been called.

Ancillary service is typically associated with establishing customer load commitments in advance. Participants whose market bids are accepted are paid the market price for committing to be standby to provide load reductions, usually with less than one-hour notice. Ancillary service is usually provided by ISOs and mainly offered to large commercial and industrial customers. Reference [28] analyzed the characteristics of simultaneous auctions of integrated systems and the pricing mechanisms for simultaneously procured energy and ancillary service using an AC-OPF formulation.

Peak time rebate rewards customers for using less electricity during peak hours. Peak-time rebate is different from peak-time pricing programs which change prices more for electricity use during peak times. Utilities usually prefer to reward their customers for using less electricity rather than punishing them for using more power during peak hours. On the other hand, customers also prefer a rate structure with no penalties. Therefore, peak-time rebate becomes a popular demand response program.

Time of use is the most common example of price-based demand response [23]. In time-of-use programs, the electricity prices are determined based on the production costs in the same period [29]. A typical time-of-use program may have three time blocks: low-load period with cheap rates, off-peak period with moderate rates and peak period with high rates. The prices are usually determined months ahead of time to reflect electricity prices under anticipated and average market conditions. By running time-of-use programs, it is expected that consumers adjust their electricity usage by prices so that the peak demand is reduced and loads is transferred to off-peak or low-load periods. In reference

[29], demand response was modeled considering time-of-use programs by using the single and multi period load models as well as the concepts of self and cross price elasticity. It was shown that demand profiles could be changed due to the running of the time-of-use program.

In critical peak pricing, the basic rate structure resembles time-of-use, but there is a short-term rate increase during critical grid conditions. The critical period occurs during a certain time on a peak day. For example, in the critical time pricing program of Pacific Gas and Electric Company (PG&E), prices will increase either from 2 p.m. to 6 p.m. or from 12 noon to 6 p.m. in event days. Participants in critical peak pricing programs are expected to shed or shift load in response to the dramatically higher electricity prices in the critical period. Critical time prices are used for a limited number of days or hours per year [23]. Reference [30] analyzed the results of critical peak pricing experiments in 483 households. A statistically significant response was found. It was also found that customer response to the \$0.68/kWh critical-peak price was not higher than response to the \$0.50/kWh critical-peak price.

Real-time pricing are programs in which customers are charged based on hourly fluctuating prices reflecting the real cost of electricity in the wholesale market [23]. Unlike the time-of-use programs whose electricity prices are determined months ahead of time, participants of real-time pricing programs are typically notified of prices on a day-ahead or hour-ahead (sometimes near- or real-time) basis. Reference [31] proposed an optimization model to perform hourly load dispatch given the hourly electricity prices. The objective of the model was to maximize the utility of the consumer. A robust optimization technique is used to model the price uncertainty.

After a customer joins certain demand response programs, the optimal energy management is one of the most important issues faced by the customer. Many studies have been performed on the optimal operation with demand response programs in the existing literature. The study in [11] proposes a direct load control scheme for large-scale residential demand response based on a consensus algorithm. The objective is to achieve the optimal aggregated demand consumptions in a decentralized way. The study in [32] proposes an agent-based energy management system with demand response and distributed energy storage systems to minimize the supply-demand gap in multiple microgrids. A virtual market with demand side management, DGs and energy storage is designed to allow neighboring microgrids to trade with each other. The study in [12] analyzes scenarios of a household with photovoltaic generators, batteries, and demand side management in the electricity market of Texas. The battery capacity and total revenue of the household are optimized with real-time market prices. The study in [10] proposed a framework to maximize the payoff of a demand response aggregator in a wholesale market based on a mixed-integer linear program. Energy storage systems, DGs, and demand response programs are used to reduce load consumptions. The study in [33] discussed the demand side management for large-scale data centers based on the stochastic optimization approach. By optimally shifting the cloud service tasks among data centers, the financial benefits can be improved. The study in [34] proposed new operation strategies of energy storage systems to facilitate demand response. The proposed methods allow energy storage devices be controlled jointly by end customers and network operators. The study in [8] proposed an energy management system to facilitate power trading among multiple microgrids by using the energy availability from

demand response, DGs and distributed energy storage systems. The study in [5] presented a central demand response algorithm to regulate frequency in a microgrid. The study in [9] introduced three models to characterize the behaviors and load shifting capabilities of some domestic appliances, so as to facilitate the implementation of demand response programs. The study in [6] proposed a demand shifting and peak shaving measures to improve the generation-load balance for a power system with a high wind integration.

The above mentioned literature assumes that a consumer is already participating in a certain demand response program. However, many utilities offer various types of demand response programs for customers to participate. For example, PG&E provides time-of-use, peak-time rebate and critical time pricing programs. The existing literature only considers one demand response program and cannot assist customers to select the program/programs to participate. Energy storage systems play an important role in demand side management. The joint optimization of energy storage integration and demand response participations has not been covered in the above literature. Moreover, if a customer joins multiple demand response programs, the corresponding energy management problem becomes more challenging.

2.3 Review of Implementation and Assessment of Voltage/VAR Control

2.3.1 Implementation of Voltage/VAR Control

Voltage/VAR control is a secondary control scheme to the daily operation of distribution systems. voltage/VAR control is achieved by on-load tap changers and VAR compensation devices such as capacitors. The main purpose of voltage/VAR control is to coordinate the schedules of tap positions of on-load tap changers and statuses of switched capacitors to improve the power quality and operations of distribution systems. The

increasing penetration of distributed generators has great impacts on conventional voltage/VAR control because of the uncertain outputs of renewable energy sources-based DGs [16, 35].

Many papers in the literature have investigated the voltage/VAR control problems in distribution networks. Reference [36] treated the regulation of on-load tap changers and capacitors as two decoupled problems and provided an optimal real-time control scheme. Reference [15] studied the coordination of voltage regulators and capacitors. A multi-objective genetic algorithm was used to deal with the integrated voltage/VAR control so as to minimize power losses and voltage deviations. In reference [37], the on-load tap changer and capacitors were dispatched hourly based on day-ahead load forecast. Reference [38] proposed a two-stage coordinated control between on-load tap changers and capacitor banks. The dispatch schedules of capacitor banks were generated using a heuristic algorithm based on the forecasted load, and the on-load tap changer was controlled in real time. Reference [39] presented an artificial neural network (ANN)-based optimal coordination control scheme for on-load tap changer and STATCOM in a distribution system. However, the existence of DGs was not considered in these papers.

As the penetration level of DGs has grown, their impacts on voltage and reactive power in distribution systems have attracted more and more attention [40]. The outputs of RES-based DGs can be highly stochastic. Meanwhile, the value of resistance can be close to that of reactance in a distribution circuit, which highlights the impacts of real power outputs of DGs on voltage profiles [16]. Reference [41] investigated the coordination of the on-load tap changer and capacitors to minimize power losses in a distribution system with DGs. The DGs were assumed to be synchronous machine-based ones whose outputs

were controllable. Reference [13] proposed a combined centralized and local control scheme for voltage/VAR control to minimize losses in the presence of induction machine-based DGs. Loads were assumed to be constant-power loads. It was also assumed that the wind power can be forecasted without errors. Reference [42] proposed an optimal control of distribution voltages with the coordination of voltage regulators, capacitors, shunt reactors and static VAR compensators in a distribution system with photovoltaic (PV) generation. However, the output of photovoltaic generators was assumed to be known. Reference [20] proposed an optimal reactive power coordination strategy to minimize the number of tap operations of line voltage regulators in distribution systems with high penetration of photovoltaic generators. Reference [43] proposed a hybrid voltage/VAR control for a distribution system with photovoltaic generators. There are only a few papers considering the stochastic nature of renewable energy source-based DGs in solving the voltage/VAR control problems. Reference [16] applied a teaching-learning algorithm to schedule voltage/VAR control dispatch, the stochastic outputs of DGs were converted to a series of equivalent deterministic scenarios. The study in [14] used the genetic algorithm for optimal VAR control considering wind farms to minimize system losses.

All of the above literature ignores the load-to-voltage relationship and use constant-power models to represent load behaviors, which may not be accurate in practice [2]. Load models have significant impacts on power system operation and analysis [44, 45]. The studies of power system stability, operation and planning strongly depend on the accuracy of load models and their parameters. The conventional constant-power load models which are normally used in previous studies assume that the load is insensitive to

voltage, which may not be realistic and lead to inaccurate voltage/VAR control dispatches. This is especially true in distribution systems since the load-to-voltage sensitivities may vary from one node to another due to the complicated load compositions. The load-to-voltage sensitivities greatly impact the effectiveness of voltage/VAR control. Meanwhile, the ever-increasing penetration of DGs has introduced additional constraints and uncertainties into the voltage control of power systems.

In recent years, there is a trend to use inverters to perform voltage/VAR control. Reference [46] proposed a decentralized control technique to perform voltage/VAR control based on inverters. Reference [47] analyzed the impacts of fluctuations of solar generation on voltage stability, and found that reactive power support provided by inverters can improve the system stability. The study in [48] developed an algorithm to apply inverters to flatten voltage profile and minimize power losses. This dissertation focuses on traditional voltage/VAR control based on load tap changers and capacitors. The inverter-based voltage/VAR control is not taken into account since the technique is still not widely accepted by utilities in the United States [49].

2.3.2 Concept of conservation voltage reduction

Besides providing high-quality power supply to the customer and increase system reliability, voltage/VAR control can also make the system run more efficiently by applying conservation voltage reduction. Conservation voltage reduction is an established idea and one of the most cost-effective ways to save energy. By lowering voltages on the distribution system in a controlled manner, conservation voltage reduction can reduce peak demand, losses and achieve more energy savings while keeping the lowest customer utilization voltage consistent with levels determined by regulatory agencies and

standards-setting organizations [50]. Considerable conservation voltage reduction tests were performed in the 1980s and 1990s, and achieved significant peak demand or energy reduction. More efforts have been made in the industry and academia in conservation voltage reduction recently, which is particularly influenced by the increasingly stringent requirements for energy saving and environmental protection as well as accommodating emerging smart monitoring and control technologies in distribution systems.

American National Standards Institute (ANSI) Standard C84.1 [51] sets the range for voltages at the distribution transformer secondary terminals at 120 Volts $\pm 5\%$ or between 114 Volts and 126 Volts. Conservation voltage reduction works on the principle that the acceptable voltage band can be easily and inexpensively operated in the lower half (114-120 volts), without causing any harm to consumer appliances [52]. Conservation voltage reduction effects can be evaluated by the Conservation Voltage Regulation factor, which is defined as the percentage of load consumption change divided by the percentage of voltage reduction.

There are two ways to perform conservation voltage reduction: short-term demand reduction and long-term energy reduction, as shown in Fig. 2.4. The left plot of Fig. 2.4 shows the short-term conservation voltage reduction, voltage reduction is applied during peak hours to reduce peak demand. In long-term energy reduction, as shown in the right plot of Fig. 2.4, the voltage is reduced permanently to save energy.

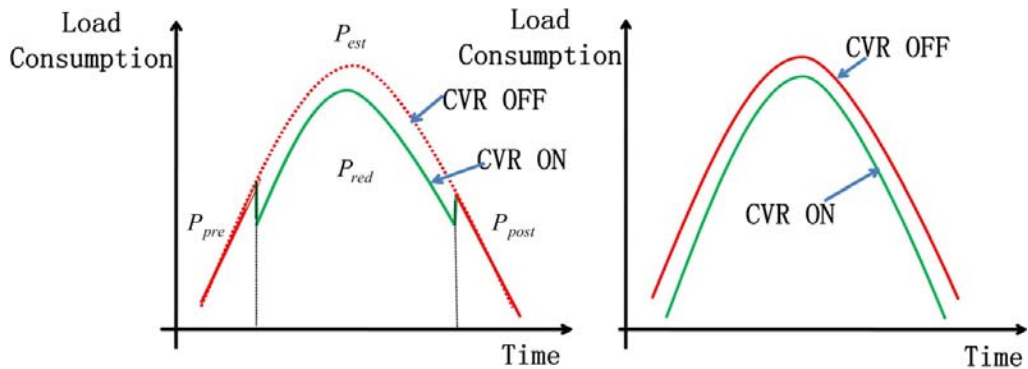


Figure 2.4. Demonstration of conservation voltage reduction.

The earliest reported conservation voltage reduction test was performed by American Electric Power System (AEP) in 1973 [53]. After that, many utilities such as Southern California Edison (SCE) [54], Northeast Utilities (NU) [55], Bonneville Power Administration (BPA) [56], BC Hydro [57], Northwest Energy Efficiency Alliance (NEEA) [58], Hydro Quebec (HQ) [59] and Dominion Virginia Power [60] conducted their CVR tests and obtained significant outcomes of energy savings associated with voltage reduction, usually ranging from 0.3% to 1% load reduction per 1% voltage reduction. Recent studies show that deployment of conservation voltage reduction on all distribution feeders of the United States could provide a 3.04% reduction in the annual national energy consumption [61]. Conservation voltage reduction was also widely tested in other countries, such as Australia [62] and Ireland [63]. It was found that 2.5% voltage reduction resulted in 1% energy savings on residential circuits in Australia. Applying conservation voltage reduction to circuits in Ireland could achieve 1.7% energy reductions.

Consumers can benefit from the reduced energy consumption from conservation voltage reduction. However, the utilities may lose revenues, which is a common problem for many demand-response programs [64]. The conservation voltage reduction benefits

for utilities can be summarized as: peak loading relief of distribution network; net loss reduction considering both the transformers and distribution lines; potential incentives and requirements from regulatory bodies (e.g., California Public Utilities Commission encouraged utilities to implement conservation voltage reduction, Northwest Power and Conservation Council performed extended research on conservation voltage reduction incentives [64]); increasing social welfare such as fuel consumption and emission reduction.

2.3.3 Performance Assessment of Conservation Voltage Reduction

Assessing the performance of conservation voltage reduction on feeder circuits has always been a critical issue in deciding its implementation, selecting target feeders to apply voltage reduction and performing cost/benefit analyses. The load consumption without voltage reduction during the conservation voltage reduction period cannot be measured and provide a benchmark for comparison. How to quantify a credible estimated energy-saving effect is the driving force for research and implementation of conservation voltage reduction. Skepticism regarding the effect of conservation voltage reduction remains a barrier to its acceptance. The major challenge to quantify conservation voltage reduction effects is to distinguish the changes in load and energy consumption due to voltage reduction from other impact factors. The methodologies for assessing conservation voltage reduction effects can be classified into four categories: comparison-based, regression-based, synthesis-based and simulation-based.

There are two basic comparison methods for measuring conservation voltage reduction effects. The first one is to select two similar feeders in the same performance period. In other words, the two feeders have similar configurations, topologies, load

conditions, load mix and are close in location. Voltage reduction is applied to one feeder (treatment group), while normal voltage is applied to the other feeder at the same time (control group). The second way is to perform a conservation voltage reduction test on a feeder (treatment group) and apply normal voltage to the same feeder but during another time period with similar weather conditions (control group). The conservation voltage reduction effects can then be calculated based on the measurements from the two tests. The comparison-based method is the most straightforward to calculate the conservation voltage reduction factor. However, there are some shortcomings: 1) a good control group may not exist; 2) the noises such as weather impacts are not very well considered and simple averages may not be sufficient to cancel noises; 3) after averaging the data, it is not possible to obtain the conservation voltage reduction factor for a particular time on a particular test day, which loses the time-dependant nature of the conservation voltage reduction factor.

In regression-based methods, loads are modeled as a function of their impact factors. In references [64-66], loads are modeled as a function of temperature. Models for the normal-voltage load process are identified using linear regression, and their outputs are compared with the measured reduced-voltage load to calculate the conservation voltage reduction factor. As the regression methods are based on linear regression models that decompose the load, usually into basic and weather dependent components, they are widely used to assess conservation voltage reduction effects because some physical interpretations may be attached to model components, allowing utilities to understand the model behavior. The regression models can also be used to forecast the conservation voltage reduction factors. However, since the conservation voltage reduction effects are

usually a few percent of energy reduction, it may fall within the error bound of the regression models. It is necessary to distinguish conservation voltage reduction effects from the estimation errors. Moreover, the regression methods are heavily dependent on the accuracy of regression models. Models used by most papers are basically linear, but the load series they try to explain are known to be distinctly nonlinear functions of the exogenous variables.

Synthesis-based methods aggregate load-to-voltage sensitivities to estimate the conservation voltage reduction effects of a circuit. There are two ways to perform the aggregation: synthesis from load components and synthesis from customer classes. In the component-based synthesis, the energy consumption of major appliance loads is modeled as a function of voltage, which is identified through laboratory tests. The load shares of each appliance are obtained through surveys. Synthesis-based methods can be used to obtain a quick estimation of conservation voltage reduction effects before its implementation. The basic assumptions of synthesis methods are that all of the appliances behave as they did during the lab test and the load composition information is correct. However, it is difficult to collect accurate load share information as well as the load-to-voltage response of every existing electric appliance. Thus, the results obtained from synthesis methods should be used with caution.

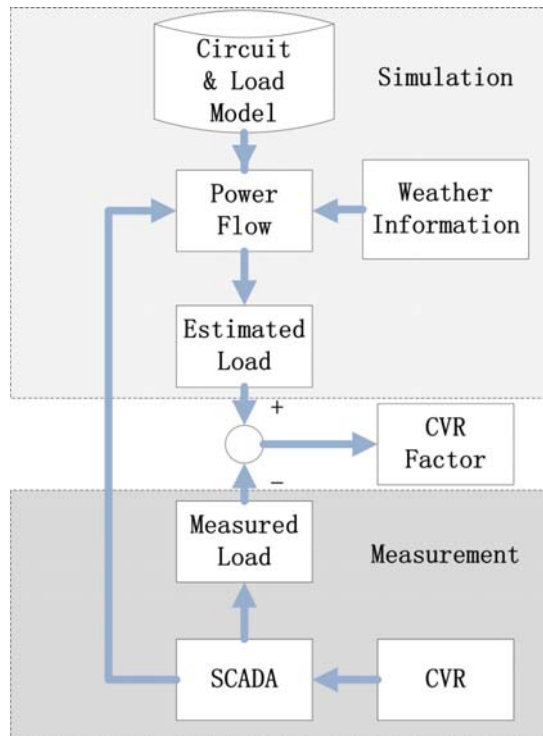


Figure 2.5. Simulation based methods.

Simulation methods simulate load behaviors using system modeling and power flow calculation. This method estimates what the load consumption would be if there were no conservation voltage reduction. Fig. 2.5 shows the flowchart of this method.

Load can be modeled as a function of voltage, time and weather factors. Power flow is run based on measured operation data and weather information. The difference between power-flow results and measured load consumption is used to calculate the conservation voltage reduction factor. The circuits that have detailed models can be of high precision. The challenge is how to model the load which contributes to the major energy saving effect. Traditional load models such as exponential and ZIP (i.e., a model that combines constant power, constant impedance and constant current models) models can be used to represent open-loop appliances. For closed-loop loads such as heating, ventilation, and air conditioning (HVAC) systems, the equivalent thermal parameter

model should be used. In the equivalent thermal parameter model, the power demand of the HVAC system is modeled as a function of solar input, temperature, humidity, voltage and thermostatic set points. Simulation methods have high precision if the models can accurately represent the load behaviors. However, the current simulation methods are component-based while it may be too difficult to build models for all existing and emerging load components. A better method is to identify the aggregated load models at the circuit level. Moreover, it is clear that conservation voltage reduction effects change with time, but the current load models are all time-invariant, which may impact the estimation results of the conservation voltage reduction factor. Thus, it is necessary to make the model adaptive to dynamic changes of feeders and load behaviors.

Table 2.1 summarizes the existing assessment methodologies. Since it is impossible to know the load consumption under normal voltage during the conservation voltage reduction period, lack of validity becomes the common roadblock for all assessment methodologies. The accuracy of the comparison-based methods depends on the selection of comparable groups [67]. The synthesis-based methods require load-share information which is difficult to be obtained. The regression-based methods are widely used in assessing conservation voltage reduction effects. Simulation methods have the potential to be used for validation, if the load behaviors could be accurately modeled. Some of the four methods can be combined in certain cases, e.g., simulation-based methods can be used to validate regression-based methods. If there is no benchmark for comparison, the reported conservation voltage reduction effects cannot be well accepted. Using load-to-voltage sensitivities for assessing conservation voltage reduction effects is another attractive method, since it can reflect the nature of conservation voltage reduction. More

sophisticated identification algorithms are needed to filter out noises and detect load-to-voltage sensitivities.

Table 2.1. Demonstration of conservation voltage reduction.

Utilities	EST	Attributes	CVRf
Snohomish PUD	CO	(+) easy and straightforward, (-) dependent on control group, (-) noise vulnerable	0.50
Northeast Utilities	CO		1.00
American Electric Power	RE	(+) clear physical meaning, (+) capable of forecasting conservation voltage reduction effects, (-) regression error, (-) load model is linear	0.62
California Public Utilities Commission	RE		1.00
Northwest Energy Efficiency Alliance	RE		0.61
Avista Utility	RE		0.84
BC Hydro	RE		0.70
Southern California Edison	RE		1.00
Bonneville Power Administration	SY	(+) quick estimation and forecast of conservation voltage reduction effect, (-) accurate load information is difficult to collect	0.99

EST: assessment method, **RE:** regression based, **CO:** comparison based, **SY:** synthesis based, **SI:** simulation based, (+) means positive attributes, (-) means negative attributes, **CVRf:** conservation voltage reduction factor

2.3.4 Implementation of Conservation Voltage Reduction

The early techniques to reduce voltage are open-loop without voltage feedback, such as load tap changer, line drop compensation and capacitor-based reduction. The installation of supervisory control and data acquisition system and advanced metering infrastructure has led many utilities to implement closed-loop voltage/VAR control. Conservation voltage reduction becomes an operation mode in these close-loop VVCs, while many other control objectives such as loss reduction, power factor improvement and voltage deviation minimization are also included.

Load tap changer/line drop compensation is the most used method to implement voltage reduction. Load tap changer is typically used to control the secondary voltage of a substation. To apply voltage reduction merely by load tap changer, the circuits should be carefully selected. For a feeder with large voltage drops, the depth of voltage reduction may be limited. Line drop compensation can lower the average voltage by 2% to 3% [68]. Line drop compensation involves setting the controls on substation voltage regulators or load tap changer to keep the most distant portion of the circuit at some minimum acceptable voltage levels, such as 114 volts, while the rest of the circuit voltage is allowed to vary with load conditions. However, settings of line drop compensation are difficult to determine and cannot adapt to the dynamic nature of distribution loads and DGs. As most utilities include some safety margin to ensure that the voltage levels remain above the minimum requirements, the voltage reduction potential is relatively small, which will decrease conservation voltage reduction effects. Switched capacitors can be coordinated with voltage control methods to conduct voltage/VAR control to implement conservation voltage reduction. For a feeder with a certain conservation voltage reduction factor, deeper voltage reduction within the permissible range can lead to more energy-savings. The depth of voltage reduction is limited for circuits that experience a significant voltage drop. A relatively flat voltage profile along the feeder is preferable to achieve an effective implementation of conservation voltage reduction. By placing capacitors at multiple locations, it is possible to flatten the voltage profile, correct the power factor to near unity, and reduce power losses [69]. The closed-loop voltage/VAR control takes advantage of various measurements to determine the best

voltage/VAR control actions during certain time periods [70]. Table 2.2 summarizes voltage reduction techniques.

Table 2.2. Voltage reduction techniques.

Utilities	VR	Attributes	VD
California Public Utilities Commission	LT	(+) easy and economical, (-) small volt reduction, (-) no volt feedback, may result in low volt	2.5%
Northwest Energy Efficiency Alliance	LD	(+) end-of-line voltage is controlled, (+) larger volt reduction than LT, (-) complicated settings, (-) no volt feedback, (-) cannot adapt to dynamic changes	2-3.9%
Duke Energy	LD		2%
Snohomish PUD	LD,CA	(+) end-of-line voltage is controlled, (+) larger volt reduction than LD, (+) less power losses, flattened volt profile and improved power factor (-) capacitor placement is complicated, (-) no volt feedback, (-) lack of coordination between LD and CA, (-) cannot adapt to dynamic changes, (-) high cost	2.1%
Bonneville Power Administration	LD,CA		4.6%
Northeast Utilities	LD,CA		3%
Georgia Power Company	LD,CA		4.1%
BC Hydro	LD,CA		3%
Avista Utility	LD,CA	(+) larger volt reduction, (+) more reliable with volt feedback, (+) adaptive to dynamic changes, (-) complicated and high cost	2.3%
Dominion Virginia Power	VVO		4%

VR: voltage reduction method, **VD:** percentage of voltage reduction, **LT:** load tap changer, **LD:** line drop compensation, **CA:** capacitor, **VVO:** closed-loop voltage/VAR control. (+) means positive attributes, (-) means negative attributes.

Integrating DGs into distribution networks is a major trend in a smart grid. There are two main research topics on the relationship between DG integration and conservation voltage reduction: 1) sizing and placement of DGs for loss reduction and voltage profile improvement; 2) the coordination between controls of DGs and voltage/VAR control to further optimize conservation voltage reduction effects. A number of objectives can be associated with sizing and placement of DGs, among which, to minimize voltage

deviation along the feeder and to minimize power losses are closely related to conservation voltage reduction.

2.4 Planning of DG Penetration in Distribution Grids

This section presents a brief literature survey on the state of the art of the formulation and algorithm for the optimal integration of distributed generators.

The integration of DG in distribution feeders has increased rapidly. DG has impacts on voltage profile, power quality, energy efficiency, and reliability of distribution systems. The location and size of DG units should be carefully selected in order to take advantage of DGs and limit their negative impacts on system operations. The placement of DGs is typically a mixed-integer multi-objective optimization problem. A variety of objectives have been investigated in the literature, such as loss reduction [71], voltage improvement [45], reliability improvement [72], stability enhancement [73], and economic considerations [74].

A wide range of methods have been proposed for DG placement, which can be divided into three categories: sensitivity analysis [73, 75], analytical approaches [76, 77], and intelligence algorithms (IAs) [78-80]. The authors of [73] used continuous power flow to identify the voltage sensitivity of each bus and then allocate DG at the most sensitive bus to improve the voltage security margin and reduce power losses. The study in [76] presented an analytical approach to identify the optimal location to place a DG to minimize power losses. IA is one of the most popular methods to determine the size and location of DG. Several works [78, 79] claimed that IAs were suitable for multi-objective problems and could achieve a near optimal solution. However, many IAs are sensitive to algorithm settings and initial conditions. IAs converge slowly and are easy to converge to

a suboptimal solution. All the above existing work assumes that DG is dispatchable and controllable, which is clearly not accurate since renewable energy source (RES)-based DGs are mostly non-dispatchable power sources with intermittent output. Only a few papers have considered the uncertain nature of DG outputs and load consumptions in system planning. The authors of [81] presented a probabilistic planning method to determine the optimal mix of wind, solar, and biomass units to minimize annual energy losses, but the placement of DG units is not considered. The authors of [82] allocated DG to improve voltage stability. The probabilistic nature of DG output was mentioned but not taken into account in the solution algorithm.

The integration of DGs increases energy efficiency on the generation side while conservation voltage reduction saves energy on the demand side. However, none of the above papers optimize the placement of DGs for the purpose of assisting voltage reduction. This research proposes a new method to simultaneously consider conservation voltage reduction and DG placement for energy saving and peak demand reduction.

2.5 Load Forecasting Techniques

Load forecasting plays an important role in the planning, control and operation of power systems. Load forecasting is a challenging task for many reasons: the load behavior is complex and the load at a given hour is dependent not only on the load at the previous hour, but also on the load at the same hour on the previous day, and on the load at the same hour on the day with the same denomination in the previous week; there are many important exogenous variables that must be considered, specially weather-related variables [83]. Many studies have been made in the area of load forecasting and its applications. Most forecasting models and methods that have already been tried out on

load forecasting can be classified into two categories: time series models, in which the load is modeled as a function of its past observed values; and causal models, in which the load is modeled as a function of some exogenous factors, specially weather and social variables.

Some methods such as multi-variant linear regression, autoregressive models, and Kalman filter-based models are in the first category. Methods such as Autoregressive–moving-average with exogenous inputs (ARMAX) models, nonparametric regression, structural models, and curve-fitting procedures are in the second category. The most popular causal models are still the linear regression ones that decompose the load, usually into basic and weather-dependent components. Although the linear models cannot fully capture the non-linear behaviors of loads, these models are attractive because some physical interpretation may be attached to their components, allowing engineers and system operators to understand their behavior.

In recent times, much research has been carried out on the application of artificial intelligence techniques and machine learning techniques to the load forecasting problem. The study in [84] applied particle swarm optimization and neural networks in load forecasting. The investigation in [85] used a support vector machine in mid-term load forecasting (i.e., predicting daily load of the next 31 days). Reference [86] combined self-organized map and support vector machine to solve the short-term load forecasting problem (i.e., day-ahead prediction). The study in [87] developed a support vector regression model based on locally weighted vectors for load forecasting. However, these methods are not designed to analyze the conservation voltage reduction effects. The major issue in evaluating the conservation voltage reduction effect is to find what the

load would be without voltage reduction during the conservation voltage reduction period. This research proposes a short-term load forecasting method to estimate the normal-voltage load during the voltage-reduction period.

2.6 Load Modeling and Identification

Load modeling has significant impacts on power system analysis. Although much research has been done in load modeling and identification, it is still a challenging problem because of the complexity, stochasticity and time variability of load. Load models can be divided into two categories: static load models and dynamic load models. Static models describe the relationship among power consumption, voltage and frequency. Frequently used static models include exponential and ZIP models. Dynamic models use differential equations to represent the relationship between the load and its impact factors. Examples of dynamic models are exponential recovery, induction motor and composite ZIP-induction motor models. At present, static load models are still commonly used for power system analysis. Dynamic models, which can capture dynamic responses of loads to disturbances, are used for transient analysis. As shown in [2], load modeling is still a challenging topic which receives interests from both industry and academia. The time-varying and stochastic nature of load behaviors makes it difficult to model loads. In this dissertation, the exponential load model as defined in (2.1) is used to represent the load-to-voltage relationship.

$$P = P_0 \left(\frac{V}{V_0} \right)^{k_p} \quad (2.1)$$

where P represents the active power consumption, P_0 represents the nominal active power, k_p represents the load-to-voltage dependence, V and V_0 represent the measured

and nominal voltage, respectively. The exponential load model is one of the most widely accepted load models to express the input-output relationship between the voltage and the power. It has been used by many papers and utilities to represent load behaviors [88]. The study in reference [89] claimed that the exponential load model could be used to represent the load with respect to the voltage change. The study in [3] even provided typical model parameters of the exponential load model for industrial, commercial and residential customers.

Load model parameters can be estimated by solving an optimization problem to minimize the difference between measured system outputs and model outputs. The methods used to identify load models can be classified into two groups: component-based identification [90] and measurement-based identification [91]. The component-based approach is an aggregated method, which requires prior knowledge on load models and corresponding load model parameters of individual load components. Load characteristics at a bus can be derived from known load components and their composition. However, since it is very difficult to collect information about load components, this method is not popular. The measurement-based approach applies system identification techniques to practical data at selected substations and feeders, which are readily available for power flow and transient stability measurements. The field measurements are obtained in two ways: stage tests and continuous monitoring. In stage tests, a certain level of voltage perturbations is artificially imposed on system loads by changing tap ratios of transformers. The permissible voltage variation is limited to several percent of the operating voltage. The continuous monitoring method records load behaviors during faults and small disturbances.

After collecting enough measurements, load model parameters can be estimated by solving an optimization problem to minimize the difference between measured system outputs and model outputs. Some of the published methods to solve this problem include [92]: least square-based parameter estimation, on-line recursive identification, gradient-based parameter estimation [11], genetic algorithms, adaptive simulated annealing-based algorithms and artificial neural network-based estimation. All these identification methods can be applied to estimate a time-invariant deterministic load model. However, the time-dependant property and randomness of load make it difficult to select appropriate model parameters for power system simulation and analysis.

In this dissertation, the load is modeled as a function of voltage by the exponential load model, and the conservation voltage reduction effects are assessed using the identified load-to-voltage sensitivities.

2.7 Summary

This chapter presents an overall description and related work on the research topics of this dissertation. In particular, Section 2.2 gives a summary of the demand response programs and the corresponding energy management techniques. Section 2.3 summarizes the present practices on voltage/VAR control and its limitations. The assessment of conservation voltage reduction effects is also discussed. The advantages and disadvantages of each assessment method are discussed. Section 2.4 provides a brief literature review of the methods on load forecasting. Finally, in Section 2.5, the technologies on load modeling and identification are summarized.

As discussed in Section 2.2 and 2.3, the energy management with demand response and the voltage/VAR optimization with DGs can be formulated as stochastic optimization problems. In the next chapter, the stochastic optimization in power systems is introduced.

CHAPTER 3 INTRODUCTION TO STOCHASTIC OPTIMIZATION OF POWER SYSTEMS

3.1 Overview

In this chapter, the stochastic optimization in power systems and its related topics on scenario generation, reduction and solution validation are discussed. Stochastic optimization is widely used in this dissertation to solve the voltage/VAR control problem and DG allocation problem in Chapter 4, and the two-stage demand response planning and operation problem in Chapter 6.

3.2 Stochastic Optimization

This section summarizes the pertinent contents on stochastic optimization in reference [93]. Consider a stochastic problem of the following type

$$\min_{x \in X} \{f(x) := E[F(x, \xi(\omega))]\} \quad (3.1)$$

where $X \subseteq R^n$, F is a real-valued function measuring the performance of the system of interest, x is a decision vector constrained to obey physical and policy rules represented by the set X , $\xi(\omega)$ is a random vector, and E is the associated expectation operator. For example, the following class of linear models of F has been widely studied and employed in practice:

$$\begin{aligned} F(x, \xi(\omega)) &= cx + \min_{y \geq 0} gy \\ \text{s.t. } Dy &= Bx + d \end{aligned} \quad (3.2)$$

where c , g , and d are known vectors, D and B are known matrices, and ξ is a random vector. In nature, this is a two-stage program which designs a system via x under system-

operating conditions known through a probability distribution on ξ . Then, y represents an operational recourse decision that is made after those operating conditions become known, i.e., after ξ is realized. The system design which is represented by x could involve continuous decisions such as the size of DGs, and discrete decisions such as the location of DGs, on/off status of capacitor banks, and tap positions of tap changers.

The expectation of F can be approximated using a sample of the random parameter $\xi(\omega)$, which is,

$$E[F(x, \xi(\omega))] \approx \frac{1}{N} \sum_{i=1}^N F(x, \xi^i) \quad (3.3)$$

where ξ^1, \dots, ξ^N is a sample of ξ . Most of the theory on sampling approximation for stochastic problems has been developed for independent and identically distributed random variables sampling. The identically distributed random variables sampling is also applied to this research.

Given an identically distributed random sample ξ^1, \dots, ξ^N of parameter $\xi(\omega)$, and the sample average approximation of equation (3.1) can be defined as

$$\min_{x \in X} \left\{ f_N(x) := \frac{1}{N} \sum_{i=1}^N F(x, \xi^i) \right\} \quad (3.4)$$

The basic idea of the sample average approximation is to approximate the true distribution of random variables with an empirical distribution by Monte Carlo sampling technology.

Assume v^* to be the optimal value of $f(x)$ and consider the set of ε -optimal solutions:

$$X^\varepsilon = \{x \in X : f(x) \leq v^* + \varepsilon\} \quad (3.5)$$

Let v_N be the optimal solution of a N-sample average approximation of $f(x)$, $f_N(x)$:

$$v_N = \min \left\{ f_N(x) = \frac{1}{N} \sum_{i=1}^N F(x, \xi^i) : x \in X \right\} \quad (3.6)$$

where ξ^1, \dots, ξ^N is a sample of ξ . Assume X_N^δ be the set of δ -optimal solution of $f_N(x)$:

$$X_N^\delta = \{x \in X : f_N(x) \leq v_N + \delta\} \quad (3.7)$$

To guarantee that the sample average approximation problem returns an ε -optimal solution to the true problem with probability at least $(1-\alpha)$, it is necessary to have

$$1 - |X| e^{-N\gamma(\delta, \varepsilon)} \geq 1 - \alpha \quad (3.8)$$

which means that N must satisfy

$$N \geq \frac{4\sigma_{\max}^2}{(\varepsilon - \delta)^2} \log \frac{|X|}{\alpha} \quad (3.9)$$

where σ_{\max}^2 represents the maximum variance. It can be seen from equation (3.9) that small changes in ε imply that N must be increased significantly. Similarly, the variance is also an important impact factor. The detailed proof of equations (3.8) and (3.9) can be found in [93].

3.3 Scenario Generation and Reduction

In the previous section, the general formulation and solution method of a stochastic problem have been discussed. In power system planning and operation, the uncertainties come from various aspects such as renewable and intermittent generation, load

consumption, electricity prices, customer behaviors, etc. This research considers two types of renewable DGs: wind turbines and photovoltaic generators. The predicted wind and solar power is used in the study. It is known that errors exist in prediction models. The normal distribution and beta distribution are used by previous papers to represent the wind power prediction errors. It has been shown that the beta function is more appropriate than the standard normal distribution in representing prediction errors of wind power [16]. The prediction errors of solar power are still under study. In [16], the beta function has also been used in representing the prediction errors of solar power. In Chapter 4, the dispatches of voltage/VAR control devices are calculated based on predicted DG outputs. Each time slot corresponds to two beta functions for prediction errors: one for wind power and the other for solar power. Similarly, beta functions are also used to represent uncertainties of predictions of wind and solar power when solving the stochastic DG allocation problem. For a predicted power P^{pred} , the beta function can be defined by two corresponding parameters α and β [16]:

$$f(x) = x^{\alpha-1}(1-x)^{\beta-1} \quad (3.10)$$

The above beta function models the occurrence of real power values x when a certain prediction value P^{pred} has been forecasted. Shape parameters α and β can be calculated as

$$\frac{P^{pred}}{S_{base}} = \frac{\alpha}{\alpha + \beta} \quad (3.11)$$

$$\sigma^2 = \frac{\alpha\beta}{(\alpha + \beta)^2(\alpha + \beta + 1)} \quad (3.12)$$

where S_{base} is the power base for the system, is maximum, σ is the error variance and can be represented as

$$\sigma = 0.2 \times \frac{P^{pred}}{P^{cap}} + 0.21 \quad (3.13)$$

where P^{cap} is the maximum power output. Using the predicted DG outputs and the equations (3.11)-(3.13), the parameters of beta functions for the current prediction horizon can be calculated. A normal distribution is frequently used to represent the forecasting uncertainty of load consumptions. Monte-Carlo simulation (MCs) is run based on forecasted power and uncertain prediction errors to generate scenarios for DG outputs and load consumptions.

In order to reduce the computation efforts, a scenario reduction technique is implemented to reduce the number of scenarios while maintaining a good approximation of the system uncertainty. In this dissertation, the simultaneous backward reduction method [94] is used for scenario reduction. Let τ_s ($s=1, \dots, N$) denote N different scenarios, each with a probability of ρ_s , a distance function $d(\tau_s, \tau_{s'})$ can be defined for the scenario pair $(\tau_s, \tau_{s'})$:

$$d(\tau_s, \tau_{s'}) := \max\{1, \|\tau_s - \bar{\tau}\|, \|\tau_{s'} - \bar{\tau}\|\} \|\tau_s - \tau_{s'}\| \quad (3.14)$$

where $\bar{\tau}$ is the average value of scenarios. Denote S as the initial set of scenarios (N initial elements) and J (initially null) as the set of scenarios to be deleted. Assume there are N scenarios and it is necessary to reduce them into n scenarios. The steps can be summarized as follows:

Step 1: compute the distances of all scenario pairs $d_{s,s'} = d(\tau_s, \tau_{s'})$ ($s, s' = 1, \dots, N$). For each scenario l , $\phi_l^{[1]} := \min_{j \neq l} d_{l,j}$ ($j = 1, \dots, N$), let $l_1 \in \arg \min_{l \in \{1, \dots, N\}} \rho_l \phi_l^{[1]}$, the first element of J , $J^{[1]} = \{l_1\}$ can be obtained and S is updated by $S^{[1]} = S / \{l_1\}$.

Step i (i>1) : for each scenario $l, l \in S^{[i-1]}$, compute $\phi_{kl}^{[i]} := \min_{k' \in J^{[i-1]} \cup \{l\}} d_{k,k'}, k \in J^{[i-1]} \cup \{l\}$, then compute $z_l^{[i]} := \sum_{k \in J^{[i-1]} \cup \{l\}} \rho_k \phi_{kl}^{[i]}$, let $l_i \in \arg \min z_l^{[i]}$, update J and S by $J^{[i]} = J^{[i-1]} \cup \{l_i\}$, $S^i = S^{i-1} / \{l_i\}$, repeat this step for N-n times.

Step N-n+1: after obtaining the final J set (with N elements) and the S set (with n elements), for the each remaining scenario $s \in S$, its new probability ρ'_s can be calculated as:

$$\rho'_s = \rho_s + \sum_{j \in J_j} \rho_j \quad (3.15)$$

where J_j can be calculated as follows: for each $j \in J$, $J_j = \{\psi \mid \psi \in \arg \min_{h \in J} d(\tau_h, \tau_j)\}$.

The number of scenarios can be reduced from N to n through the above procedures.

3.4 Multiple Replication Procedure

It is important to assess whether a candidate solution of an optimization problem is an optimal or near-optimal solution. Karush-Kuhn-Tucker conditions [79] provide necessary and sufficient optimality conditions for certain problems. However, the function values and gradients needed to test these conditions for a stochastic program are challenging to compute. An alternative approach in stochastic programming is to use Monte Carlo sampling-based estimators to assess the optimality gap. Multiple replication procedure is a kind of these Monte Carlo sampling-based methods.

Let x^* denote an optimal solution of the stochastic program defined in (3.1), and z^* denote the corresponding optimal value. Let x_n^* denote an optimal solution of the problem defined in (3.4) through a sampling procedure, and z_n^* denote the corresponding optimal value. In solving the original problem defined in (3.1), a decision x that hedges against all realizations of ξ can be obtained. When solving the problem defined in (3.4) by the sample average approximation, the problem is optimized with respect to a subset of ξ , which means that the original problem is over-optimized. Therefore, z_n^* gives a lower bound of the optimal solution value z^* .

In a multiple replication procedure [95], the quality of a candidate solution \hat{x} , e.g., $\hat{x} = x_n^*$, can be measured by the optimality gap, $\mu_{\hat{x}} = Ef(\hat{x}, \xi) - z^*$. If the gap is sufficiently small, then \hat{x} is of high quality. An upper bound on the optimality gap for \hat{x} is given by $Ef(\hat{x}, \xi) - Ez_n^*$, because $Ez_n^* < z^*$. This quantity can be estimated by [95]

$$G_n(\hat{x}) = \frac{1}{n} \sum_{j=1}^n F(\hat{x}, \xi^j) - \min_{x \in X} \frac{1}{n} \sum_{j=1}^n F(x, \xi^j) \quad (3.16)$$

where ξ^1, \dots, ξ^N are i.i.d. from the distribution of ξ . A multiple replications procedure can be used to construct a confidence interval (CI) of the form

$$P(EF(\hat{x}, \xi) - z^* \leq \varepsilon) \approx 1 - \alpha \quad (3.17)$$

where $\hat{x} \in X$ is a candidate solution, $EF(\hat{x}, \xi)$ is its true and unknown expected performance measure, ε is the random CI width, and $1 - \alpha$ is the confidence level, e.g., 0.95. Let $t_{n, \alpha}$ be the $1 - \alpha$ quantile of the t distribution with n degrees of freedom, and, let

z_α be that of the standard normal. The multiple replication procedure can be summarized as follows [95]:

1. For $k=1,2,\dots,n_g$

1.1 Sample i.i.d. observations $\xi^{k1}, \xi^{k2}, \dots, \xi^{kn}$ from the distribution of ξ .

1.2 Apply sample average approximation to solve the stochastic program using $\xi^{k1}, \xi^{k2}, \dots, \xi^{kn}$ to obtain x_n^{k*} .

1.3 Calculate $G_n^k(\hat{x}) = \frac{1}{n} \sum_{j=1}^n (F(\hat{x}, \xi^{kj}) - F(x_n^{k*}, \xi^{kj}))$.

2. Calculate gap estimate and sample variance by

$$\bar{G}_n(n_g) = \frac{1}{n_g} \sum_{k=1}^{n_g} G_n^k(\hat{x}) \quad (3.18)$$

$$s_G^2(n_g) = \frac{1}{n_g - 1} \sum_{k=1}^{n_g} (G_n^k(\hat{x}) - \bar{G}_n(n_g))^2 \quad (3.19)$$

3. Let $\varepsilon_g = t_{n_g-1, \alpha} s_G(n_g) / \sqrt{n_g}$, and output the one-sided CI on $\mu_{\hat{x}}$,

$$\left[0, \bar{G}_n(n_g) + \varepsilon_g \right] \quad (3.20)$$

It can be seen that step 1 produces n_g i.i.d. replicates and step 2 forms the resulting sample mean $\bar{G}_n(n_g)$ and sample variance $s_G^2(n_g)$.

3.5 Summary

This chapter introduces the general formulation of stochastic programs and the sample average approximation method to solve the problems. Since wind turbines and solar panels are considered as renewable DGs in the following chapters, a method to generate scenarios to represent prediction errors of wind power and solar power has been

presented. A backward scenario reduction technique is applied to enhance a tradeoff between the accuracy of the solution and the computational burden. This chapter also discusses a multiple replication procedure to quantify the optimality of solutions obtained from sample average approximation.

In the next chapter, the sample average approximation is used to solve the stochastic voltage/VAR control and the DG allocation problems. Scenario generation and reduction are used to simulate the output of wind turbines and photovoltaic generators. Multiple replication procedure is applied to evaluate the optimality of the solutions.

CHAPTER 4 IMPLEMENTATION OF VOLTAGE/VAR CONTROL IN DISTRIBUTION GRIDS

4.1 Overview

Voltage/VAR control can be implemented by a utility to improve the operation of distribution grids. The ever-increasing penetration of renewable DGs and the complicated load behaviors make the voltage/VAR control problems more challenging. A modern voltage/VAR control framework should consider the stochasticity on both the generation and demand sides. The uncertain outputs of renewable DGs and load consumptions will impact the voltage/VAR control of a distribution grid. However, if well planned, the integration of DGs can also assist the implementation of voltage/VAR control and improve the system operation. In this chapter, a rolling horizon optimization-based method for the optimal dispatches of on-load tap changer and capacitor banks is proposed. The stochasticity of DG outputs and load consumption is taken into account by a bi-level stochastic formulation. The various load-to-voltage sensitivities for different types of customers are considered. This chapter also proposes a novel stochastic model for DG placement to assist the implementation of voltage/VAR control. The model is solved and verified by a method combining sample average approximation and multiple replication procedure.

Section 4.2 gives the general models for a distribution grid and loads, section 4.3 introduces the rolling horizon optimization and the stochastic voltage/VAR control model, section 4.4 gives the simulation results for the voltage/VAR control, section 4.5 presents the stochastic model for DG placement and the combined sample average approximation

and multiple replication procedure, and section 4.6 provides the simulation and validation results for DG placement.

4.2 Models for Distribution Grids and Loads

Consider a distribution system as shown in Fig. 4.1 which includes m buses indexed by $i = 0, 1, \dots, m$.

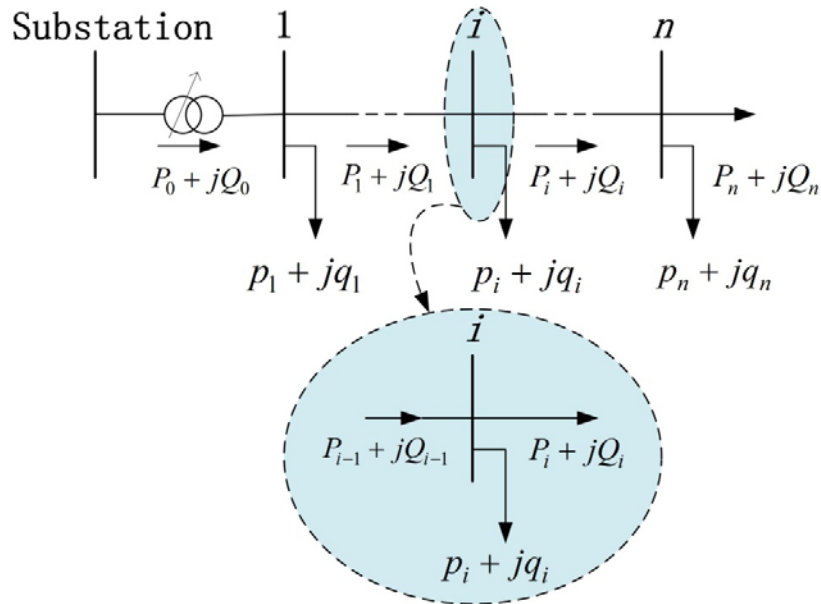


Figure 4.1. Schematic diagram of a radial distribution grid.

The following equations can be used to describe the complex power flows at each node i , which are known as DistFlow equations [48, 96]:

$$P_{i+1} = P_i - r_i \frac{P_i^2 + Q_i^2}{V_i^2} - p_{i+1} \quad (4.1)$$

$$Q_{i+1} = Q_i - x_i \frac{P_i^2 + Q_i^2}{V_i^2} - q_{i+1} \quad (4.2)$$

$$V_{i+1}^2 = V_i^2 - 2(r_i P_i + x_i Q_i) + (r_i^2 + x_i^2) \frac{P_i^2 + Q_i^2}{V_i^2} \quad (4.3)$$

$$P_{i+1} = P_{i+1}^l - P_{i+1}^g, \quad Q_{i+1} = Q_{i+1}^l - Q_{i+1}^g \quad (4.4)$$

where P_i and Q_i are the active and reactive power flow between nodes i and $i+1$, respectively; V_i is the voltage at node i ; r_i and x_i are the line resistance and reactance between nodes i and $i+1$, respectively; p_i and q_i are the active and reactive power consumption at node i , respectively; p_i^g is generated by DGs, which is subject to uncertainties and q_i^g is generated by VAR compensation devices such as capacitor banks; p_i^l and q_i^l are the active and reactive power consumption at node i , respectively.

The DistFlow equations are effective for radial networks. For a meshed network, it can be converted to a radial network by breaking the loops through adding dummy buses [97]. The DistFlow equations can be simplified using linearization. The linearized power flow equations have been extensively used and justified in the literature [96].

$$P_{i+1} = P_i - p_{i+1} \quad (4.5)$$

$$Q_{i+1} = Q_i - q_{i+1} \quad (4.6)$$

$$V_{i+1} = V_i - \frac{r_i P_i + x_i Q_i}{V_0^2} \quad (4.7)$$

$$P_{i+1} = P_{i+1}^l - P_{i+1}^g, \quad Q_{i+1} = Q_{i+1}^l - Q_{i+1}^g \quad (4.8)$$

Many load models have been developed in the past, among which, exponential load model is widely used to represent load-to-voltage relationship [3]. The exponential load model is defined as

$$p_i^l = P_i^b V_i^{k_{pi}} \quad (4.9)$$

$$q_i^l = Q_i^b V_i^{k_{qi}} \quad (4.10)$$

where P_i^b and Q_i^b are the basic active and reactive power for the exponential load model, respectively; k_{pi} and k_{qi} are the active power exponent and reactive power exponent for the exponential load model, respectively.

In the constant-power load model, k_{pi} and k_{qi} are assumed to be zero. In fact, the exponents k_{pi} and k_{qi} are related with load compositions. Table 4.1 shows the example exponent values for different types of loads [3], which are used in this dissertation for illustration. In practice, a feeder is not explicitly residential, commercial or industrial [45]. Thus, a load class mix should be implemented.

Table 4.1. Load types and exponent values.

Load Type	k_p	k_q
Residential	1.04	4.19
Commercial	1.50	3.15
Industrial	0.18	6.00

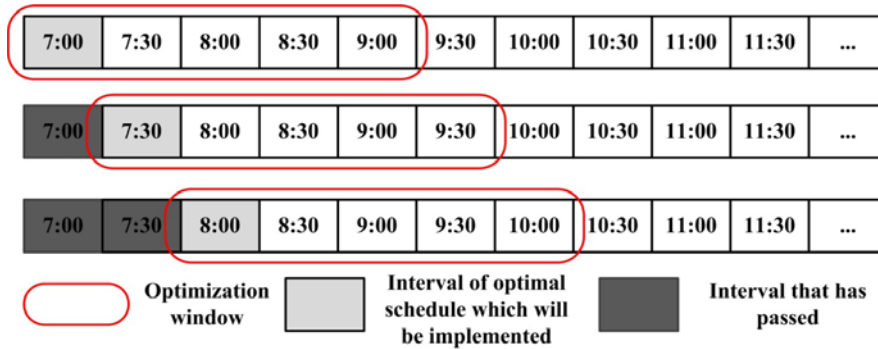


Figure 4.2. Demonstration of rolling-horizon optimization.

4.3 Stochastic Rolling Horizon Optimization-Based Voltage/VAR

Control

This section presents the rolling horizon optimization method [86, 87] and the proposed mathematical formulation of the stochastic voltage/VAR control.

4.3.1 Rolling Horizon Optimization

In analogy to model predictive control [98, 99], a rolling-horizon optimization is employed to make optimal operation decisions [100, 101]. Fig. 4.2 is an illustration of the rolling-horizon optimization. An optimization problem is formulated and solved to obtain optimal decisions over the optimization window. However, only the decisions for the first time interval in the window are implemented in practice. The solutions for other time intervals will be discarded. The above process is repeated. It is assumed that a prediction algorithm generates estimated load consumption and DG outputs. In practice, the prediction errors should be considered. The details on prediction errors have been discussed in Chapter 3.

4.3.2 Mathematical Formulation for Stochastic Voltage/VAR Control

This subsection proposes a new formulation for voltage/VAR control in a distribution grid with renewable DGs and voltage-sensitive loads. Consider using power losses of the distribution system and voltage deviations along the feeder as control objectives, the multi-objective voltage/VAR control problem for a certain control period can be formulated as follows, Table 4.2 shows the nomenclature:

Table 4.2. Nomenclature for stochastic voltage/VAR control formulation.

$P_{t,s}^{loss}$	Active system loss at time t in s th scenario	$\Delta V_{t,s}$	Maximum voltage deviation at time t in s th scenario
------------------	---	------------------	--

$V_{i,t,s}$	Voltage at node i at time t in s th scenario	k_{pi} / k_{qi}	Active/reactive power exponent at node i in s th scenario
$P_{i,t,s} / Q_{i,t,s}$	Active/reactive power flow from node i to node i+1 at time t in s th scenario	r_i / x_i	Line resistance/reactance between node i and i+1
$P_{i,t,s}^l / Q_{i,t,s}^l$	Active/reactive load at node i at time t in s th scenario	$P_{i,t,s}^g / Q_{i,t,s}^g$	Active/reactive power output of the P at node I at time t in s th scenario
$P_{i,t}^{pred}$	Predict output of the DG at node i at time t	$\omega_{i,t,s}$	Prediction error at node i at time t in scenario s
Q_i^{cap}	Size of the capacitor at node i	$C_{i,t}$	Binary indicator of the switch status of the capacitor at node i at time t
V_r	Input voltage of the regulator	\mathcal{E}	Max. allowable voltage deviation
TAP_t	Tap position at time t	CAP^{\max} / TAP^{\max}	Max. number of tap operations/capacitor switch times during time t to time t+Tp

$$\min E \left[\sum_{t=t_k}^{t_k+T_p} (P_{t,s}^{loss} + \Delta V_{t,s}) \right], \quad (4.11)$$

Subject to

$$\Delta V_{t,s} = \max_i \{ \Delta V_{i,t,s} \}, \Delta V_{i,t,s} = |V_{i,t,s} - V_{1,t,s}|, \forall i, t, s, \quad (4.12)$$

$$P_{t,s}^{loss} = \sum_i r_i (P_{i,t,s}^2 + Q_{i,t,s}^2) / V_1, \forall t, s, \quad (4.13)$$

$$P_{i+1,t,s} = P_{i,t,s} - p_{i+1,t,s}^l + p_{i+1,t,s}^g, \forall i, t, s, \quad (4.14)$$

$$Q_{i+1,t,s} = Q_{i,t,s} - q_{i+1,t,s}^l + q_{i+1,t,s}^g, \forall i, t, s, \quad (4.15)$$

$$V_{i+1,t,s} = V_{i,t,s} - (r_i P_{i,t,s} + x_i Q_{i,t,s}) / V_1, \forall i, t, s, \quad (4.16)$$

$$p_{i,t,s}^g = P_{i,t}^{pred} + \omega_{i,t,s}, \forall i, t, s, \quad (4.17)$$

$$q_{i,t,s}^g = c_{i,t} Q_i^{cap}, \forall i, t, \quad (4.18)$$

$$V_{1,t} = TAP_t V_s, \forall t \quad (4.19)$$

$$p_{i,t,s}^l = (P_{i,t}^{b,pred} + \omega_{i,t,s}) V_{i,t,s}^{k_{pi}}, \forall i, t, s, \quad (4.20)$$

$$q_{i,t,s}^l = (Q_{i,t}^{b,pred} + \omega_{i,t,s}) V_{i,t,s}^{k_{qi}}, \forall i, t, s, \quad (4.21)$$

$$1 - \varepsilon \leq V_{i,t,s} \leq 1 + \varepsilon, \forall i, t, s, \quad (4.22)$$

$$\sum_{t=t_k}^{t_k+T_p} |c_{i,t+t_{k+1}-t_k} - c_{i,t}| \leq CAP^{\max}, \quad (4.23)$$

$$\sum_{t=t_k}^{t_k+T_p} |TAP_{t+t_{k+1}-t_k} - TAP_t| \leq TAP^{\max}. \quad (4.24)$$

In the above formulation, the objective function (4.11) minimizes the expectation of active power losses and voltage deviations along the feeder during the prediction horizon. For illustration, this study assumes that the two objectives are equally weighted. However, the distribution system operators can change the weighting factors (priorities) according to the specific operational requirements. Equation (4.12) represents the maximum voltage deviation of all nodes. Equation (4.13) describes active power losses of the distribution network. Equations (4.14)-(4.16) are the linear form of the DistFlow equations defined in (4.5)-(4.8), which have been extensively verified and used in the literature. The linearization is based on the fact that the nonlinear terms in (4.1)-(4.4) are much smaller than the linear terms. The outputs of DG units and capacitors are represented as negative loads in constraints (4.14)-(4.15). Equation (4.17) assumes outputs of DG units equal the predicted values plus the predicted errors ω . ω belongs to an uncertainty set, which may vary with predicted values and will be discussed in next section. In constraint (4.18), $c_{i,t}$ represents the on/off status of the capacitor at node i during the time interval t . For nodes without capacitors, Q_i^{cap} equals zero. In constraint (4.19), V_s represents the primary voltage of the transformer at the substation, which is assumed to be 1.0 p.u. in

this paper. The secondary voltage is modeled as a function of the primary voltage [15, 36]. The detailed model can be found in [15]. Voltage regulators are voltage control devices often used on long lines and can participate in voltage/VAR control. A single-phase voltage regulator with an open-delta configuration, 32 taps ($[-16, \dots, +16]$) and $\pm 10\%$ tap range can be modeled as follows [15]:

$$V_{i,t} = V_r \sqrt{1 + 3(TAP_{i,t} / 16) + 3(TAP_{i,t} / 16)^2} \quad (4.25)$$

where V_r is the input voltage of the VR, $TAP_{i,t}$ represents the tap position of the VR of node i at time t . Equation (4.25) can be integrated into the voltage/VAR control formulation when voltage regulators exist in the distribution system.

Constraints (4.20) and (4.21) use the exponential load model to represent active and reactive load consumptions. $P_{i,t}^{b,pred}$ and $Q_{i,t}^{b,pred}$ change with a load profile which can be obtained by using short-term load forecasting techniques. Constraint (4.22) indicates the voltage of each node should be within a certain range for proper operation of the distribution circuit, ε is usually set to be 0.05. Constraints (4.23) and (4.24) describe the maximum number of daily switching operations of load tap changers and capacitors, respectively. In some practical cases, a bank of capacitors may be installed at node i . Then, the discrete output of the capacitor bank at node i can be represented as equation (4.18) and constraint (4.23) can be modified accordingly as shown in equations (4.26) and (4.27).

$$q_{i,t}^g = \sum_k c_{ik,t} Q_{ik}^{cap} \quad (4.26)$$

$$\sum_{t=t_k}^{t_k+T_p} |c_{ik,t+t_k+1-t_k} - c_{ik,t}| \leq CAP^{\max} \quad (4.27)$$

where c_{ik} is a binary indicator of the switch status of the k-th capacitor in the capacitor bank at node i and Q_{ik}^{cap} represents the size of the k-th capacitor in the capacitor bank at node i . This study considers the case that one capacitor is installed at one node. However, it is clear that the proposed method can be applied to solve the voltage/VAR control problem with capacitor banks. The maximum number of daily switching operations of on-load tap changer and capacitors should be less than the predefined values. For illustration, CAP^{max} is set to be 3 and TAP^{max} is set to be 5 in this paper. The DSOs can change these settings according to the characteristics of a specific system. To further reduce the non-linearity of the above problem, some constraints can be reformulated. Equation (4.12) can be reformulated as follows:

$$\lambda_{t,s} \geq V_{1,t,s} - V_{i,t,s}, \forall i, t, s \quad (4.28)$$

$$\lambda_{t,s} \geq V_{i,t,s} - V_{1,t,s}, \forall i, t, s \quad (4.29)$$

In constraint (4.23), assume that $s_{i,t} = (c_{i,t+t_{k+1}-t_k} - c_{i,t})^2$, since $c_{i,t}$ is a binary, $c_{i,t}^2 = c_{i,t}$,

$$s_{i,t} = c_{i,t+t_{k+1}-t_k} + c_{i,t} - 2c_{i,t+t_{k+1}-t_k}c_{i,t} \quad (4.30)$$

where $s_{i,t}$ indicates whether the capacitor at node i has changed its status from time t_k to time t_{k+1} ($s_{i,t} = 1$, if the status has changed).

To linearize the multiplication of $c_{i,t+t_{k+1}-t_k}c_{i,t}$, it is assumed that $a_{i,t} = c_{i,t+t_{k+1}-t_k}c_{i,t}$, and $a_{i,t}$ is a binary. Equation (4.23) can be represented as (4.31)-(4.34).

$$s_{i,t} = c_{i,t+t_{k+1}-t_k} + c_{i,t} - 2a_{i,t} \quad (4.31)$$

$$a_{i,t} \leq c_{i,t} \quad (4.32)$$

$$a_{i,t} \leq c_{i,t+t_{k+1}-t_k} \quad (4.33)$$

$$a_{i,t} \geq c_{i,t} + c_{i,t+t_{k+1}-t_k} - 1 \quad (4.34)$$

Table 4.3. The relationship among s, a and c.

$s_{i,t}$	$a_{i,t}$	$c_{i,t+t_{k+1}-t_k}$	$c_{i,t}$
0	0	0	0
0	1	1	1
1	0	0	1
1	0	1	0

In constraints (4.24), TAP_t is an integer whose range is dependent on the number of taps of the load tap changer. Equation (4.24) can be reformulated as follows:

$$\varphi_t \geq TAP_{t+t_{k+1}-t_k} - TAP_t \quad (4.35)$$

$$\varphi_t \geq TAP_t - TAP_{t+t_{k+1}-t_k} \quad (4.36)$$

$$\sum_{t=t_k}^{t_k+T_p} \varphi_t \leq TAP^{\max} \quad (4.37)$$

The stochastic optimization problem can be represented as follows:

$$\begin{aligned} \min E \left[\sum_{t=t_k}^{t_k+T_p} (P_{t,s}^{loss} + \Delta V_{t,s}) \right] \\ \text{s.t. (4.13) - (4.22), (4.28) - (4.29), (4.31) - (4.37)} \end{aligned} \quad (4.38)$$

To solve the formulation defined in (4.38), Monte-Carlo simulations [81] are used to generate scenarios to represent the prediction errors of wind power, solar power and load

consumption. The number of scenarios can be reduced from N to n through the simultaneous backward scenario reduction method as described in Chapter 3. The problem defined in (4.38) can be reformulated using the reduced scenarios as follows:

$$\begin{aligned} \min \sum_{s=1}^n \rho'_s [\sum_{t=t_k}^{t_k+T_p} (P_{t,s}^{loss} + \Delta V_{t,s})] \\ \text{s.t. (4.13) - (4.22), (4.28) - (4.29), (4.31) - (4.37)} \end{aligned} \quad (4.39)$$

The problem is a mix-integer non-linear programming problem, which can be solved by the general algebraic modeling system [102]. The above formulation schedules the dispatches of voltage/VAR control devices for the current prediction horizon based on predicted DG outputs so as to minimize active power losses and voltage deviations. The process is repeated when new observations come at t_{k+1} . DG outputs can be predicted by regression-based methods or machine learning-based techniques, which are beyond the contents of this paper. The comprehensive procedure for rolling horizon optimization-based voltage/VAR control can be summarized as follows (start from $t = t_k$):

Step 1: Predict DG outputs for the time period $[t, t + T_p]$;

Step 2: Calculate corresponding beta functions for the predicted DG outputs; obtain N scenarios of prediction errors using Monte-Carlo simulations; reduce the number of scenarios to n ;

Step 3: Solve the mixed-integer nonlinear problem in (4.39) and obtain the voltage/VAR control schedule for the time period $[t, t + T_p]$;

Step 4: Implement the voltage/VAR control schedule for the time period $[t, t + t_{k+1} - t_k]$. When $t = t_k + t_{k+1} - t_k = t_{k+1}$, go to step 1.

It is necessary to show how much improvement can be achieved if the stochastic prediction errors are taken into account in model predictive control. Define the solution of (4.38) as \hat{x} . For the problem defined in (4.39), the corresponding expected value problem can be formulated by replacing the random error ω by its expected value. The expected value problem is a deterministic optimization problem that can be defined as

$$\text{EV} = \min \sum_{t=t_k}^{t_k+T_p} (P_{t,s}^{\text{loss}}(\bar{\omega}_t) + \Delta V_{t,s}(\bar{\omega}_t)) \quad (4.40)$$

where $\bar{\omega}_t = E(\omega_t)$ denotes the expectation of ω_t . The expected value solution can be defined as \bar{x} . The expected results of using the expected value solution can be represented as

$$\text{EEV} = \frac{1}{N'} \sum_{h=1}^{N'} (P_{t,s}^{\text{loss}}(\bar{\omega}_t) + \Delta V_{t,s}(\bar{\omega}_t)) \quad (4.41)$$

The expected results of using the expected value solution measures the performance of \bar{x} , allowing second-stage decision variables to be chosen optimally as functions of \bar{x} and ω . The N' scenarios of prediction errors are generated by Monte-Carlo simulations. The expected results of using the expected value solution and the objective value of (4.39) can be compared to see how the stochastic programming outperforms the deterministic programming.

4.3.3 Simulation Results

For illustration, the proposed method has been examined on the modified IEEE 33-bus radial distribution network as shown in Fig. 4.3. Details about the test system can be found in [96].

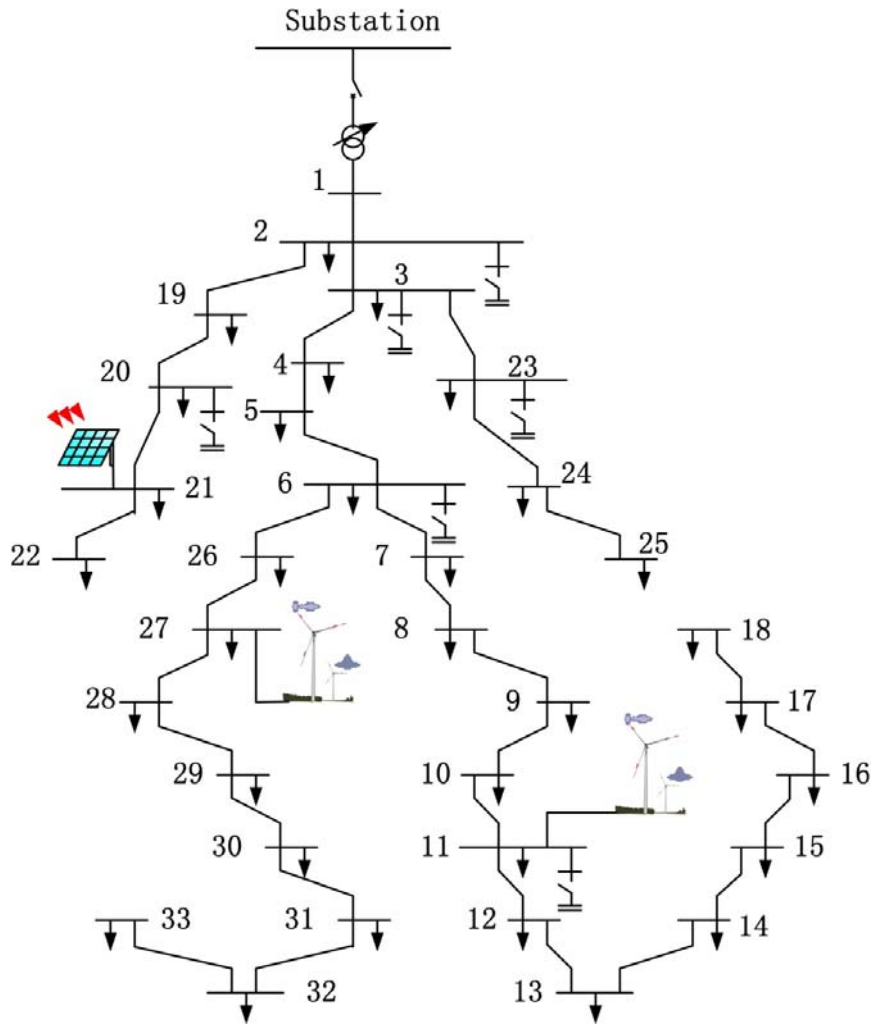


Figure 4.3. Test distribution system [82].

Assume the substation transformer has a $\pm 10\%$ tap range. Switched capacitors are installed at nodes 2, 3, 6, 11, 21 and 23, each is 30 kVAR. Photovoltaic generators are installed at node 21, wind turbines are located at nodes 11 and 27. The node types are listed in Table 4.4. This example sets T_p to be 6 hours, $t_{k+1} - t_k$ to be 15 minutes. For every 15 minutes, the DG outputs and load consumptions are predicted for the next 6 hours and the control decisions are made.

Table 4.4. Node types for stochastic voltage/VAR control simulations.

Type	Residential	Commercial	Industrial
Node number	2, 3, 4, 5, 6, 7, 8, 9, 12, 13, 14, 15, 26, 28, 29	10, 11, 16, 17, 19, 20, 21, 22, 27, 30, 33	18, 23, 24, 25, 31, 32

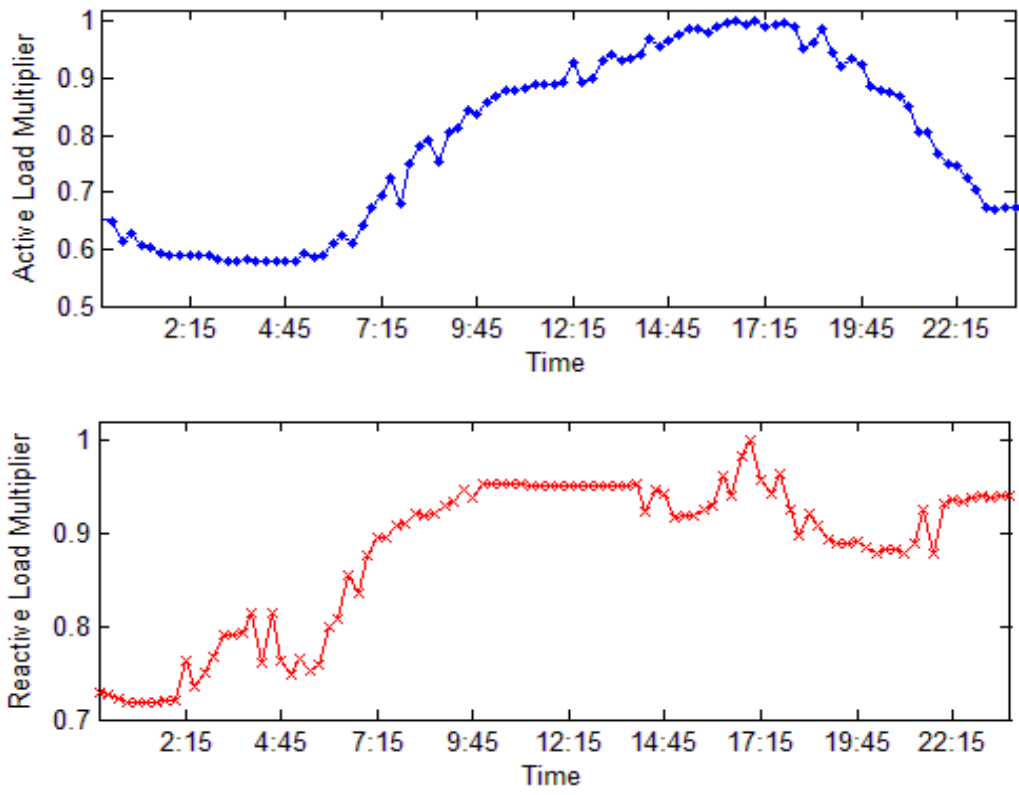


Figure 4.4. Profiles of active and reactive load multipliers.

All loads are represented by exponential load models and the load consumption of node i at time t can be represented as:

$$p_{i,t}^l = P_i^b M_t^p V_{i,t}^{k_{pi}} \quad (4.42)$$

$$q_{i,t}^l = Q_i^b M_t^q V_{i,t}^{k_{q_i}} \quad (4.43)$$

The values of basic components P_i^b and Q_i^b can be found in [96], the exponents of each type of load are shown in Table 4.5. The multipliers M_t^p and M_t^q , as shown in Fig. 4.4, are used to make the load profile change with time. It is assumed that multipliers of all nodes are the same. Fig. 4.5 shows the normalized predicted wind and solar power that is used in this study [103]. The power base of the system S_{base} is set to be 1 MVA.

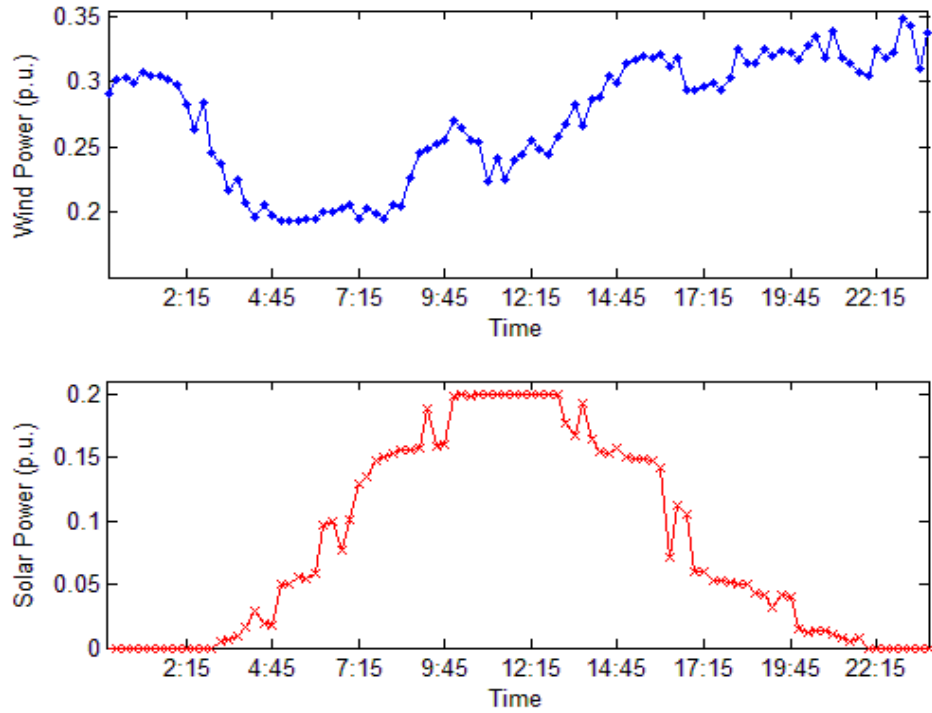


Figure 4.5. Profiles of solar power and wind power.

As introduced in section 3.3, a beta distribution is used to represent the prediction errors of wind/solar power, and the normal distribution is used to represent the prediction errors of the load consumption [16]. For the load profiles in Fig. 4.4, the mean value of

the normal distribution is the forecasted load and the standard deviation is set to 2% of the forecasted value [104]. Each time slot in Fig. 4.5 corresponds to two beta functions for prediction errors: one for wind power and the other for solar power. For a predicted power point P^{pred} , the beta function can be defined by two corresponding parameters α and β ; they can be calculated using (3.11-3.13) and the present predicted wind/solar power.

Different scenarios of prediction errors of DG generation and load consumption can be generated by using the beta and normal distributions. 100 scenarios (N=100) are generated using Monte-Carlo simulations to represent the prediction errors in the prediction horizon. As discussed in the previous section, scenario reduction is applied to reduce the computation efforts while maintaining the solution accuracy. The 100 generated scenarios are reduced to 15 scenarios (n=15) in this case. The above procedure is repeated for the whole day.

The proposed formulation in (4.39) is a mixed-integer nonlinear and nonconvex problem. Therefore, it cannot be solved directly by CPLEX. In this simulation, the Discrete and Continuous Optimizer (DICOPT) in the General Algebraic Modeling System (GAMS) is used to solve the problem. The simulation is performed by using a computer with Intel Quad Core 2.40 GHz and 8 GB memory. The computation time for the stochastic program with 15 scenarios is around 5 minutes.

The stochastic voltage/VAR control problem defined in (4.39) is solved with the 15 scenarios for every prediction horizon. Fig. 4.6 shows the resulting daily dispatch of on-load tap changer's tap positions, in which, "Tap EXL" refers to tap positions with exponential load model and "Tap CP" refers to tap positions with the constant-power

model. It can be seen that the optimal taps of on-load tap changer are quite different for exponential load model and the constant-power model. Since the proposed formulation is a mixed-integer non-linear program, a global optimum cannot be guaranteed. The following messages from GAMS indicate that there is no mathematical error in the proposed formulation, and the solution of the problem could be one of the local optimal solutions.

GAMS Message:

```

“REPORT SUMMARY:      0  NONOPT
                      0  INFEASIBLE
                      0  UNBOUNDED
                      0  ERRORS”

```

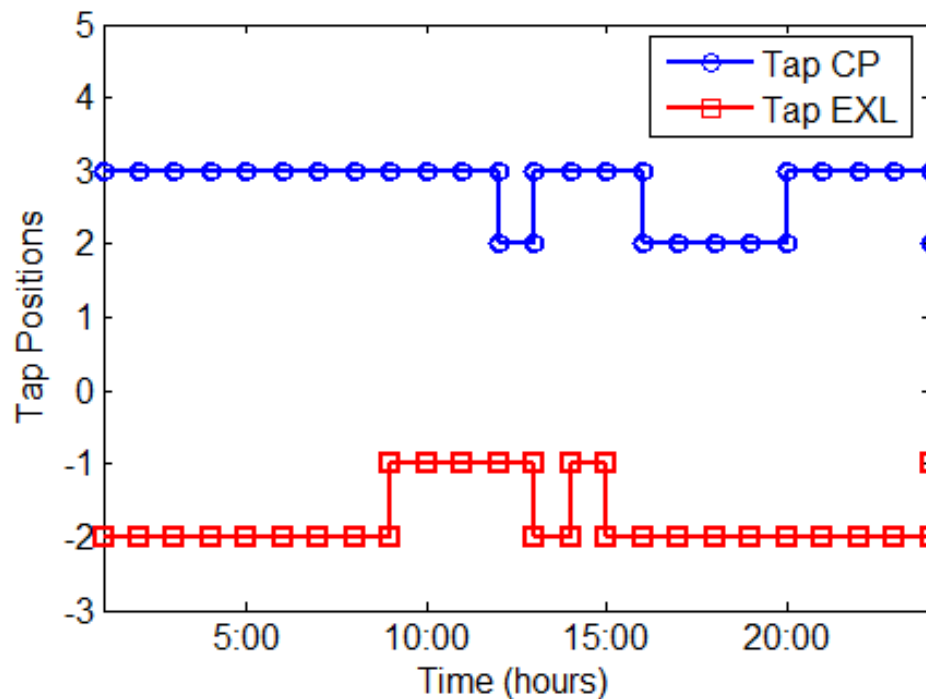


Figure 4.6. Tap positions with exponential model (Tap EXL) and constant power model (Tap CP).

Figs. 4.7-4.9 show the switch statuses of capacitors, where “EXL” represents the results with the exponential load model, “CP” represents the results with the constant-power load model. It can be seen that daily dispatches of most capacitors change with different load models (capacitor at node 3 does not change).

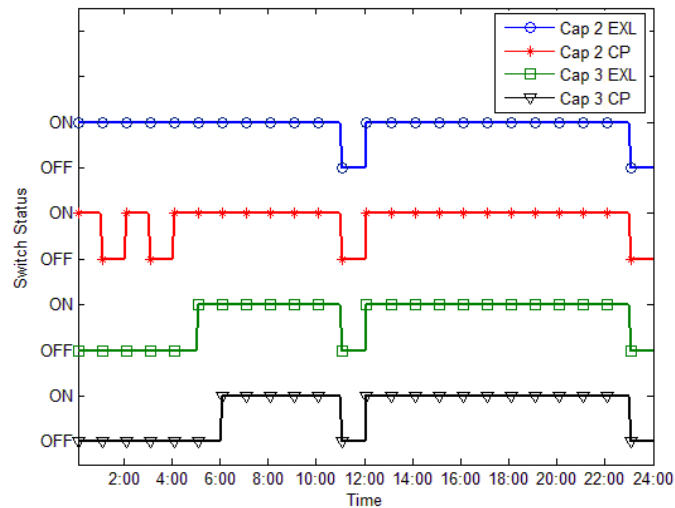


Figure 4.7. Switch status of capacitors at nodes 2 and 3 with exponential model (Cap EXL) and constant power model (CAP CP).

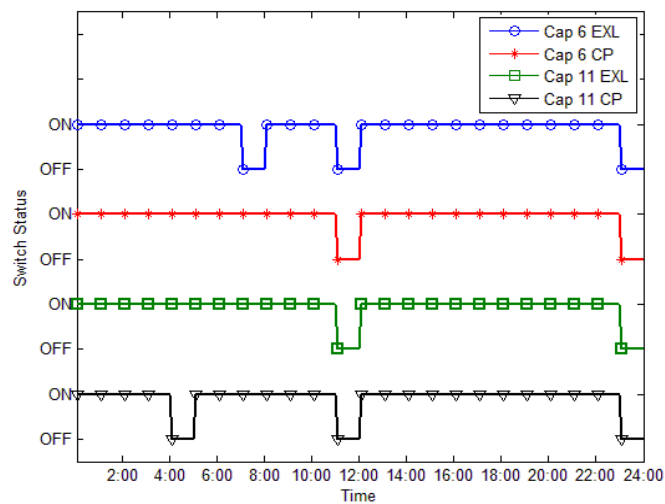


Figure 4.8. Switch status of capacitors at nodes 6 and 11 with exponential model (Cap EXL) and constant power model (CAP CP).

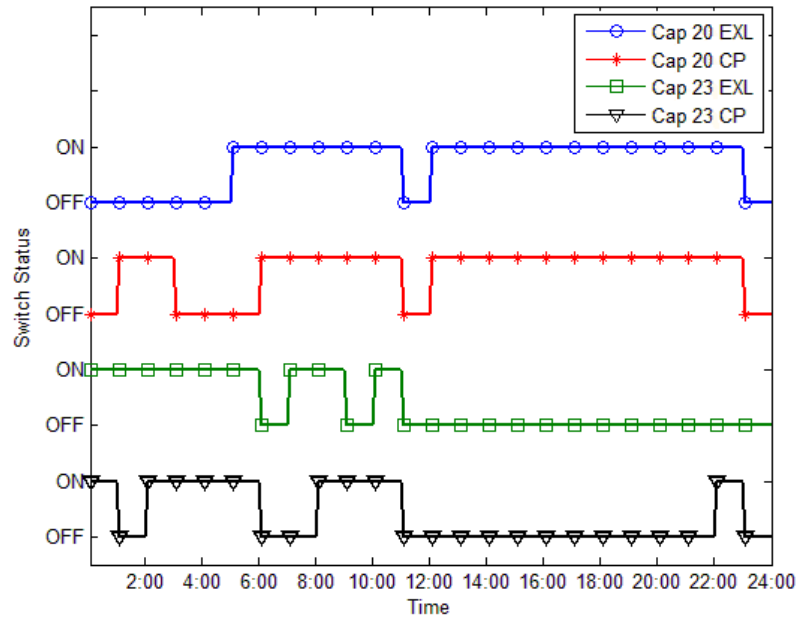


Figure 4.9. Switch status of capacitors at nodes 20 and 23 with exponential model (CAP EXL) and constant power model (CAP CP).

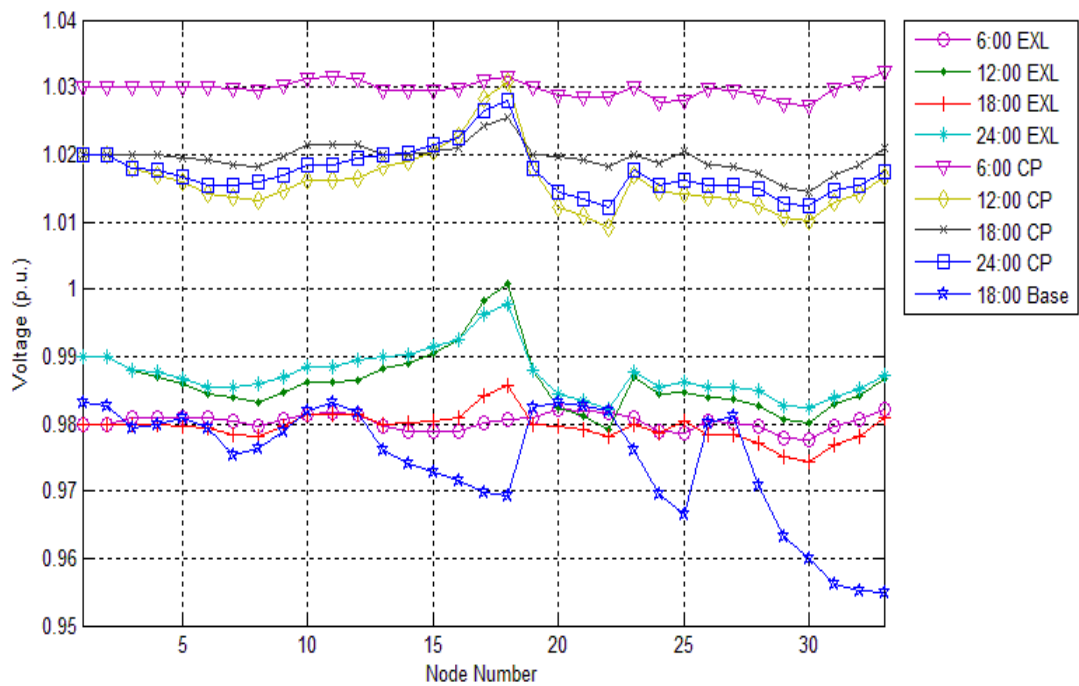


Figure 4.10. Voltage profiles.

Fig. 4.10 shows the voltages of all nodes. Voltage levels at 6:00, 12:00, 18:00 and 24:00 are selected to be shown due to the space limit. “EXL” represents the voltages with the exponential load model, “CP” represents the voltages with the constant-power load model and “Base” represents the voltages with DGs and exponential load model, but without on-load tap changer or capacitors. Compared with the base case, the proposed stochastic voltage/VAR control method considering DGs can largely improve the voltage profile no matter which kind of load models is used. All the voltages are within 0.95 p.u. to 1.05 p.u., which satisfies the voltage constraint. The optimal voltage levels with the constant-power load model are relatively higher than those with exponential load model. The reason is that losses are proportional to the square of the current, and the current of a constant-power load is inversely proportional to the voltage [13]. Thus, the on-load tap changer operates the feeder in the upper bound of the allowable voltage range to reduce losses.

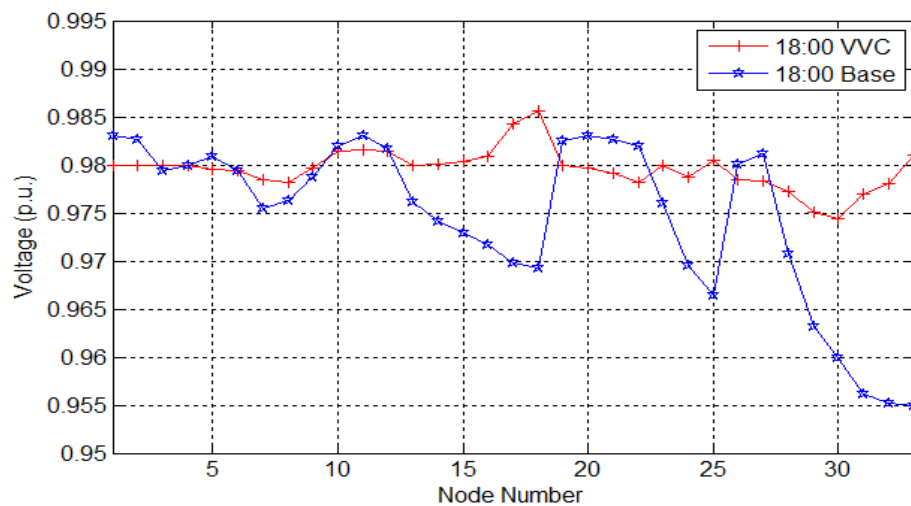


Figure 4.11. Peak-time voltage profiles.

Fig. 4.11 compares the peak-time voltage profiles with and without the proposed voltage/VAR control. The voltage profile becomes flatter by applying the proposed voltage/VAR control technique. The total numbers of daily switching operations of capacitors are 24 for exponential load models and 31 for constant power load models.

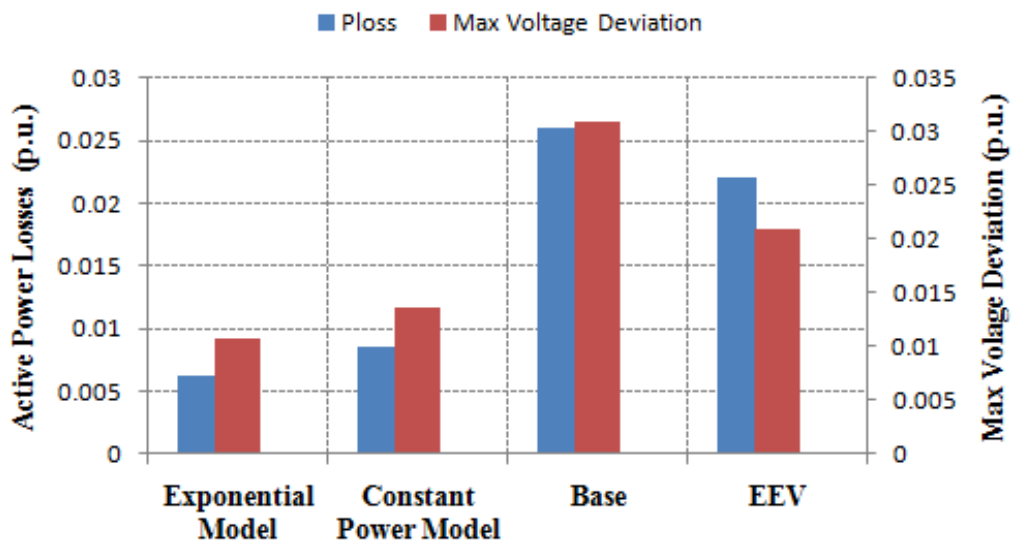


Figure 4.12. Active power losses and max voltage deviations (EEV refers to the expected results of using the expected value solution).

Fig. 4.12 shows the active power losses and maximum voltage deviation of voltage/VAR control with exponential load model, constant-power load model, the expected results of using the expected value solution, and the base case without voltage/VAR control. It can be seen that the stochastic rolling horizon optimization-based voltage/VAR control method can improve the system operation. For example, compared with the base case with DGs and without voltage/VAR control, the proposed stochastic voltage/VAR control with exponential load model reduces the maximum voltage deviation by 65%, and power losses by 77%. Compared with the deterministic

voltage/VAR control (labeled as “EEV” in Fig. 4.12), the proposed stochastic voltage/VAR control considering prediction errors and exponential load model (labeled as “exponential model” in Fig. 4.12) can reduce the maximum voltage deviation by 49% and power losses by 72%. Meanwhile, the objective function values of systems with exponential load models and the constant-power models are different, i.e., the objective function values with exponential load models are slightly lower than those with constant power load models. Since loads are sensitive to voltage in practice and different types of loads may have various load-to-voltage sensitivities, the proposed voltage/VAR control with DGs and different load models are more realistic and effective.

4.4 Stochastic DG Placement for Voltage/VAR Control

Energy deficit, load growth, environmental consciousness and constraints on building new transmission and distribution lines have created increasing interest in voltage/VAR control and conservation voltage reduction as well as DGs. Both techniques can be used to save energy and reduce peak load demand. Conservation voltage reduction is typically utilized at substations to regulate voltage and operate feeders at the lowest acceptable voltage levels [35, 55]. It is known that many loads are voltage dependent and consume less power when the supplied voltage is reduced [35, 105]. Conservation voltage reduction has been successfully implemented to reduce peak demand/energy consumption and increase the system stability margin at a number of utilities such as Northwest Energy Efficiency Alliance and BC Hydro. Previous tests indicate that significant energy savings can be achieved through voltage reduction. The energy-saving effects usually range from 0.3% to 1% load reduction per 1% voltage reduction.

The depth of voltage reduction is an important impact factor on the effectiveness of conservation voltage reduction. It can be seen from Fig. 4.13 that the level of voltage reduction is closely related with the voltage profile along the feeder.

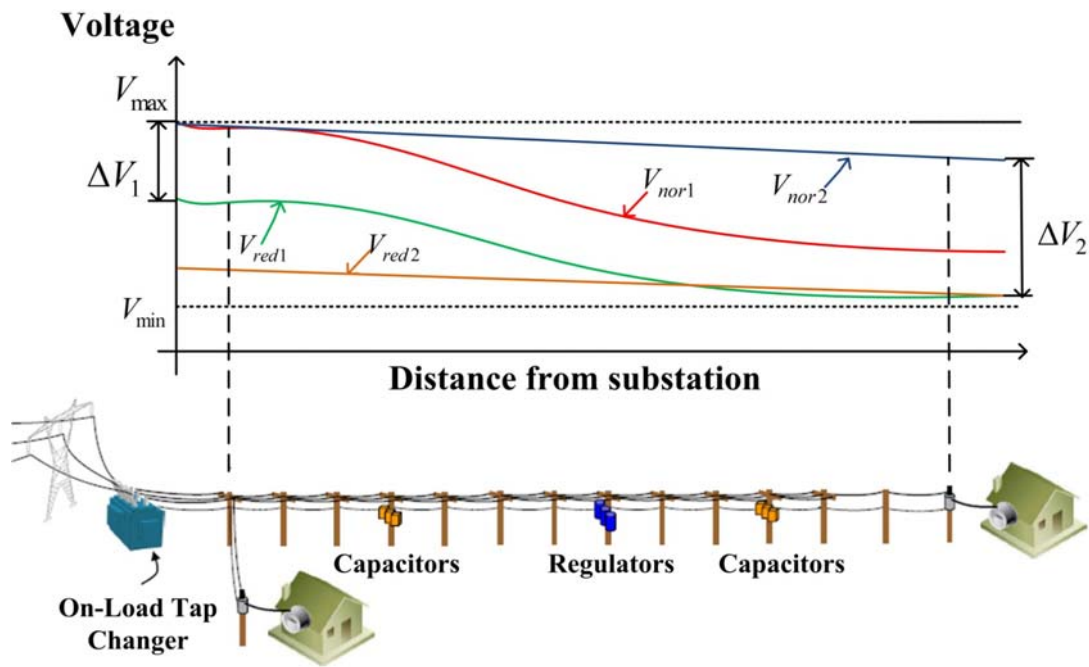


Figure 4.13. Demonstration of voltage drop along a feeder.

The ANSI standard [40] requires that the lowest voltage level remains within 5 percent from the nominal value. If the end-of-line voltage is much lower than the substation voltage, then the substation voltage cannot be reduced too much, in order to maintain the end-of-line voltage above 114 V on a 120V scale. Deeper voltage reduction can be achieved if the end-of-line voltage is maintained near the same level as the voltage at the beginning of the feeder. The most popular way to flatten the voltage profile is to place capacitor banks to provide reactive power compensation along the feeder. Recently, the integration of DGs in distribution feeders has increased rapidly. DG has impacts on

voltage profile, power quality, energy efficiency, and reliability of distribution systems. The location and size of DG units should be carefully selected in order to take advantage of DG and limit its negative impacts on system operations. This dissertation presents a new method to simultaneously consider conservation voltage reduction and DG placement for energy saving and peak demand reduction. A novel DG placement model is proposed to minimize load consumptions of the system and maintain the voltage deviations along the feeder within a predefined range. The proposed method assumes a centralized decision maker such as the distribution system operator that can make the DG placement plan for the conservation voltage reduction implementation since conservation voltage reduction is a measure initiated by the utilities. In order to effectively deal with the probabilistic nature of DG outputs and load consumption, the DG placement is formulated as a two-stage stochastic programming problem.

4.4.1 Mathematical Formulation for Stochastic DG Placement

This subsection proposes a novel formulation for the stochastic DG placement to assist the implementation of conservation voltage reduction. The objective of conservation voltage reduction is to minimize total load consumption through voltage reduction. The conservation voltage reduction effect is closely related to load-to-voltage sensitivity. In this study, an exponential load model is used to represent load consumption as a function of voltage. In order to effectively deal with the uncertain nature of DG outputs and load consumptions, it is necessary to formulate the problem into a stochastic optimization program. The detailed formulation is described as follows, Table 4.5 shows the nomenclature:

Table 4.5. Nomenclature for stochastic DG placement formulation.

$P_{y,s}^{load}$	Total active load consumption in s-th scenario	$\Delta V_{t,s}$	Maximum voltage deviation at time t in s th scenario
$V_{i,y,s}$	Voltage at node i in s-th scenario in year y	α_s / β_s	Active/reactive power exponent for the exponential model in s-th scenario
$P_{i,y,s} / Q_{i,y,s}$	Active/reactive power flow from node i to node i+1 in s-th scenario in year y	r_i / x_i	Line resistance/reactance between node i and i+1
$P_{i,t,s}^l / q_{i,t,s}^l$	Active/reactive load at node i in s-th scenario in year y	$P_{i,t,s}^g / q_{i,t,s}^g$	Active/reactive power output of the P at node I at time t in s-th scenario
$P_{i,y}^b / Q_{i,y}^b$	Base active/reactive load for the exponential load model at node i in year y	T_{ft} / T_{fh}	Cooling/heating reference temperature
$T_{i,y,s}$	Temperature at node i in scenario s in year y	μ / γ	Parameters for active/reactive load regression model w,r,t, temperature
a_i^{wt} / a_i^{pv}	0 if there is no wind turbine/photovoltaic generator at node i; 1 if there is a wind turbine/photovoltaic generator at node i	$q_{i,y,s}^g$	Reactive power generation at node i in scenario s in year y
Q_i^C	Size of the capacitor at node i	$X_{i,y,n}^C$	Switch on (1)/off (0) status of the capacitor at node i in scenario s in year
$P_{i,y,s}^{g,wt} / P_{i,y,s}^{g,pv}$	Active power output of the wind turbine /photovoltaic generator at node i in scenario s in year y	$\omega_{i,y,s}^{wt} / \omega_{i,y,s}^{pv}$	Stochastic wind turbine/photovoltaic generator output of one discrete increment at node i in scenario s in year y
s^{wt} / s^{pv}	One discrete increment of wind turbine/photovoltaic generator size (MVA)	$F_{i,y}^{wt} / F_{i,y}^{pv}$	Probabilistic distribution of $\omega_{i,y,s}^{wt} / \omega_{i,y,s}^{pv}$
F_i^α / F_i^β	Probabilistic distribution of α_s / β_s	$F_{i,y}^T$	Probabilistic distribution of $T_{i,y,s}$
$b_{i,j}^{wt} / b_{i,j}^{pv}$	0 if the j-th increment in size is not necessary to compose the wind turbine/photovoltaic generator at node i; 1 if the j-th increment in size is necessary to compose the wind turbine/photovoltaic generator at node i	$c_{i,j}$	Binary indicator $c_{i,j} = a_i b_{i,j}$
N_a / N_b	Maximum number of	ζ	Binary indicator

	DGs/size increments in the feeder/at a node		
$V_{i,y,s}^{in} / V_{i,y,s}^{out}$	Input/Output voltage of the voltage regulator at node i in scenario s in year y	V^{tap}	Voltage adjustment corresponding to one tap step
$T_{i,y,s}^{tap}$	Tap position of the regulator at node i in scenario s in year y	T_i^{\max} / T_i^{\min}	Maximum/Minimum tap position of the regulator at node i
f_{obj}	The value of the objective function	ϕ / φ	Parameters of a beta distribution
z^* / \hat{z}	True/Approximate objective value of the original SP/SP _N	z_M^{*k}	The objective value approximated by SP_{Mk} in the k -th multiple replication procedure
\hat{z}_M^{*k}	The objective value calculated by using $(\hat{a}, \hat{b}, \hat{c})$ and newly generated M scenarios in the k -th multiple replication procedure	G_k	Optimality gap in the k -th multiple replication procedure

$$\min \sum_y \sum_s P_{y,s}^{load} \quad (4.44)$$

Subject to

$$P_{y,s}^{load} = \sum_i p_{i,y,s}^l, \forall y, s, \quad (4.45)$$

$$p_{i,y,s}^l = (\mu_0 + \mu_1(T_{fh} - T_{i,y,s}) + \mu_2(T_{fc} - T_{i,y,s}))P_{i,y}^b V_{i,y,s}^{\alpha_s}, \forall i, y, s, \quad (4.46)$$

$$q_{i,y,s}^l = (\gamma_0 + \gamma_1(T_{fh} - T_{i,y,s}) + \gamma_2(T_{fc} - T_{i,y,s}))Q_{i,y}^b V_{i,y,s}^{\beta_s}, \forall i, y, s, \quad (4.47)$$

$$P_{i+1,y,s} = P_{i,y,s} - p_{i+1,y,s}^l + p_{i+1,y,s}^{g,wt} + p_{i+1,y,s}^{g,pv}, \forall i, y, s, \quad (4.48)$$

$$Q_{i+1,y,s} = Q_{i,y,s} - q_{i+1,y,s}^l + q_{i+1,y,s}^g, \forall i, y, s, \quad (4.49)$$

$$V_{i+1,y,s} = V_{i,y,s} - \frac{r_i P_{i,y,s} + x_i Q_{i,y,s}}{V_1}, \forall i, y, s, \quad (4.50)$$

$$\delta V_{i,y,s} = |V_{i,y,s} - V_1| \leq \zeta, \forall i, y, s, \quad (4.51)$$

$$p_{i,y,s}^{g,wt} = \sum_j a_i^{wt} b_{i,j}^{wt} \omega_{i,y,s}^{wt}, \forall i, y, s, \quad (4.52)$$

$$p_{i,y,s}^{g,pv} = \sum_j a_i^{pv} b_{i,j}^{pv} \omega_{i,y,s}^{pv}, \forall i, y, s, \quad (4.53)$$

$$\omega_{i,y,s}^{wt} \in F_{i,y}^{wt}, \forall i, y, s, \quad (4.54)$$

$$\omega_{i,y,s}^{pv} \in F_{i,y}^{pv}, \forall i, y, s, \quad (4.55)$$

$$\alpha_s \in F_i^\alpha, \forall i, s, \quad (4.56)$$

$$\beta_s \in F_i^\beta, \forall i, s, \quad (4.57)$$

$$T_{i,y,s} \in F_{i,y}^T, \forall i, y, s, \quad (4.58)$$

$$\sum_i a_i^{wt} + \sum_i a_i^{pv} \leq N_a, \quad (4.59)$$

$$\sum_j b_{i,j}^{wt} + \sum_j b_{i,j}^{pv} \leq N_b \quad (4.60)$$

In the above formulation, the objective function (4.44) minimizes the total load consumptions of the system during the planning horizon. The horizon is modeled in discrete time with 1-year time step.

In order to represent the load-to-voltage and load-to-temperature relationships, the combined exponential and regression models in [3] are used in constraints (4.46-4.47). This study sets $\mu_0 = \gamma_0 = 0.1$, $\mu_1 = \gamma_1 = 0.01$, $\mu_2 = \gamma_2 = 0.02$, $T_{fh} = 60$ F and $T_{fc} = 70$ F [35, 106]. The parameters can be obtained using minimum covariance determinant procedure as introduced in [31]. The values of $P_{i,1}^b$ and $Q_{i,1}^b$ used in this dissertation can be found in [45]. It is also assumed that the annual increasing rate of load is 1% during the planning

horizon. The above values are used to demonstrate the effectiveness of the proposed stochastic DG placement model.

Constraints (4.48)-(4.50) are linearized DistFlow equations as discussed in the previous section. Constraint (4.51) guarantees that the voltage deviation along the feeder is within a predefined range so as to achieve a deeper voltage reduction. In this paper, it is assumed the DGs to be connected with the system are wind turbines and photovoltaic generators. Constraint (4.52) decides whether there is a wind turbine connected with the node, while constraint (4.53) decides whether there is a photovoltaic generator connected with the node. To make the formulation more practical, it is assumed that a DG is made up by several DG units, which means the size of a DG is discrete as described by constraints (4.52) and (4.53) [81]. The sizes of a wind turbine and a photovoltaic generator can be represented as $\sum_j b_{i,j}^{wt} s^{wt}$ and $\sum_j b_{i,j}^{pv} s^{pv}$, respectively. Constraints (4.54) and (4.55) represent the stochastic output of one discrete increment of a wind turbine/photovoltaic generator at node i , which has been discussed in Chapter 3. Constraints (4.56) and (4.57) assume that the load-to-voltage sensitivities of each node are random variables that can be represented using normal distributions [88]. In this dissertation, the mean and variance of F_i^α are set to be 1.0 and 0.08, respectively; the mean and variance of F_i^β are set to be 3.6 and 0.1, respectively. All input parameters can be changed according to the available system information. Constraint (4.58) assumes the stochasticity of the temperature at node i can be represented by a normal distribution $F_{i,y}^T$. It is assumed that the mean and standard deviation of $F_{i,y}^T$ are 55 F and 25 F, respectively, and the temperature distribution during the planning horizon remains the same. Constraint (4.59) indicates that the total number of DGs that can be connected to the

system is less than or equal to N_a . Constraint (4.60) indicates that the total number of DG units that can be connected to a node is less than or equal to N_b . In this paper, it is assumed that $N_a=3$ and $N_b=6$. The purpose of DG placement is to decide the values of a_i and $b_{i,j}$. The system reconfiguration is not considered in the above formulation due to the low frequency of reconfigurations in current distribution systems.

Some of the above constraints can be reformulated to further reduce the non-linearity of the problem. Equation (4.51) can be linearized as

$$\lambda_{i,y,s} \geq V_{i,y,s} - V_0, \forall i, y, s \quad (4.61)$$

$$\lambda_{i,y,s} \geq V_0 - V_{i,y,s}, \forall i, y, s \quad (4.62)$$

$$\lambda_{i,y,s} \leq \zeta, \forall i, y, s \quad (4.63)$$

Equations (4.52) and (4.53) include multiplications of two binary variables a_i and $b_{i,j}$.

The bi-linear term $a_i b_{i,j}$ can be replaced by

$$c_{i,j} \leq a_i, \forall i, j \quad (4.64)$$

$$c_{i,j} \leq b_{i,j}, \forall i, j \quad (4.65)$$

$$c_{i,j} \geq a_i + b_{i,j} - 1, \forall i, j \quad (4.66)$$

$$c_{i,j} \geq 0, \forall i, j \quad (4.67)$$

Table 4.6. The relationship among a, b and c.

a_i	$b_{i,j}$	$c_{i,j}$
1	1	1

1	0	0
0	1	0
0	0	0

For a feeder with voltage regulators and capacitors, it is necessary to model these voltage/VAR control devices as follows [107]:

$$q_{i,y,s}^s = X_{i,y,s}^C Q_i^C, \forall y, s \quad (4.68)$$

$$V_{i,y,s}^{out} = V_{i,y,s}^{in} + Tap_{i,y,s} V^{tap}, \forall y, s \quad (4.69)$$

$$Tap^{\min} \leq Tap_{i,y,s} \leq Tap^{\max}, \forall y, s \quad (4.70)$$

Constraint (4.68) represents the on/off status of the capacitor at node i . Constraints (4.69) and (4.70) model the input-output voltage relationship of the voltage regulator at node i .

4.4.2 Proposed Solution Algorithm

The mathematical formulation proposed in section 4.4.1 is a stochastic optimization problem. There are many methodologies to solve a stochastic optimization problem, among which, sample average approximation is shown to be an easy and effective method. The intuitive idea of sample average approximation is to approximate the expectation term in the objective function by sampling. Based on the law of large numbers [81], when the size of samples is large enough, the value of the reformulated objective function converges to the value of the original objective function. At the same time, the feasible region of the reformulated problem would be equivalent to the feasible region of the original problem. However, as the sample size is finite in reality, it is important to test the quality of the solution, which is performed by the multiple

replications procedure in this dissertation. In this section, a combined multiple replication procedure-sample average approximation algorithm is proposed to solve the problem.

The first step of sample average approximation is to generate scenarios using Monte-Carlo simulations to replace the true distributions of uncertain variables by an empirical distribution which can be obtained using the Kolmogorov-Smirnov test with historical data. The Kolmogorov-Smirnov test is a nonparametric test to compare a sample with a reference probability distribution. Kolmogorov-Smirnov statistics quantify a distance between the empirical distribution function of the sample and the cumulative distribution function of the reference distribution to find the best cumulative distribution function to represent the empirical distribution function. The Monte-Carlo simulation generates N scenarios for year y , each with the same probability $1/N$. Thus, there are totally S ($S=N*y$) scenarios. The objective is to obtain the minimum expected load. The general form of the problem can be written as

$$z^* = \min f(a,b,c,W) \quad (4.71)$$

where $f(a,b,c,W) = \sum_y \sum_s P_{y,s}^{load} | (4.45) - (4.67)$ and W represents random variables such as wind turbine/photovoltaic generator outputs, load model exponents and temperature.

Equation (4.71) can be denoted as a stochastic program (SP) which depends on the priori knowledge of the probability distributions of the uncertain variables. Sample average approximation is to sample S independent and identically distributed observations from the distribution of W and then solve the approximating problem (denoted as SP_s):

$$\hat{z} = \min \frac{1}{S} \sum_y \sum_{s=1}^N f(a,b,c,W_{y,s}) \quad (4.72)$$

Thus, the original problem in (4.44)-(4.60) can be reformulated to be a mixed-integer non-linear program as:

$$\hat{z} = \min \frac{1}{S} \sum_y \sum_{s=1}^N f(a, b, c, W_{y,s}) \quad (4.73)$$

subject to (4.45)-(4.67).

In the above mixed-integer non-linear formulation, variables $a_i, b_{i,j}$ and $c_{i,j}$ are first-stage variables; variables P, Q, V, p^s and q^s are selected to be second-stage ones which change according to the uncertainty realizations. For a specific set of first-stage decisions, different costs can be associated with various scenarios.

It is known from sample average approximation that the solutions $(\hat{a}, \hat{b}, \hat{c})$ are optimal to the stochastic program as the sample size grows into infinity. However, since $(\hat{a}, \hat{b}, \hat{c})$ is obtained by solving SP_N with a finite sample size in practice, it is necessary to test the quality of the solution, which is performed by the multiple replications procedure in this dissertation.

The true optimal solution of the stochastic program is (a^*, b^*, c^*) with the optimal value z^* ($z^* = \min f(a, b, c, W)$). While $(\hat{a}, \hat{b}, \hat{c})$ is obtained from S scenarios in solving the stochastic program, new samples with M new scenarios (M is usually larger than or equal to N) are generated by K times in multiple replication procedure. This study defines the individual problem in the K*M samples as $SP_{Mk}, k = 1, \dots, K$. A new objective value z_M^{*k} can be obtained by using the same sample average approximation procedure for each SP_{Mk} . Since $\mathbb{E}z_M^{*k} \leq z^*$, an upper bound on the optimality gap of $(\hat{a}, \hat{b}, \hat{c})$ in the k-th multiple replication procedure (denote as G_k) can be estimated by

$$\frac{1}{M} \sum_{m=1}^M f(\hat{a}, \hat{b}, \hat{c}, W_m^k) - \min \frac{1}{M} \sum_{m=1}^M f(a, b, c, W_m^k) \quad (4.74)$$

where the M scenarios are independent and identically distributed random variables from the distribution of W , $\frac{1}{M} \sum_{m=1}^M f(\hat{a}, \hat{b}, \hat{c}, W_m^k)$ is calculated by using $(\hat{a}, \hat{b}, \hat{c})$ in the newly generated M scenarios. Multiple replication procedure is to repeat this procedure for multiple times (K times in this paper) and construct the confidence interval for the optimality gap. The form of the confidence interval can be describes as

$$P(f(\hat{a}, \hat{b}, \hat{c}, W) - z^* \leq \varepsilon) \approx 1 - \alpha \quad (4.75)$$

where ε is the confidence interval width, and $1 - \alpha$ is the confidence, e.g., 0.95.

Fig. 4.14 shows the flowchart of the combined sample average approximation and multiple replication procedure. The complete steps are as follows.

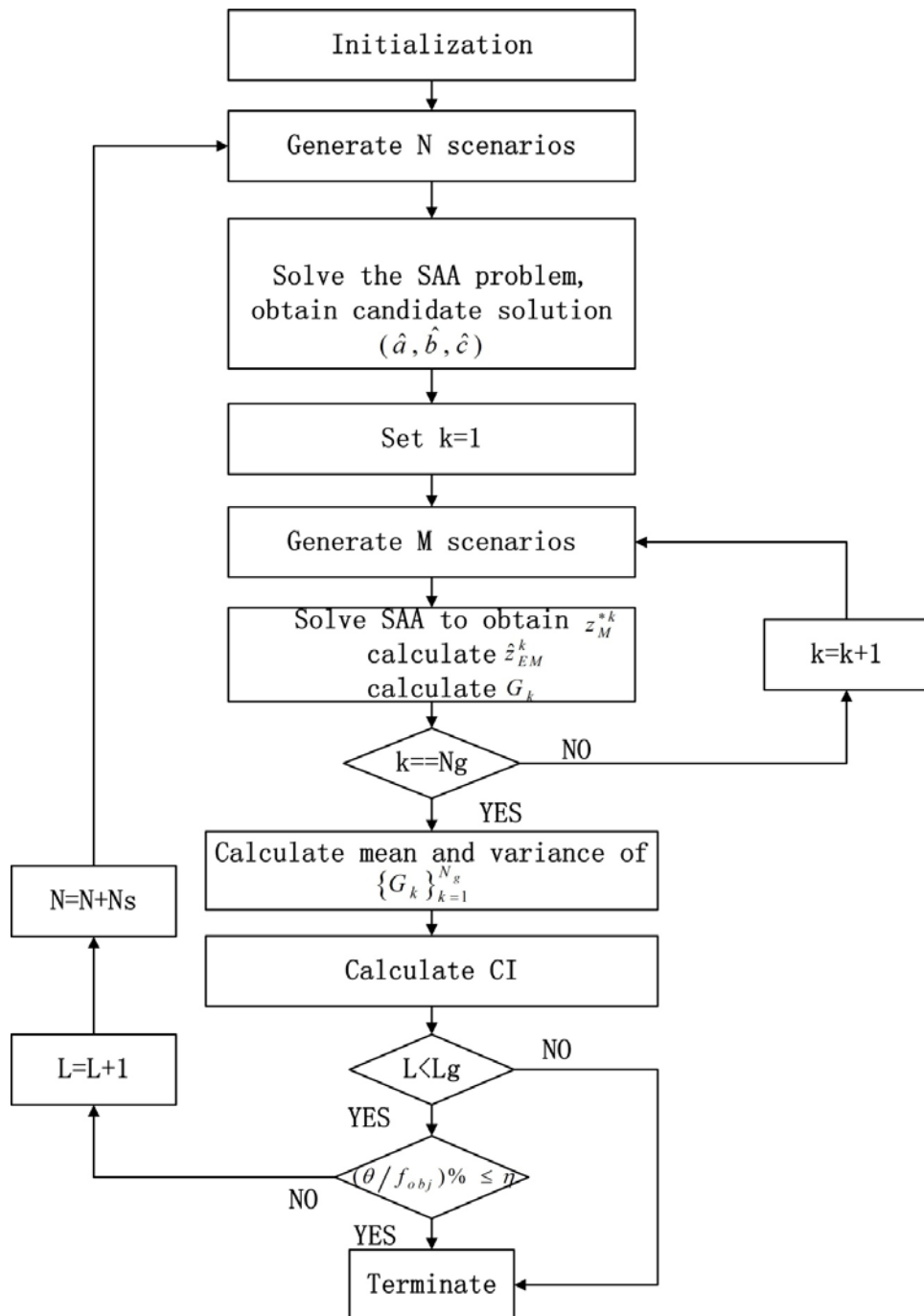


Figure 4.14. Flowchart of combined multiple replication procedure and sample average approximation.

Step1: generate S scenarios and use sample average approximation to solve the stochastic programming problem as defined in (4.73), obtain the candidate solution $(\hat{a}, \hat{b}, \hat{c})$;

Step2: generate M scenarios and use sample average approximation to solve the SP_M problem and obtain the solution (a^{*k}, b^{*k}, c^{*k}) and the objective value z_M^{*k} ;

Step3: use the solution of stochastic programming problem $(\hat{a}, \hat{b}, \hat{c})$ and the M scenarios to calculate $\hat{z}_M^{*k} = \frac{1}{M} \sum_{m=1}^M f(\hat{a}, \hat{b}, \hat{c}, W_m^k)$;

Step4: calculate the optimality gap: $G_k(\hat{a}, \hat{b}, \hat{c}) = \hat{z}_M^{*k} - z_M^{*k}$;

Step5: repeat steps 2-4 for $k = 1, 2, \dots, K$;

Step6: calculate the mean and variance of the optimality gap by $\bar{G} = \frac{1}{K} \sum_{k=1}^K G_k(\hat{a}, \hat{b}, \hat{c})$

and $s^2 = \frac{1}{K-1} \sum_{k=1}^K (G_k(\hat{a}, \hat{b}, \hat{c}) - \bar{G})^2$, then the one-sided confidence interval of the optimality gap is $[0, \bar{G} + t_{K-1, \alpha} / \sqrt{K}]$, where $t_{K-1, \alpha}$ is the α -quantile of the t -distribution with $K-1$ degrees of freedom, this study denotes the confidence interval as $[0, \theta]$, where $\theta = \bar{G} + t_{K-1, \alpha} / \sqrt{K}$;

Step7: if the number of iterations exceeds the maximum value Lg, terminate the process; otherwise, go to step 8;

Step8: if $(\theta / f_{obj}) \times 100\%$ is less than a predefined value η , terminate the process; otherwise, increase the number of scenarios by N_s and go to step1, η is defined to be 5% in this dissertation.

Since most of the previous work in DG placement uses deterministic optimization, it is necessary to show how much improvement can be achieved if the stochastic nature of DG is taken into account. For the problem defined in equation (4.71), the random variable ω is replaced by its expected value. The expected value problem (EV), which is a deterministic optimization problem, can be defined as

$$EV = \min f(a, b, c, \bar{W}) \quad (4.76)$$

where $\bar{W} = E(\bar{W})$ denotes the expectation of \bar{W} . The expected value solution can be defined as $(\bar{a}, \bar{b}, \bar{c})$. The expected results of using the EV solution can be represented as

$$EEV = \frac{1}{N'} \sum_{h=1}^{N'} f(\bar{a}, \bar{b}, \bar{c}, W_h) \quad (4.77)$$

The expected results of using the expected value solution measure the performance of $(\bar{a}, \bar{b}, \bar{c})$, allowing second-stage decision variables to be chosen optimally as functions of $(\bar{a}, \bar{b}, \bar{c})$ and W . In order to measure how good or, more frequently, how bad the decision $(\bar{a}, \bar{b}, \bar{c})$ is, when compared with $(\hat{a}, \hat{b}, \hat{c})$, Monte Carlo simulation is used. S' scenarios (S' is usually larger than S) are generated. The solution of the SPs problem $(\hat{a}, \hat{b}, \hat{c})$ is used in each of S' scenarios to calculate $f(\hat{a}, \hat{b}, \hat{c}, \omega_h)$, $h = 1, \dots, N'$. The difference between The expected results of using the expected value solution and the Monte-Carlo simulation result can be defined as

$$D = EEV - \frac{1}{N'} \sum_{h=1}^{N'} f(\hat{a}, \hat{b}, \hat{c}, W_h) \quad (4.78)$$

Since the formulation is a minimization problem, the larger the D, the more the stochastic programming outperforms deterministic programming. The proposed solution algorithm is used to solve the stochastic DG placement model in Section 4.4.1.

4.4.3 Case Study

In this research, the proposed DG placement model and solution algorithm are illustrated for a 37-bus radial distribution network as shown in Fig. 4.15. Details about the 37-bus distribution system can be found in [45]. Appendix B describes the parameters of the 37-bus distribution system. Assume the substation transformer is with $\pm 5\%$ tap range and 10 tap positions. Switched capacitors are installed at nodes 3, 16 and 32, each is 30 kVAR. Details about the test system can be found in Appendix A. The power base is 10 MVA, the voltage base is 12.66 kV. Table 4.7 shows the base case (without DG and conservation voltage reduction) of the test system.

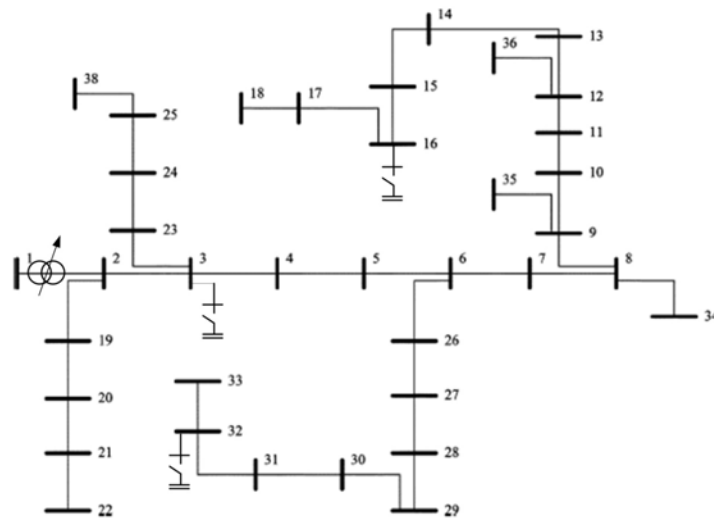


Figure 4.15. The 37-bus distribution system.

It is assumed that one size increment of a wind turbine and a photovoltaic generator is 0.01 p.u. The Monte Carlo simulation is used to generate scenarios of wind turbine/photovoltaic generator output to calculate the candidate solution for the 37-node network. The planning horizon is assumed to be 10 years and 200 scenarios are generated for each year ($S = 200$), thus there are totally 2000 scenarios ($N = 2000$). The stochastic

program defined in section 4.4.1 is a mixed-integer nonlinear and non-convex problem. In this simulation, the Discrete and Continuous Optimizer (DICOPT) in the General Algebraic Modeling System (GAMS) is used to solve the problem. The simulation is performed by using a computer with Intel Quad Core 2.40 GHz and 8 GB memory. The computation time is around 30 minutes for the stochastic planning problem with 2000 scenarios.

Table 4.7. Base case of the test system.

Maximum Voltage Deviation (p.u.)	Active loss (p.u.)	Total Active Load (p.u.)	Substation Voltage (p.u.)
0.09	0.028	0.3715	1.05

Table 4.8 shows the placement results. The DG penetration level can be defined as the total DG generation divided by the system peak load. For the planning results, the DG penetration level is 30%.

Table 4.8. DG placement results.

Node No.	Type	Size (p.u.)
8	Wind turbine	0.01
	Photovoltaic generator	0.01
13	Wind turbine	0.03
	Photovoltaic generator	0.01
31	Wind turbine	0.03
	Photovoltaic generator	0.02

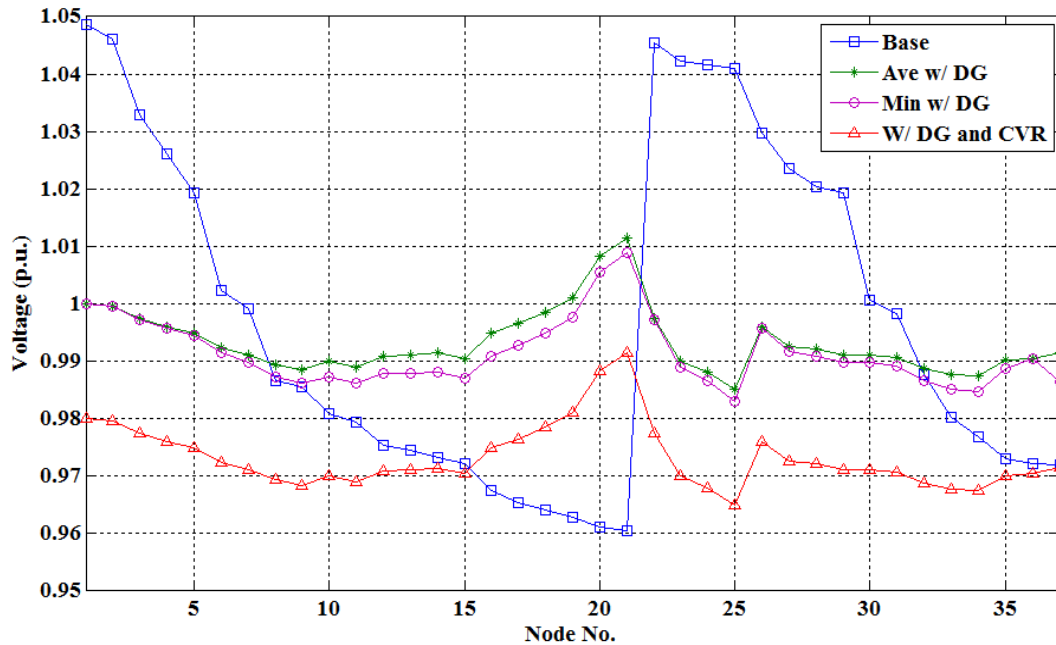


Figure 4.16. Voltage profile of the 37-buse distribution system.

Fig. 4.16 shows the voltage profiles of the test system. There are four profiles in the figure: 1) base case without DG or conservation voltage reduction; 2) average voltages of all N scenarios without voltage reduction; 3) minimum voltages of all N scenarios without voltage reduction; 4) average voltages of all N scenarios with conservation voltage reduction. In the base case, there is almost no potential for voltage reduction since the largest voltage deviation is 0.09 p.u., and the substation voltage is set to be 1.05 p.u. in order to make sure the end-of-line voltage is within the standard. After DG integration, the voltage profiles are improved largely. The voltage deviations are within 0.03 p.u. even for the worst case, which provides enough space for implementing voltage reduction. The substation voltage can be reduced from 1.05 p.u. to 0.98 p.u. with optimal placement of wind turbines.

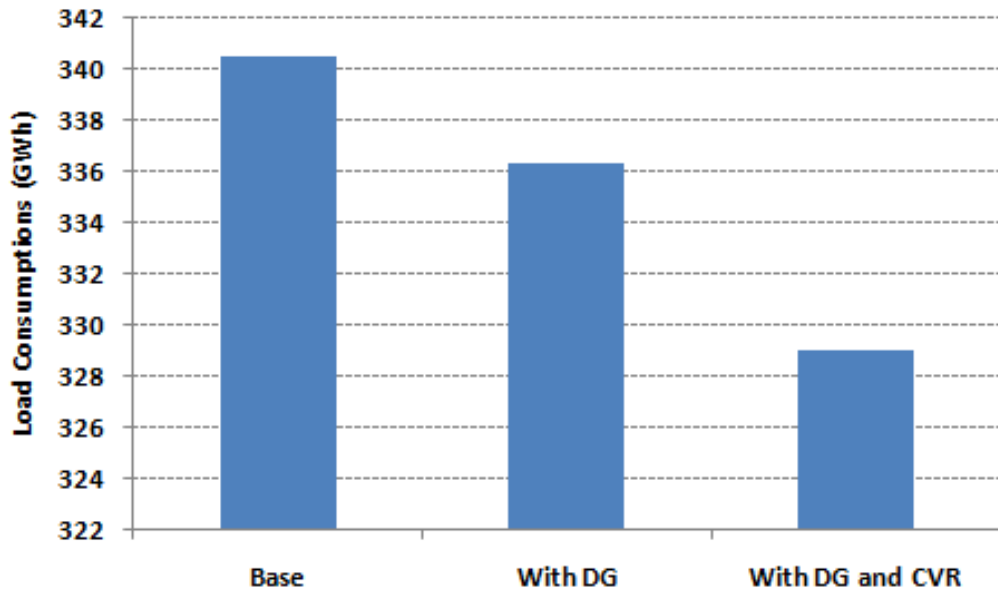


Figure 4.17. Active load consumption of the 37-buse distribution system.

Fig. 4.17 shows the active total load consumptions of three cases during the planning horizon (one year consists of 8760 hours): 1) the base case without DG or conservation voltage reduction; 2) the case with stochastic optimal DG placement (the results of the stochastic DG placement are shown in Table 4.8) but without voltage reduction; 3) the case with stochastic optimal DG placement and with conservation voltage reduction. It can be seen that the load consumptions of the base case are much higher than the other two cases. This shows the effectiveness of the stochastic optimal DG placement in improving the system operation. Moreover, significant load consumptions can be reduced by conservation voltage reduction, which shows that more energy savings can be achieved if the implementation of conservation voltage reduction and the placement of DG are considered simultaneously.

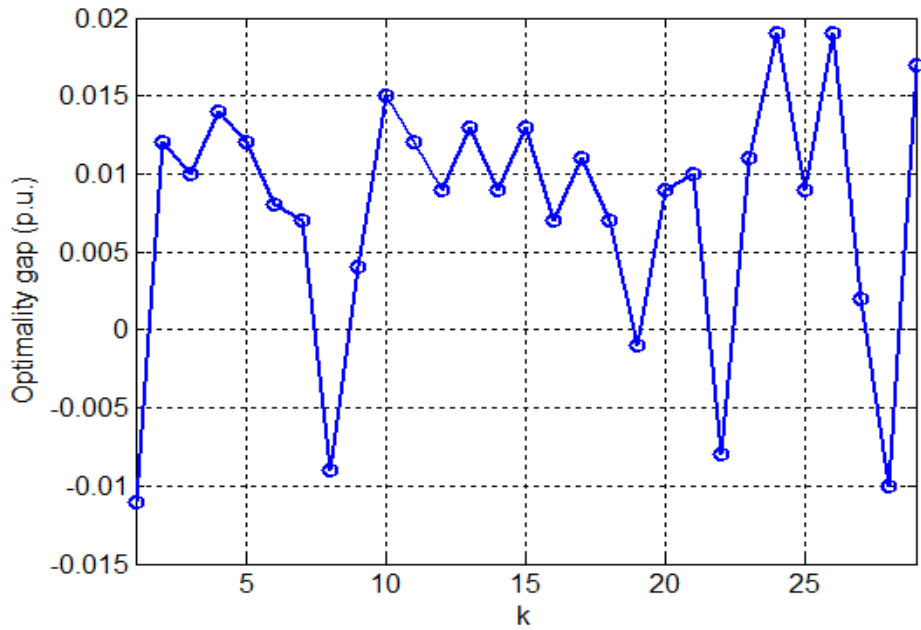


Figure 4.18. Optimality gap in multiple replication procedure (the optimality gap is defined in equation 4.74).

Table 4.9. Values of optimality gaps in multiple replication procedure.

K*	1	2	3	4	5	6	7	8	9
Optimality gap	-0.011	0.012	0.010	0.014	0.012	0.008	0.007	-0.009	0.004
K	10	11	12	13	14	15	16	17	18
Optimality gap	0.015	0.012	0.009	0.013	0.009	0.013	0.007	0.011	0.007
K	19	20	21	22	23	24	25	26	27
Optimality gap	-0.001	0.009	0.01	-0.008	0.011	0.019	0.009	0.019	0.002
K	28	29							
Optimality gap	-0.010	0.017							

*K is the number of iterations in the multiple replication procedure

As discussed in sections 3.4 and 4.4.2, the multiple replication procedure can be used to validate the quality and stability of the candidate solutions of the stochastic program. The candidate solution is tested against 29 samples ($K = 29$), each with a sample size of 2500 ($M = 2500$). The optimality gaps are shown in Fig. 4.18, and the values are listed in

Table 4.9. The mean value of gaps is $\bar{G}=0.007586$, and the standard deviation is $s=0.008231$. The confidence interval for the optimality gap is $[0, 0.0102]$ with $\alpha=0.05$, which means that there is a chance of 95% that the optimality gap is within the confidence interval. Thus, the candidate solution of the stochastic programming is very stable and of high quality.

To show the performance of the stochastic program, $N'=3000$ scenarios are generated, and use \bar{W} in solving the deterministic optimal DG placement. The formulation of the deterministic optimal problem is similar to the stochastic formulation; the only difference is that all random variables are substituted by their mean values. The problem is solved by the general algebraic modeling system [90]. Recall the solution of this deterministic problem is defined as the expected results of using the expected value solution.

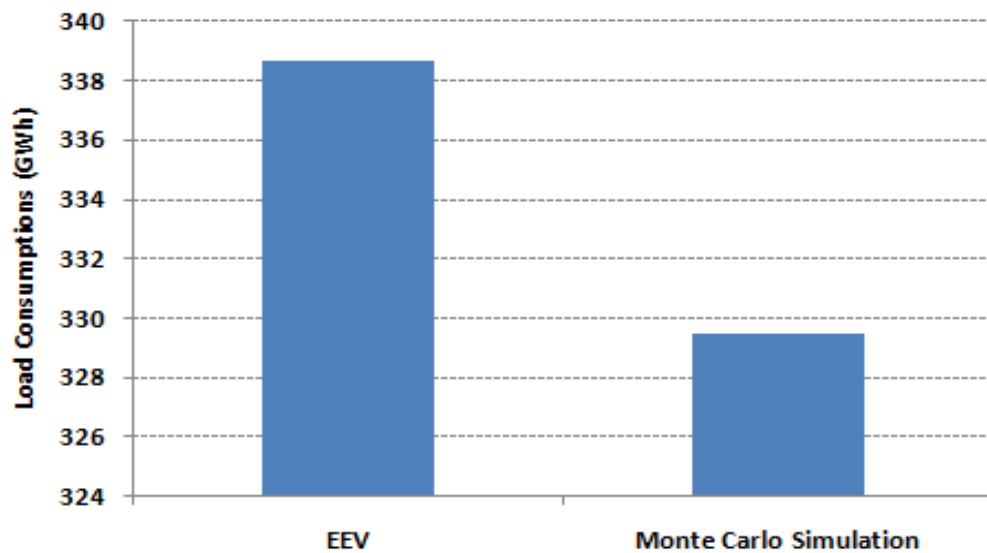


Figure 4.19. Comparison of the expected results of using the expected value solution (EEV) and Monte Carlo simulation.

The DG placement results are: wind turbines should be placed at nodes 6, 8 and 30, with the sizes of 0.01 p.u., 0.02 p.u. and 0.03 p.u., respectively, and photovoltaic generators should be placed at nodes 6, 8 and 30, with the size of 0.01 p.u., 0.02 p.u. and 0.01 p.u. As shown in (4.78), Monte Carlo simulation is run to compare the performances of the deterministic placement and the stochastic placement. Fig. 4.19 shows the comparison results. The deterministic solution is worse when wind turbine output is stochastic. Considering the probabilistic nature of DG output in practice, the proposed stochastic programming is more suitable and realistic.

4.5 Summary

This chapter applies the stochastic optimization theory in Chapter 3 to develop a rolling horizon optimization-based method for voltage/VAR control based on forecasted DG outputs and load consumptions. The model considers exponential load models and the probabilistic nature of prediction errors of DG outputs and load consumptions. The voltage/VAR control problem is formulated as a stochastic mixed-integer nonlinear program (MINLP) with the purposes to minimize power losses and feeder voltage deviations. Different types of customers (residential, commercial and industrial customers) in a distribution system are taken into account by assigning corresponding exponents in the load models. Monte-Carlo simulations are run to generate scenarios of DG outputs. The MINLP is solved with reduced scenarios. Case studies on the modified 33-bus test system with two wind turbines, one photovoltaic generator and different types of loads verify the effectiveness of the proposed voltage/VAR control technique. The proposed voltage/VAR control can reduce losses by up to 77% and reduce maximum voltage deviations by up to 65%. The stochastic voltage/VAR control technique produces

from two to three times greater benefits than the deterministic approach. Finally, it appears that significant differences exist in voltage/VAR control dispatches when load models are taken into account. Since the practical load is a mixture of constant-power loads and voltage-dependent loads, it is more reasonable to use the voltage dependent load model to represent load behaviors. Moreover, Fig. 4.12 shows that using the exponential load model, the analysis estimates both active power losses and maximum voltage deviations to be slightly lower compared to simulations using constant power loads. The main differences between the proposed formulation and the existing voltage/VAR control techniques are: (1) the proposed formulation uses exponential load models to capture the load-to-voltage relationship, while most existing papers use constant power load models which cannot correctly represent the load-to-voltage behaviors; (2) the uncertainties of load consumption and renewable DG generation are fully considered in the proposed formulation. The simulation is only illustrated on an IEEE 33-bus distribution system. It would be beneficial to test the proposed method on this IEEE 33-bus system with different penetration levels of DGs, and on larger IEEE benchmark test systems.

Based on the sample average approximation and multiple replication procedure introduced in Chapter 3, this chapter also presents a new DG placement strategy to assist the implementation of conservation voltage reduction. The DG placement is defined as a stochastic optimization problem to enable the distribution system to realize deeper voltage reduction to decrease load consumptions. In order to deal with the uncertain nature of DG outputs and load consumptions, a combined sample average approximation -multiple replication procedure-based algorithm is developed to obtain the optimal

solution. The quality of the optimal solution is validated by calculating its confidence interval using multiple replication procedure. The case studies show the effectiveness of the proposed formulation and prove that significant power reduction can be achieved, if the integration of DG and implementation of conservation voltage reduction is considered simultaneously. The main contribution of this work is the proposed solution method which has combined the sample average approximation and the multiple replication procedure.

This chapter focuses on the implementation of conservation voltage reduction. The next chapter discusses methods to assess the conservation voltage reduction effects.

CHAPTER 5 ASSESSMENT OF VOLTAGE/VAR CONTROL/CONSERVATION VOLTAGE REDUCTION EFFECTS

5.1 Overview

One important function of voltage/VAR control is conservation voltage reduction. Conservation voltage reduction lowers voltages on the distribution system in a controlled manner. Conservation voltage reduction can reduce peak demand and achieve energy savings, while keeping the lowest customer-utilization voltage consistent with levels determined by regulatory agencies and standards setting organizations. Unlike demand response programs, conservation voltage reduction is imposed by utilities. Conservation voltage reduction is shown to be an established and cost-effective way to reduce peak demand and energy consumption, which has motivated many utilities to investigate its application in individual systems [52, 55, 108, 109]. The conservation voltage reduction effect is evaluated by the Conservation Voltage Reduction factor (CVR_f), which is the change in load consumptions to the change in voltage, defined as follows [23]:

$$CVR_f = \frac{\%Load\ Change}{\%Voltage\ Reduction} = \frac{(P_{cvroff} - P_{cvron}) / P_{cvroff}}{(V_{cvroff} - V_{cvron}) / V_{cvroff}} \quad (5.1)$$

where P_{cvron} and P_{cvroff} represent the active load consumption with and without conservation voltage reduction, respectively; V_{cvron} and V_{cvroff} represent the voltage with and without conservation voltage reduction, respectively.

Utilities would like to know which feeders are suitable to implement conservation voltage reduction. There are two challenges to answer this question: firstly how to

quantify the conservation voltage reduction factor of tested feeders; secondly how to select preferred feeders when conservation voltage reduction factors vary from time to time and from feeder to feeder. The major issue in evaluating the conservation voltage reduction effect is to find what the load would be without voltage reduction during the conservation voltage reduction test period. As shown in Fig. 5.1, lines AE, BC and FD represent a measured load profile with voltage reduction. The challenge is to estimate the dotted line EF.

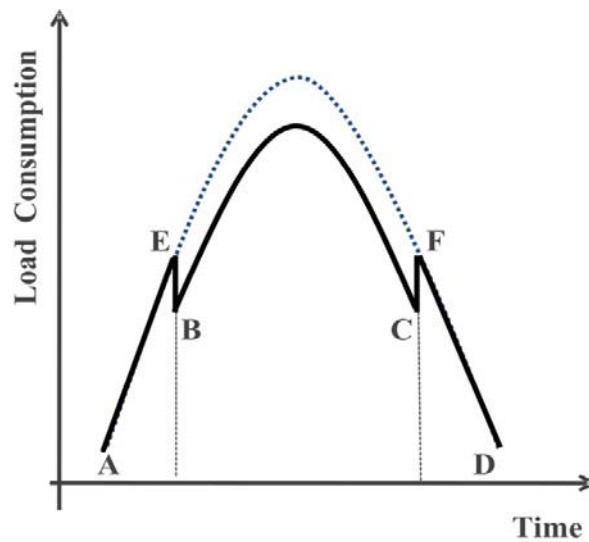


Figure 5.1. Load profiles with and without voltage reduction.

In this chapter, a data-driven method based on multistage support vector regression is proposed to estimate the normal-voltage load consumption during the conservation voltage reduction period. To consider the probabilistic nature of conservation voltage reduction effects, a statistical method is proposed to assist utilities to select feeders with the best conservation voltage reduction performance. In addition, this chapter also proposes a model-driven method to assess the conservation voltage reduction effects.

This new method is based on load model identification. The model-driven method is completely different from the existing methods and calculates conservation voltage reduction factors through load-to-voltage sensitivities.

5.2 Data-driven Assessment by Multistage Support Vector Regression

This section proposes a multistage support vector regression method to assess the conservation voltage reduction effects. In section 5.2.1, the basic concepts of support vector machine and support vector regression are introduced. In section 5.2.2, a multistage support vector regression method is developed to estimate what the load would be if there were no voltage reduction during the conservation voltage reduction period.

5.2.1 Support Vector Machine and Support Vector Regression

In machine learning, support vector machines are supervised learning models [73] with associated learning algorithms that analyze data and recognize patterns, used for classification and regression analysis. A support vector machine constructs a hyperplane or set of hyperplanes in a high- or infinite-dimensional space, which can be used for classification, regression, or other tasks. The two key ideas of support vector machines are: the maximum margin solution for a linear classifier; and the “kernel trick” which is a method of expanding up from a linear classifier to a non-linear one in an efficient manner. The basic concept of support vector regression is summarized from references [73-75] in the following parts.

Suppose there is a set of training data $\{x_i, y_i\}_{i=1}^n$, where x_i is the input pattern, and $y_i = \pm 1$ which denotes the associated output value of x_i . Let the perpendicular distance

from the hyperplane to the nearest +1 class point be denoted d_+ , and similarly d_- for -1 class. The margin is defined as $\min(d_+, d_-)$ and the support vector machine solution looks for the weight vector that maximizes this margin. If the equation $f(x) = \tilde{\mathbf{w}} \cdot \mathbf{x} + \omega_0$ defines a discriminant function, i.e., the output is $\text{sgn}(f(x))$, then the hyperplane $c\tilde{\mathbf{w}} \cdot \mathbf{x} + c\omega_0$ defines the same discriminant function for any $c > 0$. Thus, the scaling of \mathbf{w} can be chosen so that $|\tilde{\mathbf{w}} \cdot \mathbf{x} + \omega_0| = 1$. Therefore,

$$\tilde{\mathbf{w}} \cdot \mathbf{x} + \omega_0 \geq +1 \quad \text{for } y_i = +1 \quad (5.2)$$

$$\tilde{\mathbf{w}} \cdot \mathbf{x} + \omega_0 \leq -1 \quad \text{for } y_i = -1 \quad (5.3)$$

Equations (5.2) and (5.3) can be combined into one set of constraints

$$y_i(\tilde{\mathbf{w}} \cdot \mathbf{x} + \omega_0) \geq 1 \quad \text{for } i = 1, \dots, n \quad (5.4)$$

By considering the geometry that for the maximum margin solution $d_+ = d_-$, there is at least one data point in each class for which $y_i(\tilde{\mathbf{w}} \cdot \mathbf{x} + \omega_0) = 1$. Consider a point x_+ for which the quality in (5.2) holds; this gives $x_+ \cdot \tilde{\mathbf{w}} + \omega_0 = 1$. Similarly, for a point x_- for which the quality in (5.3) holds; this gives $x_- \cdot \tilde{\mathbf{w}} + \omega_0 = -1$. Let these two hyperplanes be denoted as H_+ and H_- , respectively. The perpendicular distance ($d_+ d_-$) between the two hyperplanes can be calculated as $\hat{\mathbf{w}} \cdot (x_+ - x_-) = 2/\|\tilde{\mathbf{w}}\|$, where $\hat{\mathbf{w}}$ is the unit vector $\tilde{\mathbf{w}}/\|\tilde{\mathbf{w}}\|$. Therefore, to maximize the margin, $\|\tilde{\mathbf{w}}\|^2$ can be minimized subject to the constraints in (5.4) as follows:

$$\tilde{\mathbf{w}} = \sum_i \alpha_i y_i x_i \quad (5.5)$$

The constrained optimization problem can be set up using Lagrange multipliers, and solved using numerical methods. The form of the solution is

$$\begin{aligned} \min \quad & \|\tilde{\mathbf{w}}\|^2 \\ \text{s.t.} \quad & y_i(\tilde{\mathbf{w}} \cdot \mathbf{x} + \omega_0) \geq 1, \forall i = 1, \dots, n \end{aligned} \quad (5.6)$$

where α_i represents non-negative coefficient determined numerically. It can be seen that the solution in the form of (5.5) is a linear combination of x_i . The key feature of equation (5.5) is that α_i equals zero for every x_i except those which lie on the hyperplanes H_+ or H_- , and these points are the support vectors. It is clear that not all of the training points contribute to the final solution, which is referred to as the sparsity of the solution. The support vectors lie closest to the decision boundary. The optimization problem for finding the α_i is convex, which means there are no local minima. This is in contrast to the optimization problem for neural networks, where there are local minima. After obtaining the solution as shown in (5.5), predictions for a new input \mathbf{x} can be made as follows:

$$g(\mathbf{x}) = \text{sgn}(\tilde{\mathbf{w}} \cdot \mathbf{x} + \omega_0) = \text{sgn}\left(\sum_i \alpha_i y_i(x_i \cdot \mathbf{x})\right) + \omega_0 \quad (5.7)$$

It can be seen that \mathbf{x} enters this expression on terms of the inner product $\mathbf{x} \cdot x_i$.

The problem defined in (5.6) is suitable for the linearly separable cases. In practice, there are many cases in which the data is not linearly separable. An objective function that trades off misclassifications against minimizing $\|\tilde{\mathbf{w}}\|^2$ can be set up to find an optimal compromise. A slack variable $\xi_i \geq 0$ should be added for (5.2) and (5.3) to find the compromise:

$$\tilde{\mathbf{w}} \cdot x_i + \omega_0 \geq +1 - \xi_i \quad \text{for } y_i = +1 \quad (5.8)$$

$$\tilde{\mathbf{w}} \cdot x_i + \omega_0 \leq -1 + \xi_i \quad \text{for } y_i = -1 \quad (5.9)$$

Fig. 5.2 shows the idea of adding the slack variable, i.e., the constraints (5.2) and (5.3) can be violated, but a penalty will be added [110]. Therefore, the function to be optimized is given by

$$J = \|\mathbf{w}\|^2 + C(\sum_i \xi_i) \quad (5.10)$$

where C is the parameter that determines the weights of the slack variables and $\|\tilde{\mathbf{w}}\|^2$.

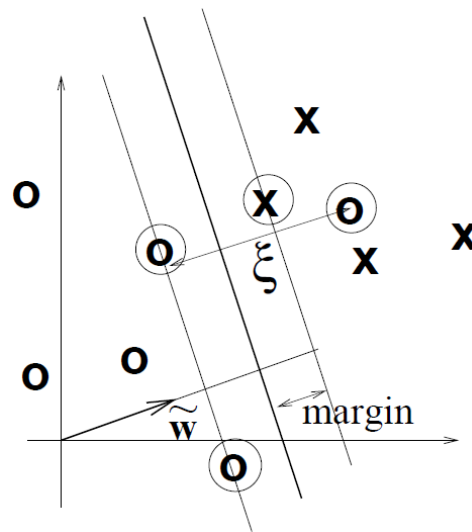


Figure 5.2. A non-separable example with support vectors shown in ringed points.

The solution of (5.10) is given by

$$\tilde{\mathbf{w}} = \sum_i \alpha_i y_i x_i \quad (5.11)$$

where α_i is obtained from solving a quadratic programming problem. In this case, the support vectors with $\alpha_i \neq 0$ are not only those data points which lie on the separating hyperplanes, but also those that have non-zero ξ_i .

The discriminant function in (5.8) and (5.9) is linear. In order to generalize support vector machine to non-linear discriminant functions, it is necessary to apply a kernel trick as shown in [110]. It should be noted that the only way the data points appear in the

testing phase with a new input \mathbf{x} is as $\mathbf{x} \cdot \mathbf{x}_i$. Suppose an input \mathbf{x} can be mapped into some other space Γ with a dimension N_Γ by the mapping $\phi: R^d \rightarrow \Gamma$. Γ is the feature space defined by the mapping ϕ . The maximum margin algorithm can construct a separating hyperplane in the feature space by evaluating inner products in feature space of the form $\phi(x_i) \cdot \phi(x_j)$. If there was a function so that $k(x_i, x_j) = \phi(x_i) \cdot \phi(x_j)$, then the function k can be used in the algorithm. The function k is called the kernel function. Thus, predictions for a new input \mathbf{x} can be made by modifying equation (5.7) as:

$$\begin{aligned} g(\mathbf{x}) &= \text{sgn}\left(\sum_i \alpha_i y_i (\phi(x_i) \cdot \phi(\mathbf{x})) + \omega_0\right) \\ &= \text{sgn}\left(\sum_i \alpha_i y_i k(x_i, \mathbf{x}) + \omega_0\right) \end{aligned} \quad (5.12)$$

with the α_i and ω_0 determined by a quadratic programming problem.

Support vector regression (SVR) is based on the similar idea of support vector machine as discussed above. Support vector regression finds a nonlinear map from the input space to the output space and maps the input data to a higher dimensional feature space through this map. For the classification problem as shown in (5.7), the sgn function can be removed and the prediction be expressed as

$$f(\mathbf{x}) = \tilde{\mathbf{w}} \cdot \mathbf{x} + \omega_0 \quad (5.13)$$

A ε -insensitive error function can be defined as follows:

$$E_\varepsilon(z) = \begin{cases} |z| - \varepsilon & \text{if } |z| \geq \varepsilon \\ 0 & \text{otherwise} \end{cases} \quad (5.14)$$

By minimizing the following error function

$$C \sum_i E_\varepsilon(y_i - f(x_i)) \quad (5.15)$$

a solution can be obtained as

$$\tilde{\mathbf{w}} = \sum_i \beta_i x_i \quad (5.16)$$

where many of the coefficients β_i are zero. The data points which lie inside the ε -tube have $\beta_i = 0$, those on the edge or outside have non-zero β_i . Similarly, the problem can be kernelized so that the prediction is expressed as

$$f(x) = \sum_i \beta_i k(x, x_i) + \omega_0 \quad (5.17)$$

In general, linear regression in the feature space is made by the following estimation function:

$$f(x) = \langle \omega, \phi(x) \rangle + b \quad (5.18)$$

Where $\phi(x)$ is the nonlinear mapping from the input space to the high-dimensional feature space, ω denotes the coefficients that need to be estimated, and b is a real constant that also has to be estimated. The support vector regression solves an optimization problem [86]:

$$\min \frac{1}{2} \omega^T \omega + C \sum_{i=1}^n (\xi_i + \xi_i^*) \quad (5.19)$$

subject to

$$y_i - \langle \omega, \phi(x_i) \rangle + b \leq \varepsilon + \xi_i^* \quad (5.20)$$

$$\langle \omega, \phi(x_i) \rangle + b - y_i \leq \varepsilon + \xi_i \quad (5.21)$$

$$\xi_i, \xi_i^* \geq 0 \quad (5.22)$$

where ξ_i^* is the slack variable of the upper training error (ξ_i is the lower one) subject to the ε -insensitive tube $|y - (\langle \omega, \phi(x) \rangle + b)| \leq \varepsilon$, The constant $C > 0$ determines the tradeoff between the flatness of f and its accuracy in capturing the training data. The constraints of (5.20)-

(5.22) imply that most of the data x_i are placed inside the tube ε . If x_i is outside the tube, there is an error ξ_i or ξ_i^* that needs to be minimized in the objective function. Support vector regression avoids underfitting and overfitting of the training data by minimizing the regularization term $\omega^T \omega$ as well as the training error $C \sum_{i=1}^n (\xi_i + \xi_i^*)$.

By introducing the Lagrange multipliers α_i and α_i^* , the support vector regression training procedure is to solve the dual problem of (5.19):

$$\min_{\alpha, \alpha^*} \frac{1}{2} \sum_{i,j=1}^n (\alpha_i - \alpha_i^*)(\alpha_j - \alpha_j^*) Q(x_i, x_j) + \varepsilon \sum_{i=1}^n (\alpha_i + \alpha_i^*) - \sum_{i=1}^n y_i (\alpha_i - \alpha_i^*) \quad (5.23)$$

subject to

$$\sum_{i=1}^n (\alpha_i - \alpha_i^*) = 0 \quad (5.24)$$

$$0 \leq \alpha_i, \alpha_i^* \leq C \quad (5.25)$$

where $Q(x_i, x_j) = \langle \phi(x_i), \phi(x_j) \rangle$ is the kernel function. In this dissertation, the Gaussian kernel as defined in (5.26) is used.

$$Q(x_i, x_j) = \exp(-\|x_i - x_j\|^2 / 2\sigma^2) \quad (5.26)$$

The support vector regression output is:

$$\hat{f}(x) = \sum_{i=1}^n (\alpha_i - \alpha_i^*) Q(x_i, x) + b \quad (5.27)$$

5.2.2 Data-driven Assessment by Multistage Support Vector Regression

The major issue in calculating the conservation voltage reduction factor is to estimate P_{cvroff} , which represents what the load would be if there were no voltage reduction during the conservation voltage reduction period. Fig. 5.3 demonstrates a peak-time conservation voltage reduction test result. The dark bold line represents the measured

load profile which can be divided into three parts: P_{pre} , P_{red} and P_{post} . P_{pre} represents the load consumption before voltage reduction is applied. P_{red} represents the load consumption during the voltage reduction period. P_{post} represents the load consumption after voltage reduction ends. Therefore, P_{pre} and P_{post} represent load consumption with the normal voltage level, and P_{red} represents the load consumption with reduced voltage level. The dotted line P_{est} in the figure shows what the load would be if there were no voltage reduction during the conservation voltage reduction period. The value of P_{est} cannot be measured, and has to be estimated if required.

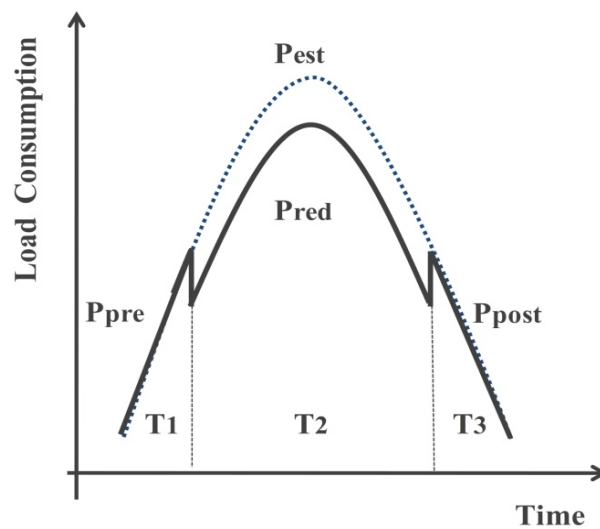


Figure 5.3. Demonstration of conservation voltage reduction test.

If P_{est} can be estimated, then the conservation voltage reduction factor can be calculated as follows:

$$CVR_f = \frac{(P_{est}(T_2) - P_{cvron}) / P_{est}(T_2)}{(V_{cvroff} - V_{cvron}) / V_{cvroff}} \quad (5.28)$$

where P_{cvroff} represent the active load consumption without conservation voltage reduction; V_{cvron} and V_{cvroff} represent the voltage with and without conservation voltage reduction, respectively.

In this dissertation, a multistage support vector regression-based technique is applied to estimate P_{est} so that the conservation voltage reduction factor can be calculated. One important characteristic of the conservation voltage reduction test data (i.e., load profiles with voltage reduction) is that P_{pre} and P_{post} can be used to find non-test load profiles (i.e., load profiles without voltage reduction) that are similar to the test profile. In order to estimate what the load consumption would be if there were no voltage reduction, the first step is to reconstruct the time series of the load consumption. In this dissertation, the load is represented by (5.29).

$$L_j = f(L_{j-1}, L_{j-7}, T_j, H_j) \quad (5.29)$$

where L_j represents load of day j , L_{j-1} and L_{j-7} are vectors representing load profiles of the previous day and of the same day in the previous week, T_j is a vector representing temperature profile of day j , H_j is a vector representing humidity profile of day j .

A load estimation model that is trained based on the entire available data is called global estimators. However, a better model can be trained by using only the set of points that are close to the point under estimation, which is defined as local estimators [87]. P_{pre} and P_{post} can be used to select load profiles that are similar to the current profile under estimation from the entire available load data so as to construct the local-estimator subset. Based on the above analysis, a multi-stage support vector regression framework is proposed in this dissertation and used to estimate P_{est} . As shown in Fig. 5.4, measurement

data such as power and voltage of both test days (i.e., reduced voltage is applied during test days) and non-test days (i.e., normal voltage is applied during non-test days) are stored in the database. The rest of the flowchart can be classified into three stages.

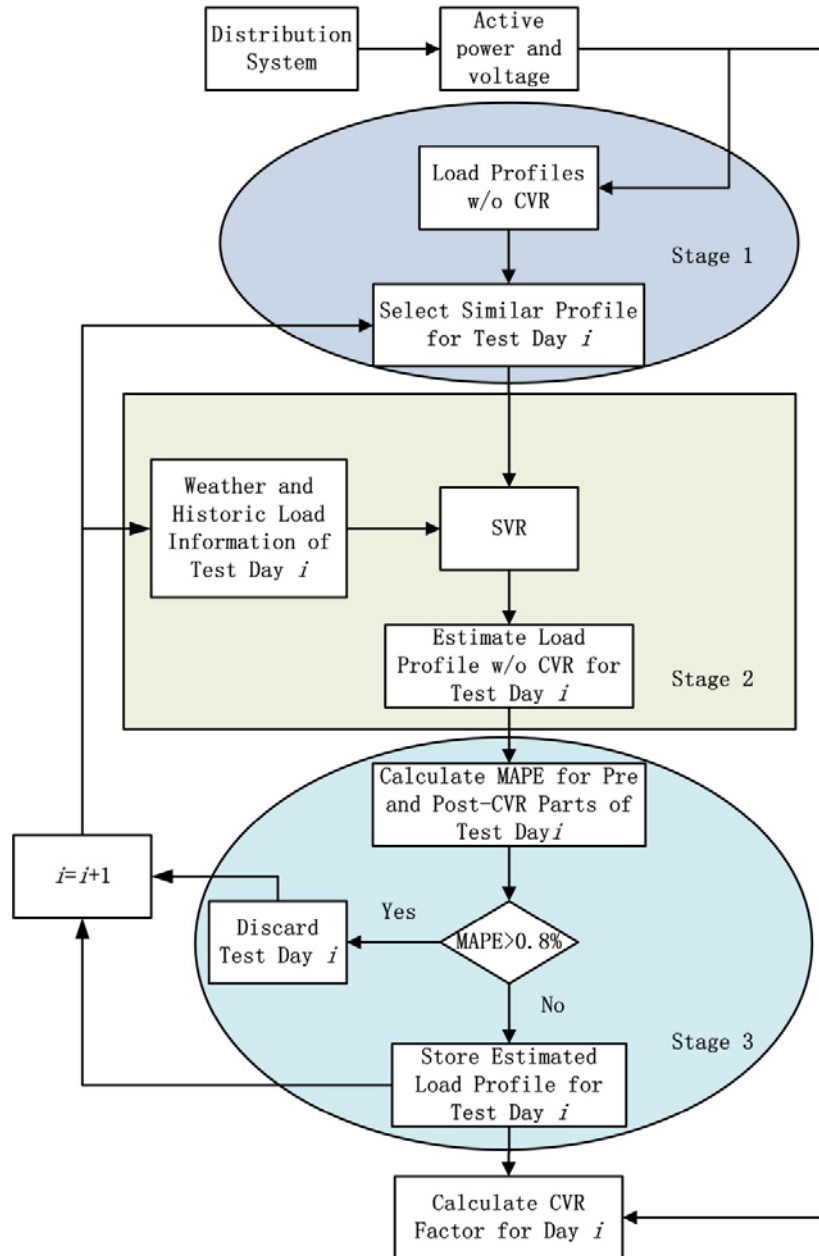


Figure 5.4. Multistage support vector regression framework for conservation voltage reduction analysis (MAPE represents mean average percentage error).

(1) First-stage: Select Similar Profiles by Euclidian Distance

The purpose of the first stage is to select load profiles that are similar to the current profile under estimation from all available historic data. The similarity between a non-test day k and the test day i is defined by a Euclidian distance-based index:

$$\varepsilon_{pk} = \sum_{\substack{i=1 \\ i \in T_1, T_3}}^N \frac{\sqrt{(P_i - P_{ik})^2}}{\max(P) \cdot N} \times 100\% \quad (5.30)$$

where ε_{pk} is the Euclidian distance-based power index for the k -th non-test day, P_i represents active load at time i on a conservation voltage reduction test day, P_{ik} represents active load at time i on k -th non-test day, T_1 and T_3 represent the pre-conservation voltage reduction period and post-conservation voltage reduction period as shown in Fig. 5.3, and $\max(P)$ represents the maximum active power of all load profiles under investigation. By this action, the differences of peak loads of all profiles are maintained. It is clear that the smaller the index, the closer the profile is to the one under estimation.

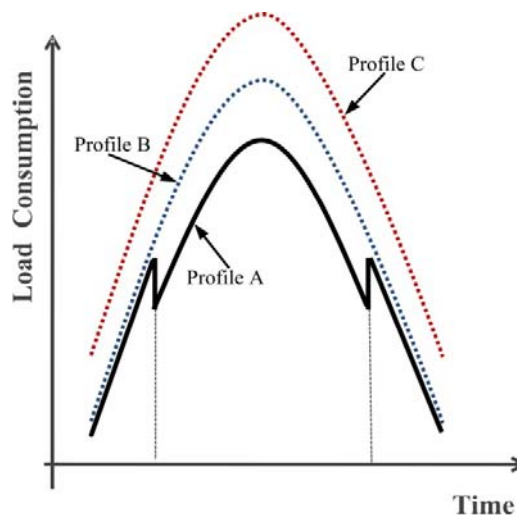


Figure 5.5. Load profiles with and without voltage reduction.

For example, Fig. 5.5 shows three measured load profiles. Profile A represents the load consumption on a voltage-reduction day. The purpose is to estimate what the load

would be if there were no voltage reduction in profile A. Profiles B and C represent the load consumption on two normal-voltage days. Compared with profile C, profile B is closer to profile A. Therefore profile B is included in the training set.

(2) Second-stage: Load Consumption Estimation

Support vector regression is used as the core algorithm in the second stage to estimate P_{est} . In order to show the performance of support vector regression, the support vector regression is compared with multi-linear regression using a practical dataset. Typical peak-time voltage reduction tests are performed by a utility company on five feeders. Overall, data of 275 days are recorded, of which 120 days are voltage-reduction days. Data of the 155 days without voltage reduction are used to evaluate the performances of support vector regression and multi-linear regression. For the 155 normal-voltage days, the load data of 55 days are randomly selected to be the validation set, and data of the remaining 100 normal-voltage days belong to the training set. The estimated load is represented as shown in (5.29). The multi-linear regression model used in this section is defined as

$$\begin{aligned} \hat{L}_j = & \beta_0 + \sum_{l=1,3,7} \beta_{1,l} L_{j-l} + \sum_{l=0,1,7} \beta_{2,l} T_{j-l} \\ & + \sum_{l=0,1,7} \beta_{3,l} T_{j-l}^2 + \sum_{l=0,1,7} \beta_{4,l} T_{j-l}^3 + \sum_{l=0,1,7} \beta_{5,l} H_{j-l} \\ & + \sum_{l=0,1,7} \beta_{6,l} H_{j-l}^2 + \sum_{l=0,1,7} \beta_{7,l} H_{j-l}^3 \end{aligned} \quad (5.31)$$

Fig. 5.6 shows estimation results of Feeder 1 on a day in February. The SVR model developed in this study has a better performance than the MLR benchmarking model as specified in (5.31).

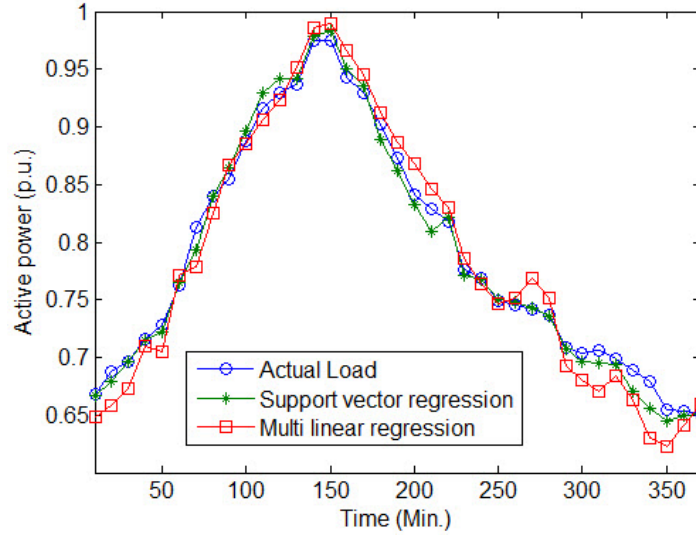


Figure 5.6. Comparison of support vector regression and multi-linear regression.

The estimation errors of support vector regression and the multi-linear regression benchmarking model in (5.31) are quantified by the mean absolute percentage error (MAPE), normalized mean square error (NMSE) and relative error percentage (REP). The definitions of mean absolute percentage error, normalized mean square error and relative error percentage are listed as follows [73]:

$$MAPE = \frac{1}{n} \sum_{i=1}^n \left| \frac{A_i - F_i}{A_i} \right| \quad (5.32)$$

$$NMSE = \frac{1}{n} \sum_{i=1}^n \frac{(A_i - F_i)^2}{\bar{A}\bar{F}}$$

$$\bar{A} = \frac{1}{n} \sum_{i=1}^n A_i \quad (5.33)$$

$$\bar{F} = \frac{1}{n} \sum_{i=1}^n F_i$$

$$REP = \sqrt{\frac{\sum_i (A_i - F_i)^2}{\sum_i A_i^2}} \times 100 \quad (5.34)$$

where A_i is the actual value and F_i is the forecasted value. Estimation errors of the days in the validation dataset are averaged and shown in Table 5.1. It can be seen that the support vector regression model provides better estimation than the MLR model.

Table 5.1. Estimation errors of support vector regression and multi-linear regression

	MAPE	REP	NMSE
Support vector regression	1.20	1.48	0.02
Multi-linear regression	3.81	4.22	0.06

The support vector regression model has smaller estimation errors than the multi-linear regression benchmarking model. Thus, support vector regression is used in the second stage for time-series learning and prediction. The results shown in Fig. 5.6 are calculated by models that are trained with the entire-period data. If the support vector regression model and the multi-linear regression model are trained with partial-period data (e.g., data of only periods T1 and T3 in Fig. 5.3), the performance may be different, but a detailed comparison and evaluation of this effect is not included in this study.

(3) Third-stage: Re-select Load Profiles

By taking advantage of the pre-selecting step, the proposed method is expected to have lower errors. However, the accuracy of conservation voltage reduction effect estimation is highly dependent on the accuracy of the estimated load. Detailed analysis of impacts of load estimation errors on conservation voltage reduction factor calculation can

be found in section 5.2.3. Lower conservation voltage reduction factors and higher mean absolute percentage errors can result in larger errors of the estimated conservation voltage reduction factors. In this stage, the estimated load profiles are re-selected to further reduce the estimation errors. Since P_{cvroff} is unknown on a voltage-reduction day, the mean absolute percentage errors between $P_{est}(T_1, T_3)$ and P_{pre} , P_{post} are used for re-selection. If the mean absolute percentage error is smaller than 0.8, P_{est} is stored for further analysis, otherwise, it is discarded.

In order to show the performance of the proposed multistage support vector regression model, this study calculates the relative errors between forecasted loads and actual loads in the validation dataset. The relative error of an estimation point i can be defined as

$$RE_i = \frac{A_i - F_i}{A_i} \quad (5.35)$$

where A_i is the actual value and F_i is the forecasted value. The mean of all the RE values is 0.134, and the variance is 0.0692.

The first stage of the proposed method is to select load profiles to form a training dataset. The data of voltage-reduction days cannot be used to verify whether the pre-selection of the training data can improve the accuracy of the load estimation since the load at the normal-voltage is unknown. As introduced before, data of 275 days are recorded, of which 120 days are voltage-reduction days. Data of the 155 days without voltage reduction are used to evaluate the performance improvement by conducting pre selection. Fig. 5.9 shows the load profile of one normal-voltage day. It is assumed that the first 50-minute data and the last 50-minute data are used to perform the pre-selection.

The Euclidian distance based indices of the remaining 154 normal-voltage days are calculated by (5.30) and ranked. For illustration, 120 days of these 154 days are selected to form the training dataset. If there is no pre-selection, all of the 154 normal-voltage days are included in the training set. Fig. 5.9 shows that the estimation performance of support vector regression is improved by performing the pre-selection. The mean average percentage estimation errors with pre-selection and without pre-selection are 0.29 and 0.78, respectively.

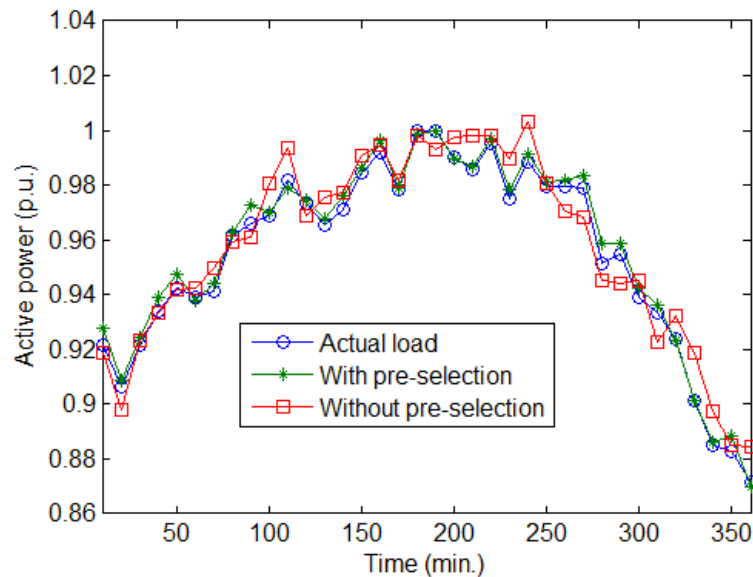


Figure 5.7. Comparison of support vector regression with and without pre-selection in forming the training dataset for a single normal-voltage day.

5.2.3 Impacts of Load Estimation Error on Conservation Voltage Reduction Assessment

Equations (5.36a)-(5.36d) show how load estimation errors impact the accuracy of conservation voltage reduction effect estimation. In (5.36d), CVR_{fe} represents the estimated conservation voltage reduction factor, and CVR_{fact} represents the actual conservation voltage reduction factor which is impossible to know. V_{cvron} and V_{cvroff}

represent voltage levels with and without voltage reduction, respectively. P_{cvron} represents the load consumption with voltage reduction, P_e represents the estimated load consumption without voltage reduction, P_{act} represents the actual load consumption if there were no voltage reduction and is unknown. $\tau = (P_{act} - P_e)/P_{act}$ represents the estimation error of the load consumption without voltage reduction. If there is no estimation error ($\tau = 0$), CVR_{fe} equals CVR_{fact} . Though CVR_{fact} is unknown, it can be seen that as $|\tau|$ becomes larger, CVR_{fe} differs more from CVR_{fact} . Moreover, the impacts of $|\tau|$ are enlarged if the conservation voltage reduction effect is small (γ approximates 1).

$$CVR_{fe} = \frac{(P_e - P_{cvron}) / P_e}{(V_{cvroff} - V_{cvron}) / V_{cvroff}} \quad (5.36a)$$

$$CVR_{fact} = \frac{(P_{act} - P_{cvron}) / P_{act}}{(V_{cvroff} - V_{cvron}) / V_{cvroff}} \quad (5.36b)$$

$$P_{act} = (1 + \tau)P_e, \gamma = P_{red} / P_{act} \quad (5.35c)$$

$$\frac{CVR_{fe}}{CVR_{fact}} = 1 + \tau + \frac{\tau}{1 - \gamma} + \frac{\tau^2}{1 - \gamma} \quad (5.36d)$$

Equation (5.36) has shown that the load estimation errors result in the errors of the calculated conservation voltage reduction factors.

In (5.36b), assume $\Delta V = (V_{cvroff} - V_{cvron}) / V_{cvroff}$, then

$$CVR_{fact} = \frac{(P_{act} - P_{red}) / P_{act}}{\Delta V} = \frac{1 - \gamma}{\Delta V} \quad (5.37)$$

$$1 - \Delta V \cdot CVR_{fact} = \gamma \quad (5.38)$$

By using (5.36d) and (5.38),

$$CVR_{fact} = \frac{CVR_{fe} - \tau/\Delta V - \tau^2/\Delta V}{1 + \tau} \quad (5.39)$$

For a calculated conservation voltage reduction profile, the band for the corresponding actual conservation voltage reduction factors can be calculated by (5.39) and using assumed load estimation errors.

Fig. 5.7 demonstrates the relationship among the mean absolute percentage errors of estimation, assumed actual conservation voltage reduction factors and errors of conservation voltage reduction effect estimation.

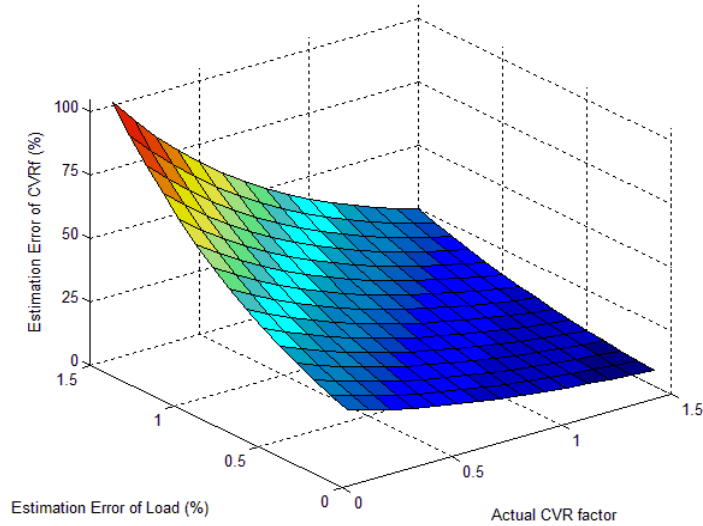


Figure 5.8. Relationship of estimation errors of load, actual conservation voltage reduction factors and estimation errors of conservation voltage reduction factors.

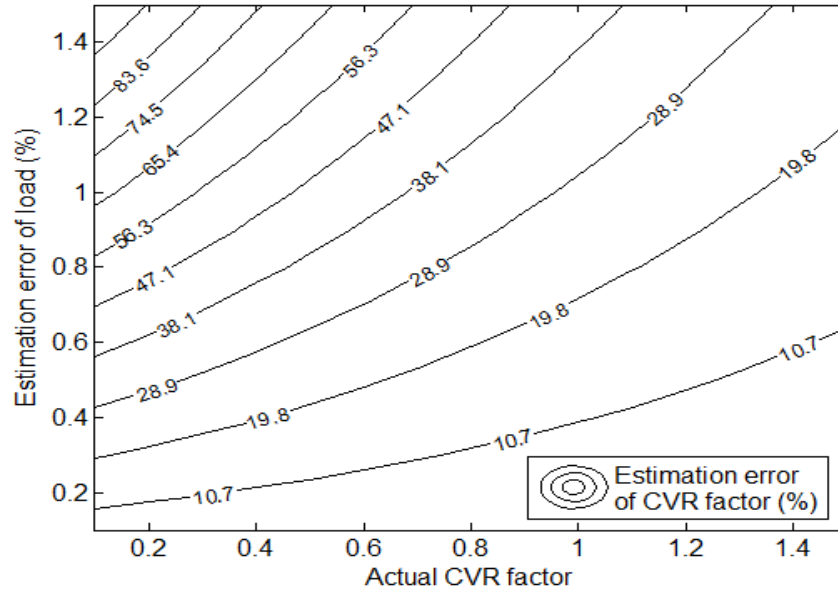


Figure 5.9. Contour of estimation errors of load, actual conservation voltage reduction factors and estimation errors of conservation voltage reduction factors.

Fig. 5.8 shows the contour of the relationship among estimation errors of load, actual conservation voltage reduction factors and estimation errors of conservation voltage reduction factors. For a certain conservation voltage reduction factor, higher load estimation errors indicate larger errors in the assessment of conservation voltage reduction effects. For a certain load estimation error, smaller conservation voltage reduction factors indicate larger errors in the assessment results, i.e., small conservation voltage reduction effects are more sensitive to the accuracy of load estimation. The above analysis of impacts of load estimation errors on conservation voltage reduction assessment can be used for all assessment methods that are based on estimating what the load would be if there were no voltage reduction. For example, the conservation voltage reduction factor is 0.84 for Avista Utility in Table 2.1. If the load estimation error is assumed to be $\tau = \pm 1\%$, and the voltage reduction level is assumed to be $\Delta V = 4\%$, then

the range of the actual conservation voltage reduction factors can be calculated by (5.39), and the actual CVR factors are within the range between 0.58 and 1.10 .

5.2.4 Numerical Studies for Data-driven Assessment

As discussed in section 5.2.2, the typical test data for a day can be divided into three parts: pre-conservation voltage reduction period, conservation voltage reduction period, and post-conservation voltage reduction period. The proposed multistage support vector regression is applied to estimate what the load would be if there were no voltage reduction. For illustration, Fig. 5.10 shows how the proposed method works to evaluate the conservation voltage reduction effect of Feeder 1 on one of the 120 voltage-reduction days. As shown in the figure, conservation voltage reduction starts at 140 minutes and ends at 420 minutes; this part of data is defined as P_{red} in Section 5.2.2. The first 140-minute data and the last 180-minute data are defined as pre-conservation voltage reduction (T_1) and post-conservation voltage reduction data (T_3), respectively. The load consumption without conservation voltage reduction on that test day is estimated by a trained model. The model is trained by data of 63 pre-selected normal-voltage days. To assess the conservation voltage reduction effects of other days, the model needs to be retrained by a new training set with reselected data. The estimated load and the load data with conservation voltage reduction are shown in Fig. 5.10.

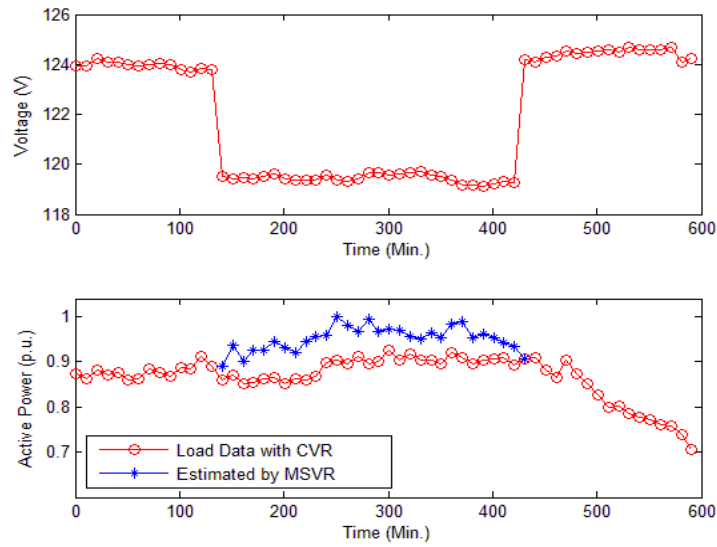


Figure 5.10. Voltage profile, actual load profile (with conservation voltage reduction) and estimated load profile by multistage support vector regression (MSVR based on 63 training days).

Fig. 5.11 shows conservation voltage reduction factors calculated by the multistage support vector regression. The conservation voltage reduction factors are not constant but always fluctuating and tend to decrease during test periods. Therefore, continuous monitoring and real-time conservation voltage reduction factor calculations are necessary.

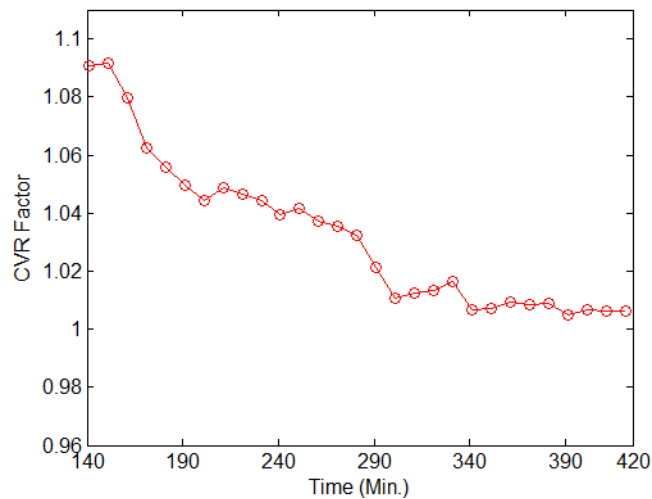


Figure 5.11. Conservation voltage reduction factors calculated by multistage support vector regression.

For the estimated CVR factors shown in Fig. 5.11, the band for the corresponding actual CVR factors can be calculated by (5.39) with the assumption that $\Delta V = 4\%$ and an assumed load estimation error of $\tau = \pm 1\%$, and the results are shown in Fig. 5.12. The upper bound of the actual CVR factors is about 125% of the estimated CVR factors, and the lower bound of the actual CVR factors is around 75% of the estimated CVR factors.

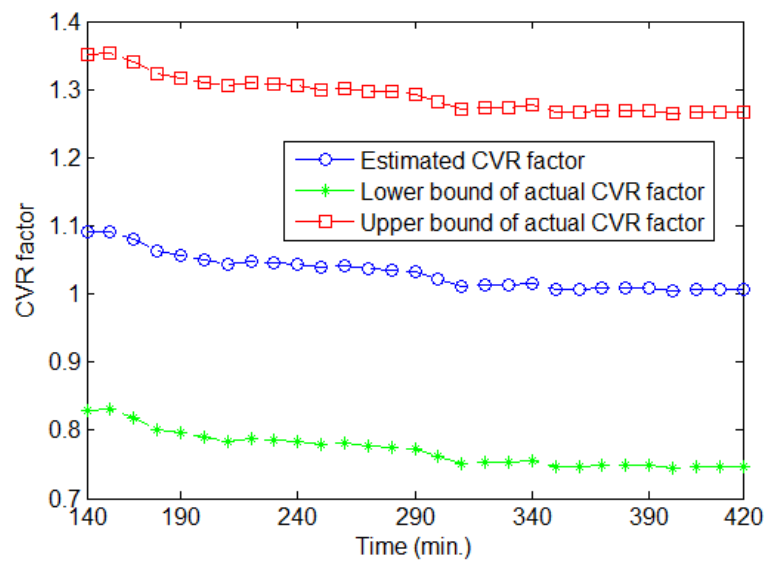


Figure 5.12. Band for actual conservation voltage reduction factors in data-driven assessment.

5.2.5 Statistical Analysis

Because of the variability of conservation voltage reduction factors, it is necessary to evaluate the conservation voltage reduction effect of each feeder in a probabilistic way. In order to compare the conservation voltage reduction performances of different feeders, the Kolmogorov-Smirnov goodness-of-fit test is applied in this study. The purpose of the test is to find a distribution (e.g., Normal distribution, Gamma distribution, etc) that can represent a dataset. The Kolmogorov-Smirnov test computes the test error ψ , which is the maximum vertical distance between an empirical cumulative distribution function and

a fitted cumulative distribution function. This error is compared to a critical value ψ_{crit} , and a probability distribution fit that satisfies $\psi \leq \psi_{crit}$ could be accepted. Fig. 5.12 shows the conservation voltage reduction factor for one voltage-reduction day of Feeder 1. Similar analyzes are performed for 10 voltage-reduction days of the same feeder and the results are summarized in Figs. 5.13 and 5.14.

Fig. 5.13 shows the differences between the cumulative distribution function of conservation voltage reduction factors of Feeder 1 and various other cumulative distribution functions (normal, Weibull with 2 parameters, Rayleigh and Exponential). The normal distribution is closest to the cumulative distribution of the feeder.

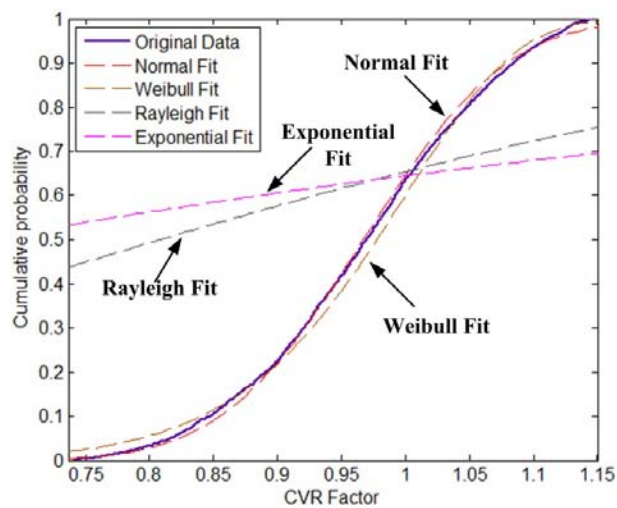


Figure 5.13. Cumulative probability of conservation voltage reduction factors of Feeder 1

Fig. 5.14 shows the histogram of the conservation voltage reduction factors of Feeder 1.

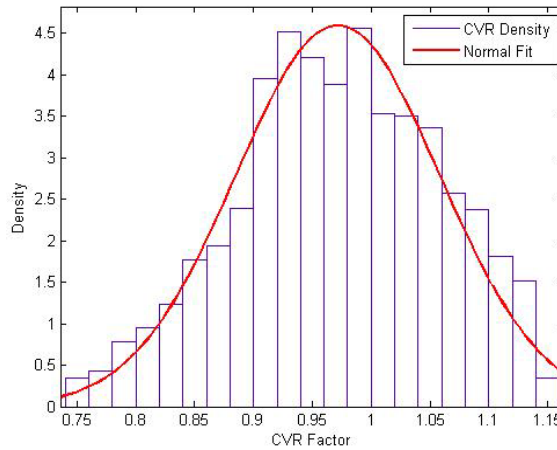


Figure 5.14. Histogram of CVR factors of Feeder 1.

Similar analyses can be performed for 10 voltage-reduction days of the other 4 feeders. Table 5.2 shows the Kolmogorov-Smirnov test errors subject to a normal distribution and the maximum likelihood estimates for parameters. μ is the mean and σ is the standard deviation, $\psi_{crit} = 0.0258$ for the normal distribution fit to the empirical distribution with a level of significance 5%.

Table 5.2. Results of conservation voltage reduction factor calculations of feeders

Feeder No.	ψ	μ (MEAN)	σ (STD)
1	0.0205	0.9716	0.0868
2	0.0122	1.1061	0.0697
3	0.0195	1.0191	0.0687
4	0.0209	1.0503	0.1056
5	0.0185	0.9702	0.1532

ψ represents the Kolmogorov-Smirnov test error, μ represents the mean, σ represents the standard deviation

Fig. 5.15 shows the cumulative normal distribution functions of conservation voltage reduction performances of all feeders. The cumulative normal distribution function gives

the probability that the variable CVR_f takes a value less than or equal to some specified value CVR_{f-spec} .

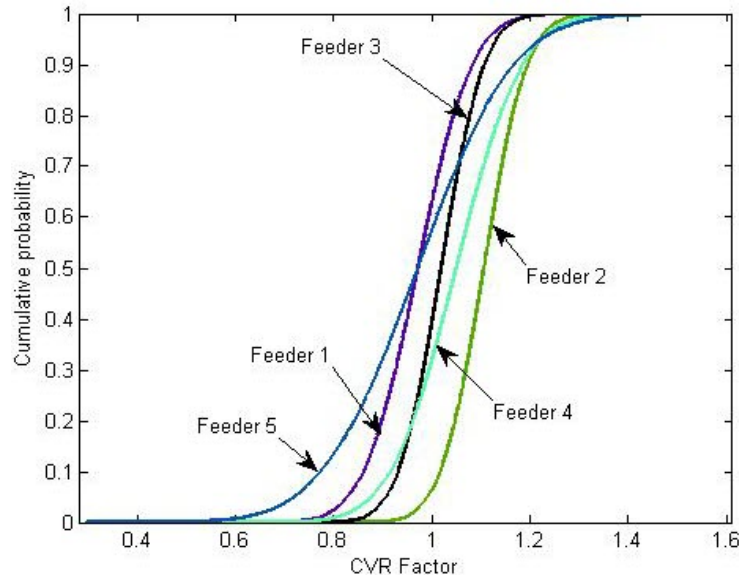


Figure 5.15. Cumulative normal distribution functions of conservation voltage reduction factors of all test feeders.

Table 5.3 summarizes conservation voltage reduction effects of the five studied feeders. It shows the percentiles, which represent the certainty level of achieving a conservation voltage reduction factor below a particular threshold. The CVR_{f-max} and CVR_{f-min} represent maximum and minimum conservation voltage reduction factors at different percentile levels. For example, if a line is drawn at 25% cumulative probability in Fig. 5.15, the intersections between the line and the cumulative distribution curves indicate that $CVR_{f-max}=1.0593$ (the rightmost intersection) and $CVR_{f-min}=0.8673$ (the leftmost intersection). For all five feeders, the minimum conservation voltage reduction factor is 0.6137; and the maximum conservation voltage reduction factor is 1.3279.

Table 5.3. Summary of conservation voltage reduction factors of all test feeders

Percentile	0%	25%	50%	75%	100
CVR_{f-max}	0.9444	1.0593	1.1062	1.1531	1.3279
CVR_{f-min}	0.6137	0.8673	0.9708	1.0303	1.1737

If there are no intersections among the cumulative distribution function curves like Feeders 1 and 3 in Fig. 5.15, then the cumulative distribution function on the far right of the cumulative distribution function chart offers the best opportunity for achieving the highest conservation voltage reduction factor at every confidence level, and this feeder is the best conservation voltage reduction candidate. If the cumulative distribution function curves intersect (as they are in this example), then the best feeder is the one that gives the highest conservation voltage reduction factor with the predefined certainty level. For the cumulative distribution function curves in Fig. 5.15, if the certainty level is defined to be 90% for example, then it is clear that Feeder 2 is the best candidate and Feeder 1 exhibits the worst performance.

5.3 Model-driven Assessment

In section 5.2, a multistage support vector regression-based method is proposed to assess the conservation voltage reduction effects. This method requires historic load data to train the support vector regression model. Moreover, it can only be applied to assess the peak-time conservation voltage reduction since the load consumption before voltage reduction and after voltage reduction ends is needed in the first stage of the proposed method. In this section, a new method based on load model identification is presented to assess the conservation voltage reduction effects. The proposed method in this section

can be applied to assess the load reduction effects of both peak-time and continuous conservation voltage reduction. Most of the previous methods to assess conservation voltage reduction effects are based on the idea to estimate what the load would be if there were no voltage reduction during the conservation voltage reduction period and then do the comparison. In this section, a new method to assess conservation voltage reduction effects is proposed. It is assumed in this method that loads can be modeled as functions of the supplied voltage. The conservation voltage reduction effects can be assessed by estimating the load-to-voltage sensitivities in these functions. For example, conservation voltage reduction effects decrease when load-to-voltage sensitivities change from a constant-impedance type load to a constant-power type. Conservation voltage reduction factors can be calculated by identifying the time-varying load-to-voltage sensitivities.

5.3.1 Load Model Identification

Load model identification refers to the process of finding a particular model that satisfactorily (in some sense) describes the observed load behaviors, which is in fact a parameter estimation problem [92]. Let $z(t)$ denote the piece of data received at time t . $z(t)$ is in general a vector, composed of several different measurements. By assuming that the data acquisition takes place in a discrete manner, a sequence of measurements $z(1)$, $z(2)$, ..., $z(t)$ is assumed to be received at time t . The objective of identification is to infer a model of the system from the record $z(t)$, $z(t-1)$, ..., $z(1)$. For example, $z(t)$ can be the voltage and power measurements at a substation, and the objective is to find a model to represent the load-to-voltage relationship from $z(t)$.

Normally, a model is parameterized in terms of a parameter vector θ , so the objective of identification is actually to determine this vector. Consider the following model:

$$y(t) = \theta^T \varphi(t) + \varepsilon(t) \quad (5.40)$$

where θ represents the parameter set to be estimated, $y(t)$ and $\varphi(t)$ represent measurements, $\varepsilon(t)$ represents the model error, and $t=1,2,\dots, N$. The following objective function can be minimized with respect to θ to estimate the parameter set.

$$\varepsilon_N(\theta) = \frac{1}{N} \sum_1^N [y(t) - \theta^T \varphi(t)]^2 \quad (5.41)$$

Since the objective function (5.41) is quadratic in θ , it can be minimized analytically as follows:

$$\hat{\theta}(N) = \left[\sum_{t=1}^N \varphi(t) \varphi^T(t) \right]^{-1} \sum_{t=1}^N \varphi(t) y(t) \quad (5.42)$$

where $\hat{\theta}$ represents the estimated parameter values. Equation (5.42) is the least squares estimation and can be written in a recursive fashion as shown in [92].

It has been shown in [111] that the normal operating data of power system variables (e.g., load consumption, voltage, etc) with small variations can be used to estimate the parameters of load models.

5.3.2 Model-Driven Assessment of Conservation Voltage Reduction Effects

As shown in equation (5.1), the conservation voltage reduction factor can be defined as the relating change in active load consumption to the change in voltage. Since active power consumption has a direct economic impact on distribution network operators and

customers, this section focuses on active power reduction effects. The reactive power reduction effects are not included in this study. The conservation voltage reduction factor and conservation voltage reduction effects discussed in this section specifically refer to the active conservation voltage reduction factor and active conservation voltage reduction effects. Conservation voltage reduction factors are calculated in this section by identifying the time-varying load-to-voltage sensitivities. The first step is to model the load as a function of voltage. A substation supplies power to thousands of load components, such as lights, motors and so on. As it is impossible to model every individual load, the load model for a substation is usually an aggregate model to represent the overall load behaviors of all downstream loads and associated equipments.

Karlsson and Hill proposed an exponential recovery load model as follows [78]:

$$T_p \dot{P}_r(t) = -P_r(t) + P_0 \left(\frac{V}{V_0}\right)^{k_{ps}} - P_0 \left(\frac{V}{V_0}\right)^{k_{pt}} \quad (5.43)$$

$$P_d = P_r + P_0 \left(\frac{V}{V_0}\right)^{k_{pt}} \quad (5.44)$$

$$T_q \dot{Q}_r(t) = -Q_r(t) + Q_0 \left(\frac{V}{V_0}\right)^{k_{qs}} - Q_0 \left(\frac{V}{V_0}\right)^{k_{qt}} \quad (5.45)$$

$$Q_d = Q_r + Q_0 \left(\frac{V}{V_0}\right)^{k_{qt}} \quad (5.46)$$

where P_r and Q_r represent the recovery load states for real and reactive power, respectively, P_d and Q_d represent the real and reactive power demand, respectively, P_0 and Q_0 represent the nominal real and reactive power, respectively, T_p and T_q represent the real and reactive load recovery time constant, respectively, k_{ps} and k_{qs} represent the

steady-state real and reactive load-to-voltage dependences, respectively, k_{pt} and k_{qt} represent the transient-state real and reactive load-to-voltage dependences, respectively, V and V_0 represent the measured and nominal voltage, respectively.

Equations (5.43-5.46) use an exponential recovery process to express the relationship between power consumption and voltage reduction. The active part of the steady-state model is in the following form:

$$P_d = P_0 \left(\frac{V}{V_0} \right)^{k_{ps}} \quad (5.47)$$

Equation (5.47) represents the exponential load model which is one of the most widely used load models to express the input-output relationship between power and voltage. Since the purpose of this study is to analyze energy-saving effects, the steady-state model defined in (5.47) can be used. As it is obvious that the load consumption is changing with time due to factors such as human behaviors, weather conditions and continuous on/off switches of different kinds of loads, parameters of the load model are not constants. Even for the same circuit, different load models may be found at different times. Hence, a time-varying exponential load model is proposed in this study as:

$$P = P_0(t) \left(\frac{V(t)}{V_0} \right)^{k_p(t)} \quad (5.48)$$

where $P_0(t)$ and $k_p(t)$ are time-varying model parameters that need to be identified. Since these two parameters are continuously varying with the time, a recursive identification is required. In this dissertation, a nonlinear Kalman-filter based estimator, also called the unscented Kalman filter [98] is used to perform the recursive estimation of model parameters. The unscented Kalman filter has long been used as a dynamic state estimator.

Compared to the extended Kalman filter, the unscented Kalman filter does not require the model to be linearized.

The unscented Kalman filter is an efficient recursive filter able to solve state estimation problems [98]. This filter eliminates the inaccuracies introduced by the extended Kalman filter by utilizing a nonlinear unscented transform, which does not require the calculation of derivatives or linearization of the nonlinear model. Consider a nonlinear system modeled by the discrete time state equation

$$\begin{aligned}x_k &= f(x_{k-1}) + q_k \\y_k &= h(x_k) + r_k\end{aligned}\tag{5.49}$$

where $x \in \mathfrak{R}^L$ is a discrete state vector; $y \in \mathfrak{R}^p$ is a discrete measurement vector; $f(\cdot)$ and $h(\cdot)$ are non-linear mapping functions representing the system and measurement models in term of the state variables; q and r are a Gaussian process and measurement noise with zero mean and covariance matrices Q and R , respectively. The values of q and r affect the performance of the unscented Kalman filter, and the impacts of these values on the state estimation are discussed in section 5.3.4. The procedure for implementation of an unscented Kalman filter is as follows [112]:

A. Sigma Points Calculation

The calculation of sigma points is based only on the knowledge about variable x . Given a $L \times 1$ state vector \hat{x}_{k-1} at time step $k-1$ and state error covariance matrix P_{k-1} , compute a set of $2L+1$ sigma points from:

$$\begin{aligned}\chi_{1,k-1} &= \hat{x}_{k-1} \\ \chi_{i,k-1} &= \hat{x}_{k-1} + (\sqrt{(L+\lambda)P_{k-1}})_i, \quad i = 2, \dots, L+1 \\ \chi_{i,k-1} &= \hat{x}_{k-1} - (\sqrt{(L+\lambda)P_{k-1}})_i, \quad i = L+2, \dots, 2L+1\end{aligned}\tag{5.50}$$

where the parameter λ decides the spread of i -th sigma point around \hat{x}_{k-1} . The points are scaled further from \hat{x}_{k-1} if $\lambda > 0$ and are scaled towards \hat{x}_{k-1} if $\lambda < 0$. λ can be defined as

$$\lambda = \alpha^2(L + \kappa) - L \quad (5.51)$$

where α is a small constant, usually set to 10^{-3} , and can be used to control the amount of the higher-order nonlinearities around \hat{x}_{k-1} . κ is another scaling parameter which is usually set to 0 or $3-L$ to ensure that the kurtosis of the sigma point distribution agrees with the kurtosis of a Gaussian distribution. The square root of the positive definite matrix $(L + \lambda)P_{k-1}$ can be computed by using the Cholesky decomposition. Each column of the sigma point matrix is propagated one step ahead through the dynamic process function $f(\cdot)$ to calculate the transformed sigma points at time step k :

$$\mathcal{X}_{i,k} = f(\mathcal{X}_{i,k-1}), \quad i = 1, \dots, 2L + 1 \quad (5.52)$$

B. Time Update

A prior state estimate \hat{x}_k^- and its corresponding covariance matrix P_k^- are approximated by the weighted mean and covariance of the transformed sigma points:

$$\begin{aligned} \hat{x}_k^- &= \sum_{i=1}^{2L+1} W_i^{(m)} \mathcal{X}_{i,k} \\ P_k^- &= \sum_{i=1}^{2L+1} W_i^{(c)} [(\mathcal{X}_{i,k} - \hat{x}_k^-)(\mathcal{X}_{i,k} - \hat{x}_k^-)^T] + Q \end{aligned} \quad (5.53)$$

where Q is the process noise covariance matrix. The weights $W_i^{(m)}$ and $W_i^{(c)}$ are defined as:

$$W_1^{(m)} = \frac{\lambda}{L + \lambda} \quad (5.54)$$

$$W_i^{(m)} = \frac{1}{2(L + \lambda)}, \quad i = 2, \dots, 2L + 1 \quad (5.55)$$

$$W_1^{(c)} = \frac{\lambda}{L + \lambda} + (1 - \alpha^2 + \beta) \quad (5.56)$$

$$W_i^{(c)} = \frac{\lambda}{2(L + \lambda)}, \quad i = 2, \dots, 2L + 1 \quad (5.57)$$

where β is a parameter used to incorporate prior knowledge of the higher order moments of the state distribution. The optimal choice of β for Gaussian distribution is 2.

C. Measurement Update

The measurements are taken into account in this step. The observations at time step k are calculated as the weighted sum of the projection of transformed sigma points through the measurement function $h(\cdot)$:

$$\begin{aligned} Y_{i,k} &= h(\chi_{i,k}), \quad i = 1, \dots, 2L + 1 \\ \hat{y}_k^- &= \sum_{i=1}^{2L+1} W_i^{(m)} Y_{i,k} \\ P_{\hat{y}_k} &= \sum_{i=1}^{2L+1} W_i^{(c)} [(Y_{i,k} - \hat{y}_k^-)(Y_{i,k} - \hat{y}_k^-)^T] + R \\ P_{\hat{x}_k, \hat{y}_k} &= \sum_{i=1}^{2L+1} W_i^{(c)} [(\chi_{i,k} - \hat{x}_k^-)(Y_{i,k} - \hat{y}_k^-)^T] \end{aligned} \quad (5.58)$$

where R is the measurement noise covariance matrix. The posterior state estimate and its error covariance matrix can be calculated as:

$$\begin{aligned}
K_k &= P_{\hat{x}_k, \hat{y}_k} P_{\hat{y}_k}^{-1} \\
\hat{x}_k &= \hat{x}_k^- + K_k (y_k - \hat{y}_k^-) \\
P_k &= P_k^- - K_k P_{\hat{y}_k} K_k^T
\end{aligned} \tag{5.59}$$

In order to estimate parameters of the time-varying exponential load model, the problem has to be represented in the state-space form required by unscented Kalman filter as follows:

$$\begin{aligned}
x_1 &= P_0 \\
x_2 &= k_p
\end{aligned} \tag{5.60}$$

which are related through a linear state mapping and a nonlinear measurement mapping as follows:

$$\begin{aligned}
x_{1,k+1} &= x_{1,k} \\
x_{2,k+1} &= x_{2,k} \\
y_{k+1} &= x_{1,k+1} (V_{k+1})^{x_{2,k+1}}
\end{aligned} \tag{5.61}$$

The proposed identification algorithm therefore requires only load consumption data and voltage, which can be easily obtained from utilities [89].

Fig. 5.16 shows a schematic of the time-varying framework for conservation voltage reduction assessment.

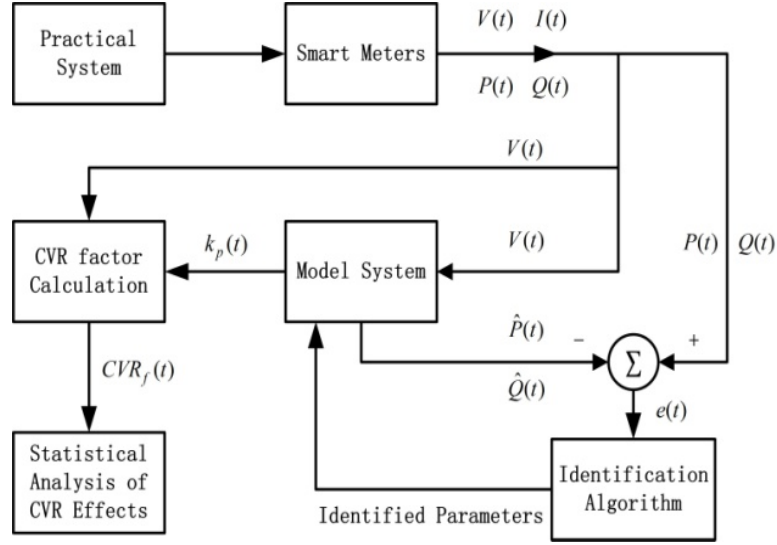


Figure 5.16. Time-varying load modeling framework for assessing conservation voltage reduction effects.

Measurement devices are installed at substations to continuously monitor system operations. The measurement devices provide the basic operation data, such as real and reactive power and voltage. To identify load models in (5.48), the identification algorithm, which is the unscented Kalman filter in this dissertation, tunes the parameter set so as to minimize the difference between model output $\hat{P}(t)$ and measured system output $P(t)$. The time step for the time-varying load modeling is set to be one-minute in this dissertation.

For the identified load parameters, the corresponding conservation voltage reduction factors can be calculated as follows:

$$CVR_f = \frac{\%Load\ Change}{\%Voltage\ Reduction} = \frac{(P_{cvroff} - P_{cvron}) / P_{cvroff}}{(V_{cvroff} - V_{cvron}) / V_{cvroff}} \quad (5.62)$$

$$CVR_f = \frac{(P_{cvroff} - P_{cvron}) / P_{cvroff}}{(V_{cvroff} - V_{cvron}) / V_{cvroff}} \quad (5.63)$$

$$P_{cvroff} = P_0 \left(\frac{V_{cvroff}}{V_0} \right)^{k_p(t)} \quad (5.64)$$

$$P_{cvron} = P_0 \left(\frac{V_{cvron}}{V_0} \right)^{k_p(t)} \quad (5.65)$$

$$CVR_f = \left(1 - \left(\frac{V_{cvron}}{V_{cvroff}} \right)^{k_p(t)} \right) / \left(1 - \left(\frac{V_{cvron}}{V_{cvroff}} \right) \right) \quad (5.66)$$

The proposed identification algorithm requires only load consumption data and voltage, which can be easily obtained from utilities.

As discussed in section 2.3.3, two frequently used methods to assess the performance of conservation voltage reduction are the comparison method and the regression method. In the comparison method, the reduced voltage is applied to one feeder, and the normal voltage is applied to another feeder. The difference of load consumptions of the two feeders are compared, and used to calculate the conservation voltage reduction factor. In the regression method, a linear regression model is used to represent loads. The load consumption without voltage reduction can be estimated from the regression model. The basic idea of these two existing methods is to estimate what the load would be if there were no voltage reduction (i.e., P_{est} in Fig. 5.3). In contrast, the proposed method in this section is to calculate conservation voltage reduction factors by using exponential load models to represent loads and estimating the load-to-voltage sensitivities. Therefore, the proposed method does not estimate P_{est} , and no comparison is needed.

Table 5.4 summarizes the ideas and attributes of the existing approaches and the proposed solution in this section.

Table 5.4. Comparison of existing approaches and proposed method for assessment of conservation voltage reduction effects

Methods	Descriptions	Attributes
Comparison method	Compare load with and without voltage reduction	Easy and straightforward Difficult to find a good control group
Regression method	Estimate by P_{est} regression method	Clear physical meaning Linear model and regression errors
Proposed method in section 5.3	Model loads as a function of voltage without estimating P_{est} , and calculate CVR factor from load-to-voltage sensitivity	No control group is needed, no day on/day off tests

5.3.3 Simulation Verification

Example 1

In practice, noise can exist in the measurement data. Meanwhile, load-to-voltage sensitivities can change in a continuous manner. Therefore, it is necessary to verify the performance of the proposed method before applying it to the field data. The purposes of this simulation example are: (1) test the performance of the proposed method in noise-filtering; (2) test the performance of the proposed method in estimating and tracking the non-linear and continuous change of load-to-voltage sensitivities.

The non-linear signal considered is given by

$$y_k = A_k c_k^{b_k} + \varepsilon_k \quad (5.67)$$

where A_k , c_k , b_k and ε_k are the amplitude, base, exponent and Gaussian noise, respectively. For tracking the non-linear change, A_k and b_k are set as follows for purposes of illustration:

$$A_k = 0.2 * \sin(k) + 1 \quad (5.68)$$

$$b_k = 0.5 * \sin(k) + 1 \quad (5.69)$$

Fig. 5.17 shows the profile of c_k , which is used in this example. The variation of c_k in Fig. 5.17 is set to be relatively small since the natural variation of the voltage in (5.48) is small in power systems. The signal-to-noise ratio (SNR) of c_k shown in Fig. 5.17 is 35 dB.

The non-linear signal y_k becomes

$$y_k = [0.2 * \sin(k) + 1] * c_k^{[0.5 * \sin(k) + 1]} + \varepsilon_k \quad (5.70)$$

where ε_k represents the white noise with a standard deviation of $0.9\% \times y_k$.

To test the estimation performance of the unscented Kalman filter, it is assumed that y_k and c_k are measurements, and A_k and b_k are the parameters that need to be estimated. The problem can be summarized as follows:

- Signal is represented by an exponential model $y = Ac^b$
- Measurements: y_k and c_k
- Parameters to be estimated: \hat{A}_k and \hat{b}_k

The values of process noise q and measurement noise r affect the estimation results of the unscented Kalman filter. To illustrate the effects of q and r , it is assumed that q and r can have values that vary within the following set,

$$q, r \in (0.01, 0.02, 0.03, 0.04, 0.05, 0.06, 0.07, 0.08, 0.09, 0.10) \quad (5.71)$$

The above set has ten elements. Therefore, there are 100 combinations of q and r . The unscented Kalman filter based estimation is run for each combination of q and r . Fig. 5.18 shows the mean average estimation errors between the actual y_k and the estimated \hat{y}_k . The smallest error in Fig. 5.18 (MAPE=0.0190) is the result with the combination of $q=0.05$, and $r=0.04$. Fig. 5.19 compares the actual values of b_k which is defined in (5.69) and the estimated values of \hat{b}_k by the unscented Kalman filter with $q=0.05$, and $r=0.04$. Fig. 5.20 shows the actual values of A_k which is defined in (5.68) and the estimated values of \hat{A}_k . For this simulated signal, the results show that the unscented Kalman filter can track the non-linear change of the parameters.

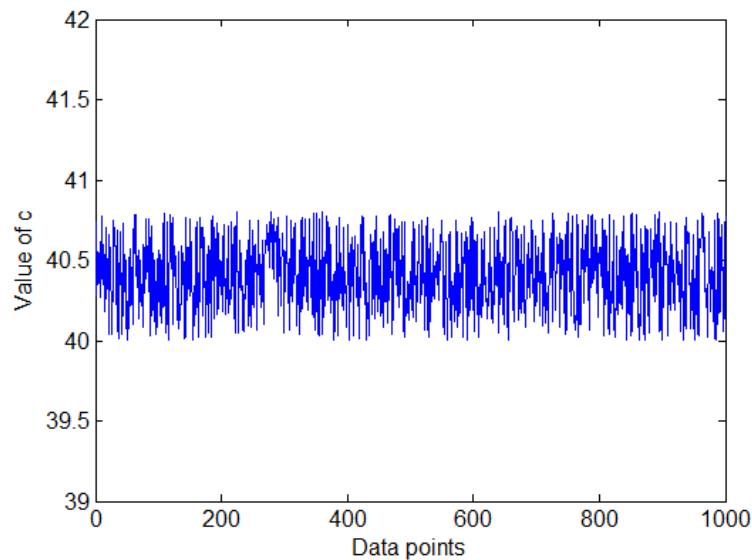


Figure 5.17. Values of c .

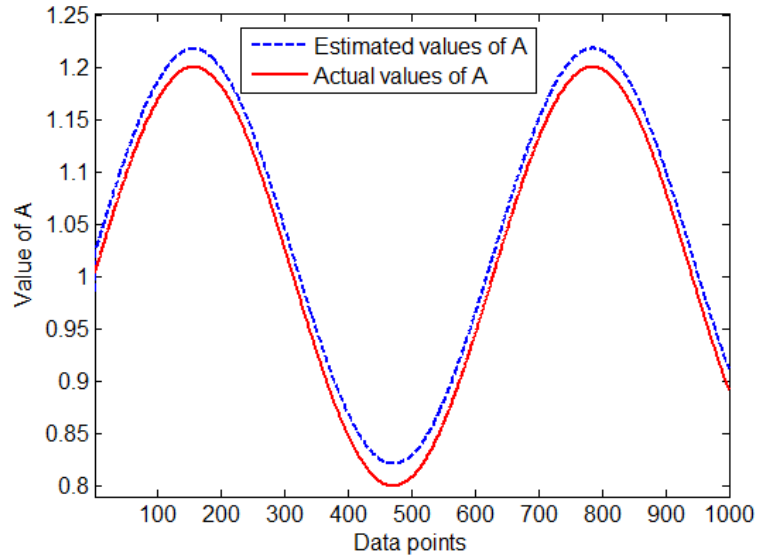


Figure 5.20. Actual and estimated values of A.

Example 2

In this example, the conservation voltage reduction is illustrated on the IEEE 123-bus distribution system as shown in Fig. 5.21. Detailed descriptions about the distribution system can be found in [113]. OpenDSS [114] is used to simulate the load and voltage profiles with and without voltage reduction. By using OpenDSS, it is possible to simulate what the load would be if there were no voltage reduction. Therefore, the actual conservation voltage reduction factors can be calculated by (5.1).

Fig. 5.22 shows the simulated voltage profiles with and without voltage reduction. A 3% voltage reduction is applied to the substation transformer. The voltage reduction starts at 20 minutes and ends at 80 minutes. The load consumption profiles with and without voltage reduction measured at the substation is shown in Fig. 5.23.

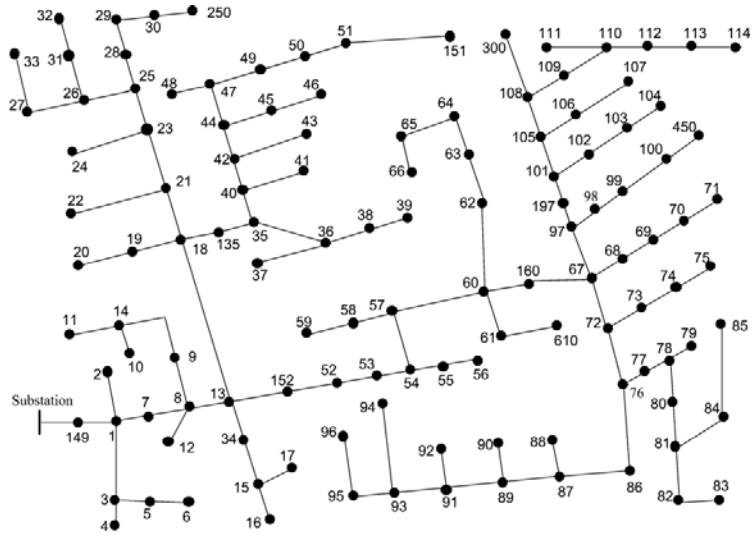


Figure 5.21. IEEE 123-bus distribution system.

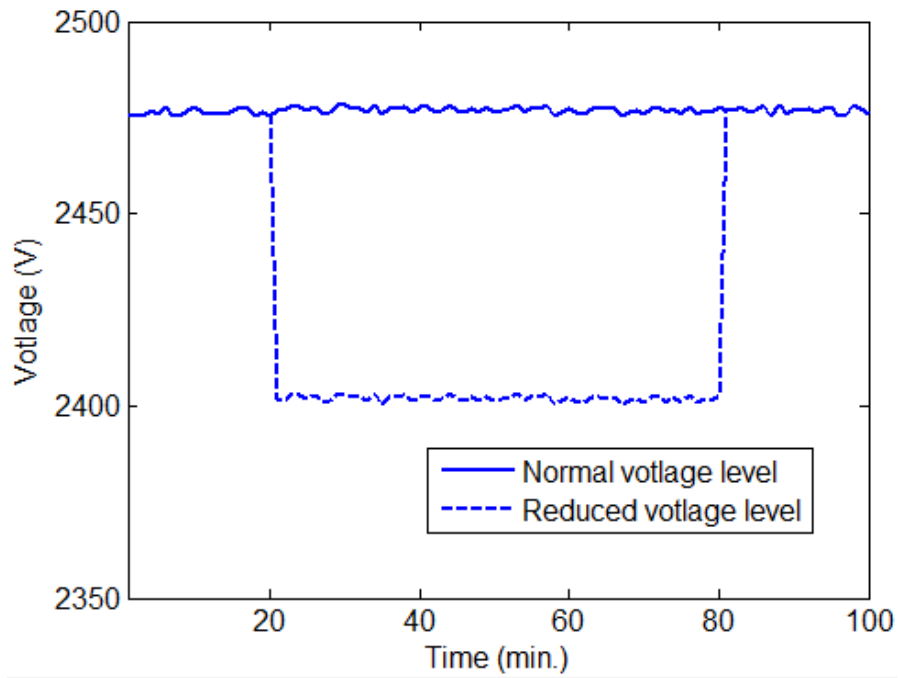


Figure 5.22. Voltage profiles with and without conservation voltage reduction in simulation example 2.

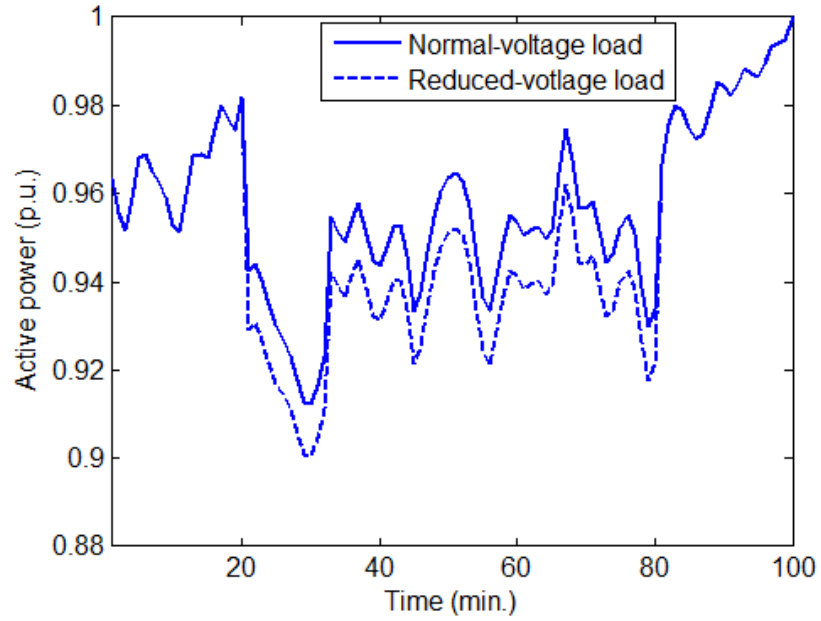


Figure 5.23. Load profiles with and without voltage reduction in simulation example 2.

The exponential load model defined in (5.48) is used to represent the load. The unscented Kalman filter algorithm is then applied to estimate the load-to-voltage sensitivities and the conservation voltage reduction factors are calculated from the estimated load-to-voltage sensitivities by using (5.66).

The initial values of P_0 and k_p as well as the values of process noise q and measurement noise r affect the estimation results. To illustrate these affects, it is assumed that $P_0(0)$, $k_p(0)$ could have values that vary within the following set,

$$P_0(0), k_p(0) \in (0.1, 0.2, 0.3, 0.4, 0.5, 0.6, 0.7, 0.8, 0.9, 1.0) \quad (5.72)$$

It is also assumed that q and r could have values that vary within the following sets,

$$\begin{aligned} q &\in (0.01, 0.02, 0.03, 0.04, 0.05) \\ r &\in (0.001, 0.002, 0.003, 0.004, 0.005) \end{aligned} \quad (5.73)$$

Therefore, there are 2500 combinations of $P_0(0)$, $k_p(0)$, q and r . The unscented Kalman filter based estimation is run for each combination of $P_0(0)$, $k_p(0)$, q and r . Fig. 5.24 shows the mean average estimation errors. In Fig. 5.24, the smallest error (MAPE=0.0086) is the result with the combination of $P_0(0)=0.5$, $k_p(0)=0.4$, $q=0.02$, and $r=0.005$.

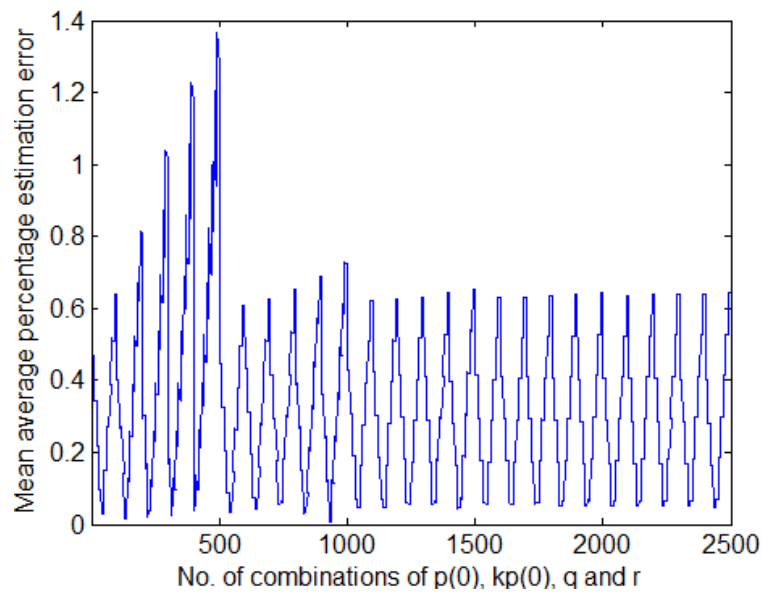


Figure 5.24. Mean average percentage estimation errors with different values of $P(0)$, $k_p(0)$, q and r in simulation example 2.

Fig. 5.25 shows the model outputs $\hat{P}(t)$ calculated from the estimated load model and the simulated active power $P(t)$. The solid line represents the simulated active power. The dashed line represents the active power calculated from the estimated load models with the combination of $P_0(0)=0.5$, $k_p(0)=0.4$, $q=0.02$, and $r=0.005$. To demonstrate the impacts of initial values of P_0 and k_p as well as the values of q and r on

the estimation, the results by using the combination of $P_0(0)=0.5$, $k_p(0)=0.4$, $q=0.02$, $r=0.005$ and $P_0(0)=0.5$, $k_p(0)=0.4$, $q=0.02$, $r=0.005$ are also shown.

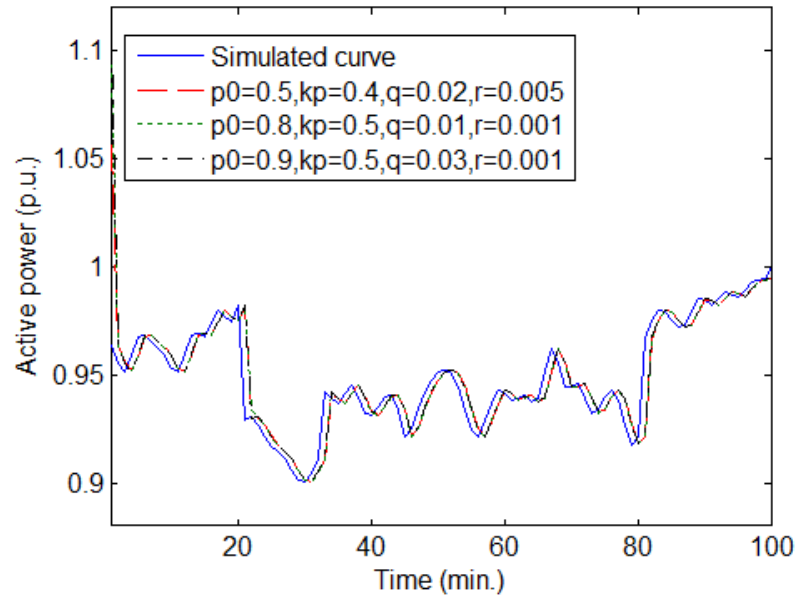


Figure 5.25. Simulated and estimated load profiles with different combinations of $P(0)$, $k_p(0)$, q and r in simulation example 2.

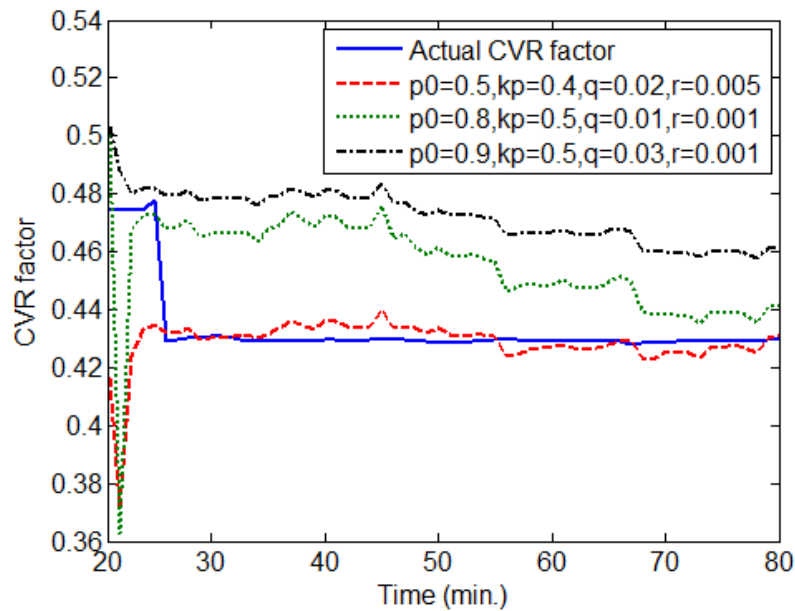


Figure 5.26. Comparison of actual and estimated conservation voltage reduction factors in simulation example 2.

Since the load and voltage profiles with and without voltage reduction can be simulated, the actual conservation voltage reduction factor can be calculated and is shown in Fig. 5.26. This figure also shows the estimated conservation voltage reduction factors by using three combinations of $P_0(0)$, $k_p(0)$, q and r . The values of $P_0(0)$, $k_p(0)$, q and r of the unscented Kalman filter affects the assessment results. The calculated conservation voltage reduction factors vary with different values of $P_0(0)$, $k_p(0)$, q and r . It is therefore suggested to select the combination that results in the smallest mean average percentage estimation error as the values of the unscented Kalman filter algorithm (i.e., $P_0(0)=0.5$, $k_p(0)=0.4$, $q=0.02$, $r=0.005$ in this example). In Fig. 5.26, the unscented Kalman filter with the combination of $P_0(0)=0.5$, $k_p(0)=0.4$, $q=0.02$, $r=0.005$ also results in an estimated conservation voltage reduction factor that is closest to the actual conservation voltage reduction factor.

5.3.4 Numerical Studies for Model-driven Assessment

As discussed in section 5.3.2, an exponential load model is used to represent the load-to-voltage relationship. Then conservation voltage reduction factors can be calculated from parameters of the exponential load model as shown in (5.66). There are two ways to show the performance of the proposed method. The first way is to compare the model output $\hat{P}(t)$ and the measured active power $P(t)$. $P(t)$ represents the active power consumption at the substation, and can be measured directly from measurement devices. In (5.74), $\hat{P}(t)$ represents the output of the exponential load model with the estimated model parameters.

$$\hat{P}(t) = \hat{P}_0 \left(\frac{V(t)}{V_0} \right)^{\hat{k}_p(t)} \quad (5.74)$$

where $V(t)$ is the measured voltage at the substation, $\hat{P}_0(t)$ and $\hat{k}_p(t)$ are model parameters estimated by the unscented Kalman filter.

If $\hat{P}(t)$ is close to $P(t)$, then the model parameters estimated by the unscented Kalman filter are reasonable, and the exponential load model can track the load behaviors. In this section, the mean average percentage error (MAPE) is used to measure the difference between the model output $\hat{P}(t)$ and the measured active power $P(t)$. The mean average percentage error is defined as follows:

$$MAPE = \frac{1}{n} \sum_{i=1}^n \left| \frac{P_i - \hat{P}_i}{P_i} \right| \quad (5.75)$$

The closer the model output to the measured active power, the smaller the mean square percentage error is.

The second way to show the performance of the proposed model-driven assessment of conservation voltage reduction effects is to use a Euclidian distance based comparison method. As shown in Fig. 5.3, load and voltage profiles of a voltage-reduction day can be divided into three parts: the period before voltage reduction (T_1), voltage reduction period (T_2), and the period after voltage reduction ends (T_3). In the Euclidian distance based comparison method, a normal-voltage day whose load and voltage profiles are similar to the profile with voltage reduction is selected. The load consumption of the selected normal-voltage day is used to represent what the load would be if there were no voltage reduction. The difference between the load consumption of the selected normal-voltage

day and that of the reduced-voltage day is considered to be the load reduction effect of conservation voltage reduction. The Euclidian distance based indices for a normal-voltage day k are defined as follows,

$$\sum_{\substack{i=1 \\ i \in T_1, T_3}}^N \frac{\sqrt{(P_i^{cvr} - P_{ki}^{nocvr})^2}}{P_I^{cvr} N} = \mathcal{E}_{pk} \quad (5.76)$$

$$\sum_{\substack{i=1 \\ i \in T_1, T_3}}^N \frac{\sqrt{(V_i^{cvr} - V_{ki}^{nocvr})^2}}{V_I^{cvr} N} = \mathcal{E}_{vk} \quad (5.77)$$

Where

- \mathcal{E}_{pk} and \mathcal{E}_{vk} are the Euclidian distance-based power and voltage indices for the k-th day without voltage reduction, respectively,
- P_i^{cvr} and V_i^{cvr} represent active load and voltage at time i on a day with voltage reduction, respectively,
- P_{ki}^{nocvr} and V_{ki}^{nocvr} represent active load and voltage at time i on the k-th day without voltage reduction, respectively.
- I is the index of the $\max(P_i^{cvr}), \forall i$, i.e., the maximum power consumption of the conservation voltage reduction day is used as the denominator in (5.76) for normalization and the corresponding voltage level is used as the denominator in (5.77).
- As shown in Fig. 5.3, T_1 and T_3 represent the period before the voltage reduction and the period after the voltage reduction ends, respectively.

Practical data of voltage reduction day is used in this section to demonstrate the proposed method. Data of 11 voltage-reduction days of a feeder are analyzed. For the purposes of illustration, the results of 3 voltage-reduction days are shown in details in this section. The assessment results of all 11 days are summarized in section 5.3.5.

Example 1

Fig. 5.27 shows the voltage profile of Oct. 16 which is a voltage-reduction day. Conservation voltage reduction starts at 140 minutes and ends at 422 minutes. Fig. 5.28 shows the active power profile measured at the substation on this voltage-reduction day.

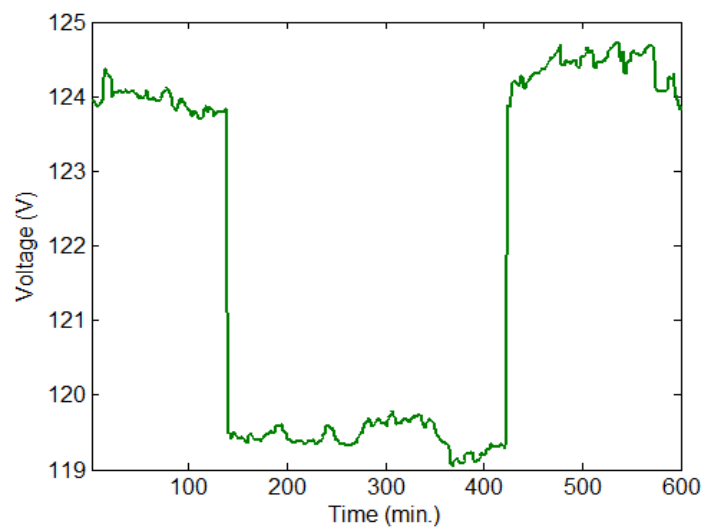


Figure 5.27. Voltage profile with conservation voltage reduction in example 1.

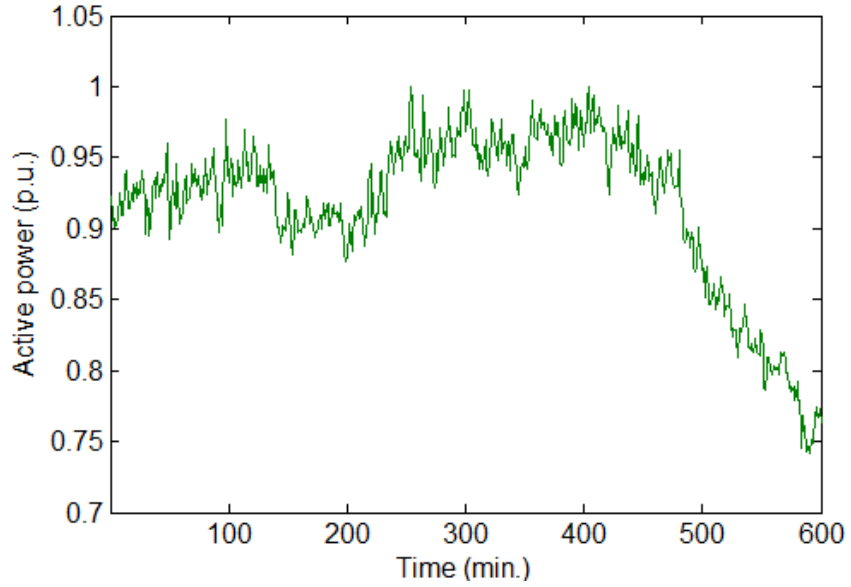


Figure 5.28. Measured load profiles in example 1.

The exponential load model defined in (5.48) is used to represent the load. The unscented Kalman filter algorithm is then applied to estimate the load-to-voltage sensitivities and the conservation voltage reduction factors are calculated from the estimated load-to-voltage sensitivities by using (5.66).

The initial values of P_0 and k_p as well as the values of process noise q and measurement noise r affect the estimation results. To illustrate the effects of q and r , it is assumed that $P_0(0) = 1.0$ and $k_p(0) = 1.0$, and q and r can have values that vary within the following set,

$$q, r \in (0.01, 0.02, 0.03, 0.04, 0.05, 0.06, 0.07, 0.08, 0.09, 0.10) \quad (5.78)$$

The above set has ten elements. Therefore, there are 100 combinations of q and r . The unscented Kalman filter based estimation is run for each combination of q and r . Fig.

5.29 shows the mean average estimation errors between the measured active power $P(t)$ and the estimated model outputs $\hat{P}(t)$ as defined in (5.74).

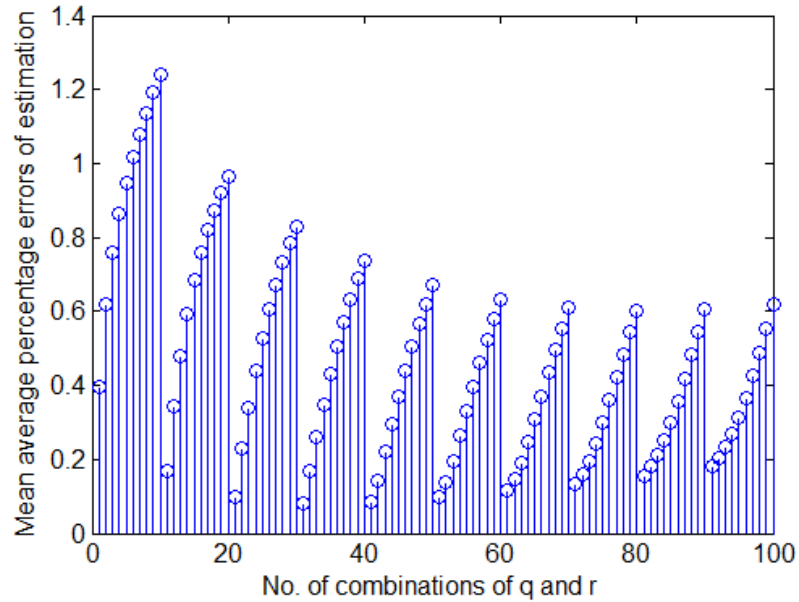


Figure 5.29. Mean average percentage estimation errors with different values of q and r in example 1.

In Fig. 5.29, the smallest error (MAPE=0.0797) is the result with the 31st combination of q and r ($q=0.04$, $r=0.01$). The second (MAPE=0.0832) and third (0.0963) smallest errors are the results with the 41st ($q=0.05$, $r=0.01$) and 51st ($q=0.06$, $r=0.01$) combinations of q and r , respectively. For illustration, the estimation results of using these three combinations of q and r are discussed.

Fig. 5.30 shows the model outputs $\hat{P}(t)$ calculated from the estimated load model and the measured active power $P(t)$. The solid line represents the measured active power. The other three lines represent the active power calculated from the estimated load models with the three combinations of q and r (i.e., $q=0.04$, $r=0.01$, $q=0.05$, $r=0.01$, and

$q=0.06$, $r=0.01$), respectively. All estimated model outputs are close to the measured power. The closest one is the result calculated by setting $q=0.04$ and $r=0.01$ since it has the smallest mean percentage estimation error (MAPE=0.0797) as shown in Fig. 5.29.

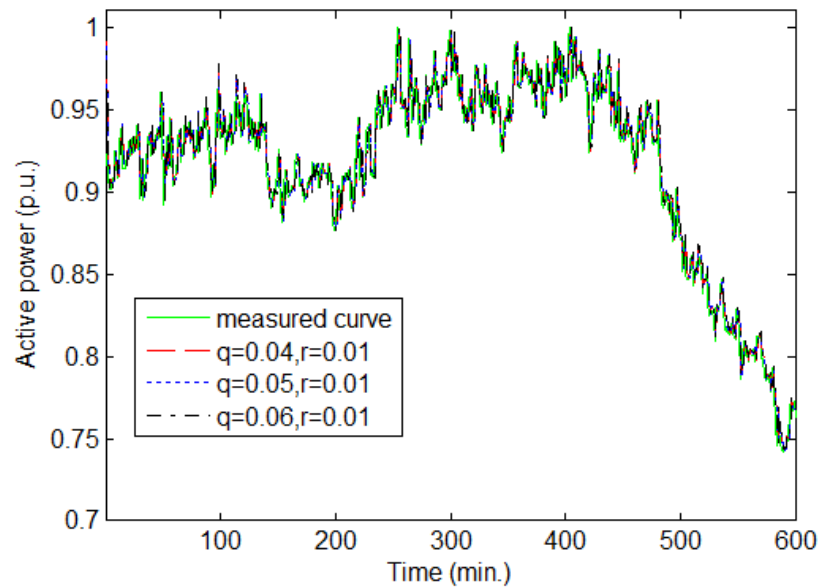


Figure 5.30. Measured and estimated load profiles with different combinations of q and r in example 1.

Fig.5.31 shows the estimated k_p for the three combinations of q and r . k_p is used to calculate conservation voltage reduction factor, and the results are shown in Fig. 5.32.

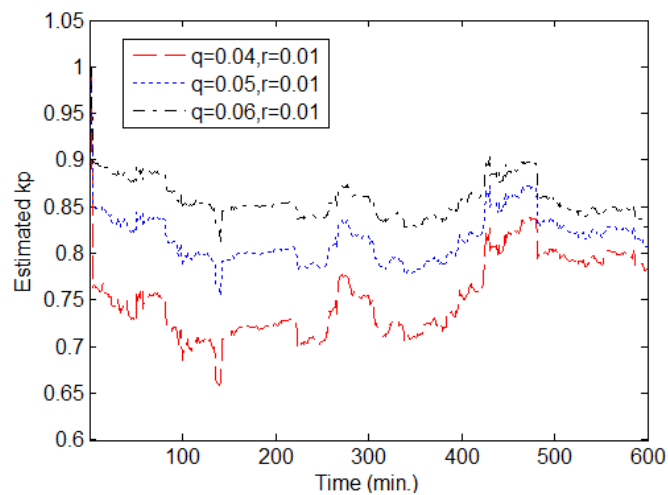


Figure 5.31. Estimated load-to-voltage sensitivities with different combinations of q and r in example 1.

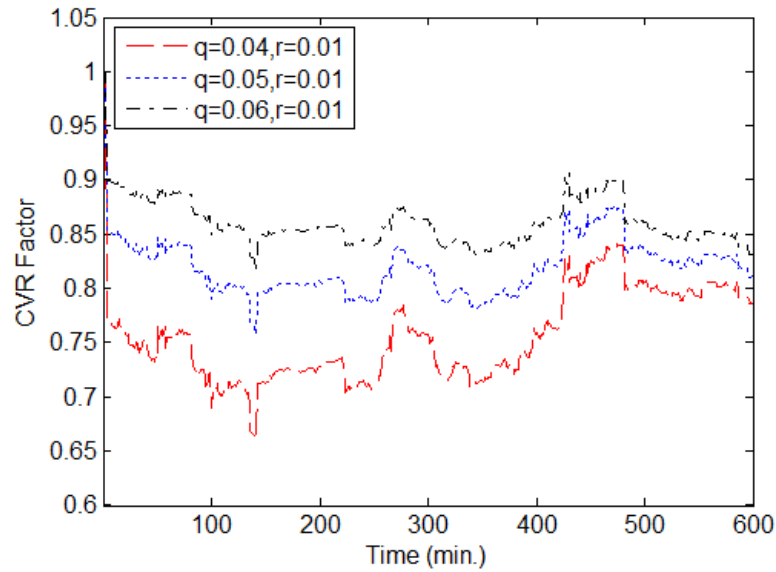


Figure 5.32. Conservation voltage reduction factors calculated by estimated load-to-voltage sensitivities in example 1 (only the period of 140-422 minutes is CVR period)

The values of q and r of the unscented Kalman filter significantly affects the assessment results. The calculated conservation voltage reduction factors vary with different settings of q and r . For determined initial values of P_0 and k_p , it is suggested to select the combination of q and r that results in the smallest mean average percentage estimation error as the values of the unscented Kalman filter algorithm (i.e., $q=0.04$, $r=0.01$ in this example).

The above example shows the impacts of q and r with $P_0(0)=1.0$ and $k_p(0)=1.0$. It is necessary to demonstrate the impacts of the combination of $P_0(0)$, $k_p(0)$, q and r on the estimation results. To illustrate these affects, it is assumed that $P_0(0)$, $k_p(0)$ could have values that vary within the following set,

$$P_0(0), k_p(0) \in (0.5, 0.6, 0.7, 0.8, 0.9, 1.0) \quad (5.79)$$

It is also assumed that q and r could have values that vary within the following sets,

$$q, r \in (0.01, 0.02, 0.03, 0.04, 0.05, 0.06, 0.07, 0.08, 0.09, 0.1) \quad (5.80)$$

Therefore, there are 3600 combinations of $P_0(0)$, $k_p(0)$, q and r . The unscented Kalman filter based estimation is run for each combination of $P_0(0)$, $k_p(0)$, q and r . Fig. 5.33 shows the mean average estimation errors. In Fig. 5.33, the smallest error (MAPE=0.0796) is the result with the combination of $P_0(0)=1.0$, $k_p(0)=0.9$, $q=0.04$, and $r=0.01$. The second smallest error is the result with the combination of $P_0(0)=1.0$, $k_p(0)=1.0$, $q=0.04$, and $r=0.01$. The third smallest error is the result with the combination of $P_0(0)=0.9$, $k_p(0)=0.9$, $q=0.04$, and $r=0.01$. For purposes of illustration, the estimation results of using these three combinations of $P_0(0)$, $k_p(0)$, q and r are discussed.

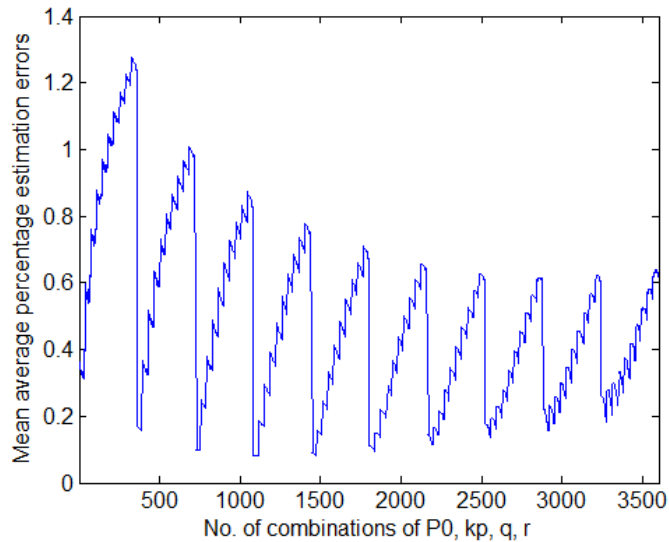


Figure 5.33. Mean average percentage estimation errors with different values of $P_0(0)$, $k_p(0)$, q and r in example 1.

Fig. 5.34 shows the model outputs $\hat{P}(t)$ calculated from the estimated load model and the measured active power $P(t)$. The solid line represents the measured active power. The other three lines represent the active power calculated from the estimated load models with the three combinations of $P_0(0)$, $k_p(0)$, q and r , respectively. All estimated model outputs are close to the measured power. The closest one is the result calculated by setting $P_0(0) = 1.0$, $k_p(0) = 0.9$, $q = 0.04$, and $r = 0.01$ since it has the smallest mean percentage estimation error as shown in Fig. 5.33.

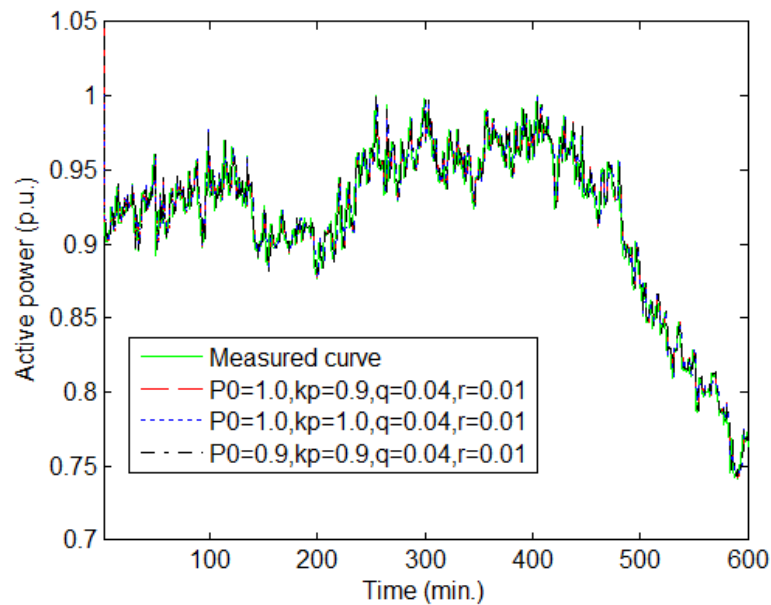


Figure 5.34. Measured and estimated load profiles with different combinations $P_0(0)$, $k_p(0)$, q and r in simulation example 1.

Fig. 5.35 shows the estimated k_p for the three combinations of $P_0(0)$, $k_p(0)$, q and r . k_p is used to calculate conservation voltage reduction factor, and the results are shown in Fig. 5.36.

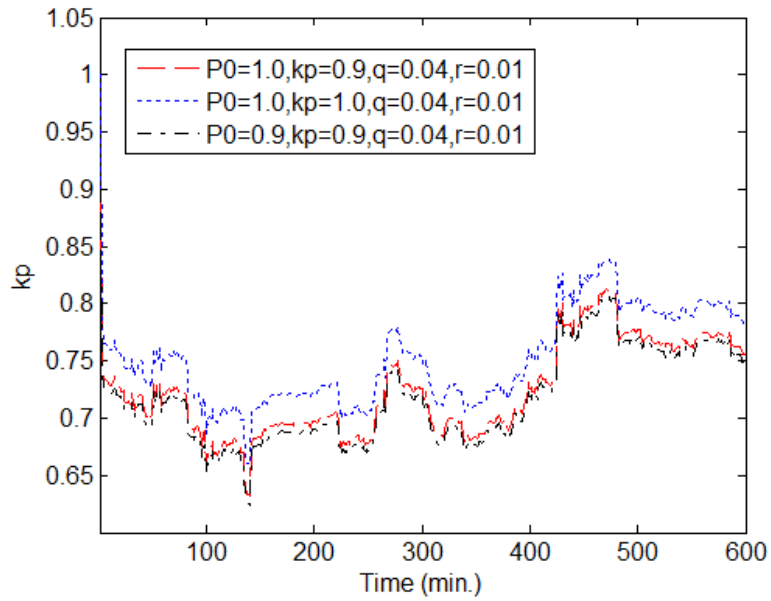


Figure 5.35. Estimated load-to-voltage sensitivities with different combinations of $P_0(0)$, $k_p(0)$, q and r in example 1.

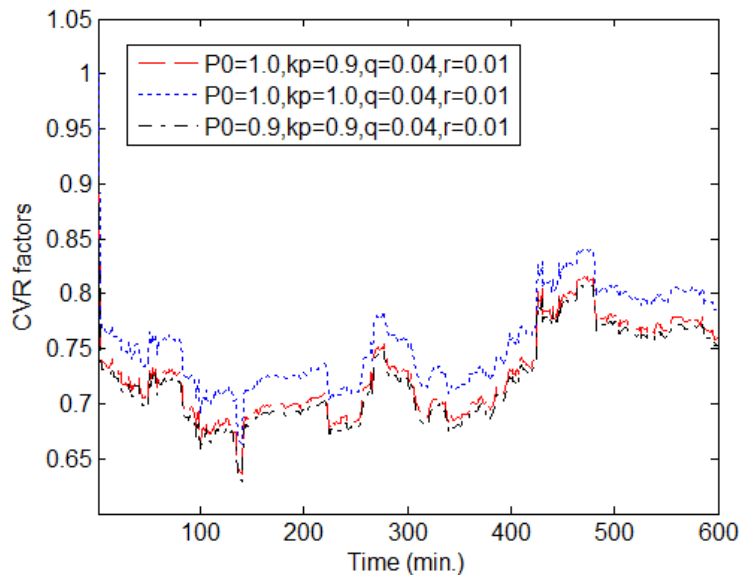


Figure 5.36. Conservation voltage reduction factors calculated by estimated load-to-voltage sensitivities in example 1 (only the period of 140-422 minutes is CVR period).

Fig. 5.37 shows the estimated conservation voltage reduction factors calculated by setting $P_0(0)=1.0$, $k_p(0)=0.9$, $q=0.04$, and $r=0.01$ during the voltage reduction period.

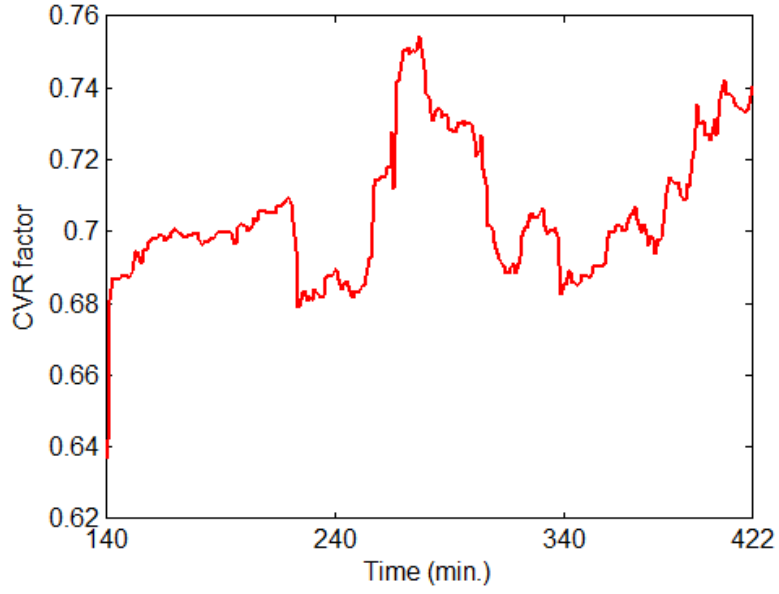


Figure 5.37. Conservation voltage reduction factors during voltage reduction period in example 1.

In sections 5.2.2 and 5.2.3, it is shown that the estimation errors of load consumption affect the accuracy of the calculated conservation voltage reduction factors in the data-driven assessment method. For the model-driven assessment method proposed in this section, the estimation errors of k_p result in the errors of the conservation voltage reduction factors calculated by (5.66). In (5.66), assume $\Delta V = V_{cvron}/V_{cvroff}$,

$$CVR_{fe} = \frac{1 - \Delta V^{\hat{k}_p}}{1 - \Delta V} \quad (5.81)$$

$$CVR_{fact} = \frac{1 - \Delta V^{k_p}}{1 - \Delta V} \quad (5.82)$$

$$\frac{CVR_{fe}}{CVR_{fact}} = \frac{1 - \Delta V^{\hat{k}_p}}{1 - \Delta V^{k_p}} \quad (5.83)$$

where CVR_{fe} is the estimated conservation voltage reduction factor, CVR_{fact} is the actual conservation voltage reduction factor which is unknown in practice, \hat{k}_p is the estimated load-to-voltage sensitivity, and k_p is the actual load-to-voltage sensitivity which is unknown in practice. Assume $\varphi = k_p / \hat{k}_p$,

$$\frac{CVR_{fe}}{CVR_{fact}} = \frac{1 - \Delta V^{\hat{k}_p}}{1 - \Delta V^{\varphi \hat{k}_p}} \quad (5.84)$$

$$\varepsilon = \frac{CVR_{fact} - CVR_{fe}}{CVR_{fact}} = \frac{\Delta V^{\hat{k}_p} - \Delta V^{\varphi \hat{k}_p}}{1 - \Delta V^{\varphi \hat{k}_p}} \quad (5.85)$$

$$CVR_{fact} = \frac{1 - \Delta V^{\varphi \hat{k}_p}}{1 - \Delta V^{\hat{k}_p}} \times CVR_{fe} \quad (5.86)$$

where ε is the estimation error of the conservation voltage reduction factor. If there is no error between \hat{k}_p and k_p (i.e., $\varphi = 1$), then $\varepsilon = 0$ and the estimated conservation voltage reduction factor is equal to the actual one. For convenience, it assumed that

$$\psi = \frac{k_p - \hat{k}_p}{k_p} = 1 - \frac{1}{\varphi} \quad (5.87)$$

where ψ represents the estimation error of k_p . Then, (5.85) can be reformulated as

$$\varepsilon = \frac{CVR_{fact} - CVR_{fe}}{CVR_{fact}} = \frac{\Delta V^{\hat{k}_p} - \Delta V^{\frac{1}{1-\psi} \hat{k}_p}}{1 - \Delta V^{\frac{1}{1-\psi} \hat{k}_p}} \quad (5.88)$$

If ΔV is set to 0.96 (i.e., 4% voltage reduction), the relationship among the estimated the load-to-voltage sensitivity \hat{k}_p , the estimation error of the load-to-voltage sensitivity ψ , and the estimation error of conservation voltage reduction factor ε can be calculated

from (5.88), and the results are plotted in Fig. 5.38. For a certain estimation error of \hat{k}_p , the estimation error of conservation voltage reduction factor slightly decreases with the increase of estimated values of \hat{k}_p . The estimation error of conservation voltage reduction factor becomes larger with an increase of the estimation error of \hat{k}_p .

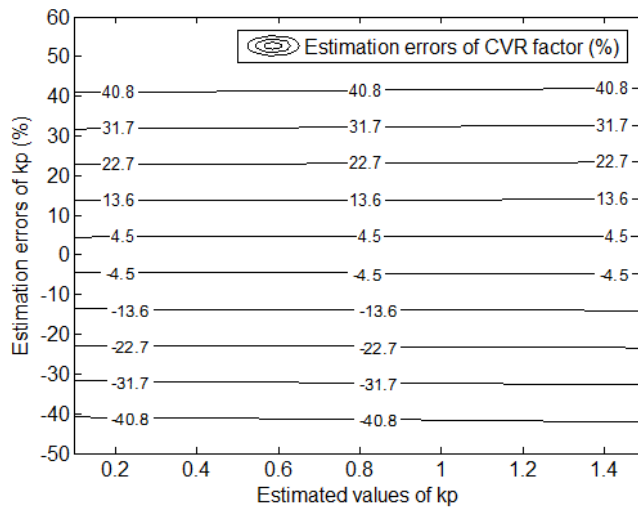


Figure 5.38. Contour of relationship of estimation errors of k_p , estimated values of k_p , and estimation errors of conservation voltage reduction factors.

For the calculated conservation voltage reduction factors shown in Fig. 5.37, the band for the corresponding actual conservation voltage reduction factors can be calculated by (5.86-5.87) with the assumption that $\Delta V = 0.96$ and $\psi = \pm 5\%$, and the results are shown in Fig. 5.39. The upper bound of the actual CVR factors is about 105% of the estimated CVR factors, and the lower bound of the actual CVR factors is around 95% of the estimated CVR factors.

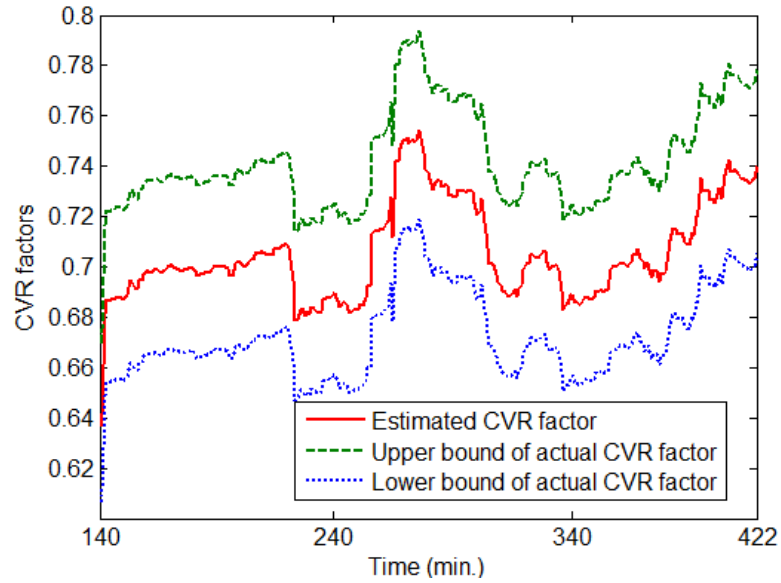


Figure 5.39. Band of conservation voltage reduction factors in example 1.

Besides applying mean average percentage estimation error to measure the performance of the proposed model-driven assessment method, the Euclidian distance based method can also be used. As shown in (5.76) and (5.77), the basic idea of the Euclidian distance based comparison method is to select a normal-voltage day whose load and voltage profiles are similar to the profiles with the voltage reduction. The load consumption of the selected normal-voltage day is used to represent what the load would be if there were no voltage reduction. The voltage reduction shown in Fig. 5.27 was conducted on Oct. 16. Table 5.5 shows the available dataset that includes all normal-voltage days. The Euclidian distance based indices defined in (5.76) and (5.77) can be calculated using the load and voltage profiles of these normal-voltage days and the day with voltage reduction as shown in Figs. 5.27 and 5.28. Table 5.5 summarizes the calculated indices for active power (ε_p) and voltage (ε_v).

Table 5.5. Calculation results of Euclidian distance-based indices in example 1

Date	ε_p (%)	ε_v (%)
Sep 03	5.25	0.025
Sep 04	5.03	0.043
Sep 05	4.91	0.034
Sep 06	4.53	0.024
Sep 07	4.55	0.030
Sep 08	4.51	0.034
Sep 09	2.81	0.026
Sep 10	2.81	0.026
Sep 11	2.16	0.031
Sep 13	1.55	0.031
Sep 15	2.79	0.034
Sep 17	3.87	0.024
Sep 18	2.18	0.031
Sep 19	1.93	0.032
Sep 20	1.35	0.029
Sep 21	2.37	0.033
Sep 22	2.71	0.034
Sep 23	2.56	0.034
Sep 25	1.31	0.032
Sep 27	1.35	2.44
Sep 29	2.49	0.029
Oct 03	1.82	0.042
Oct 04	1.82	0.030
Oct 05	2.51	0.037
Oct 06	2.71	0.037
Oct 07	3.13	0.026
Oct 09	0.19	0.034

Oct 11	0.32	0.038
Oct 13	0.86	0.023
Oct 15	1.52	0.017
Oct 17	0.22	0.019
Oct 19	0.68	0.039
Oct 20	0.21	0.029
Oct 21	0.16	0.026
Oct 22	0.25	0.033
Oct 23	0.15	0.039
Oct 25	0.71	0.030

The smallest index for power is 0.15 (Oct. 23). The second smallest one is 0.16 (Oct. 21). Fig. 5.40 shows the load profiles of Oct. 16 (the voltage-reduction day), 23 and 21. Fig. 5.41 shows the corresponding voltage profiles.

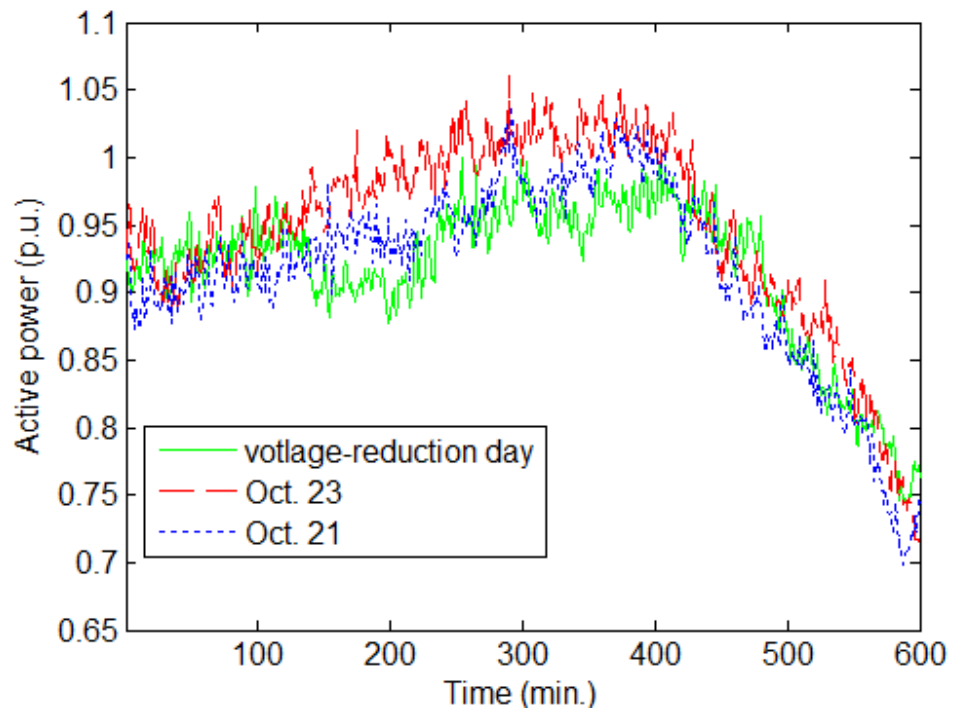


Figure 5.40. Load profiles with and without voltage reduction in example 1.

The conservation voltage reduction factors can be calculated by using the load and voltage profiles of normal-voltage days to represent what the load and voltage would be if there were no voltage reduction for the reduced-voltage day. Fig. 5.42 shows the calculated conservation voltage reduction factors.

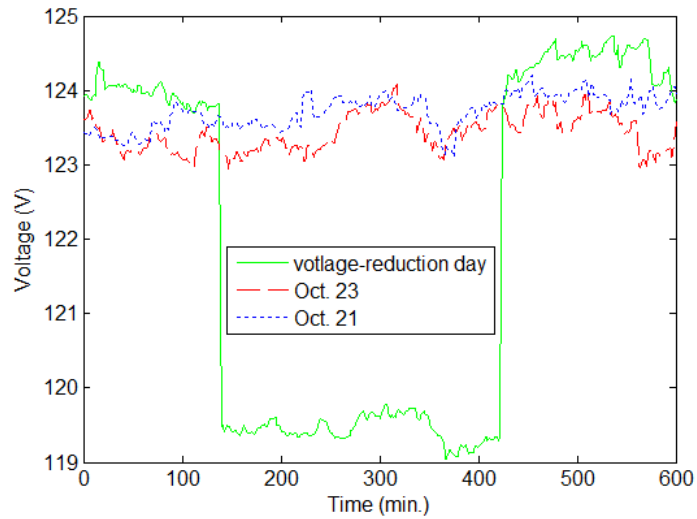


Figure 5.41. Voltage profiles with voltage reduction and without voltage reduction in example 1.

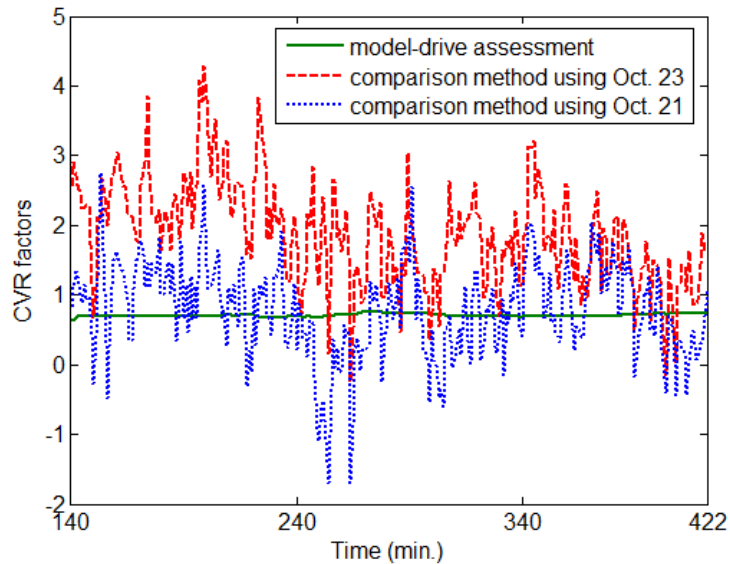


Figure 5.42. Conservation voltage reduction factors calculated by model-driven method and comparison method in example 1.

Compared to the conservation voltage reduction factors calculated by using the Euclidian distance based comparison method, the conservation voltage reduction factors estimated by the proposed model-driven method is smooth. Even though the power tracking performance is good for the model-driven method as shown in Fig. 5.34, the CVR factors calculated by the two methods do not match each other well. A possible reason is that the load profile of the single normal-voltage day selected by the Euclidian distance based method cannot accurately represent what the load would be if there were no voltage reduction during the conservation voltage reduction period. Further studies are necessary to verify the performance of the proposed model-driven assessment method.

Example 2

Fig. 5.43 shows the voltage profile of Oct. 8 which is a voltage-reduction day. Conservation voltage reduction starts at 123 minutes and ends at 181 minutes. Fig. 5.44 shows the active power profile measured at the substation on this voltage-reduction day.

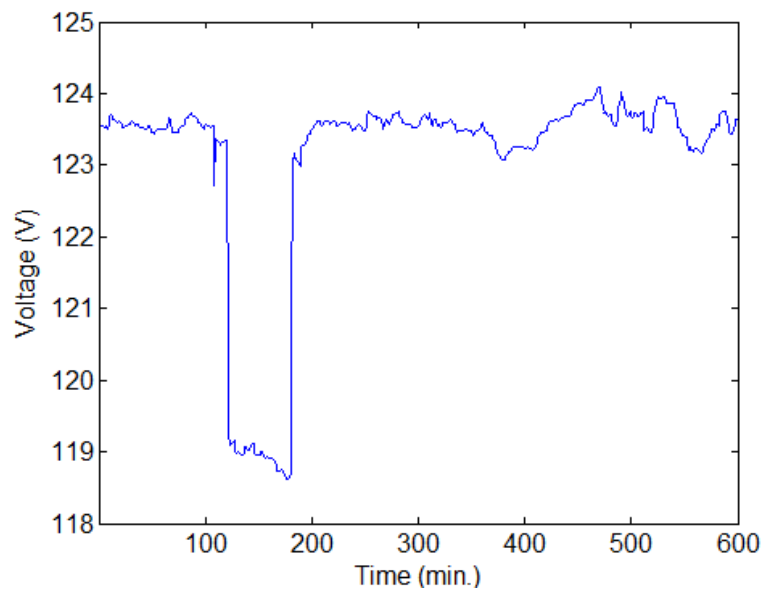


Figure 5.43. Voltage profile with conservation voltage reduction in example 2.

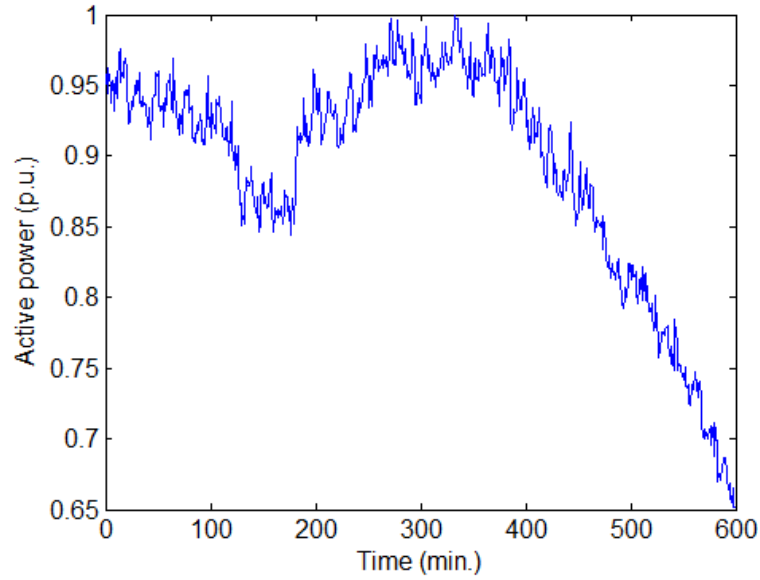


Figure 5.44. Measured load profiles in example 2.

As discussed in example 1, the initial values of P_0 and k_p as well as the values of process noise q and measurement noise r affect the estimation results. To illustrate these effects, it is assumed that $P_0(0)$, $k_p(0)$ could have values that vary within the following set,

$$P_0(0), k_p(0) \in (0.5, 0.6, 0.7, 0.8, 0.9, 1.0) \quad (5.89)$$

It is also assumed that q and r could have values that vary within the following sets,

$$q, r \in (0.01, 0.02, 0.03, 0.04, 0.05, 0.06, 0.07, 0.08, 0.09, 0.1) \quad (5.90)$$

Therefore, there are 3600 combinations of $P_0(0)$, $k_p(0)$, q and r . The unscented Kalman filter based estimation is run for each combination of $P_0(0)$, $k_p(0)$, q and r . Fig. 5.45 shows the mean average estimation errors. In Fig. 5.45, the smallest error (MAPE=0.0335) is the result with the combination of $P_0(0)=0.5$, $k_p(0)=1.0$, $q=0.08$, and $r=0.01$. The second smallest error is the result with the combination of $P_0(0)=0.6$,

$k_p(0) = 1.0$, $q=0.08$, and $r=0.01$. The third smallest error is the result with the combination of $P_0(0) = 0.7$, $k_p(0) = 1.0$, $q=0.08$, and $r=0.01$. For illustration, the estimation results of using these three combinations of $P_0(0)$, $k_p(0)$, q and r are discussed below.

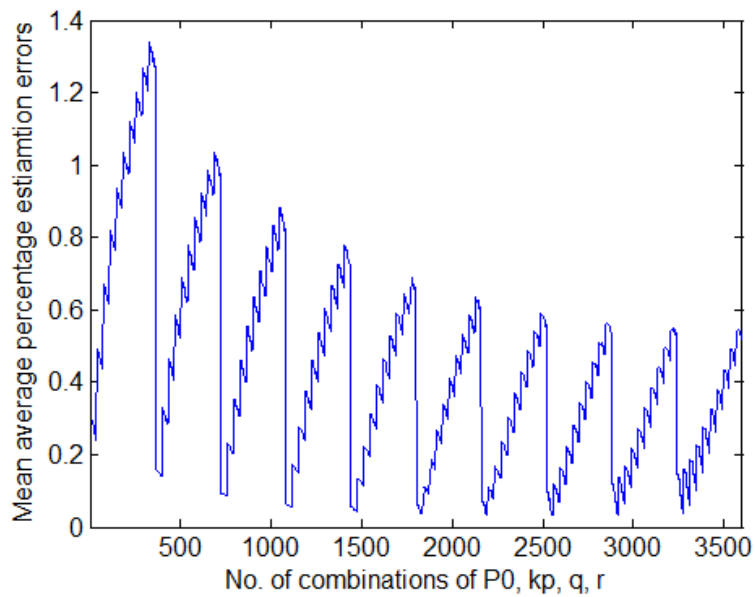


Figure 5.45. Mean average percentage estimation errors with different values of $P_0(0)$, $k_p(0)$, q and r in simulation example 2.

Fig. 5.46 shows the model outputs $\hat{P}(t)$ calculated from the estimated load model and the measured active power $P(t)$. The solid line represents the measured active power. The other three lines represent the active power calculated from the estimated load models with the three combinations of $P_0(0)$, $k_p(0)$, q and r , respectively. All estimated model outputs are close to the measured power. The closest one is the result

calculated by setting $P_0(0)=0.5$, $k_p(0)=1.0$, $q=0.08$, and $r=0.01$ since it has the smallest mean percentage estimation error as shown in Fig. 5.45.

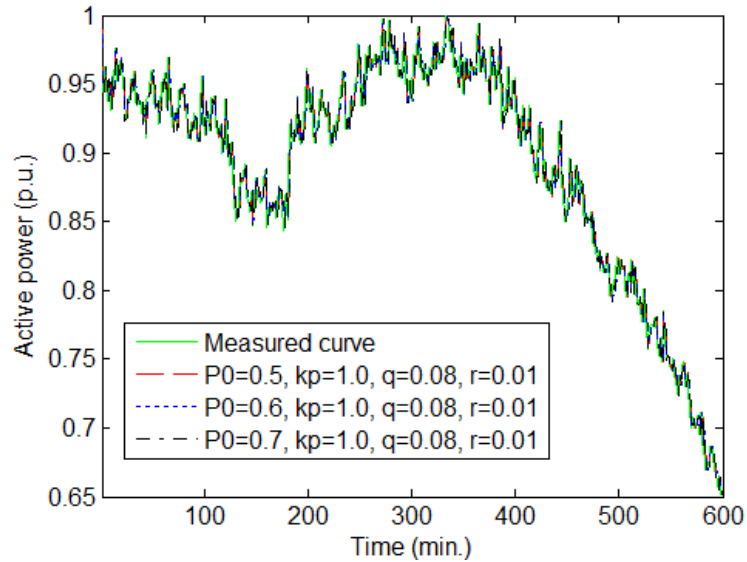


Figure 5.46. Measured and estimated load profiles with different combinations $P_0(0)$, $k_p(0)$, q and r in simulation example 2.

Fig.5.47 shows the estimated k_p for the three combinations of $P_0(0)$, $k_p(0)$, q and r . k_p is used to calculate conservation voltage reduction factor, and the results are shown in Fig. 5.48.

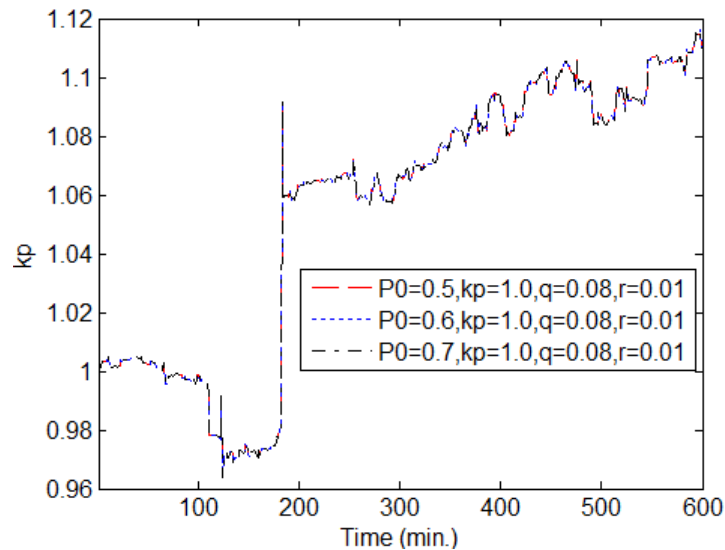


Figure 5.47. Estimated load-to-voltage sensitivities in example 2.

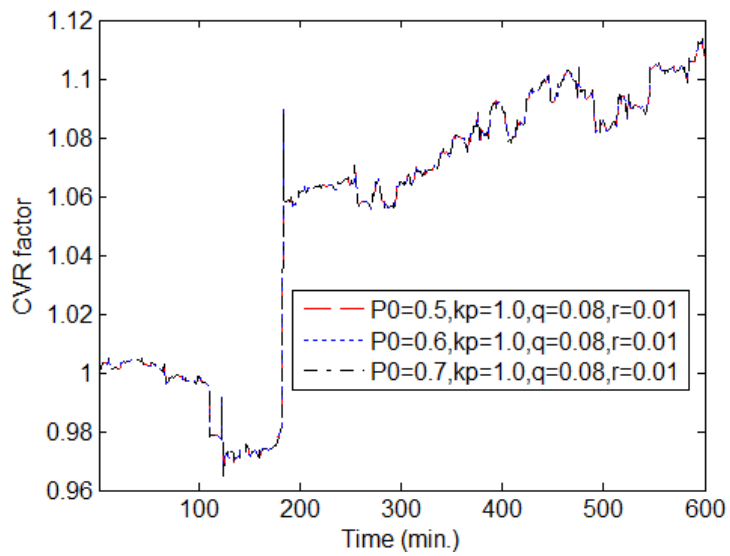


Figure 5.48. Conservation voltage reduction factors calculated by estimated load-to-voltage sensitivities in example 2 (only the period of 123-181 minutes is CVR period).

Fig. 5.49 shows the estimated conservation voltage reduction factors calculated by setting $P_0(0)=0.5$, $k_p(0)=1.0$, $q=0.08$, and $r=0.01$ during the voltage reduction period.

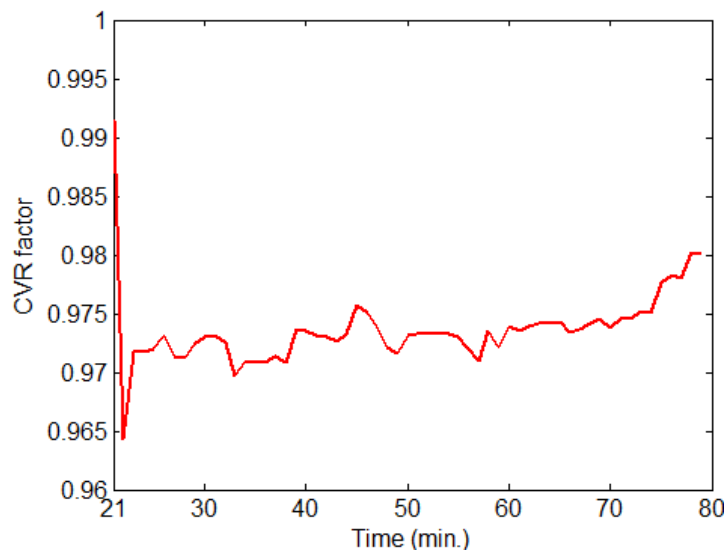


Figure 5.49. Conservation voltage reduction factors during voltage reduction period in example 2.

As discussed in example 1, the estimation errors of k_p result in the errors of the calculated conservation voltage reduction factors. For the calculated conservation voltage reduction factors shown in Fig. 5.49, the band for the corresponding actual conservation voltage reduction factors can be calculated by (5.86-5.87) with the assumption that $\Delta V = 0.96$ and $\psi = \pm 5\%$, and the results are shown in Fig. 5.50. The upper bound of the actual CVR factors is about 105% of the estimated CVR factors, and the lower bound of the actual CVR factors is around 95% of the estimated CVR factors.

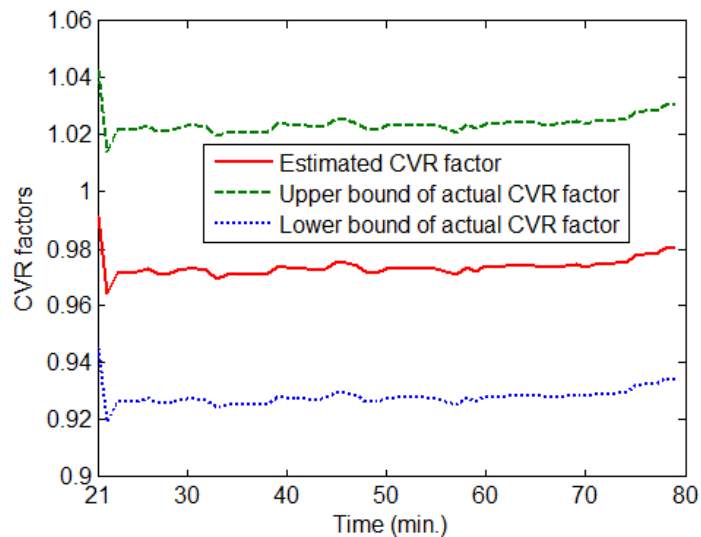


Figure 5.50. Band of conservation voltage reduction factors in example 2.

The voltage reduction shown in Fig. 5.43 was conducted on Oct. 8. Table 5.6 shows the available dataset that includes all normal-voltage days. The Euclidian distance based indices defined in (5.76) and (5.77) can be calculated using the load and voltage profiles of these normal-voltage days and the day with voltage reduction as shown in Figs. 5.43

and 5.44. Table 5.6 summarizes the calculated indices for active power (ε_p) and voltage (ε_v).

Table 5.6. Calculation results of Euclidian distance-based indices in example 2

Date	ε_p (%)	ε_v (%)
Sep 03	3.43	0.0174
Sep 04	3.35	0.0244
Sep 05	3.26	0.0139
Sep 06	3.06	0.0162
Sep 07	3.06	0.0158
Sep 08	2.79	0.0135
Sep 09	1.89	0.0157
Sep 10	1.89	0.0157
Sep 11	1.34	0.0159
Sep 13	0.90	0.0147
Sep 15	1.88	0.0157
Sep 17	2.52	0.0163
Sep 18	1.14	0.0161
Sep 19	1.39	0.0147
Sep 20	0.73	0.0143
Sep 21	1.52	0.0148
Sep 22	1.78	0.0170

Sep 23	1.63	0.0150
Sep 25	0.80	0.0128
Sep 27	0.73	1.8312
Sep 29	1.52	0.0147
Oct 03	1.12	0.0136
Oct 04	1.04	0.0127
Oct 05	1.57	0.0120
Oct 06	1.67	0.0143
Oct 07	2.06	0.0130
Oct 09	0.39	0.0117
Oct 11	0.21	0.0117
Oct 13	0.36	0.0139
Oct 15	0.90	0.0243
Oct 17	0.32	0.0230
Oct 19	0.30	0.0135
Oct 20	0.17	0.0117
Oct 21	0.34	0.0132
Oct 22	0.41	0.0111
Oct 23	0.25	0.0120
Oct 25	0.29	0.0107

The smallest index for power is 0.17 (Oct. 20). The second smallest one is 0.21 (Oct. 11). Fig. 5.51 shows the load profiles of Oct. 8 (the voltage-reduction day), 11 and 20. Fig. 5.52 shows the corresponding voltage profiles.

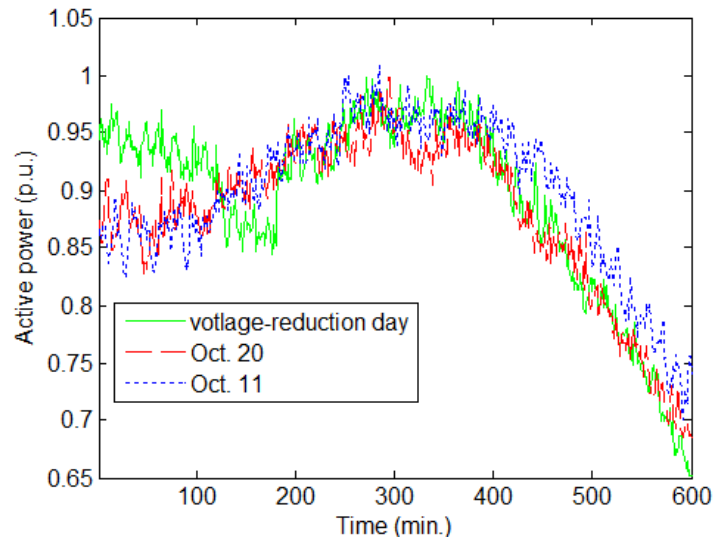


Figure 5.51. Load profiles with and without voltage reduction in example 2.

The conservation voltage reduction factors can be calculated by using the load and voltage profiles of normal-voltage days to represent what the load and voltage would be if there were no voltage reduction for the reduced-voltage day. Fig. 5.53 shows the calculated conservation voltage reduction factors.

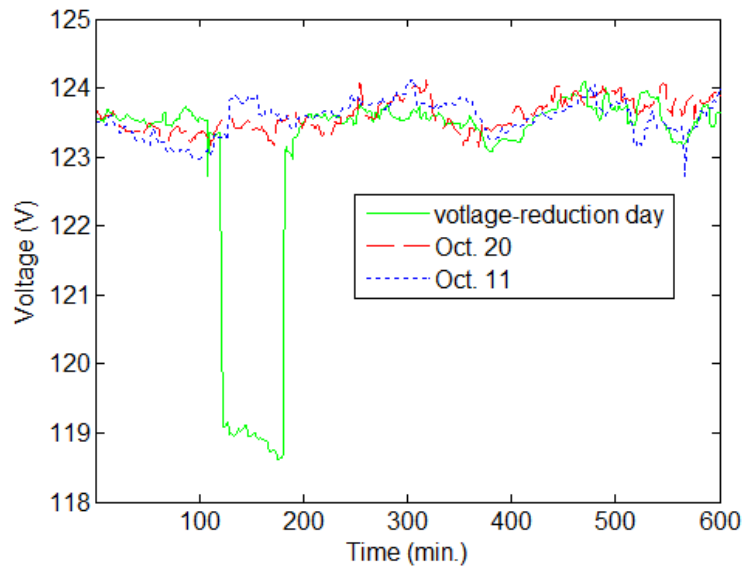


Figure 5.52. Voltage profiles with voltage reduction and without voltage reduction in example 2.

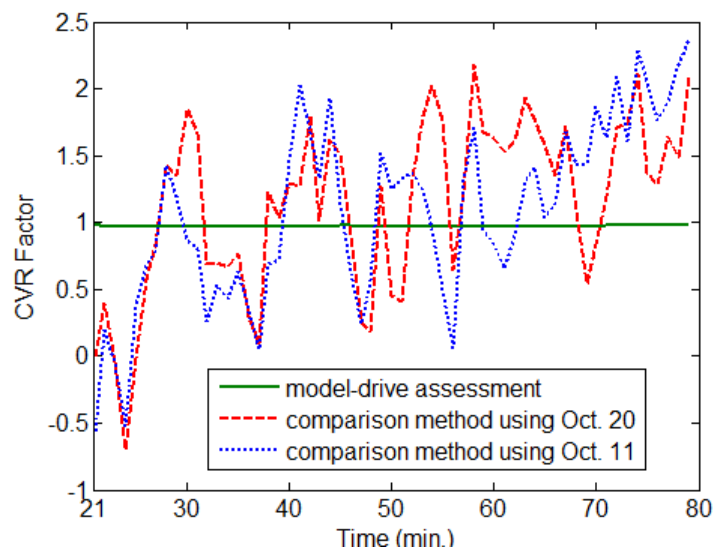


Figure 5.53. Conservation voltage reduction factors calculated by model-driven method and comparison method in example 2.

Compared to the conservation voltage reduction factors calculated by using the Euclidian distance based comparison method, the conservation voltage reduction factors estimated by the proposed model-driven method is smooth and nearly constant. Similar to the results of example 1, the CVR factors calculated by the two methods do not match

each other well. A possible reason is that the load profile of the single normal-voltage day selected by the Euclidian distance based method cannot accurately represent what the load would be if there were no voltage reduction during the conservation voltage reduction period. Further studies are necessary to verify the performance of the proposed model-driven assessment method.

Example 3

This example analyzes the conservation voltage reduction test on Sep. 24. Fig. 5.54 shows the voltage profile. Conservation voltage reduction starts at 184 minutes and ends at 363 minutes. Fig. 5.55 shows the active power profile measured at the substation on this voltage-reduction day.

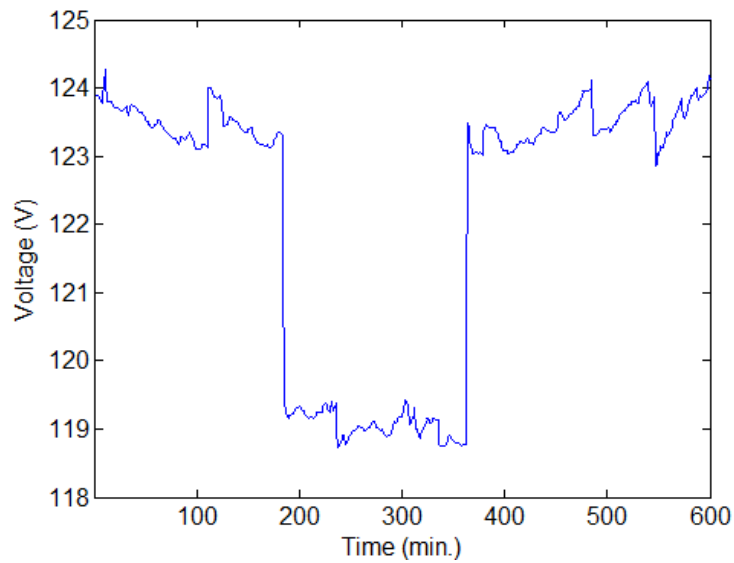


Figure 5.54. Voltage profile with conservation voltage reduction in example 3.

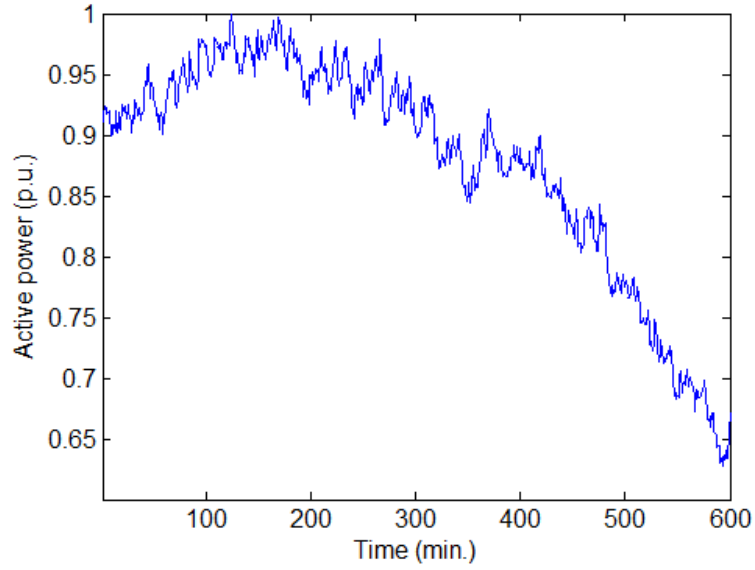


Figure 5.55. Measured load profiles in example 3.

To illustrate the impacts of the initial values of P_0 and k_p as well as the values of process noise q and measurement noise r on the assessment, it is assumed that $P_0(0)$, $k_p(0)$ could have values that vary within the following set,

$$P_0(0), k_p(0) \in (0.5, 0.6, 0.7, 0.8, 0.9, 1.0) \quad (5.91)$$

It is also assumed that q and r could have values that vary within the following sets,

$$q, r \in (0.01, 0.02, 0.03, 0.04, 0.05, 0.06, 0.07, 0.08, 0.09, 0.1) \quad (5.92)$$

Therefore, there are 3600 combinations of $P_0(0)$, $k_p(0)$, q and r . The unscented Kalman filter based estimation is run for each combination of $P_0(0)$, $k_p(0)$, q and r . Fig. 5.56 shows the mean average estimation errors. In Fig. 5.56, the smallest error (MAPE=0.0603) is the result with the combination of $P_0(0)=1.0$, $k_p(0)=1.0$, $q=0.05$, and $r=0.01$. The second smallest error is the result with the combination of $P_0(0)=0.9$, $k_p(0)=1.0$, $q=0.05$, and $r=0.01$. The third smallest error is the result with the combination

of $P_0(0)=0.8$, $k_p(0)=1.0$, $q=0.05$, and $r=0.01$. For illustration, the estimation results of using these three combinations of $P_0(0)$, $k_p(0)$, q and r are discussed.

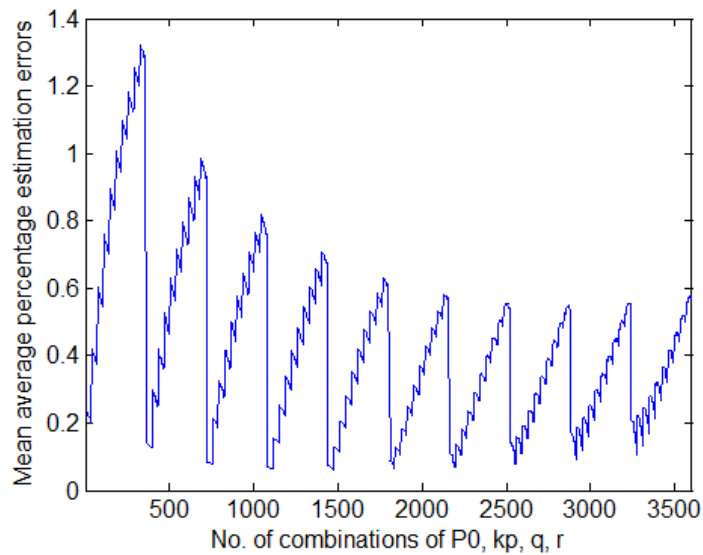


Figure 5.56. Mean average percentage estimation errors with different values of $P_0(0)$, $k_p(0)$, q and r in simulation example 3.

Fig. 5.57 shows the model outputs $\hat{P}(t)$ calculated from the estimated load model and the measured active power $P(t)$. The solid line represents the measured active power. The other three lines represent the active power calculated from the estimated load models with the three combinations of $P_0(0)$, $k_p(0)$, q and r , respectively. All estimated model outputs are close to the measured power. The closest one is the result calculated by setting $P_0(0)=1.0$, $k_p(0)=1.0$, $q=0.05$, and $r=0.01$ since it has the smallest mean percentage estimation error as shown in Fig. 5.56.

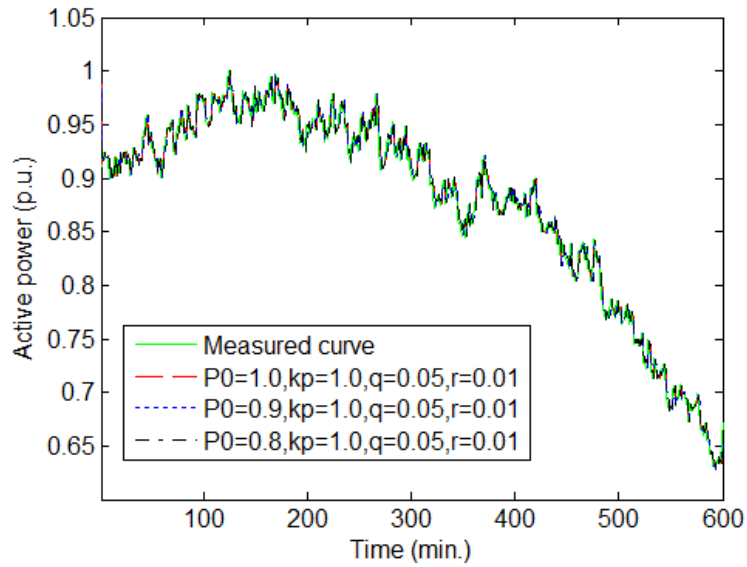


Figure 5.57. Measured and estimated load profiles with different combinations $P_0(0)$, $k_p(0)$, q and r in simulation example 3.

Fig. 5.58 shows the estimated k_p for the three combinations of $P_0(0)$, $k_p(0)$, q and r . k_p is used to calculate conservation voltage reduction factor, and the results are shown in Fig. 5.59.

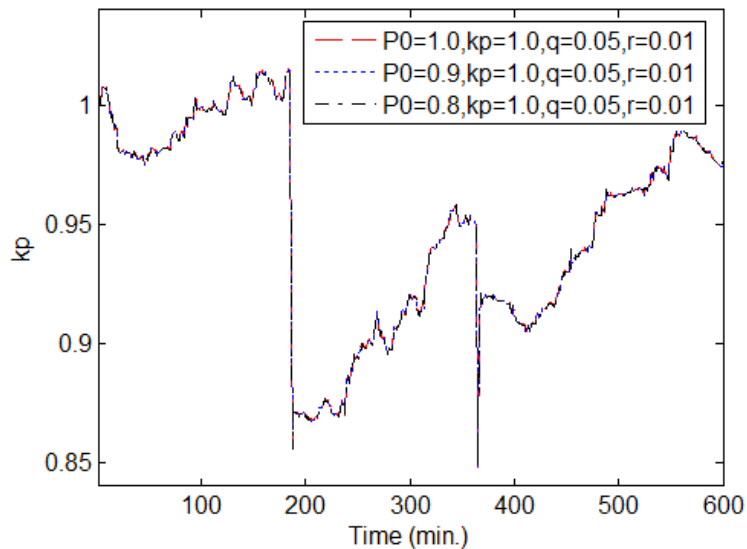


Figure 5.58. Estimated load-to-voltage sensitivities in example 2.

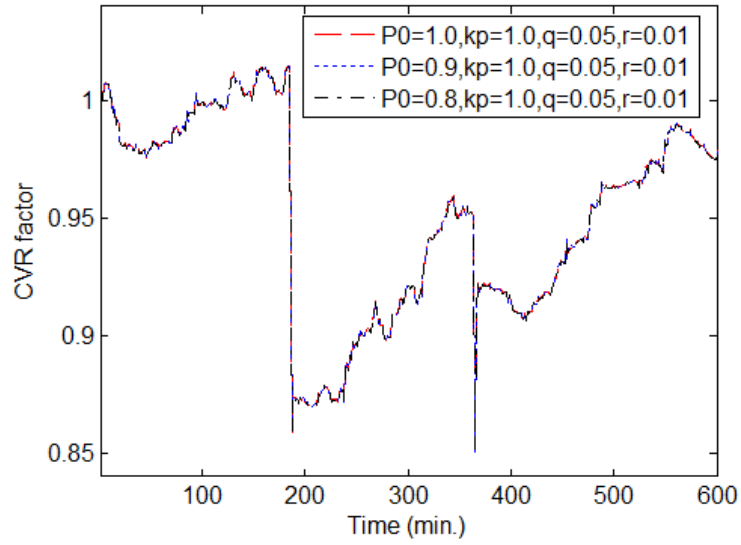


Figure 5.59. Conservation voltage reduction factors calculated by estimated load-to-voltage sensitivities in example 3 (only the period of 184-363 minutes is CVR period).

Fig. 5.60 shows the estimated conservation voltage reduction factors calculated by setting $P_0(0)=1.0$, $k_p(0)=1.0$, $q=0.05$, and $r=0.01$ during the voltage reduction period.

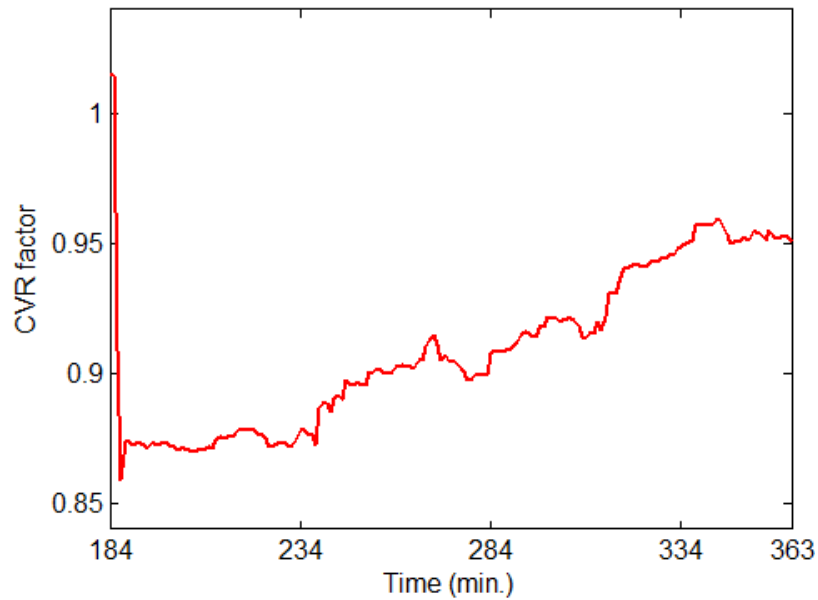


Figure 5.60. Conservation voltage reduction factors during voltage reduction period in example 3.

As discussed in example 1, the estimation errors of k_p result in the errors of the calculated conservation voltage reduction factors. For the calculated conservation voltage reduction factors shown in Fig. 5.60, the band for the corresponding actual conservation voltage reduction factors can be calculated by (5.86-5.87) with the assumption that $\Delta V = 0.96$ and $\psi = \pm 5\%$, and the results are shown in Fig. 5.61. The upper bound of the actual CVR factors is about 105% of the estimated CVR factors, and the lower bound of the actual CVR factors is around 95% of the estimated CVR factors.

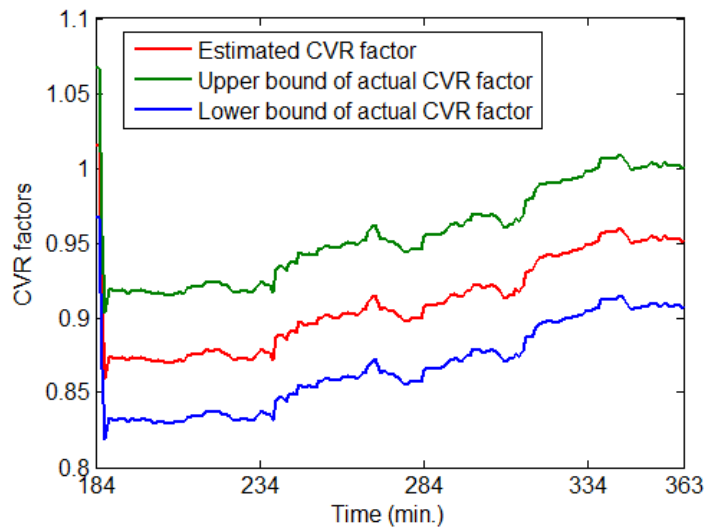


Figure 5.61. Band of conservation voltage reduction factors in example 3.

The voltage reduction shown in Fig. 5.54 was conducted on Sep. 24. Table 5.7 shows the available dataset that includes all normal-voltage days. The Euclidian distance based indices defined in (5.76) and (5.77) can be calculated using the load and voltage profiles of these normal-voltage days and the day with voltage reduction as shown in Figs. 5.54

and 5.55. Table 5.7 summarizes the calculated indices for active power (ε_p) and voltage (ε_v).

Table 5.7. Calculation results of Euclidian distance-based indices in example 3

Date	ε_p (%)	ε_v (%)
Sep 03	2.29	0.019
Sep 04	2.16	0.031
Sep 05	2.10	0.013
Sep 06	1.88	0.018
Sep 07	1.88	0.017
Sep 08	1.77	0.015
Sep 09	0.79	0.016
Sep 10	0.79	0.016
Sep 11	0.36	0.018
Sep 13	0.38	0.012
Sep 15	0.81	0.017
Sep 17	1.44	0.021
Sep 18	0.37	0.016
Sep 19	0.45	0.017
Sep 20	0.36	0.015
Sep 21	0.51	0.016
Sep 22	0.74	0.019
Sep 23	0.62	0.017
Sep 25	0.25	0.015
Sep 27	1.20	2.05
Sep 29	0.58	0.017
Oct 03	0.41	0.014
Oct 04	0.30	0.015

Oct 05	0.62	0.015
Oct 06	0.73	0.016
Oct 07	1.00	0.016
Oct 09	1.14	0.012
Oct 11	0.88	0.014
Oct 13	0.52	0.017
Oct 15	0.19	0.029
Oct 17	1.06	0.028
Oct 19	0.61	0.017
Oct 20	0.92	0.013
Oct 21	1.10	0.017
Oct 22	1.17	0.013
Oct 23	1.01	0.014
Oct 25	0.61	0.011

The smallest index for power is 0.19 (Oct. 15). The second smallest one is 0.25 (Sep. 25). Fig. 5.62 shows the load profiles of Sep. 24 (the voltage-reduction day), Sep. 25 and Oct. 15. Fig. 5.63 shows the corresponding voltage profiles.

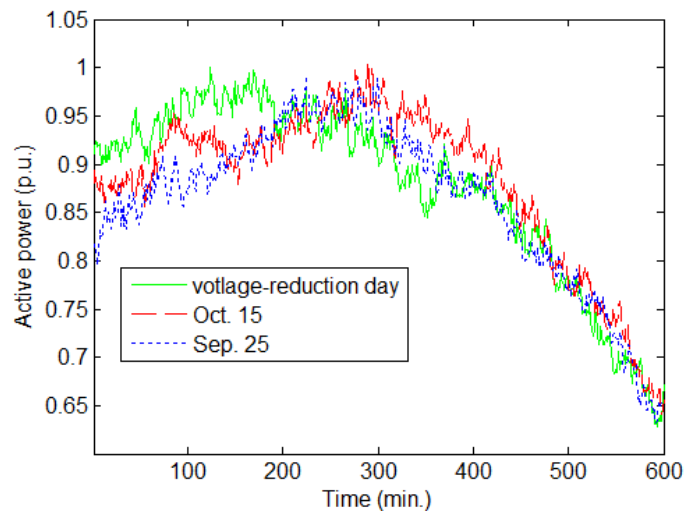


Figure 5.62. Load profiles with and without voltage reduction in example 3.

The conservation voltage reduction factors can be calculated by using the load and voltage profiles of normal-voltage days to represent what the load and voltage would be if there were no voltage reduction for the reduced-voltage day. Fig. 5.64 shows the calculated conservation voltage reduction factors.

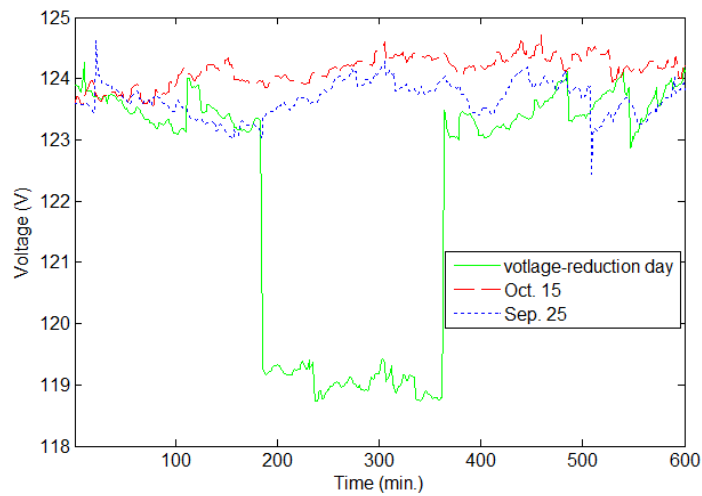


Figure 5.63. Voltage profiles with voltage reduction and without voltage reduction in example 3.

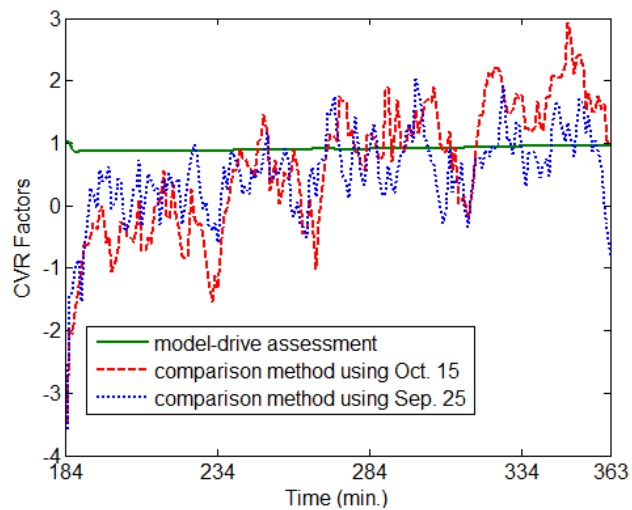


Figure 5.64. Conservation voltage reduction factors calculated by model-driven method and comparison method in example 3.

Similar to examples 1 and 2, the CVR factors calculated by the Euclidian distance based comparison method and the proposed model-driven method do not match each other well. A possible reason is that the load profile of the single normal-voltage day selected by the Euclidian distance based method cannot accurately represent what the load would be if there were no voltage reduction during the conservation voltage reduction period. Further studies are necessary to verify the performance of the proposed model-driven assessment method.

5.3.5 Statistical Analysis of Assessment Results by Unscented Kalman Filter

Section 5.3.4 discusses the assessment results of three voltage-reduction days. The unscented Kalman filter algorithm is applied to the available data of 11 voltage-reduction days of the same feeder. For each day, the settings of unscented Kalman filter that result in the smallest mean average estimation error are used. Fig. 5.65 shows the histogram of calculated conservation voltage reduction factors of all voltage-reduction days.

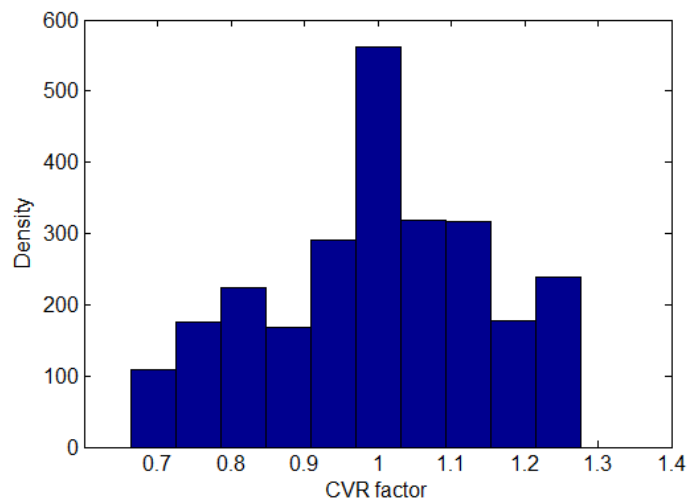


Figure 5.65. Histogram of conservation voltage reduction factors calculated by unscented Kalman filter.

As discussed in section 5.2.4, the Kolmogorov-Smirnov goodness-of-fit test is applied to find a distribution that can represent a dataset. The Kolmogorov-Smirnov test computes the test error ψ , which is the maximum vertical distance between an empirical cumulative distribution function and a fitted cumulative distribution function. This error is compared to a critical value ψ_{crit} , and the probability distribution fit that satisfies $\psi \leq \psi_{crit}$ could be accepted. For the normal distribution fit, $\psi = 0.0580$ and $\psi_{crit} = 0.0267$ with a level of significance 5%. Therefore, the normal distribution fit cannot be accepted. Similarly, the exponential distribution, Rayleigh distribution, and Weibull distribution (2 parameters) cannot represent the conservation voltage reduction factors either. The Weibull and normal distributions are close to the empirical distribution. The mean and standard deviation of the fitted normal distribution are 0.996 and 0.148, respectively. The two parameters for the fitted Weibull distribution are 1.059 and 7.741, respectively.

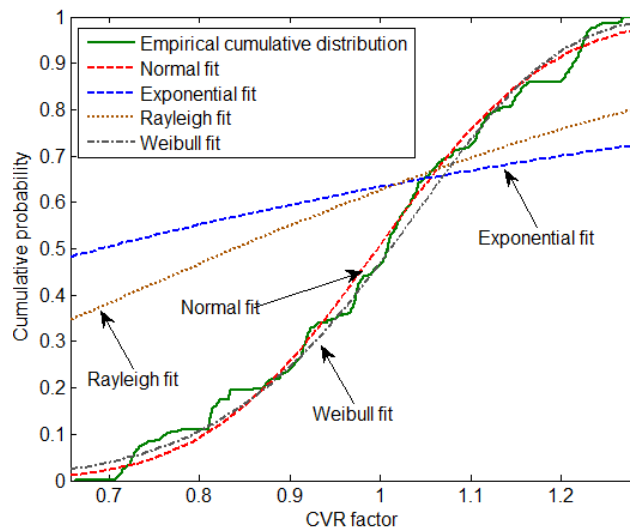


Figure 5.66. Cumulative distribution curves of conservation voltage reduction factors calculated by unscented Kalman filter.

Fig. 5.66 shows the differences between the cumulative distribution function of conservation voltage reduction factors of Feeder 1 and various other cumulative distribution functions (normal, Weibull with 2 parameters, Rayleigh and Exponential). Although none of the distributions in Fig. 5.66 passes the Kolmogorov-Smirnov test, the empirical cumulative distribution curve of the conservation voltage reduction factors can still be helpful to know the statistical behaviors of conservation voltage reduction effects.

5.4 Summary

In this chapter, two new methods to assess conservation voltage reduction effects are proposed: data-driven assessment and model-driven assessment. The two methods are applied to assess the effects of practical conservation voltage reduction tests conducted by utilities.

For the data-driven assessment method, a multi-stage support vector regression technique is proposed to estimate the load consumption without voltage reduction during a conservation voltage reduction period. The proposed method is designed for the assessment of peak-time voltage reduction. The first stage is to make full use of pre-conservation voltage reduction and post-conservation voltage reduction data to calculate a Euclidian distance-based index, and to select a set of load profiles that are closest to the profile under estimation. The selected profiles are used to train the support vector regression prediction model in the second stage. Estimated load profiles with large errors are filtered out in the third stage. The conservation voltage reduction factor can be calculated by using the estimated load profile. The impacts of load estimation errors on conservation voltage reduction factor calculation are analyzed. When selecting the preferred conservation voltage reduction feeders, the variety of conservation voltage

reduction effects is taken into account. A Kolmogorov-Smirnov-test based probabilistic framework is used to find the probabilistic conservation voltage reduction performance of each of five feeders.

Section 5.2.3 provides the analysis of impacts of load estimation errors on conservation voltage reduction assessment. It is found that larger estimation errors of load result in higher calculation errors of conservation voltage reduction factors. The relationship among the load estimation errors, values of conservation voltage reduction factors, and calculation errors of conservation voltage reduction factors are quantified by equations (5.36-5.39). The conclusion of the analysis is generic, and can be applied to all conservation voltage reduction assessment methods that require an estimation of the load consumption without voltage reduction.

For the model-driven assessment method, a time-varying exponential load model is used to represent loads and the unscented Kalman filter is applied to estimate model parameters. Then conservation voltage reduction factors can be calculated using the estimated model parameters. The results confirm that conservation voltage reduction factors change with the time. In practice, the load-to-voltage sensitivity k_p is usually smaller and less variant than the base load P_0 . Therefore, the initial guess of the states to be estimated (i.e., k_p and P_0 in this section) and the settings of the unscented Kalman filter, i.e., the values of process noise q and measurement noise r significantly affect the estimation results. These affects are shown in the examples in section 5.3.3 and 5.3.4. In this dissertation, multiple combinations of initial state guess, q and r are applied in the examples, and it is suggested to select the settings that result in the smallest mean average estimation error as the appropriate setting of the unscented Kalman filter. A Euclidian

distance based comparison method is developed to show the performance of the proposed model-driven assessment method. Simulation examples in section 5.3.3 show that the proposed method can track changes of the load consumption and the load-to-voltage sensitivity. However, it is found that the results of model-driven method and Euclidian distance based method do not match each other well. A possible reason is that the load profile of a single normal-voltage day selected by the Euclidian distance based method cannot accurately represent what the load would be if there were no voltage reduction during the conservation voltage reduction period. Since the actual conservation voltage reduction factors are unknown, the accuracy of the proposed method cannot be fully verified with the practical data. Further studies on the verification of the estimation results of conservatism voltage reduction effects are necessary in the future work.

Compared to previous efforts on evaluating conservation voltage reduction effects, the proposed methods have the following notable advantages: 1) they do not depend on the selection of control groups or assumption of a simple linear relationship between a load and its impact factors; 2) they capture the nature of conservation voltage reduction by modeling load-to-voltage sensitivities; 3) they consider the time-varying and uncertain nature of conservation voltage reduction effects. The proposed assessment method can potentially be used to guide the selection of suitable substations and appropriate time to implement voltage reduction. It can also be used to assist utilities to perform cost/benefit analyses.

Next chapter studies demand response which is implemented on the customer side to improve the energy efficiency.

CHAPTER 6 IMPLEMENTATION OF DEMAND RESPONSE WITH DGs AND ENERGY STORAGE SYSTEMS

6.1 Overview

Chapters 4 and 5 investigate voltage/VAR control and conservation voltage reduction which can be applied by utilities to improve the operating efficiency of distribution grids. This chapter investigates demand response. Unlike voltage/VAR control which is imposed by utilities, demand response is a measure that can be implemented on the customer side to operate the power system in a more efficient and reliable way. Utilities usually provide multiple options of demand response programs to customers, so as to reduce or shift the peak-time demand, and improve the system operation and reliability. On the other hand, customers have various demand profiles. The integration of customer-owned DGs and energy storage systems brings further challenges. This chapter describes a novel method to assist various types of end-use customers to make the most beneficial plan to participate in demand response programs, and to integrate customer-owned DGs and energy storage systems. Meanwhile, the developed method can also help the customers to schedule DG generation, charging/discharging of batteries, and perform load management accordingly. Multiple objectives are considered in the decision-making process, which include costs, reliability, and discomfort. The costs include electricity purchases and investments of DGs. The reliability is defined as the curtailment index of loads. The discomfort is defined as the load shifts.

The problems that need to be solved can be summarized as follows:

- In which demand response program(s) should a customer participate?
- How many battery units should be installed to coordinate with the demand response programs?
- How to perform energy management (e.g., load shifting, charging/discharging of battery units) with the selected demand response programs?

6.2 Mathematical Formulation

The proposed two-stage scheme for the selection and energy management of demand response (DR) programs is shown in Fig. 6.1.

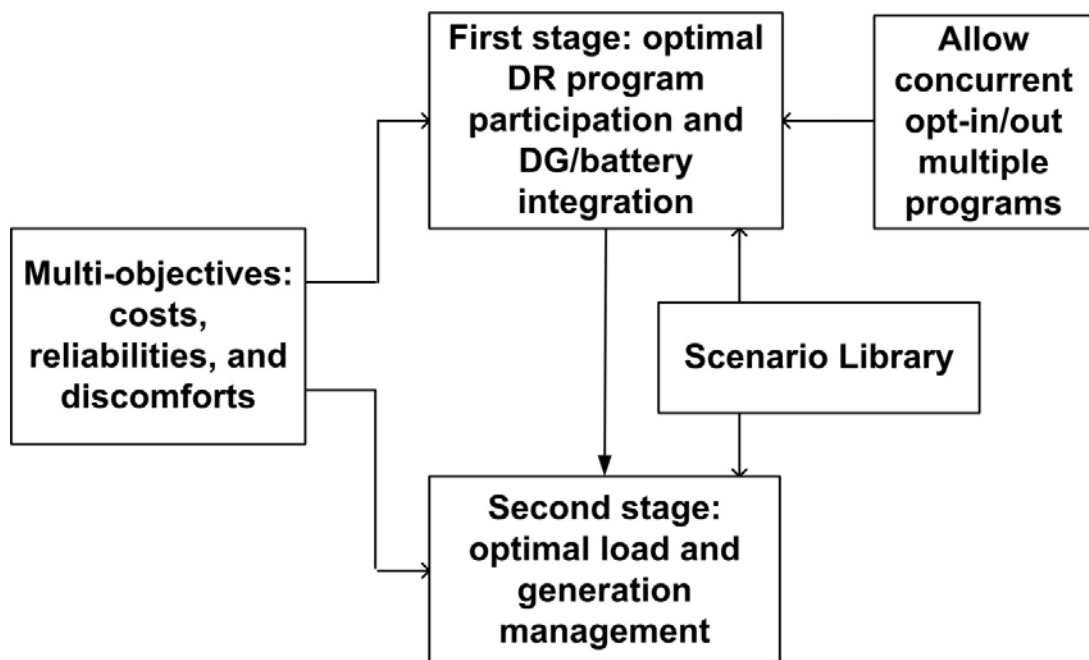


Figure 6.1. Two-stage demand response selection and energy management.

In the first stage, multiple types of demand response programs are considered, e.g., peak-time rebate, time-of-use and critical peak pricing programs. The integration of consumer-

owned DGs and energy storage is also taken into account. In the second stage, the load dispatch is performed based on the demand response programs selected in the first stage. Three objectives are taken into account: cost, reliability, and discomfort. The objectives are expected values under uncertainty. The proposed formulation is as follows, and Table 6.2 shows the nomenclature for the formulation.

Table 6.1 Nomenclature for demand response formulation.

i	Index for demand response programs: 1-Peak-time rebate; 2-Time of use (TOU); 3-Critical peak pricing (CPP)	$r_{y,w}$	Reliability index in scenario w in year y
h	Index for hour of the day	$d_{y,w}$	Discomfort index in scenario w in year y
P^r	Reliability cost	P^d	Discomfort cost
y	Index for year	β_y	Present worth factor in year y
w	Index for scenario	W^r	Weight for reliability
W^c	Weight for cost	W^d	Weight for discomfort
W_w	Probability of scenario w	OC^g	Operation cost of generators
$g_{h,y,w}$	Output of generators	IC^s	Investment cost of storage
IC^g	Investment cost of generators	$p_{h,y,w}$	Net electricity price
z^s	Number of batteries to be installed	z^g	Number of generators to be installed
$S_{i,y}^{dr}$	Sign-on bonus of program i in year y	$p_{h,y,w}^t$	Carbon tax price
$C_{y,w}^l$	Total cost of scenario w in year y	$l_{h,y,w}$	Net load consumption
p^{curt}	Curtailed payment	$L_{h,y,w}^0$	Load consumption without demand response programs
$l_{h,y,w}^s$	Shifted load	$l_{h,y,w}^c$	Curtailed load
$L_{y,w}^{\max}$	Max. load consumption without demand response programs	$\alpha_{h,w}^s$	Load shifting ratio
P_y^0	Electricity price without demand response programs	$R_{y,w}^{PTR}$	Total peak time rebate

$\Delta PTOU_{h,y,w}$	Price change due to time-of-use program	$\Delta PCPP_{h,y,w}$	Price change due to critical time pricing
$PTR_{h,y,w}$	Peak time rebate	G^{\max}	Maximum output of generator
$a_{h,y,w}$	Capacity factor of generator	γ	Aging factor of energy storage system
$q_{h,y,w}^{sd}$	Discharging power	M^s	Maximum charging/discharging of one battery unit
$q_{h,y,w}^{sc}$	Charging power	$s_{h,y,w}$	State of charge of energy storage system
η^d	Discharging efficiency	η^c	Charging efficiency
η^l	Battery leakage	p^{ocs}	Operation cost of energy storage systems
D^s	Charging/discharging duration	$\alpha_{h,w}^c$	Load curtailment ratio

$$\min (W^c (IC^s z^s + IC^g z^g - \sum_{i,y} S_{i,y}^{dr})) + 365 \sum_{y,w} W_w (W^c C_{y,w}^l + W^r P^r r_{y,w} + W^d P^d d_{y,w}) \quad (6.1)$$

Subject to

$$C_{y,w}^l = \beta_y (\sum_h (OC^g g_{h,y,w} + (p_{h,y,w} + p_{h,y,w}^l) l_{h,y,w} + p^{curt} l_{h,y,w}^c + p^{ocs} (q_{h,y,w}^{sd} + q_{h,y,w}^{sc})) - R_{y,w}^{PTR}), \forall y, w, \quad (6.2)$$

$$l_{h,y,w} = L_{h,y,w}^0 - g_{h,y,w} - l_{h,y,w}^s - l_{h,y,w}^c - q_{h,y,w}^{sd} + q_{h,y,w}^{sc}, \forall h, y, w, \quad (6.3)$$

$$l_{h,y,w} \leq L_{h,y,w}^{\max}, \forall h, y, w, \quad (6.4)$$

$$\sum_h l_{h,y,w}^s = 0, \forall y, w, \quad (6.5)$$

$$l_{h,y,w}^s \leq \alpha_{h,w}^s (\sum_i z_{i,y}) L_{h,y,w}^0, \forall h, y, w, \quad (6.6)$$

$$l_{h,y,w}^c \leq \alpha_{h,w}^c (z_{1,y} + z_{3,y}) L_{y,w}^{\max}, \forall h, y, w, \quad (6.7)$$

$$p_{h,y,w} = P_y^0 + z_{2,y} \Delta PTOU_{h,y,w} + z_{3,y} \Delta PCPP_{h,y,w} - z_{2,y} z_{3,y} \Delta PTOU_{h \in [14,18], y, w}, \forall h, y, w \quad (6.8)$$

$$R_{y,w}^{PTR} = z_{1,y} \sum_{h \in [14,18]} (L_{h,y,w}^0 - l_{h,y,w}) PTR_{h,y,w}, \forall y, w, \quad (6.9)$$

$$s_{h,y,w} = \eta^l s_{h-1,y,w} - (\eta^d)^{-1} q_{h,y,w}^{sd} + \eta^c q_{h,y,w}^{sc}, \forall h, y, w. \quad (6.10)$$

$$s_{1,y,w} = s_{24,y,w} = \gamma^{y-1} D^s z^s M^s, \forall y, w. \quad (6.11)$$

$$q_{h,y,w}^{sd} \leq \gamma^{y-1} z^s M^s, \forall h, y, w. \quad (6.12)$$

$$q_{h,y,w}^{sc} \leq \gamma^{y-1} z^s M^s, \forall h, y, w. \quad (6.13)$$

$$s_{h,y,w} \leq \gamma^{y-1} D^s z^s M^s, \forall h, y, w, \quad (6.14)$$

$$d_{y,w} = \sum_h |l_{h,y,w}^s|, \forall y, w, \quad (6.15)$$

$$r_{y,w} = \sum_h l_{h,y,w}^c, \forall y, w, \quad (6.16)$$

$$g_{h,y,w} \leq z^g a_{h,y,w} G^{\max}, \forall h, y, w, \quad (6.17)$$

$$z^s \in \text{integer}, z \in \text{binary} \quad (6.18)$$

$$C^1, r, d, l, g, l^c, q^{sd}, q^{sc}, s \geq 0 \quad (6.19)$$

In the above formulation, the objective function (6.1) minimizes the total costs during the planning horizon. The costs include the investment and operation costs of energy storage systems and distributed generators, the reliability cost, and the discomfort cost. The sign-on bonus is considered as a negative cost. It is assumed that there are 365 days in one year.

Constraint (6.2) represents the operation costs, the first item is the operation cost of distributed generators, the second item is the cost of load consumption, the third item is the cost of load curtailment, the fourth item represents the operation cost of energy storage systems, and the last item is the total peak-time rebate. Constraint (6.3) represents

the net load consumption. The first item represents the original load consumption of the customer, the second item represents the generation of distributed generators, the third item represents the shifted load, the fourth item represents the curtailed load, and the last two items represent the charging and discharging of energy storage systems. Five representative scenarios are considered, winter weekdays, winter weekends, summer weekdays, summer weekends, and event days (only applicable under certain demand response programs).

Constraint (6.4) indicates that the net load consumption with demand response programs should be no larger than the load consumption without demand response programs. In constraint (6.5), the net shifted load in a day should be zero, since all shifted load consumption can be supplied eventually. Constraint (6.6) represents the maximum allowable load shift, which should be a certain portion of the original load consumption. Constraint (6.7) represents the maximum allowable load curtailment. Constraint (6.8) represents the net electricity price with demand response programs. The first item represents the electricity price without any demand response programs. The second item represents the price adjustment of time-of-use program. The third item represents the price adjustment of critical peak pricing program. If a consumer participates in both time-of-use and critical time pricing programs, there exists a duplicate charge during peak hours, which is deducted by the last item. Constraint (6.9) represents the peak-time rebate. Peak time is defined as 2 pm to 6 pm in this dissertation. The operator can change the settings according to practical scenarios.

Constraints (6.10-6.14) represent the operating constraints of energy storage systems, which have been used by other researchers [115-118]. Constraint (6.10) calculates the

state of charge (SOC) of the energy storage systems for each time period. According to the operation requirement of energy storage systems, the state of charge at the end of the day should be equal to the state of charge at the beginning of the day, which is indicated by constraint (6.11). Constraints (6.12) and (6.13) represent the maximum discharging and charging constraints of energy storage systems, respectively. Constraint (6.14) indicates the maximum continuously charging/discharging period.

Constraint (6.15) defines the discomfort index as the total shifted load consumption. In constraint (6.16), the reliability index is defined as the total curtailed loads. Constraint (6.17) represents the maximum allowable outputs of generators.

The first-stage decision variables are z_s , z_g , and $z_{i,y}$; the second-stage decision variables are $g_{h,y,w}$, $q_{h,y,w}^{sd}$, $q_{h,y,w}^{sc}$, $l_{h,y,w}$, $l_{h,y,w}^s$, and $l_{h,y,w}^c$. The first stage of the formulation assists customers in selecting the most beneficial demand response programs (i.e., time-of-use, critical time pricing, and peak-time rebate). The first stage also makes decisions on the integration of customer-owned DGs and batteries. The second stage performs load managing and generation scheduling according to the decision made in the first stage.

6.3 Numerical Results

6.3.1 Parameter Settings of Case Studies

The proposed model in equations (6.1-6.18) is tested with two types of customers: small commercial/industrial buildings and large commercial/industrial campuses. Five demand scenarios [101] are considered in the case study: 1. summer weekdays, 2. summer weekends, 3. winter weekdays, 4. winter weekends, and 5. critical days (event days). In general, hot summer weekdays and cold winter weekdays with severe events are

considered as critical days. For purposes of illustration, the probabilities of the five demand scenarios are set to be $W_1=0.3425$, $W_2=0.1370$, $W_3=0.3425$, $W_4=0.1370$, and $W_5=0.041$. Fig. 6.2 shows the load consumption of five scenarios for small commercial/industrial buildings. Fig. 6.3 shows the load consumption of five scenarios for large commercial/industrial campuses.

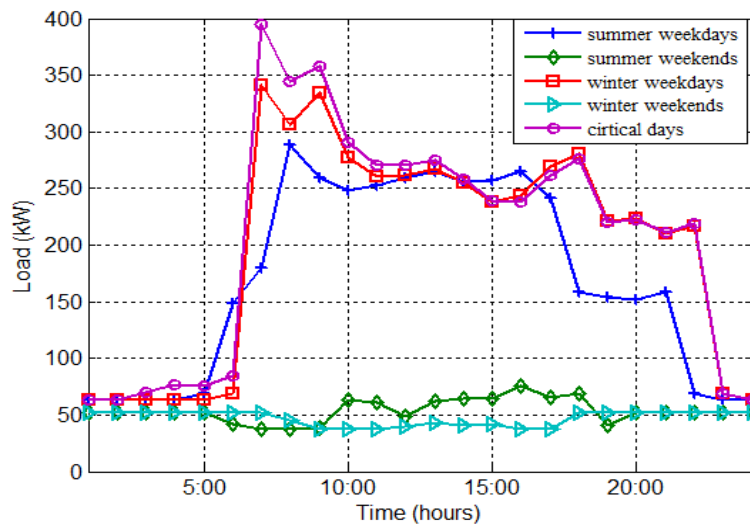


Figure 6.2. Five load scenarios for small commercial/industrial buildings.

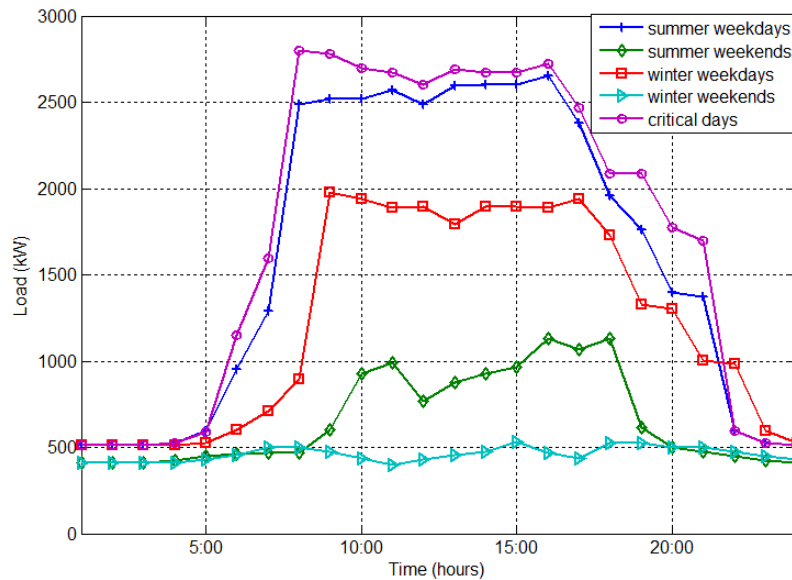


Figure 6.3. Five load scenarios for large commercial/industrial campuses.

The base electricity price P_1^0 is set at 0.20 \$/kWh, the price deviations of demand response programs are shown in Fig. 6.4 [119]. Equation (6.8) shows that the electricity price for a certain time slot is the aggregation of the base price and the corresponding price deviations. It is assumed that the annual increasing rate of base electricity price is 7%. The annual discount rate is 0.95.

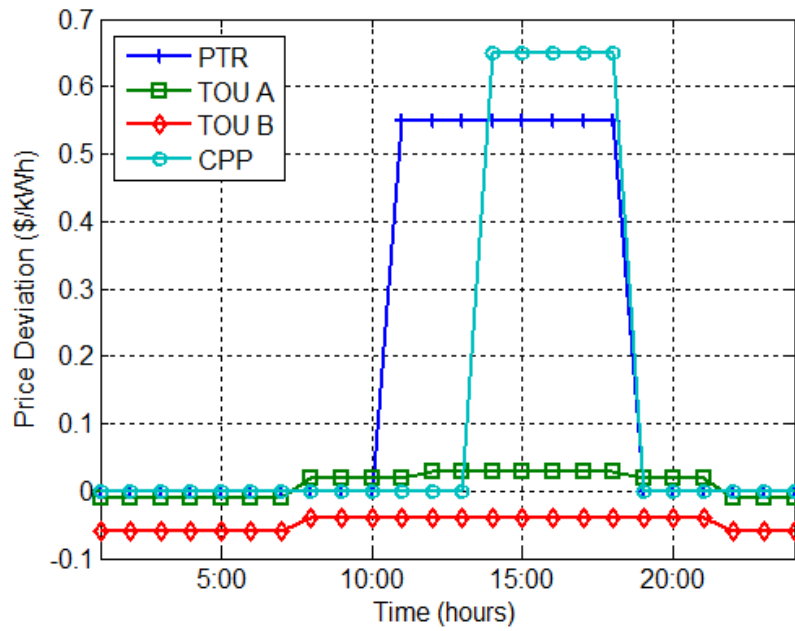


Figure 6.4. Price deviations of demand response programs.

The planning horizon is at 5 years. G^{\max} is set at 80 kW for small commercial/industrial buildings, and 600 kW for large commercial/industrial campuses. OC^s is set at \$0.1/kWh with the annual increase of 2%. Sign-on bonus is applied to the critical peak pricing program, and is set to be \$0.5/kW of the maximum load consumption. α_{hw}^s is set at 0.05 and α_{hw}^c is set at 0.05. For the energy storage systems, η^l is set at 0.95, η^c is set at 0.90, η^d is set at 0.90, γ is set at 0.9, P^{ocs} is set at 0.50 \$/kWh, D^s is set at 4 hours, and M^s is set at 3 kW. It is assumed that the weights of costs, reliability index and discomfort index are 0.45, 0.45, and 0.1, respectively. It should be

noted that all of the simulation settings are for illustration, operators can change the settings according to the operation and available information of a system. Fig. 6.5 shows the flowchart of the simulations. The proposed model in (6.1-6.18) is coded in the general algebraic modeling system. The inputs of the simulations include the parameter settings in Section 6.3.1, load profiles and electricity price. Since the proposed model represents a mixed-integer nonlinear and nonconvex problem, the Discrete and Continuous Optimizer (DICOPT) in the General Algebraic Modeling System (GAMS) [93] is used to solve the problem. The simulation is performed by using a computer with Intel Quad Core 2.40 GHz and 8 GB memory. The computation time for each simulation case is around 2 minutes. The outputs of the solver are the optimal selection of demand response programs, integration of battery units and energy management.

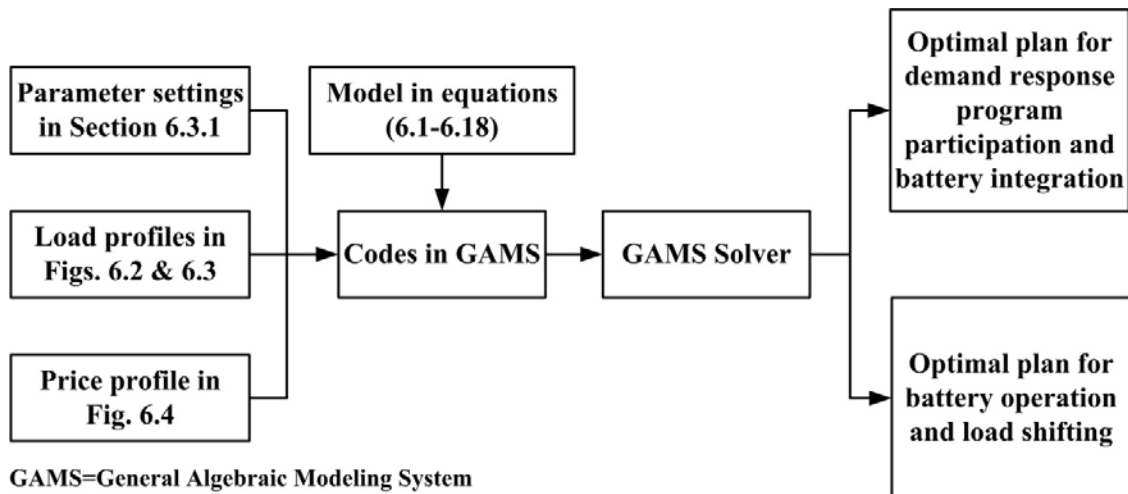


Figure 6.5. Flowchart of simulation.

6.3.2 Simulation Results for Small Commercial/Industrial Buildings

The model defined in equations (6.1-6.18) is tested with a small commercial/industrial building. The load profiles of the building are shown in Fig. 6.2. The settings of the model parameters are defined in Section 6.3.1. Five demand scenarios

[101] are considered: scenario 1. summer weekdays, scenario 2. summer weekends, scenario 3. winter weekdays, scenario 4. winter weekends, and scenario 5. critical days (event days). The model is solved by the general algebraic modeling system [90] to obtain the optimal selection of demand response programs, integration of battery units/DGs and energy management. For the selection of demand response programs and battery units/DGs, the building installs one DG and 47 battery units, and participates in all three demand response programs in the five years.

(a) Results of Load Shifting

In order to illustrate the optimal load consumption management with demand response programs, this subsection starts with Fig. 6.5 which shows the load shifting results in five demand scenarios in the first year. A positive value represents that the load is shifted from the corresponding time, and a negative value represents that the load is shifted to the time period. Scenarios 1, 4 and 5 have positive load shifting during 11:00 to 19:00 (peak-hours) and negative load shifting during other periods of a day (off-peak hours). The net shifted load consumption of scenarios 1, 4 and 5 during 24 hours is zero, which satisfies the constraint (6.5). In Fig. 6.6 the shifted load of scenarios 2 and 3 is zero during 24 hours since the two scenarios represent weekend load demand which is usually low.

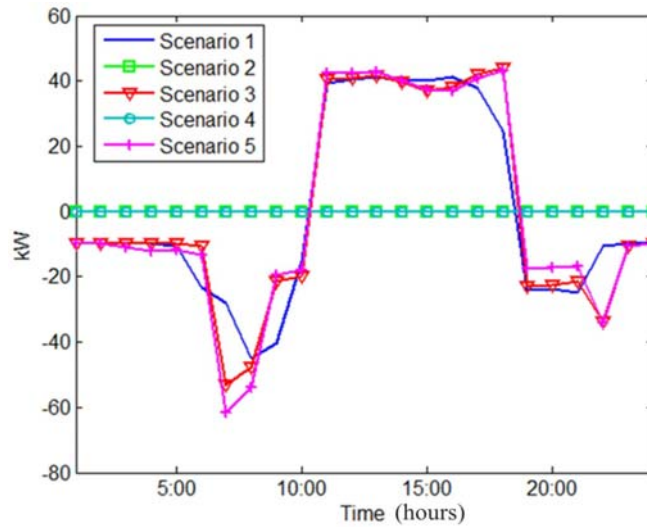


Figure 6.6. Load shifting results of a small commercial/industrial building in the first year.

(b) Results of Optimal Energy Management of Battery Units

In order to demonstrate the optimal energy management of battery units, this subsection starts with Fig. 6.7. The figure shows the aggregated charging/discharging operation of all installed battery units in the first year, which is obtained by solving the problem defined in equations (6.1-6.18).

In Fig. 6.7, a positive value represents that batteries are operating at the discharging state, and a negative value indicates that batteries are operating at the charging state. In general, the fluctuation of charging/discharging power in scenarios 2 and 4 (summer/winter weekends) is smaller than that of scenarios 1, 3 (summer/winter weekdays) and 5 (event days). In scenario 5 (event days), batteries operate in the discharging state during the critical period (14:00-18:00). The reason is that grid electricity price in the critical period is high as shown in Fig. 6.4, and the building tends to support its load using batteries.

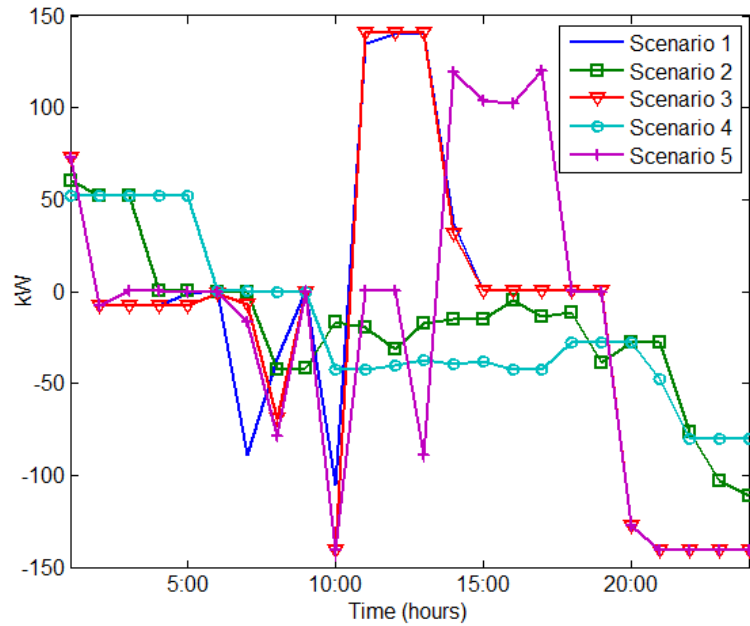


Figure 6.7. Aggregated charging/discharging of battery units of a small commercial/industrial building in the first year.

(c) Results of Imported Power from Grids

Fig. 6.8 shows the net imported power from the grid in the first year. In scenarios 2 and 4 (summer/winter weekends), the imported power is zero from 1:00 to 20:00, which indicates that the building is self-sufficient during this period. In scenarios 1 and 3 (summer/winter weekdays), the building imports electricity from the grid. During 14:00-17:00, i.e., the peak period of event days, the building uses all of its generation and storage capacities to be self-adequate, because of the extremely high electricity price as shown in Fig. 6.4.

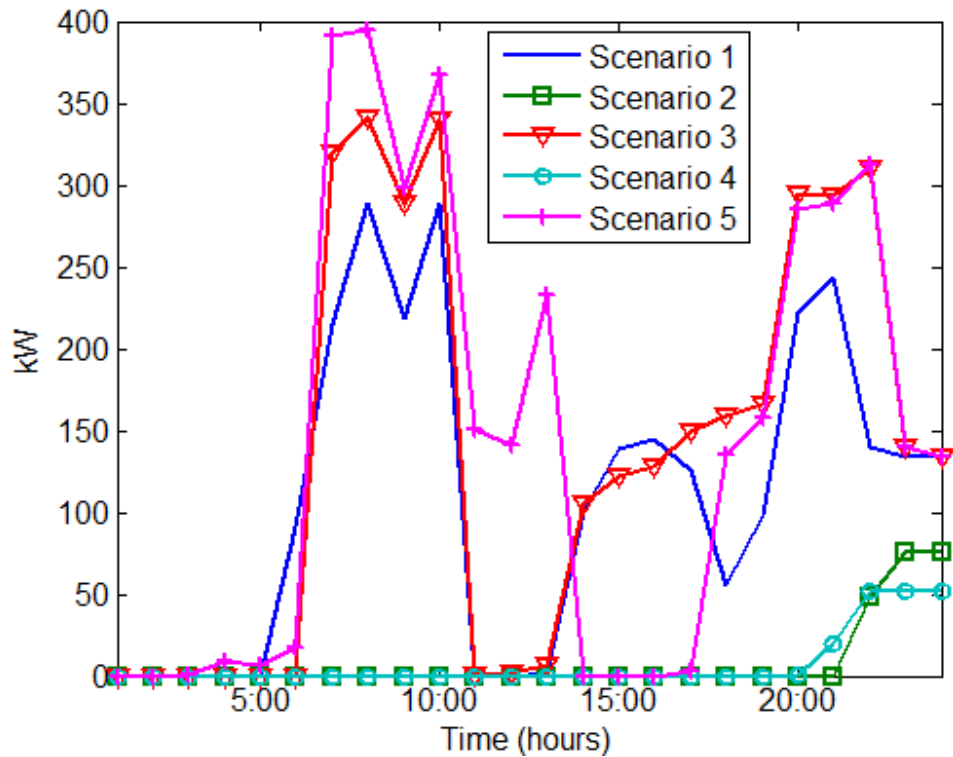


Figure 6.8. Power imported from the grid of a small commercial/industrial building in the first year.

(d) Imported Power from Grids for a Building without Battery Units

In order to show the impacts of energy storage systems on customer behaviors, it is assumed that there is no battery installed in the building. Fig. 6.9 shows the net imported power from the grid in the first year. Compared to Fig. 6.8, the imported power in Fig. 6.9 becomes smaller during the night for all five scenarios because there is no battery unit that needs to be charged. However, the peak demand (14:00 to 18:00) becomes larger in scenarios 1, 3 (summer/winter weekdays) and 5 (event days). This is because the demand can only be supplied by the grid and DG. In Fig. 6.8, the building can be self-supplied in peak hours in event days to avoid paying a much higher energy price. As shown in Fig. 6.9, the building has to buy electricity at the critical peak price in event days because there is no energy storage system.

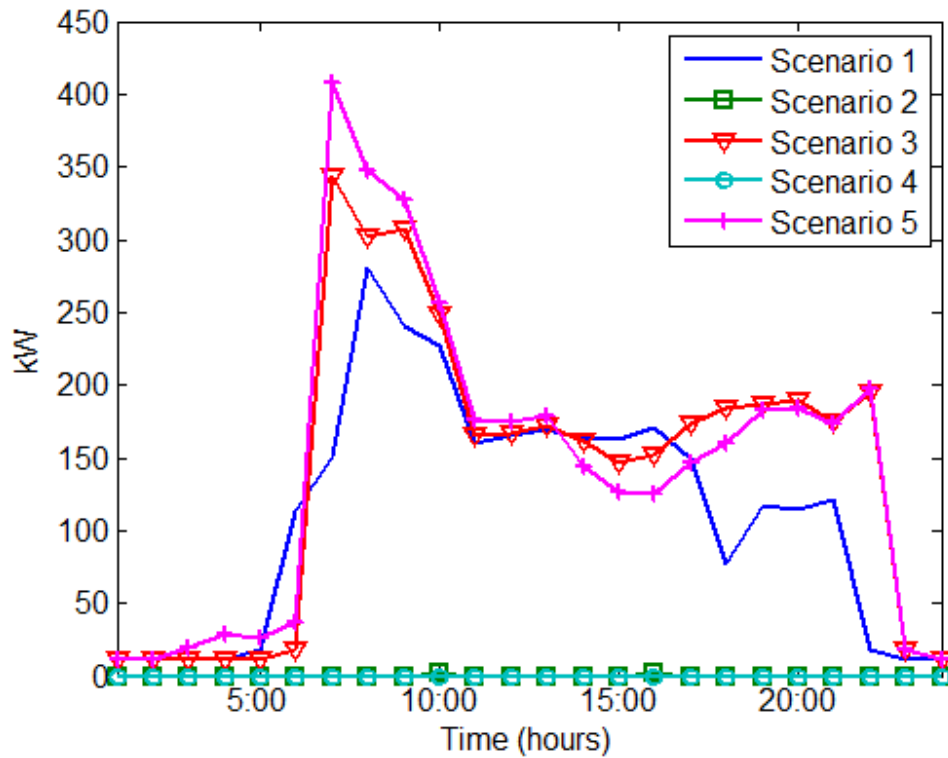


Figure 6.9. Power imported from the grid of a small commercial/industrial building without batteries in the first year.

6.3.3 Simulation Results for Large Commercial/Industrial Campuses

In this case, simulations are run for a large commercial/industrial campus with load profiles showing in Fig. 6.3. The settings of the model parameters are defined in Section 6.3.1. Five demand scenarios [101] are considered: scenario 1. summer weekdays, scenario 2. summer weekends, scenario 3. winter weekdays, scenario 4. winter weekends, and scenario 5. critical days (event days). The model is solved by the general algebraic modeling system [90] to obtain the optimal selection of demand response programs, integration of battery units/DGs and energy management. For the selection of demand response programs and battery units/DGs, the campus installs one DG and 468 battery units, and participates in all three demand response programs in the five years.

(a) Results of Load Shifting

Fig. 6.10 shows the load shifting results in five demand scenarios in the first year. A positive value represents that the load is shifted from the corresponding time, and a negative value represents that the load is shifted to the time period.

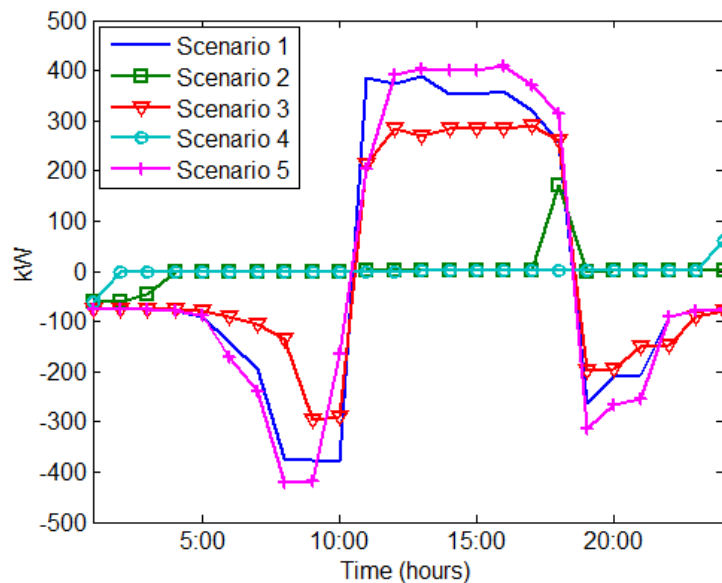


Figure 6.10. Load shifting results of a large commercial/industrial building in the first year.

Similar to the load shifting results in the small commercial/industrial building, load consumption is mostly shifted during 11:00 to 18:00 in scenarios 1, 3 (summer/winter weekdays) and 5 (event days).

(b) Load shifting for a Building without Battery Units

In order to show the impacts of energy storage systems, Fig. 6.11 shows the load shifting under the assumption that there is no battery installed on campus. Compared with Fig. 6.10, the shifted load consumption becomes larger in scenarios 2, 4 and 5, especially for scenario 2 (summer weekdays). This is because load can only be supplied by the grid and DG if there is no battery unit, more load consumption needs to be shifted to respond to the electricity price in peak periods. Shifted load consumption is close to zero for

winter weekends since the demand in this scenario is relatively low itself as shown in Fig.

6.3.

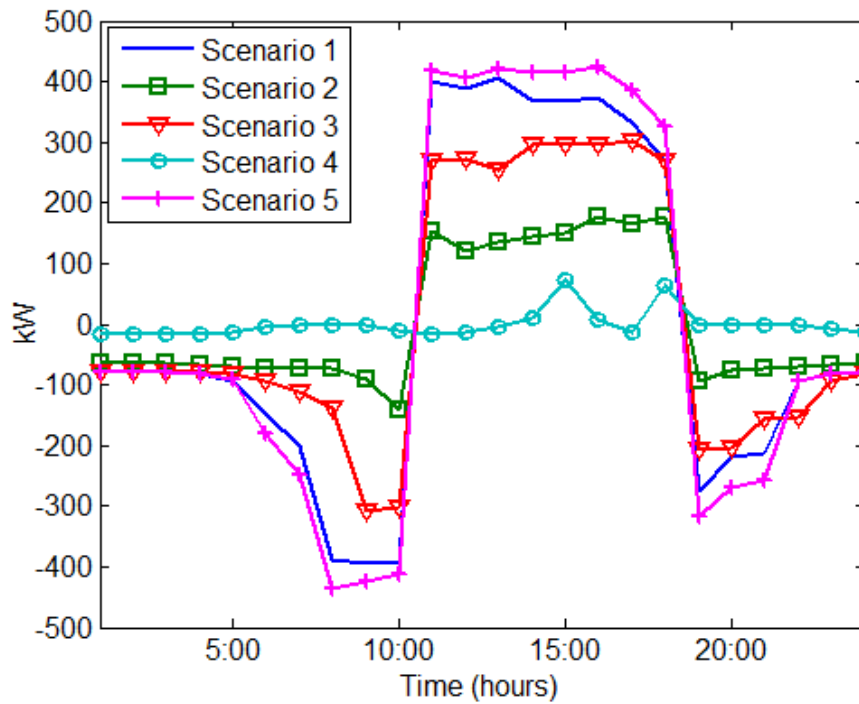


Figure 6.11. Load shifting of a large commercial/industrial campus without batteries in the first year.

(c) Results of Optimal Energy Management of Battery Units

Fig. 6.12 shows the aggregated charging/discharging operation of all installed battery units in the first year. A positive value represents that batteries are operating at the discharging state, and a negative value indicates that batteries are operating at the charging state.

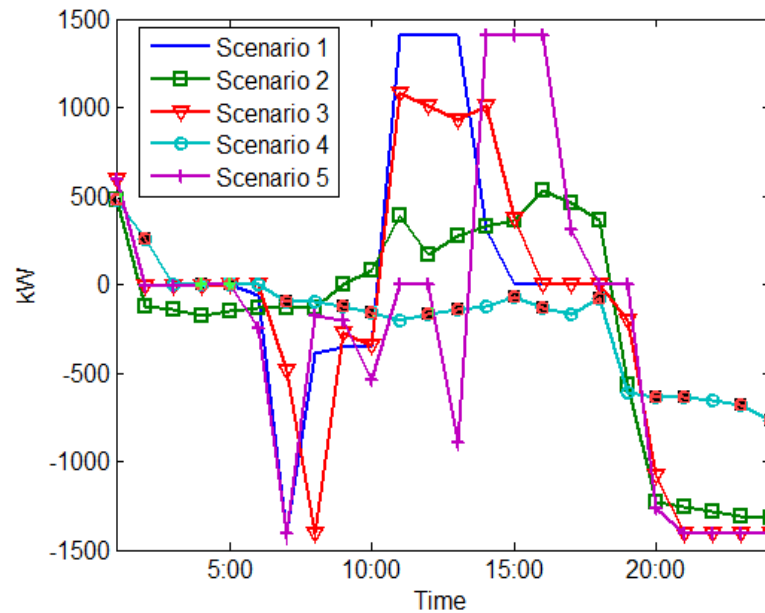


Figure 6.12. Aggregated charging/discharging of battery units of a large commercial/industrial campus in the first year.

Battery units work in the discharging mode to support demand during peak periods in summer/winter weekdays, summer weekends, and event days. The charging/discharging power in winter weekends is still small due to the relatively flat and small demand. In all five scenarios, battery units are operated in the charging state from 8:00 pm to midnight to take advantage of the relatively cheap electricity.

(d) Results of Imported Power from Grids

Fig. 6.13 shows the net imported power from the grid in the first year by solving the model defined in equations (6.1-6.18). The campus can be self-supported in most periods in scenarios 2 and 4 (summer/winter weekends) since the net imported power during these periods are zero. During the night of scenarios 2 and 4 (summer/winter weekends), the campus imports relatively cheap electricity from the grid to charge the battery units. In scenarios 1 and 3 (summer/winter weekdays), the campus needs to buy electricity from

the grid. In the peak periods (14:00-18:00) of scenario 5 (event days), the campus tends to buy less electricity from the grid, because of the extremely high electricity price in event days as shown in Fig. 6.4.

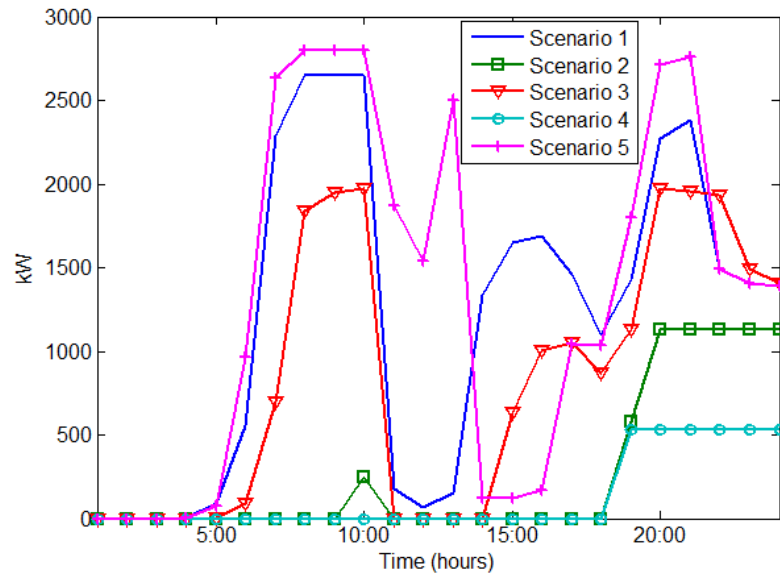


Figure 6.13. Power imported from the grid of a large commercial/industrial campus in the first year.

Fig. 6.14 shows the net imported power from the grid in the fifth year. Compared to the results shown in Fig. 6.13, the campus imports more power from the grid in the fifth year. This is because of the increasing load consumption and decreasing available capacity of energy storage systems and DGs (because of the aging problems).

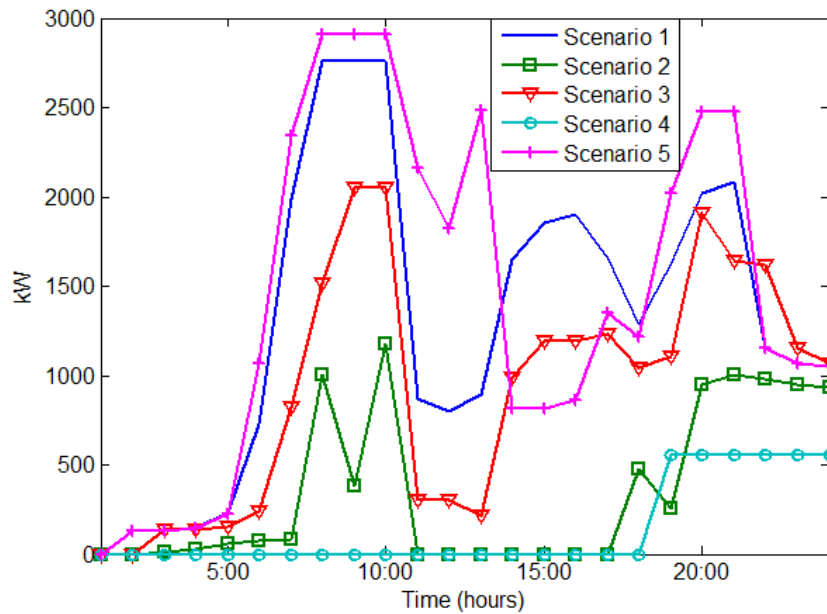


Figure 6.14. Power imported from the grid of a large commercial/industrial campus in the fifth year.

(e) Impacts of Critical Time Price on Customer Behavior

In order to show the impacts of demand response program design on customer behavior, the critical time price shown in Fig. 6.4 is increased by 150%. After running the optimization, the customer selects time-of-use and peak-time rebate programs to participate in all five years, while participating in critical time pricing programs for the first year. Fig. 6.15 shows the net imported power from the grid in the fifth year. Compared to the results in Fig. 6.14, the imported power during peak hours increases in event days. This is because the customer has already decided not to participate in critical time pricing program

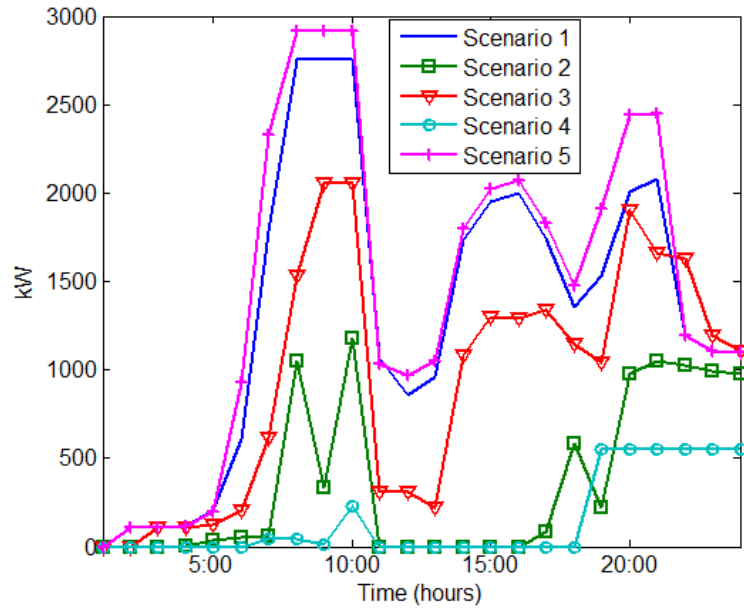


Figure 6.15. Power imported from the grid of a large commercial/industrial campus in the fifth year (with peak-time rebate and time-of-use).

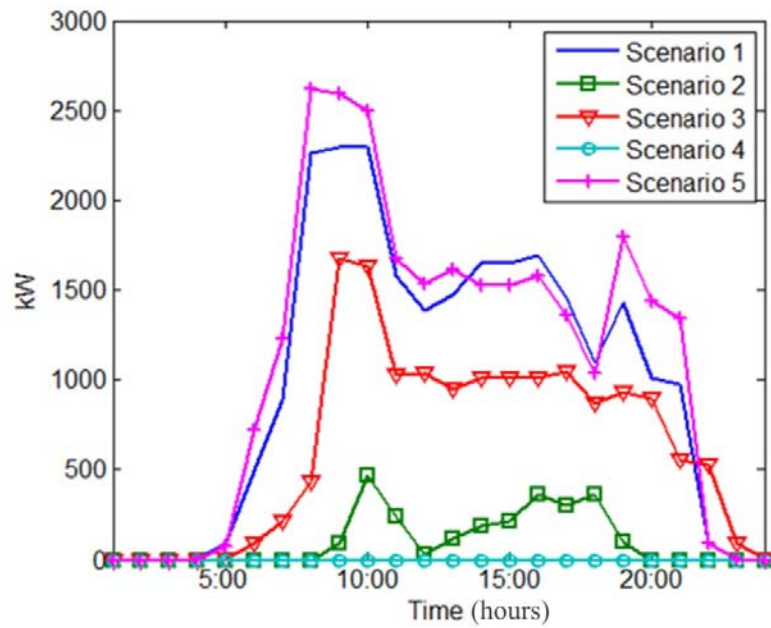


Figure 6.16. Power imported from the grid of a large commercial/industrial campus without batteries in the first year.

(f) Imported Power from Grids for a Campus without Battery Units

Fig. 6.16 shows the net imported power from the grid of the large campus under the assumption that there is no battery installed. Compared to Fig. 6.13, the campus does not need to import power in night to charge the batteries. However, it needs to buy more electricity with a higher price in the peak periods in summer/winter weekdays, winter weekends and event days. The total operation costs of the customer with and without battery units over a period of 5 years are \$693,517 and \$940,560, respectively.

6.4 Summary

This chapter proposes a two-stage framework for the planning and energy management of a customer with demand response programs. In practice, a utility usually provides multiple demand response programs to its customers. In the proposed method, the first stage is to assist the customer to select the most beneficial programs to participate and install an appropriate number of battery units. The second stage is to perform energy management according to the decisions made in the first stage, which includes dispatches of loads, DGs and energy storage systems.

For illustration, two types of customers (small commercial/industrial buildings and large commercial/industrial campuses) and five demand scenarios (summer/winter weekdays, summer/winter weekends, and event days) are considered in the case study. The simulation results demonstrate the effectiveness of our method. The impacts of batteries and demand response program designs on customer behaviors are also shown.

Chapter 7 concludes the dissertation and introduces future work direction.

CHAPTER 7 CONCLUSIONS AND FUTURE WORK

DIRECTION

7.1 Conclusions and Contributions

This research focuses on the efficient operation of modernized distribution grids on the customer side and the utility side. For the customer side, this research studies the optimal demand side management. For the utility side, this research investigates the voltage/VAR control and DG integration. Compared to the existing literature, the main contributions of this dissertation are as follows:

(1) A two-stage co-optimization framework is proposed for the planning and energy management of a customer with demand response programs. The novel method considers multiple demand response programs, various customer types and demand scenarios, and the integration of energy storage systems. The designed method can help a customer to make the most beneficial plans to join demand response programs and install energy storage systems in the planning stage, and optimally schedule the loads, DG outputs and batteries according to the decisions made in the first stage.

(2) A stochastic rolling horizon optimization-based voltage/VAR control technique is developed. The uncertainty and variability of DG outputs and load consumptions are fully considered in the proposed method. Instead of using the constant-power load model which is widely applied in existing voltage/VAR control research, the exponential load models are used to capture the load-to-voltage sensitivities of a variety of customers. Therefore, the major contribution of this work is to simultaneously consider the stochasticity of load and renewable generation, and the load-to-voltage relationship.

(3) A multistage support vector regression algorithm is developed to estimate the load consumption without voltage reduction during the conservation voltage reduction period. Compared to the existing regression-based methods to assess conservation voltage reduction effects which assume linear regression models, the proposed big data-driven method can capture the complicated load behaviors. The probabilistic nature of conservation voltage reduction effects is considered when selecting target feeders by a proposed stochastic analysis framework based on the Kolmogorov-Smirnov test.

(4) A load model identification-based method is proposed to assess the conservation voltage reduction effects. This method captures the nature of conservation voltage reduction by modeling the load as a function of voltage and calculating conservation voltage reduction factors from the identified load-to-voltage sensitivities. The proposed method does not require long-term day on/day off tests to conduct comparison. The new method can assist utilities in assessing the conservation voltage reduction effects of feeders.

(5) A solution and validation method is presented for stochastic DG placement. The objective of the DG placement is to assist the implementation of conservation voltage reduction. The uncertainties of renewable DG outputs and load consumption are considered by formulating the problem as a stochastic program. A combined sample average approximation-multiple replication procedure method is developed to solve the problem and validate the optimality of the solutions.

In particular, a two-stage framework to facilitate demand response at the customer level is proposed. The objective is to maximize the benefits to the customer. In the first stage, the proposed method can assist a customer to select multiple demand response

programs to join and install an appropriate amount of batteries to coordinate with demand response. The second stage is to perform energy management according the planning decisions in the first stage, which includes dispatches of loads, fossil-fired backup generators and batteries. The proposed method can be applied to residential, commercial and industrial customers with various demand scenarios. For illustration, the simulations study two types of customers: large commercial/industrial campuses and small commercial/industrial buildings. Five demand scenarios are considered: summer weekdays, summer weekends, winter weekdays, winter weekends and event days. Time-of-use, critical time pricing and peak-time rebate are considered as options of demand response programs. The numerical results show the impacts of demand response incentives and costs of energy storage systems on the selection and operation of demand response programs. The proposed method can be used to assist customers to make the most beneficial decisions to participate in demand response.

To guarantee the efficient and reliable operation of a modernized distribution grid, a stochastic rolling horizon optimization-based voltage/VAR control technique is proposed. The method considers exponential load models and the probabilistic nature of prediction errors of DG outputs and load consumptions. The voltage/VAR control problem is formulated as a stochastic program with the purposes to minimize power losses and voltage deviations along a feeder. Different types of customers (residential, commercial and industrial customers) in a distribution system are taken into account by assigning corresponding exponents in the load models. Case studies on the modified 33-bus test system with wind turbines, photovoltaic generators and different types of loads verify the effectiveness of the proposed voltage/VAR control technique. Compared to the case

without voltage/VAR control, the proposed method can reduce losses by up to 77% and reduce maximum voltage deviations by up to 65%. It should be noted that the stochastic voltage/VAR control produces from two to three times greater benefits than the deterministic voltage/VAR control approach. Finally, it appears that significant differences exist in voltage/VAR control dispatches when load models are taken into account. Compared with previous studies on voltage/VAR control dispatch, the proposed method considers both improved load models and uncertain DG outputs.

The conservation voltage reduction plays an essential role in a smart distribution grid. This dissertation develops two novel methods to assess load-reduction effects of conservation voltage reduction: data-driven method and model-driven method. The data-driven method is based on a proposed multi-stage support vector regression technique to estimate the load consumption without voltage reduction during a conservation voltage reduction period. The first stage is to make use of pre- conservation voltage reduction and post- conservation voltage reduction data to select a set of load profiles that are closest to the profile under estimation. The selected profiles are used to train the support vector regression prediction model in the second stage. Estimated load profiles with large errors are filtered out in the third stage. The conservation voltage reduction factors can be calculated by using the estimated load profile. In the proposed model-driven method, load is modeled as a function of voltage by a time-varying exponential load model. The model parameters are recursively identified by recursive least square. The conservation voltage reduction factors can be calculated using the identified load-to-voltage sensitivities. A conservation voltage reduction factor is subject to different types of uncertainties, depending on load mix, feeder configurations, weather conditions, human behaviors, etc.

This dissertation uses the Kolmogorov-Smirnov goodness-of-fit test to identify the most suitable probability distributions representing conservation voltage reduction effects of different feeders. The cumulative distribution functions that represent conservation voltage reduction effects of each feeder are used to select candidate feeders. The results could potentially be used to select target feeders before making any investments.

To accommodate the increasing penetration of DGs, this dissertation presents a new DG planning strategy to assist the implementation of conservation voltage reduction. The DG placement is defined as a stochastic optimization problem to enable the distribution system to decrease load consumptions. In order to deal with the uncertain nature of DG outputs and load consumptions, a combined sample average approximation-multiple replication procedure-based algorithm is developed to obtain the optimal solution. The quality of the optimal solution is validated by calculating its confidence interval using a multiple replication procedure. The case studies show the effectiveness of the proposed formulation and prove that the power reduction can be achieved, if the integration of DG and implementation of conservation voltage reduction is considered simultaneously.

7.2 Future Work Directions

7.2.1 Future Work for Voltage/VAR Control and DG Placement

The dissertation proposes a centralized voltage/VAR control technique which considers the stochasticity of DG outputs and load behaviors. Possible future work directions can be summarized as follows:

(1) The exponential load model is used to represent the load-to-voltage relationship since the model has been widely used in existing papers. However, further investigations are needed for the validation of using this model in practice. A possible way is to run a few

trials to change the tap positions of tap changers to check if the exponential load model can track the load-to-voltage behaviors.

(2) The proposed voltage/VAR control technique is illustrated on a modified IEEE 33-bus test system in section 4.3.3. The penetration of renewable DGs affects the voltage/VAR control. It would be beneficial to further validate the proposed method on the 33-bus test system with different penetration levels of renewable DGs and on larger IEEE standard test systems. Simulations and even field tests on real utility systems are necessary in the future.

(3) The costs of the implementation of the proposed voltage/VAR control and the benefits of a flattened voltage profile and reduced power losses need to be studied. A flattened voltage profile can assist the implementation of conservation voltage reduction since the end-of-line voltage is higher than the minimum voltage limit.

(4) The dissertation does not consider inverter-based VAR control since it is still not widely accepted by utilities in the U.S. However, it is a trend to use inverters to provide fast-response VAR control of a distribution system. The coordination of inverters and traditional voltage/VAR control devices should be studied. Moreover, a fast-response voltage/VAR control requires a decentralized communication and control framework for voltage regulators and VAR compensation devices.

(5) Chapter 4 also proposes a stochastic DG placement method to assist voltage/VAR control. In practice, many DGs are owned by customers. It is necessary to investigate the standards and incentives for the integration of customer-owned DGs.

7.2.2 Future Work for Assessment of Conservation Voltage Reduction

The dissertation proposes two methods for the assessment of conservation voltage reduction effects: data-driven assessment method and model-driven assessment method.

Possible future work directions include:

- (1) Similar to the work on voltage/VAR control, an exponential load model is used to represent the load-to-voltage behavior in section 5.3. Even though the load model is frequently used in papers, further validations by field tests are necessary.
- (2) The verification of the assessment results by the proposed two methods is still outstanding. For the data-driven assessment method, the performance of the support vector regression model is better than a multi-linear regression model with normal-voltage data. For the reduced-voltage data, it is still necessary to study whether the proposed model can accurately estimate what the load would be if there were no voltage reduction. Tests on more voltage-reduction days are still necessary. The support vector regression model needs to be re-trained for a new voltage-reduction day, which is complicated. It would be beneficial to investigate model adaptation techniques to construct a general support vector regression model that can be easily adjusted by new datasets. The proposed model-driven method can track the changes of model parameters in the simulation examples in section 5.3.3. But the verification with simulated data cannot be directly applied to practical test cases. For the assessment of utility data in section 5.3.4, the proposed model-driven method demonstrates good performance on tracking the measured load consumption (i.e., the mean average percentage error between the model output and the measured active power is small). A Euclidian distance based comparison method is developed to show the performance of the proposed method.

However, it is found that the calculated conservation voltage reduction factors of the proposed method do not match those of the Euclidian distance based method in a good way. A possible reason is that the load profile of the normal-voltage day selected by the Euclidian distance based method is not an accurate estimation of what the load would be if there were no voltage reduction for the day with conservation voltage reduction. Therefore, the verification of the assessment results should be further evaluated.

(3) For the proposed model-driven assessment method, it is found in sections 5.3.3 and 5.3.4 that the parameter values of the identification algorithm (i.e., the values assumed for the process noise level q and measurement noise level r) have impacts on the calculation of conservation voltage reduction factors. Different values of q and r lead to different assessment results of conservation voltage reduction. In this dissertation, it is suggested to use the values of q and r that result in the smallest mean average estimation error. Further studies are necessary to evaluate the impacts of algorithm settings on the assessment results of conservation voltage reduction.

7.2.3 Future Work for Demand Response

The dissertation develops a co-optimization framework for the planning and energy management with demand response. Possible future work directions include:

(1) The developed method in chapter 6 requires significant computation. A customer may not have the required computational abilities. A possible solution is to develop an online optimization platform that integrates the proposed model so that a customer can upload the data and use an online server to perform the computation.

(2) The demand response program designs have great impacts on customer behaviors. Changes in program designs may lead to significantly different cost-effectiveness results

and customer reactions. The role of energy storage systems and fossil-fired and renewable DGs in the design and operation of demand response programs needs further research. The planning of distribution systems considering demand response programs is also a promising topic.

(3) Demand response has been applied by others to conduct peak shaving and frequency regulation. It is necessary to study the coordination of demand response programs, operation of DGs, batteries and plug-in electric vehicles, and microgrids to improve the system-wide efficiency and operation.

(4) As more measurement data from smart meters become available, the assessment of conservation voltage reduction and demand response effects will be more accurate. Big data-driven techniques provide abilities to deal with large amounts of data, which can be used to analyze and predict the performance of demand response and energy efficiency programs.

CHAPTER 8 OUTCOMES

Journal Papers

1. **Z. Wang**, B. Chen, J. Wang, and J. Kim, "Decentralized Energy Management System for Networked Microgrids in Grid-connected and Islanded Modes," *IEEE Transactions on Smart Grid*, accepted for publication.
2. **Z. Wang**, B. Chen, J. Wang, and C. Chen, "Networked Microgrids for Self-healing Power Systems," *IEEE Transactions on Smart Grid*, accepted for publication.
3. **Z. Wang** and J. Wang, "Self-healing Resilient Distribution Systems based on Sectionalization into Microgrids," *IEEE Transactions on Power Systems*, accepted for publication.
4. C. Chen, J. Wang, Z. Li, H. Sun, and **Z. Wang**, "PMU Uncertainty Quantification in Voltage Stability Analysis," *IEEE Transactions on Power Systems*, accepted for publication.
5. **Z. Wang**, B. Chen, J. Wang, and M. Begovic, "Stochastic DG Placement for Conservation Voltage Reduction based on Multiple Replications Procedure," *IEEE Transactions on Power Delivery*, vol. 30, no. 3, pp. 1039-1047, June 2015.
6. **Z. Wang**, B. Chen, J. Wang, M. Begovic, and C. Chen, "Coordinated Energy Management of Networked Microgrids in Distribution Systems," *IEEE Transactions on Smart Grid*, vol. 6, no. 1, pp. 45-53, Jan. 2015.
7. **Z. Wang**, B. Chen, J. Wang, and M. Begovic, "Inverter-less Hybrid Voltage/Var Control for Distribution Circuits with Photovoltaic Generators," *IEEE Transactions on Smart Grid*, vol. 5, no. 6, pp. 2718-2728, Nov. 2014.
8. B. Chen, J. Wang, L. Wang, Y. He, and **Z. Wang**, "Robust Optimization for Transmission Expansion Planning: Minimax Cost vs. Minimax Regret," *IEEE Transactions on Power Systems*, vol. 29, no. 6, pp. 3069-3077, Nov. 2014.

9. **Z. Wang**, H. Chen, J. Wang, M. Begovic, and D. Zhao, "MPC-based Voltage/Var Optimization for Distribution Circuits with Distributed Generators and Exponential Load Models," *IEEE Transactions on Smart Grid*, vol. 5, no. 5, pp. 2412-2420, Sep. 2014.
10. **Z. Wang** and J. Wang, "Time-Varying Stochastic Assessment of Conservation Voltage Reduction Based on Load Modeling," *IEEE Transactions on Power Systems*, vol. 29, no. 5, pp. 2321-2328, Sep. 2014.
11. **Z. Wang**, B. Chen, J. Wang, J. Kim, and M. Begovic, "Robust Optimization based Optimal DG placement in Microgrids," *IEEE Transactions on Smart Grid*, vol. 5, no. 5, pp. 2173-2182, Sep. 2014.
12. **Z. Wang** and J. Wang, "Review on Implementation and Assessment of Conservation Voltage Reduction," *IEEE Transactions on Power Systems*, vol. 29, no. 3, pp. 1306-1315, May 2014.
13. **Z. Wang**, M. Begovic, and J. Wang, "Analysis of Conservation Voltage Reduction Effects Based on Multistage SVR and Stochastic Process," *IEEE Transactions on Smart Grid*, vol. 5, no. 1, pp. 431-439, Jan. 2014.

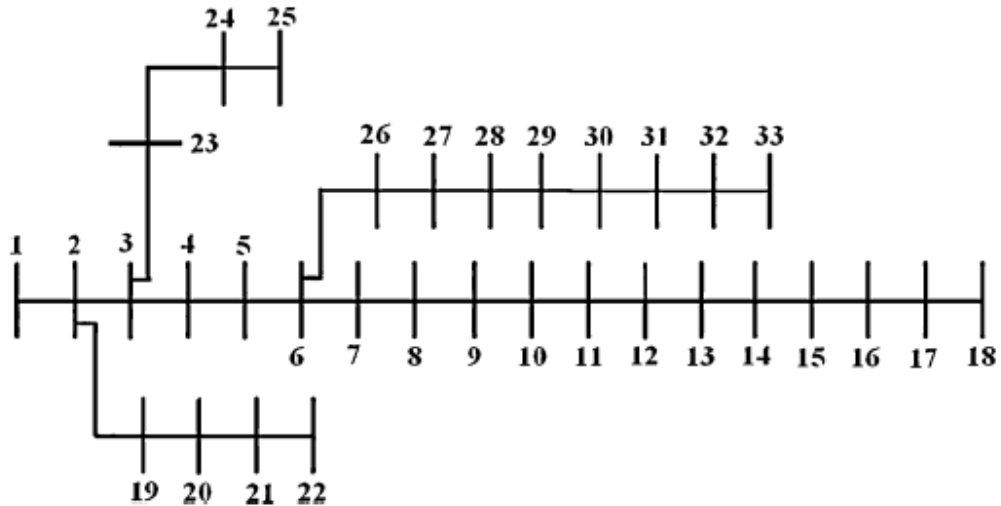
Patent Disclosures

1. Z. Wang, M. Begovic, and F. Lambert, "Method to Evaluate CVR Effects by Short-term Load Forecasting Technique," Georgia Tech Research Cooperation, filed on Sep. 17, 2013.
2. Z. Wang, M. Begovic, and F. Lambert, "Method to Evaluate CVR Effects with Load Model Identification Technique," Georgia Tech Research Cooperation, filed on Sep. 17, 2013.

CHAPTER 9 APPENDICES

Appendix A: IEEE 33-Node Distribution Test System

The following figure shows the IEEE 33-node distribution test system.



FigureA.1. IEEE 33-node distribution test system.

The line data for the 33-node test system is listed as follows:

Line No.	From Node	To Node	r (ohm)	x (ohm)
1	1	2	0.0922	0.0470
2	2	3	0.4930	0.2511
3	3	4	0.3660	0.1864
4	4	5	0.3811	0.1941
5	5	6	0.8190	0.7070
6	6	7	0.1872	0.6188
7	7	8	0.7114	0.2351

8	8	9	1.0300	0.7400
9	9	10	1.0440	0.7400
10	10	11	0.1966	0.0660
11	11	12	0.3744	0.1238
12	12	13	1.4680	1.1550
13	13	14	0.5416	0.7129
14	14	15	0.5910	0.5260
15	15	16	0.7463	0.5450
16	16	17	1.2890	1.7210
17	17	18	0.7320	0.5740
18	2	19	0.1640	0.1565
19	19	20	1.5042	1.3554
20	20	21	0.4095	0.4784
21	21	22	0.7089	0.9373
22	3	23	0.4512	0.3083
23	23	24	0.8980	0.7091
24	24	25	0.8960	0.7011
25	6	26	0.2030	0.1034
26	26	27	0.2842	0.1447
27	27	28	1.0590	0.9337
28	28	29	0.8042	0.7006
29	29	30	0.5075	0.2585
30	30	31	0.9744	0.9630

31	31	32	0.3105	0.3619
32	32	33	0.3410	0.5302

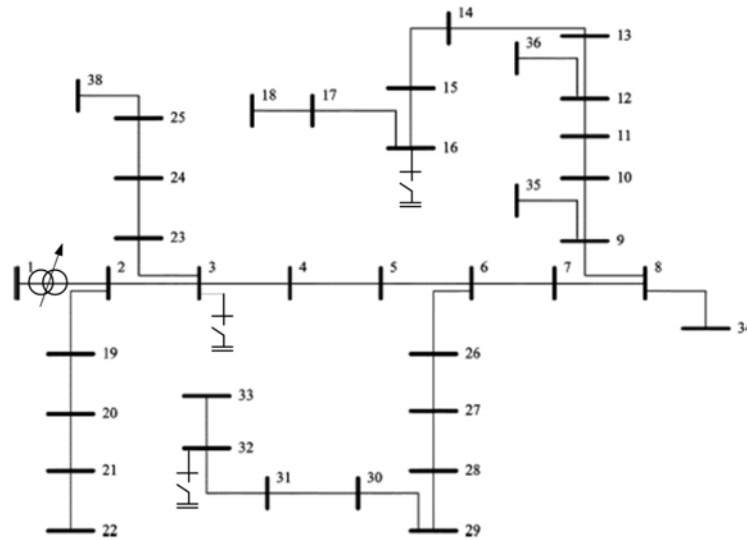
Load data for the 33-node test system is listed as follows:

Node No.	P (kw)	Q (kvar)
2	100.0	60.0
3	90.0	40.0
4	120.0	80.0
5	60.0	30.0
6	60.0	20.0
7	200.0	100.0
8	200.0	100.0
9	60.0	20.0
10	60.0	20.0
11	45.0	30.0
12	60.0	35.0
13	60.0	35.0
14	120.0	80.0
15	60.0	10.0
16	60.0	20.0
17	60.0	20.0
18	90.0	40.0

19	90.0	40.0
20	90.0	40.0
21	90.0	40.0
22	90.0	40.0
23	90.0	50.0
24	420.0	200.0
25	420.0	200.0
26	60.0	25.0
27	60.0	25.0
28	60.0	20.0
29	120.0	70.0
30	200.0	600.0
31	150.0	70.0
32	210.0	100.0
33	60.0	40.0

Appendix B: 37-Bus Distribution Test System

The following figure shows the 37-bus distribution test system.



FigureB.2. 37-bus distribution test system.

The line data for the 37-bus test system is listed as follows, the base power is 100 MVA, and the base voltage is 23 kV:

Line No.	From Node	To Node	r (p.u.)	x (p.u.)
1	1	2	0.000574	0.000293
2	2	3	0.00307	0.001564
3	3	4	0.002279	0.001161
4	4	5	0.002373	0.001209
5	5	6	0.0051	0.004402
6	6	7	0.001166	0.003853
7	7	8	0.00443	0.001464
8	8	9	0.006413	0.004608
9	9	10	0.006501	0.004608
10	10	11	0.001224	0.000405

11	11	12	0.002331	0.000771
12	12	13	0.009141	0.007192
13	13	14	0.003372	0.004439
14	14	15	0.00368	0.003275
15	15	16	0.004647	0.003394
16	16	17	0.008026	0.010716
17	17	18	0.004558	0.003574
18	2	19	0.001021	0.000974
19	19	20	0.009366	0.00844
20	20	21	0.00255	0.002979
21	21	22	0.004414	0.005836
22	3	23	0.002809	0.00192
23	23	24	0.005592	0.004415
24	24	25	0.005579	0.004366
25	6	26	0.001264	0.000644
26	26	27	0.00177	0.000901
27	27	28	0.006594	0.005814
28	28	29	0.005007	0.004362
29	29	30	0.00316	0.00161
30	30	31	0.006067	0.005996
31	31	32	0.001933	0.002253
32	32	33	0.002123	0.003301
33	8	34	0.012453	0.012453

34	9	35	0.012453	0.012453
35	12	36	0.012453	0.012453
36	18	37	0.003113	0.003113
37	25	38	0.003113	0.003113

Load data for the 37-bus test system is listed as follows:

Node No.	P (p.u.)	Q (p.u.)
2	0.1	0.06
3	0.09	0.04
4	0.12	0.08
5	0.06	0.03
6	0.06	0.02
7	0.2	0.1
8	0.2	0.1
9	0.06	0.02
10	0.06	0.02
11	0.045	0.03
12	0.06	0.035
13	0.06	0.035
14	0.12	0.08
15	0.06	0.01
16	0.06	0.02

17	0.06	0.02
18	0.09	0.04
19	0.09	0.04
20	0.09	0.04
21	0.09	0.04
22	0.09	0.04
23	0.09	0.05
24	0.42	0.2
25	0.42	0.2
26	0.06	0.025
27	0.06	0.025
28	0.06	0.02
29	0.12	0.07
30	0.2	0.6
31	0.15	0.07
32	0.21	0.1
33	0.06	0.04
34	0	0
35	0	0
36	0	0
37	0	0
38	0	0

REFERENCES

- [1] DOE. (2006). *Benefits of demand response in electricity markets and recommendations for achieving them*. Available: <http://energy.gov/oe/downloads/benefits-demand-response-electricity-markets-and-recommendations-achieving-them-report>
- [2] J. V. Milanovic, K. Yamashita, S. Martinez Villanueva, S. Z. Djokic, and L. M. Korunovic, "International Industry Practice on Power System Load Modeling," *IEEE Trans. Power Syst.*, vol. 28, no. 3, pp. 3038-3046, Aug. 2013.
- [3] W. Price, S. Casper, C. Nwankpa, R. Bradish, H. Chiang, C. Concordia, *et al.*, "Bibliography on load models for power flow and dynamic performance simulation," *IEEE Power Engineering Review*, vol. 15, no. 2, pp. 523-538, Feb. 1995.
- [4] H. A. Aalami, M. P. Moghaddam, and G. R. Yousefi, "Modeling and prioritizing demand response programs in power markets," *Electric Power Systems Research*, vol. 80, no. 4, pp. 426-435, Apr. 2010.
- [5] S. A. Pourmousavi and M. H. Nehrir, "Real-Time Central Demand Response for Primary Frequency Regulation in Microgrids," *IEEE Trans. Smart Grid*, vol. 3, no. 4, pp. 1988-1996, Dec. 2012.
- [6] K. Dietrich, J. M. Latorre, L. Olmos, and A. Ramos, "Demand Response in an Isolated System With High Wind Integration," *IEEE Trans. Power Syst.*, vol. 27, no. 1, pp. 20-29, Feb. 2012.
- [7] Z. Peng, Q. Kejun, Z. Chengke, B. G. Stewart, and D. M. Hepburn, "A Methodology for Optimization of Power Systems Demand Due to Electric Vehicle Charging Load," *IEEE Trans. Power Syst.*, vol. 27, no. 3, pp. 1628-1636, Aug. 2012.
- [8] H. S. V. S. Kumar Nunna and S. Doolla, "Energy Management in Microgrids Using Demand Response and Distributed Storage-A Multiagent Approach," *IEEE Trans. Power Deli.*, vol. 28, no. 2, pp. 939-947, Apr. 2013.
- [9] M. C. Vlot, J. D. Knigge, and J. G. Slootweg, "Economical Regulation Power Through Load Shifting With Smart Energy Appliances," *IEEE Trans. Smart Grid*, vol. 4, no. 3, pp. 1705-1712, Sep. 2013.
- [10] M. Parvania, M. Fotuhi-Firuzabad, and M. Shahidehpour, "Optimal Demand Response Aggregation in Wholesale Electricity Markets," *IEEE Trans. Smart Grid*, vol. 4, no. 4, pp. 1957-1965, Dec. 2013.

- [11] C. Chen, W. Jianhui, and S. Kishore, "A Distributed Direct Load Control Approach for Large-Scale Residential Demand Response," *IEEE Trans. Power Syst.*, vol. 29, no. 5, pp. 2219-2228, Sep. 2014.
- [12] L. Meng, L. Wei-Jen, and L. K. Lee, "Financial Opportunities by Implementing Renewable Sources and Storage Devices for Households Under ERCOT Demand Response Programs Design," *IEEE Trans. Ind. Applic.*, vol. 50, no. 4, pp. 2780-2787, July 2014.
- [13] F. A. Viawan and D. Karlsson, "Combined local and remote voltage and reactive power control in the presence of induction machine distributed generation," *IEEE Trans. Power Syst.*, vol. 22, no. 4, pp. 2003-2012, Nov. 2007.
- [14] Y.-Y. Hong and Y.-F. Luo, "Optimal VAR control considering wind farms using probabilistic load-flow and gray-based genetic algorithms," *IEEE Trans. Power Deli.*, vol. 24, no. 3, pp. 1441-1449, Jul. 2009.
- [15] B. A. De Souza and A. M. F. de Almeida, "Multiobjective Optimization and Fuzzy Logic Applied to Planning of the Volt/Var Problem in Distributions Systems," *IEEE Trans. Power Syst.*, vol. 25, no. 3, pp. 1274-1281, Aug. 2010.
- [16] T. Niknam, M. Zare, and J. Aghaei, "Scenario-Based Multiobjective Volt/Var Control in Distribution Networks Including Renewable Energy Sources," *IEEE Trans. Power Deli.*, vol. 27, no. 4, pp. 2004-2019, Oct. 2012.
- [17] H. E. Z. Farag, E. F. El-Saadany, and R. Seethapathy, "A Two Ways Communication-Based Distributed Control for Voltage Regulation in Smart Distribution Feeders," *IEEE Trans. Smart Grid*, vol. 3, no. 1, pp. 271-281, Mar. 2012.
- [18] A. Borghetti, "Using mixed integer programming for the volt/var optimization in distribution feeders," *Electric Power Systems Research*, vol. 98, pp. 39-50, May 2013.
- [19] A. C. Rueda-Medina and A. Padilha-Feltrin, "Distributed Generators as Providers of Reactive Power Support-A Market Approach," *IEEE Trans. Power Syst.*, vol. 28, no. 1, pp. 490-502, Feb. 2013.
- [20] Y. P. Agalgaonkar, B. C. Pal, and R. A. Jabr, "Distribution Voltage Control Considering the Impact of PV Generation on Tap Changers and Autonomous Regulators," *IEEE Trans. Power Syst.*, vol. 29, no. 1, pp. 182-192, Jan. 2014.
- [21] F. Capitanescu, I. Bilibin, and E. Romero Ramos, "A Comprehensive Centralized Approach for Voltage Constraints Management in Active Distribution Grid," *IEEE Trans. Power Syst.*, vol. 29, no. 2, pp. 933-942, Mar. 2014.

- [22] FERC. (2012). *Assessment of demand response and advanced metering*. Available: <http://www.ferc.gov/legal/staff-reports/12-20-12-demand-response.pdf>
- [23] M. H. Albadi and E. El-Saadany, "A summary of demand response in electricity markets," *Electric Power Systems Research*, vol. 78, pp. 1989-1996, 2008.
- [24] J. Bode, S. George, and A. Savage, "Cost-effectiveness of CECONY Demand Response Programs," Freeman, Sullivan & CO., Nov. 2013.
- [25] K.-Y. Huang and Y.-C. Huang, "Integrating direct load control with interruptible load management to provide instantaneous reserves for ancillary services," *IEEE Trans. Power Syst.*, vol. 19, no. 3, pp. 1626-1634, Aug. 2004.
- [26] K.-H. Ng and G. B. Sheble, "Direct load control-A profit-based load management using linear programming," *IEEE Trans. Power Syst.*, vol. 13, no. 2, pp. 688-694, May 1998.
- [27] H. Aalami, M. P. Moghaddam, and G. Yousefi, "Demand response modeling considering interruptible/curtailable loads and capacity market programs," *Applied Energy*, vol. 87, pp. 243-250, 2010.
- [28] T. Wu, M. Rothleder, Z. Alaywan, and A. D. Papalexopoulos, "Pricing energy and ancillary services in integrated market systems by an optimal power flow," *IEEE Trans. Power Syst.*, vol. 19, no. 1, pp. 339-347, Feb. 2004.
- [29] H. Aalami, G. R. Yousefi, and M. P. Moghadam, "Demand Response model considering EDRP and TOU programs," presented at the IEEE PES Transmission and Distribution Conference and Exposition, Chicago, IL, Apr. 21-24, 2008.
- [30] K. Herter, "Residential implementation of critical-peak pricing of electricity," *Energy Policy*, vol. 35, pp. 2121-2130, 2007.
- [31] A. Conejo, J. Morales, and L. Baringo, "Real-Time Demand Response Model," *IEEE Trans. Smart Grid*, vol. 1, no. 3, pp. 236-242, Dec. 2010.
- [32] H. S. V. S. Kumar Nunna and S. Doolla, "Multiagent-Based Distributed-Energy-Resource Management for Intelligent Microgrids," *IEEE Trans. Ind. Electron.*, vol. 60, no. 4, pp. 1678-1687, Apr. 2013.
- [33] C. Zhi, W. Lei, and L. Zuyi, "Electric Demand Response Management for Distributed Large-Scale Internet Data Centers," *IEEE Trans. Smart Grid*, vol. 5, no. 2, pp. 651-661, March 2014.
- [34] W. Zhimin, G. Chenghong, L. Furong, P. Bale, and S. Hongbin, "Active Demand Response Using Shared Energy Storage for Household Energy Management," *IEEE Trans. Smart Grid*, vol. 4, no. 4, pp. 1888-1897, Dec. 2013.

- [35] Z. Wang and J. Wang, "Review on Implementation and Assessment of Conservation Voltage Reduction," *IEEE Trans. Power Syst.*, vol. 29, no. 3, pp. 1306-1315, May 2014.
- [36] J. Grainger and S. Civanlar, "Volt/Var Control on distribution Systems with lateral branches using shunt capacitors and voltage regulators Part I: The overall problem," *IEEE Trans. Power Apparatus and Systems*, pp. 3278-3283, Nov. 1985.
- [37] R.-H. Liang and C.-K. Cheng, "Dispatch of main transformer ULTC and capacitors in a distribution system," *IEEE Trans. Power Deli.*, vol. 16, no. 4, pp. 625-630, Oct. 2001.
- [38] J.-y. Park, S.-r. Nam, and J.-k. Park, "Control of a ULTC considering the dispatch schedule of capacitors in a distribution system," *IEEE Trans. Power Syst.*, vol. 22, no. 2, pp. 755-761, May 2007.
- [39] G. W. Kim and K. Y. Lee, "Coordination control of ULTC transformer and STATCOM based on an artificial neural network," *IEEE Trans. Power Syst.*, vol. 20, no. 2, pp. 580-586, May 2005.
- [40] M. Singh, V. Khadkikar, A. Chandra, and R. K. Varma, "Grid interconnection of renewable energy sources at the distribution level with power-quality improvement features," *IEEE Trans. Power Deli.*, vol. 26, no. 1, pp. 307-315, Jan. 2011.
- [41] F. A. Viawan and D. Karlsson, "Voltage and reactive power control in systems with synchronous machine-based distributed generation," *IEEE Trans. Power Deli.*, vol. 23, no. 2, pp. 1079-1087, Apr. 2008.
- [42] T. Senjyu, Y. Miyazato, A. Yona, N. Urasaki, and T. Funabashi, "Optimal Distribution Voltage Control and Coordination With Distributed Generation," *IEEE Trans. Power Deli.*, vol. 23, no. 2, pp. 1236-1242, Apr. 2008.
- [43] Z. Wang, B. Chen, J. Wang, and M. Begovic, "Inverter-less Hybrid Voltage/Var Control for Distribution Circuits with Photovoltaic Generators," *IEEE Trans. Smart Grid*, vol. 5, no. 6, pp. 2718-2728, Nov. 2014.
- [44] P. Kundur, *Power system stability and control*: Tata McGraw-Hill Education, 1994.
- [45] D. Singh and K. Verma, "Multiobjective optimization for DG planning with load models," *IEEE Trans. Power Syst.*, vol. 24, no. 1, pp. 427-436, Feb. 2009.
- [46] B. A. Robbins, C. N. Hadjicostis, and A. D. Domínguez-García, "A two-stage distributed architecture for voltage control in power distribution systems," *IEEE Trans. Power Syst.*, vol. 28, no. 2, pp. 1470-1482, May 2013.

- [47] R. Yan and T. K. Saha, "Investigation of voltage stability for residential customers due to high photovoltaic penetrations," *IEEE Trans. Power Syst.*, vol. 27, no. 2, pp. 651-662, May 2012.
- [48] H.-G. Yeh, D. F. Gayme, and S. H. Low, "Adaptive VAR control for distribution circuits with photovoltaic generators," *IEEE Trans. Power Syst.*, vol. 27, no. 3, pp. 1656-1663, Aug. 2012.
- [49] H. Li, F. Li, Y. Xu, D. T. Rizy, and S. Adhikari, "Autonomous and adaptive voltage control using multiple distributed energy resources," *IEEE Trans. Power Syst.*, vol. 28, no. 2, pp. 718-730, May 2013.
- [50] D. Kirshner, "Implementation of conservation voltage reduction at Commonwealth Edison," *IEEE Trans. Power Syst.*, vol. 5, no. 4, pp. 1178-1182, Nov. 1990.
- [51] ANSI, "ANSI Standard C84.1-1995 Electric Power Systems and Equipment Voltage Ratings (60 Hz)," 1995.
- [52] B. Kennedy and R. Fletcher, "Conservation voltage reduction (CVR) at Snohomish County PUD," *IEEE Trans. Power Syst.*, vol. 6, no. 3, pp. 986-998, Aug. 1991.
- [53] R. Preiss and V. Warnock, "Impact of voltage reduction on energy and demand," *IEEE Trans. Power Syst.*, pp. 1665-1671, 1978.
- [54] B. Williams, "Distribution capacitor automation provides integrated control of customer voltage levels and distribution reactive power flow," presented at the IEEE Power Industry Computer Application Conference, Salt Lake City, UT, May 7-12, 1995.
- [55] D. Lauria, "Conservation voltage reduction (CVR) at Northeast Utilities," *IEEE Trans. Power Deli.*, vol. 2, no. 4, pp. 1186-1191, Oct. 1987.
- [56] J. De Steese, "Assessment of Conservation Voltage Reduction Applicable in the BPA Service Region," 1987.
- [57] A. Dwyer, R. E. Nielsen, J. Stangl, and N. S. Markushevich, "Load to voltage dependency tests at BC Hydro," *IEEE Trans. Power Syst.*, vol. 10, no. 2, pp. 709-715, May 1995.
- [58] T. A. Short and R. W. Mee, "Voltage reduction field trials on distributions circuits," presented at the IEEE PES Transmission and Distribution Conference and Exposition (T&D), Orlando, FL, May 7-10, 2012.

- [59] S. Lefebvre, G. Gaba, A.-O. Ba, and D. Asber, "Measuring the efficiency of voltage reduction at Hydro-Québec distribution," presented at the IEEE Power and Energy Society General Meeting, Pittsburgh, PA, July 20-24, 2008.
- [60] M. A. Peskin, P. W. Powell, and E. J. Hall, "Conservation Voltage Reduction with feedback from Advanced Metering Infrastructure," presented at the IEEE PES Transmission and Distribution Conference and Exposition, Orlando, FL, May 7-10, 2012.
- [61] J. F. K. Schneider, F. Tuffner, R. Singh. (2010). *Evaluation of Conservation Voltage Reduction (CVR) on a National Level*. Available: http://www.pnl.gov/main/publications/external/technical_reports/PNNL-19596.pdf
- [62] W. Ellens, A. Berry, and S. West, "A quantification of the energy savings by Conservation Voltage Reduction," in *IEEE International Conference on Power System Technology*, Auckland, Oct. 30-Nov. 2, 2012, pp. 1-6.
- [63] E. Diskin, T. Fallon, G. O'mahony, and C. Power, "Conservation voltage reduction and voltage optimisation on Irish distribution networks," presented at the CIRED Workshop on Integration of Renewables into the Distribution Grid Lisbon, May 29-30, 2012.
- [64] R.W.Beck. (2007). *Distribution Efficiency Initiative Final Report*. Available: <http://neea.org/docs/default-source/rfp's/long-term-monitoring-and-tracking-distribution-efficiency.pdf?sfvrsn=4>
- [65] T. L. Wilson, "Measurement and verification of distribution voltage optimization results " presented at the IEEE Power and Energy Society General Meeting, Minneapolis, MN, July 25-29, 2010.
- [66] K. Fagen and C. Bernier, "Efficiencies in Distribution Design and Operating Practices Mid-Study Analysis," presented at the IEEE Rural Electric Power Conference, Rapid City, SD, May 6-8, 2007.
- [67] E. Vega-Fuentes, S. Leon-del Rosario, J. M. Cerezo-Sanchez, and A. Vega-Martinez, "Combined comparison-regression method for assessment of CVR effects," in *55th International Scientific Conference on Power and Electrical Engineering of Riga Technical University (RTUCON)*, Riga, Oct. 14, 2014, pp. 172-176.
- [68] R. H. Fletcher and A. Saeed, "Integrating engineering and economic analysis for conservation voltage reduction," presented at the IEEE Power Engineering Society Summer Meeting, Chicago, IL, July 25-29, 2002.

- [69] B. Milosevic and M. Begovic, "Capacitor placement for conservative voltage reduction on distribution feeders," *IEEE Trans. Power Deli.*, vol. 19, no. 3, pp. 1360-1367, July 2004.
- [70] R. Uluski, "VVC in the Smart Grid era," presented at the IEEE Power and Energy Society General Meeting, Minneapolis, MN, July 25-29, 2010.
- [71] N. Acharya, P. Mahat, and N. Mithulananthan, "An analytical approach for DG allocation in primary distribution network," *International Journal of Electrical Power & Energy Systems*, vol. 28, pp. 669-678, 2006.
- [72] D. Zhu, R. P. Broadwater, K. S. Tam, R. Seguin, and H. Asgeirsson, "Impact of DG placement on reliability and efficiency with time-varying loads," *IEEE Trans. Power Syst.*, vol. 21, no. 1, pp. 419-427, Feb. 2006.
- [73] H. Hedayati, S. Nabaviniaki, and A. Akbarimajd, "A method for placement of DG units in distribution networks," *IEEE Trans. Power Deli.*, vol. 23, no. 3, pp. 1620-1628, July 2008.
- [74] Z. Wang, B. Chen, J. Wang, J. Kim, and M. Begovic, "Robust Optimization based Optimal DG placement in Microgrids," *IEEE Trans. Smart Grid*, vol. 5, no. 5, Sep. 2014.
- [75] M. Etehad, H. Ghasemi, and S. Vaez-Zadeh, "Voltage Stability-Based DG Placement in Distribution Networks," *IEEE Trans. Power Deli.*, vol. 28, no. 1, pp. 171-178, Jan. 2013.
- [76] C. Wang and M. H. Nehrir, "Analytical approaches for optimal placement of distributed generation sources in power systems," *IEEE Trans. Power Syst.*, vol. 19, no. 4, pp. 2068-2076, Nov. 2004.
- [77] H. Duong Quoc and N. Mithulananthan, "Multiple Distributed Generator Placement in Primary Distribution Networks for Loss Reduction," *IEEE Trans. Ind. Electron.*, vol. 60, no. 4, pp. 1700-1708, Apr. 2013.
- [78] K.-H. Kim, Y.-J. Lee, S.-B. Rhee, S.-K. Lee, and S.-K. You, "Dispersed generator placement using fuzzy-GA in distribution systems," presented at the IEEE Power Engineering Society Summer Meeting, Chicago, IL, July 25-29, 2002.
- [79] N. S. Rau and Y.-h. Wan, "Optimum location of resources in distributed planning," *IEEE Trans. Power Syst.*, vol. 9, no. 4, pp. 2014-2020, Nov. 1994.
- [80] R. Srinivasa Rao, S. V. L. Narasimham, M. Ramalinga Raju, and A. Srinivasa Rao, "Optimal network reconfiguration of large-scale distribution system using harmony search algorithm," *IEEE Trans. Power Syst.*, vol. 26, no. 3, pp. 1080-1088, Aug. 2011.

- [81] Y. Atwa, E. El-Saadany, M. Salama, and R. Seethapathy, "Optimal renewable resources mix for distribution system energy loss minimization," *IEEE Trans. Power Syst.*, vol. 25, no. 1, pp. 360-370, Feb. 2010.
- [82] R. S. Al Abri, E. F. El-Saadany, and Y. M. Atwa, "Optimal Placement and Sizing Method to Improve the Voltage Stability Margin in a Distribution System Using Distributed Generation," *IEEE Trans. Power Syst.*, vol. 28, no. 1, pp. 326-334, Feb. 2013.
- [83] H. S. Hippert, C. E. Pedreira, and R. C. Souza, "Neural networks for short-term load forecasting: a review and evaluation," *IEEE Trans. Power Syst.*, vol. 16, no. 1, pp. 44-55, Feb. 2001.
- [84] Z. Bashir and M. El-Hawary, "Applying wavelets to short-term load forecasting using PSO-based neural networks," *IEEE Trans. Power Syst.*, vol. 24, pp. 20-27, 2009.
- [85] B.-J. Chen and M.-W. Chang, "Load forecasting using support vector machines: A study on EUNITE competition 2001," *IEEE Trans. Power Syst.*, vol. 19, pp. 1821-1830, 2004.
- [86] S. Fan and L. Chen, "Short-term load forecasting based on an adaptive hybrid method," *IEEE Trans. Power Syst.*, vol. 21, no. 1, pp. 392-401, Feb. 2006.
- [87] E. E. Elattar, J. Goulermas, and Q. Wu, "Electric load forecasting based on locally weighted support vector regression," *IEEE Trans. Syst., Man, and Cybernetics*, vol. 40, no. 4, pp. 438-447, July 2010.
- [88] K. Srinivasan and C. Lafond, "Statistical analysis of load behavior parameters at four major loads," *IEEE Trans. Power Syst.*, vol. 10, no. 1, pp. 387-392, Feb. 1995.
- [89] M. Begovic and R. Mills, "Load identification and voltage stability monitoring," *IEEE Trans. Power Syst.*, vol. 10, no. 1, pp. 109-116, Feb. 1995.
- [90] W. W. Price, K. A. Wirgau, A. Murdoch, J. V. Mitsche, E. Vaahedi, and M. El-Kady, "Load modeling for power flow and transient stability computer studies," *IEEE Trans. Power Syst.*, vol. 3, no. 1, pp. 180-187, Feb. 1988.
- [91] C.-J. Lin, A.-T. Chen, C.-Y. Chiou, C.-H. Huang, H.-D. Chiang, J.-C. Wang, *et al.*, "Dynamic load models in power systems using the measurement approach," *IEEE Trans. Power Syst.*, vol. 8, no. 1, pp. 309-315, Feb. 1993.
- [92] L. Ljung and T. Söderström, *Theory and practice of recursive identification*: MIT Press, 1985.

- [93] J. R. Birge and F. Louveaux, *Introduction to stochastic programming*: Springer Verlag, 1997.
- [94] H. Heitsch and W. Römisch, "Scenario reduction algorithms in stochastic programming," *Comput. Optim. Appl.*, vol. 24, nos. 2-3, pp. 187-206, Feb. 2003.
- [95] G. Bayraksan and D. P. Morton, "Assessing solution quality in stochastic programs," *Mathematical Programming*, vol. 108, no. 2-3, pp. 495-514, Sep. 2006.
- [96] M. E. Baran and F. F. Wu, "Network reconfiguration in distribution systems for loss reduction and load balancing," *IEEE Trans. Power Deli.*, vol. 4, no. 2, pp. 1401-1407, Apr. 1989.
- [97] M. Haque, "Efficient load flow method for distribution systems with radial or mesh configuration," *IEE Proceedings-Generation, Transmission and Distribution*, vol. 143, no. 1, pp. 33-38, Jan. 1996.
- [98] Z. Wang, B. Chen, J. Wang, M. Begovic, and Y. He, "MPC-based Voltage/Var Optimization for Distribution Circuits with Distributed Generators and Exponential Load Models," *IEEE Trans. Smart Grid*, vol. 5, no. 5, pp. 2412-2420, Sep. 2014.
- [99] M. Moradzadeh, R. Boel, and L. Vandeveldel, "Anticipating and Coordinating Voltage Control for Interconnected Power Systems," *Energies*, vol. 7, no. 2, pp. 1027-1047, Feb. 2014.
- [100] P. Malysz, S. Sirouspour, and A. Emadi, "An Optimal Energy Storage Control Strategy for Grid-connected Microgrids," *IEEE Trans. Smart Grid*, vol. 5, no. 4, pp. 1785-1796, July 2014.
- [101] A. O'Connell, D. Flynn, and A. Keane, "Rolling Multi-Period Optimization to Control Electric Vehicle Charging in Distribution Networks," *IEEE Trans. Power Syst.*, vol. 29, no. 1, pp. 340-348, Jan. 2014.
- [102] I. E. Grossmann, J. Viswanathan, A. Vecchiotti, R. Raman, and E. Kalvelagen, "GAMS/DICOPT: A discrete continuous optimization package," *Mathematical Methods in Applied Sciences*, vol. 24, no. 11, pp. 649-664, July 2001.
- [103] M. Marwali, M. Haili, S. Shahidehpour, and K. Abdul-Rahman, "Short term generation scheduling in photovoltaic-utility grid with battery storage," *IEEE Trans. Power Syst.*, vol. 13, no. 3, pp. 1057-1062, Aug. 1998.
- [104] L. Wu, M. Shahidehpour, and T. Li, "Cost of reliability analysis based on stochastic unit commitment," *IEEE Trans. Power Syst.*, vol. 23, no. 3, pp. 1364-1374, Aug. 2008.

- [105] Z. Wang, M. Begovic, and J. Wang, "Analysis of Conservation Voltage Reduction Effects Based on Multistage SVR and Stochastic Process," *IEEE Trans. Smart Grid*, vol. 5, no. 1, pp. 431-439, Jan. 2014.
- [106] L. Global Energy Partners. (2005). *Distribution Efficiency Initiative*. Available: http://www.smartgridnews.com/artman/uploads/1/sgrn_2007_08011.pdf
- [107] H. A. Mostafa, R. El-Shatshat, and M. M. A. Salama, "Multi-Objective Optimization for the Operation of an Electric Distribution System With a Large Number of Single Phase Solar Generators," *IEEE Trans. Smart Grid*, vol. 4, no. 2, pp. 1038-1047, Jun. 2013.
- [108] D. Kirshner and P. Giorsetto, "Statistical Test of Energy Saving Due to Voltage Reduction," *IEEE Trans. Power Apparatus and Systems*, pp. 1205-1210, June 1984.
- [109] V. Dabic, C. Siew, J. Peralta, and D. Acebedo, "BC Hydro's experience on Voltage VAR Optimization in distribution system," presented at the IEEE PES Transmission and Distribution Conference and Exposition, New Orleans, LA, Apr. 19-22, 2010.
- [110] A. Smola and B. Schölkopf, "A tutorial on support vector regression," *Statistics and Computing*, vol. 14, no. 3, pp. 199-222, August 2004.
- [111] K. Srinivasan, C. Nguyen, Y. Robichaud, A. S. Jacques, and G. Rogers, "Load response coefficients monitoring system: theory and field experience," *IEEE Trans. Power App. and Syst.*, vol. PAS-100, no. 8, pp. 3818-3827, Aug. 1981.
- [112] S. J. Julier and J. K. Uhlmann, "New extension of the Kalman filter to nonlinear systems," in *AeroSense'97*, 1997, pp. 182-193.
- [113] W. H. Kersting, "Radial distribution test feeders," *IEEE Trans. Power Syst.*, vol. 6, no. 3, pp. 975-985, Aug. 1991.
- [114] R. C. Dugan, "Reference Guide The Open Distribution System Simulator (OpenDSS)," 2009.
- [115] W. Zhe, Y. Kai, and W. Xiaodong, "Privacy-Preserving Energy Scheduling in Microgrid Systems," *IEEE Trans. Smart Grid*, vol. 4, no. 4, pp. 1810-1820, Nov. 2013.
- [116] W. Tianshu, K. Taeyoung, P. Sangyoung, Z. Qi, S. X. D. Tan, C. Naehyuck, *et al.*, "Battery management and application for energy-efficient buildings," in *2014 51st ACM/EDAC/IEEE Design Automation Conference (DAC)*, San Francisco, CA, June 1-5, 2014.

- [117] S. Kahrobaee, S. Asgarpour, and Q. Wei, "Optimum Sizing of Distributed Generation and Storage Capacity in Smart Households," *IEEE Trans. Smart Grid*, vol. 4, no. 4, pp. 1791-1801, Dec. 2013.
- [118] A. M. Dizqah, A. Maheri, K. Busawon, and A. Kamjoo, "A Multivariable Optimal Energy Management Strategy for Standalone DC Microgrids," *IEEE Trans. Power Syst.*, accepted for publication.
- [119] PG&E. *Demand Response Programs in PG&E.* Available: <http://www.pge.com/en/mybusiness/save/energymanagement/index.page>